Understanding the molecular interplay between senescence, rejuvenation, and healthy ageing.

Eleanor Tyler

A thesis presented for the degree of

Doctor of Philosophy

2016

Supervisors:

Dr Cleo L. Bishop

Prof. Mike P. Philpott

Centre for Cell Biology and Cutaneous Research

The Blizard Institute

Barts and the London School of Medicine and Dentistry

Queen Mary University of London

Statement of originality

I, Eleanor Tyler, confirm that the research included within this thesis is my own work or that where it has been carried out in collaboration with, or supported by others, that this is duly acknowledged below and my contribution indicated.

I attest that I have exercised reasonable care to ensure that the work is original, and does not to the best of my knowledge break any UK law, infringe any third party's copyright or other Intellectual Property Right, or contain any confidential material.

I accept that the College has the right to use plagiarism detection software to check the electronic version of the thesis.

I confirm that this thesis has not been previously submitted for the award of a degree by this or any other university.

Signature: Eleanor Tyler

Date: 19.12.16

Abstract

Senescence is classically defined as an irreversible cell cycle arrest. There is now convincing evidence that senescent cells accumulate during human ageing, potentially driving age-related dysfunction through depletion of mitotically active cells and stimulation of chronic inflammation. Recently, a landmark paper demonstrated that removal of $p16^{INK4A}$ (p16)-positive senescent cells in mice prolonged healthy lifespan, suggesting a direct link between senescence and age-related dysfunction. As such, restraining the senescent pool or slowing their rate of accumulation presents an attractive therapeutic strategy for extending healthspan. Previously, our laboratory has demonstrated that siRNA transfection can reverse deep senescence in p16-positive primary adult human mammary epithelial cells using a panel of senescence markers. Subsequent siRNA screening revealed 28 hits which strongly induced reversal in the deeply senescent HMECs. In this project, siRNA knockdown of p16 combined with $p21^{WAF1/CIP1}$ (p21) was found to reverse deep replicative senescence in primary adult human mammary fibroblasts, as defined by a panel of senescence markers. This discovery provided the opportunity to screen for novel siRNAs which induce reversal in both cell types. Screening in the deeply senescent HMFs of the 28 shortlisted candidates and 33 protein interactors identified using bioinformatics revealed 45 siRNAs which significantly increased cell number compared to the negative siRNA control. Subsequent immunofluorescence staining and high content analysis of the top 14 candidates identified 10 hit siRNAs which induced senescence reversal as defined by a panel of markers. Interestingly, these 10 hits were enriched for cytoskeletal and cell adhesion processes, suggesting an interplay between external forces and senescence induction. The top siRNA hit, early growth response 2 or EGR2, a transcription factor, was validated and selected for further exploration as a novel driver of senescence. Bioinformatics analysis revealed an enrichment for EGR2 binding sites within genes dynamically expressed in HMEC senescence, including p16, p21, and nine hits identified to reverse senescence in HMFs and HMECs. Furthermore, deeply senescent HMFs and HMECs were found to have a significantly increased nuclear EGR2 foci number compared to proliferating cells, and this was significantly decreased in reversed HMFs. In conclusion, it is proposed that EGR2 may represent a novel driver of both HMF and HMEC senescence.

Acknowledgements

This work was supported by a Medical Research Council PhD Studentship (Grant number: MR/K501372/1).

First and foremost, I would like to thank my supervisor, Dr Cleo Bishop, for her invaluable, unwavering support and guidance throughout my PhD. Your relentless optimism has been an inspiration. Thank you. I am also grateful for the support from my second supervisor, Prof. Mike Philpott, who has been there for me throughout all the PhD milestones.

To Deb, the members of the Bishop lab., and everyone in the Blizard (Anke, Heather, Hannah, to name but a few), thank you for making our institute such a fun place to work. In particular, I would like to thank Dr Maddi Moore. We grew up together in the lab. and I will always look to you as my academic big sister. Special thanks also to Mat for sharing his seemingly endless wealth of knowledge.

A big thank you goes to my support at home, Mike, who made sure I was always fed and watered. You are my rock. Also, to my friends and family, Kim, Sylvie, Alex, Gemma, Mum and Dad, who were always there for me and always okay when I couldn't be there. Thank you all.

Contents

List of Figures

List of Tables

List of Abbreviations

Due to the nature of this work, abbreviated gene names are not listed here but are outlined in the main text where appropriate.

Full name	**Abbreviation**
Absorbance at 230 nm	A_{230}
Absorbance at 260 nm	A_{260}
Absorbance at 280 nm	A_{280}
Analysis of variance	ANOVA
Antigen presenting cell	APC
Apical ectodermal ridge	AER
Arbitrary Unit	AU
Base pairs	bp
Bovine serum albumin	BSA
Carbon dioxide	CO_2
Celsius	C
Centimetre squared	cm^2
Chromatin immunoprecipitation	ChIP
Chromatin immunoprecipitation sequencing	ChIP-Seq
Cyclin dependent kinase	CDK
CDK inhibitor	CDKI
Cytosine-guanine dinucleotide	CpG
Deep senescence	DS

Dharmafect 2	Dh2
Dharmafect 4	Dh4
Differentially methylated region	DMR
Distilled water	dH_2O
DNA damage response	DDR
Double stranded RNA	dsRNA
Dulbecco's modified Eagle medium	DMEM
Dylight 547	DY547
Early proliferating	EP
Enhanced chemiluminescence	ECL
Enzyme-linked immunosorbent assay	ELISA
Ethylenediaminetetraacetic acid	EDTA
Extracellular matrix	ECM
Fast food diet	FFD
Fluorescence-activated cell sorting	FACS
Foetal bovine serum	FBS
Gene ontology	GO
Genome-wide association studies	GWAS
Hydrochloric acid	HCl
Human mammary epithelial cell	HMEC
Human mammary fibroblast	HMF
Kilobase	kb
Kilobase pairs	kbp

Kilodalton	KDa
Laboratory	lab.
Living skin equivalent	LSE
Loxo26 p21 double knockout	Loxo26 $p21^{-/-}$
Loxo26 wild-type	WT Loxo 26
Major histocompatibility complex	MHC
Mammary epithelial basal medium	MEBM
Matrix metalloproteinase	MMP
Messenger RNA	mRNA
Methyl-CpG-binding domain	MBD
Microgram	µg
Microlitre	µL
Micrometre	µm
Micrometre squared	μm^2
MicroRNA	miRNA
Milliamps	mA
Millijoule	mJ
Millilitre	mL
Millimolar	mM
Mitochondria dysfunction-associated senescence	MiDAS
Mitosis	M phase
Molar	M
Mouse embryonic fibroblast	MEF

Nanogram	ng
Nanomolar	nM
Nicotinamide adenine dinucleotide	NAD^+
Reduced NAD	NADH
Off target effect	OTE
O-N-Acetylglucosamine	O-GlcNAc
Oncogene-induced senescence	OIS
Paraformaldehyde	PFA
Passage	P
P29 plus three weeks	P29+3
Peripheral nervous system	PNS
Phosphate-buffered saline	PBS
PBS with Tween-20	PBS-T
PBS-T (0.05%) with 5% milk	PBS-T-milk
Polycomb repressive complex 1	PRC1
Polycomb repressive complex 2	PRC2
p16 siRNA combined with p21 siRNA	p16+p21
Quantitative real time polymerase chain reaction	qRTPCR
Radio-immunoprecipitation assay	RIPA
Reactive oxygen species	ROS
Replicative senescence	RS
Reversed	R
Revolutions per minute	rpm

Room temperature	RT
RNA-induced silencing complex	RISC
RNA interference	RNAi
Scanning ion conductance microscopy	SICM
Senescence-associated β-galactosidase	SA-β-Gal
Senescence-associated differentially methylated position	senDMP
Senescence-associated heterochromatin foci	SAHF
Senescence-associated miRNA	SA-miRNA
Senescence-associated secretory phenotype	SASP
Single nucleotide polymorphism	SNP
siRNA targeting Cyclophilin B labelled with DY547	siGLO
Small interfering RNA	siRNA
Sodium dodecyl sulphate	SDS
SDS-polyacrylamide gel electrophoresis	SDS-PAGE
Short hairpin RNA	shRNA
Standard deviation	SD
Stress induced premature senescence	SIPS
Systemic sclerosis	SSc
T cell receptor	TCR
Telomere associated foci	TAF
Telomeric repeat amplification protocol	TRAP
The Cancer Genome Atlas	TCGA
T helper 1	Th1

Ultraviolet	UV
Unit	U
Untransfected	UTC
Vascular smooth muscle cell	VSMC
Wild-type	WT
4',6-diamidino-2-phenylindole	DAPI
5-Bromo-2'-deoxyuridine	BrdU
5-Bromo-4-chloro-3-indoyl-β-D-galactopyroside	X-Gal
8-oxoguanine	8-oxoG

Chapter 1 Introduction

1.1 The cell cycle

1.1.1 Cell cycle regulation

The eukaryotic cell cycle consists of four phases: G1, a growth phase during which cell components are synthesised; S phase, where DNA synthesis occurs; G2, a second growth phase; and mitosis (M phase) where cell division takes place. Progression through these cell cycle phases requires passage through sequential checkpoints, namely G1-S, G2-M, and the Spindle checkpoint which controls entry into anaphase. The G1-S and G2-M checkpoints are controlled by cyclin-dependent kinases (CDKs) and their regulatory cyclin subunits (reviewed in Lim & Kaldis 2013), that form cyclin-CDK complexes which act to regulate cell cycle progression by modulating expression of transcription factors and crucial cell cycle components.

In most adult tissues, the majority of cells are maintained in a quiescent non-proliferating state called G_0. Recent evidence has shown that cell cycle gene expression is repressed during quiescence by a multi-subunit protein complex called DREAM, containing p130 or p107, dimerisation partner (DP), RB-like, E2F and MuvB (Figure 1.1) (Sadasivam and DeCaprio, 2013). In order to stimulate re-entry into the cell cycle for tissue homeostasis and repair, mitogenic signals, including the RAS subfamily, mitogen-activated protein kinase (MAPK) (Ladha *et al.*, 1998), and mechanistic target of rapamycin (mTOR) (Rodgers *et al.*, 2014), regulate CDK4 and CDK6 complex activity (reviewed in Asghar *et al*. 2015). Together with the D-type cyclins, CDK4 and CDK6 control the transition to S phase via phosphorylation of the retinoblastoma tumour suppressor protein (pRB) and the related family proteins p107 and p130 (Kato *et al.*, 1993; Matsushime *et al.*, 1994). Subsequently, activated cyclin E-CDK2 complexes function to hyperphosphorylate pRB, disrupting its association with the E2F family of transcription factors. Different E2F complexes either activate or repress transcription, and pRB family members inhibit E2F-mediated activation and augment E2F-mediated repression, thus disruption of pRB-E2F binding enables expression of E2F-responsive genes critical for cell cycle progression, including cyclins E and A which then reinforce progression through to S phase (reviewed in Dyson 1998; Lim & Kaldis 2013). Cyclin E-CDK2 maintains the hyperphosphorylated state of pRB throughout the remainder of the cell cycle, ensuring progression. Cyclin A-CDK2 is then responsible for the continuation

of S phase (Krude *et al.*, 1997), and, together with cyclin A- and cyclin B-CDK1, for transition through the G2/M checkpoint and entry into mitosis (Chen *et al.*, 2009; Marais *et al.*, 2010) (Figure 1.1).

Cell cycle exit can be triggered at the G1/S checkpoint by senescence or differentiation signals via two families of cyclin-dependent kinase inhibitors (CDKIs), INK4 and Cip/Kip, which function to inactivate cyclin-CDK complexes (reviewed in Buttitta and Edgar 2007). Members of the INK4 group include $p16^{INK4A}$ (chromosome 9p21), $p15^{INK4B}$ (9p21), $p18^{INK4C}$ (1p32) and $p19^{INK4D}$ (19p13) which function to inhibit CDK4 and CDK6 in G1 by inhibiting the CDK catalytic domains and weakening affinity of the cyclins for the CDKs (Figure 1.1). The Cip/Kip group comprises $p21^{WAF1/CIP1}$ (p21), $p27^{KIP1}$ (p27) and $p57^{KIP2}$ (p57) which function more broadly to inhibit cyclin D-, E-, A- and B- dependent CDKs throughout G1, S and G2 (Sherr & Roberts 1999; reviewed in Lim & Kaldis 2013). INK4 and Cip/Kip inhibition of cyclin D-CDK4 and -CDK6 and cyclin E-CDK2 at G1 results in hypophosphorylated pRB sequestration of E2F transcription factors and subsequent cell cycle arrest.

Recent evidence has suggested that G2 cell cycle progression is controlled by cyclin A-CDK2 and cyclin B-CDK1 phosphorylation of FOXM1, a member of the forkhead box (Fox) superfamily of transcription factors, thus activating transcriptional activity and promoting the expression of genes responsible for driving mitotic entry (Chen *et al*. 2009; Marais *et al*. 2010; reviewed in Lim & Kaldis 2013). Up-regulation of Cip/Kip proteins in response to DNA damage or incomplete replication leads to inhibition of cyclin A- and cyclin B-CDK1 activity, FOXM1 hypophosphorylation and subsequent loss of transcriptional activity, thus inducing G2 cell cycle arrest (Figure 1.1). Progression through the G2/M checkpoint into mitosis stimulates degradation of the A- and B-type cyclins by the anaphase-promoting complex, also known as APC/C, leading to mitotic exit and re-entry into the next G1 phase (reviewed in Peters 2006).

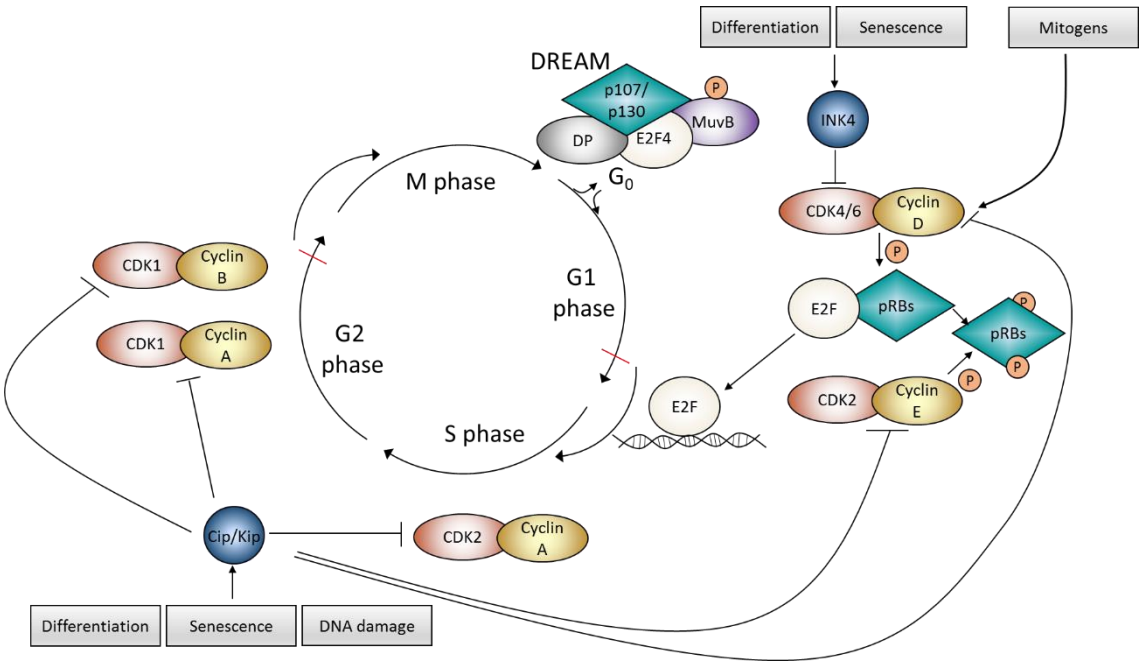

Figure 1.1 Schematic summarising the stages of the cell cycle. In most adult tissues, the majority of cells are maintained in a quiescent state (G_0). The DREAM complex (DP, p107/p130, E2F, and MuvB) represses cell cycle gene expression during quiescence. The cell cycle is regulated by complexes of cyclins (yellow) and cyclin-dependent kinases (CDKs, orange). In addition, there are various important inhibitors of these cyclin-CDK complexes (INK4 and Cip/Kip families, blue). To progress through the cell cycle, cells have to pass through the G1/S transition checkpoint (red bar) that is controlled by cyclin D-CDK4/6 and cyclin E-CDK2 pRB and p107/p130 family members (pRBs)/E2F signalling pathways. The G2/M transition checkpoint is controlled by cyclin A together with CDK2 or CDK1 or cyclin B-CDK1.

1.1.2 The INK4/ARF locus

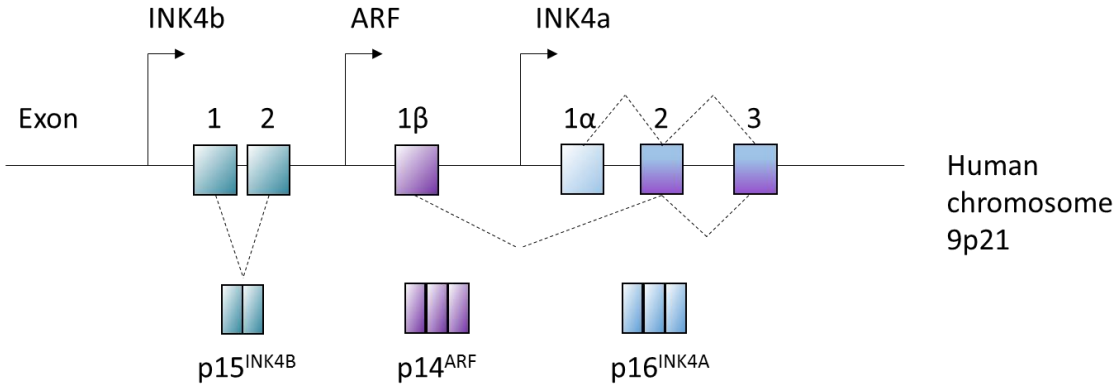

Figure 1.2 The INK4/ARF locus. Genes of the INK4/ARF locus are shown with coloured boxes representing the coding exons of INK4b (green), ARF (purple/blue) and INK4a (blue).

The INK4/ARF locus on human chromosome 9p21 comprises three tumour suppressors: p16; $p15^{INK4B}$ (p15); and $p14^{ARF}$ (ARF) (the equivalent in mice is p19Arf) genes (Figure 1.2). p15 and p16 bind directly to CDK4 and -6 preventing association with cyclin-D1, thus inhibiting kinase activity and halting cell cycle progression (Sherr & Roberts 1999), as explored in more detail in Section 1.1.1. ARF functions to stabilise tumour suppressor p53 by inhibiting MDM2, leading to up-regulation of p21, inhibition of several CDK kinase complexes and subsequent cell cycle arrest (Stott *et al*. 1998) (Figure 1.3).

Overexpression of oncogenes (e.g. HRas proto-oncogene, GTPase (HRAS); B-Raf proto-oncogene, serine/threonine kinase (BRAF); CRAF; v-myc avian myelocytomatosis viral oncogene homolog (MYC)), or loss of tumour suppressors, such as phosphatase and tensin homolog (PTEN), are known to be activators of the INK4/ARF locus (Serrano *et al.*, 1997; Zhu *et al.*, 1998; Chen *et al.*, 2005). For example, RAS signalling through the RAF-MEK-ERK kinase cascade is thought to stimulate ETS1 and 2 transcription factors to induce p16 expression (Ohtani *et al.*, 2001) as well as increasing levels of intracellular reactive oxygen species (ROS), thus enabling activation of p16 via the p38 family of stress-activated kinases (Deng *et al.*, 2004) (Figure 1.3). Additional regulators of the locus present a complex picture of INK4/ARF activation (reviewed in Gil & Peters 2006; Martin *et al*. 2014). Immediate early genes which are up-regulated in response to mitogenic signals are known to regulate the INK4/ARF locus, including members of the activator protein 1 (AP-1) family (JUNB, c-JUN, and JUND) and early growth response 1

(EGR1). In mouse embryonic fibroblasts (MEFs), overexpression of JUNB induces p16 expression, c-JUN modestly represses p16 but activates the ARF promoter (Passegué and Wagner, 2000), and JUND represses ARF in MEFs (Weitzman *et al*. 2000). EGR1, a transcription factor, is also known to repress ARF in MEFs (Krones-Herzig, Adamson and Mercola, 2003), as discussed in more detail in Section 1.8.5. Additionally, the WNT/β-catenin signalling pathway has been proposed to regulate p16 in a cell type-dependent manner (reviewed in Martin *et al*. 2014). A β-catenin binding site has been identified in the INK4a promoter (Wassermann *et al.*, 2009), and β-catenin induced ARF accumulation in MEFs (Damalas *et al.*, 2001) and stimulated expression of p16 in human colorectal cancer cell lines (Wassermann *et al.*, 2009). However, β-catenin repressed p16 in murine melanocytes (Damalas *et al.*, 2001) and was identified as a repressor of p16 in human mammary epithelial cells (HMECs) in a genome-wide RNA interference (RNAi) screen (Bishop *et al.*, 2010). SUFU, a negative regulator of hedgehog signalling, is known to interact with β-catenin and decrease β-catenin nuclear levels, and was revealed as a p16 activator in HMECs (Bishop *et al.*, 2010). There is also evidence to suggest that aberrantly high levels of E2F transcription factors stimulate up-regulation of ARF; however, there is no direct evidence that p16 is regulated by the E2Fs (Komori *et al.*, 2005).

As p16 plays a crucial role in ageing, cancer, and other diseases, it is essential for a normal cell to maintain reliable repression of the INK4/ARF locus. Thus, epigenetic regulation of the INK4/ARF locus is performed by the polycomb repressive complexes 1 and 2 (PRC1 and PRC2), which function to repress transcription through histone methylation and ubiquitination (Jacobs *et al*. 1999; Gil *et al*. 2004; reviewed in Martin *et al*. 2014). PRC2, comprised of embryonic ectoderm development (EED); SUZ12 polycomb repressive complex 2 subunit (SUZ12); and the histone methyltransferase, enhancer of zeste 1 polycomb repressive complex 2 subunit (EZH1) functions as an initiator of transcription repression by catalysing histone H3 lysine 27 trimethylation, an epigenetic mark recognised by PRC1. Subsequently, PRC1, comprised of BMI1 proto-oncogene polycomb ring finger (BMI1), polyhomeotic homolog 1 or 2 (Ph1 or 2), chromobox homolog 7 (CBX7), and the ubiquitin E3 ligases, ring finger protein 1A or B (RING1A or B), catalyses the monoubiquitination of lysine 119 of histone H2A and implements gene silencing (reviewed in Martin *et al*. 2014). Importantly, PRC1 and PRC2

have been found to bind directly to the INK4/ARF locus (Bracken *et al.*, 2007). Furthermore, reduced expression of these complexes results in increased p16 levels and activation of senescence (Gil *et al.*, 2004), and overexpression of individual PRC components extends replicative lifespan via repression of INK4/ARF (Jacobs *et al.*, 1999; Gil *et al.*, 2004; Bruggeman *et al.*, 2011). Although it is well-established that BMI1 and CBX7 levels decline during senescence in fibroblasts (Jacobs *et al.*, 1999; Gil *et al.*, 2004) the molecular pathways that regulate expression of these complexes during senescence is unclear. However, recent work has identified senescence-associated microRNAs (SA-miRNAs) which directly repress transcription of polycomb group complex members (Overhoff *et al.*, 2014).

1.1.3 p21

p21, cyclin-dependent kinase inhibitor 1A (CDKN1A), is a well-characterised member of the Cip/Kip family of CDKIs which functions mainly to inhibit cyclin/CDK2 complexes, as described in Section 1.1.1 in more detail. p21, a transcriptional target of the tumour suppressor p53, plays an important role in mediating DNA-damage induced cell-cycle arrest in G1 and G2. DNA damage sensors, including ataxia-telangiectasia mutated (ATM) (Lavin and Shiloh, 1997) and ataxia-telengiectasia mutated and Rad3-related ATR (ATR) (Cliby *et al.*, 1998), phosphorylate the checkpoint kinases CHK1 and CHK2 (Matsuoka, Huang and Elledge, 1998; Liu *et al.*, 2000), which in turn phosphorylate p53 on serine 20, preventing MDM2 binding, ubiquitination and targeting for degradation (Dumaz *et al.*, 2001). Following this, p53 then acts as a transcription factor inducing the expression of p21 which in turn inhibits several cyclin-CDK complexes and halts the cell cycle (Figure 1.1) (Turenne *et al.*, 2001). In order to maintain low levels of p53 under normal conditions, MDM2 ubiquitinates p53 to facilitate degradation (Oren, 1999). This process can be modulated by the products of the INK4/ARF locus, as ARF is known to bind to MDM2 preventing MDM2-mediated p53 degradation (Zhang, Xiong and Yarbrough, 1998) (Figure 1.3).

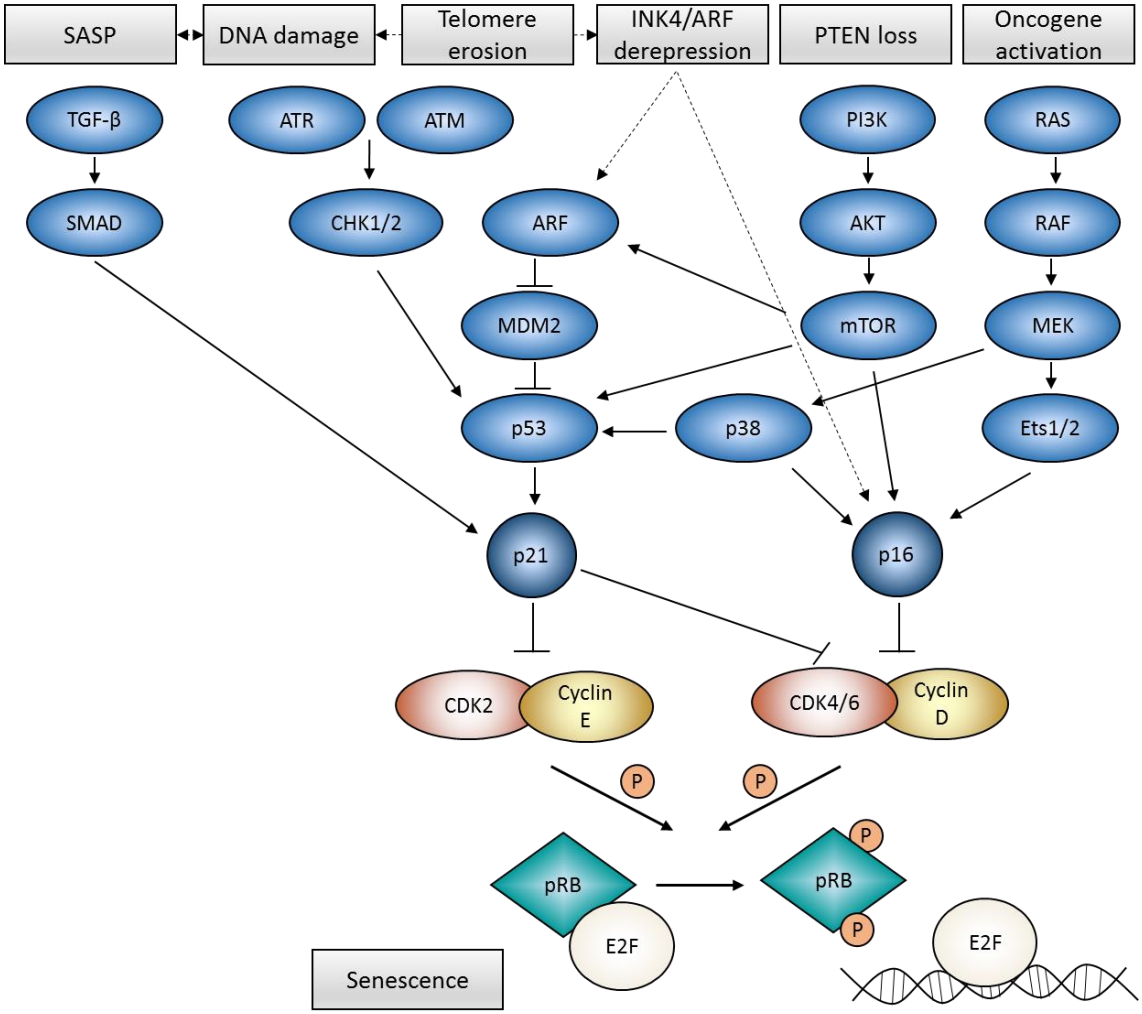

Figure 1.3 Pathways to p16 and p21 activation and senescence induction. Senescence triggers (grey boxes) stimulate downstream genes (blue) ultimately leading to up-regulation and activation of tumour suppressors p16 and p21 (dark blue), arresting the cell by inhibition of pRB phosphorylation, subsequent sequestration of E2F transcription factors and inhibition of transcription of downstream E2F-regulated genes critical for cell cycle progression.

Other mechanisms of p21 activation include PTEN loss or AKT serine/threonine kinase (AKT) activation which subsequently activates mechanistic target of rapamycin complex 1 (mTORC1), inducing p53 activity and p21 up-regulation (Astle *et al.*, 2012). Similar to the INK4/ARF locus (see Section 1.1.2), the RAS-RAF-MEK-ERK cascade induces high levels of ROS, activating p38 MAPK which leads to increased p53 transcriptional activity and up-regulation of p21 (Sun *et al.*, 2007). In addition, the senescence-associated secretory phenotype (SASP) (see Section 1.4.2) component TGF-β can induce p15 and p21 up-regulation in a paracrine manner via a mechanism that generates ROS and DNA damage (Acosta *et al.*, 2013) (Figure 1.3). It has been suggested that DNA damage signalling through p53-p21-p38-TGF-β during senescence stimulates mitochondrial

dysfunction and increases ROS levels, thus inducing further DNA damage and generating a stable self-sustaining feedback loop reinforcing senescence (Passos *et al.*, 2010).

Furthermore, p21 is a multi-functional protein which plays key roles in processes not limited to CDK inhibition. Independently of CDKs, p21 regulates cell cycle progression via inhibition of proliferating cell nuclear antigen (PCNA), subsequently blocking DNA synthesis (Luo, Hurwitz and Massagué, 1995; Warbrick *et al.*, 1995), and is also known to interact directly with and inhibit a range of transcription factors, including E2F1, c-Myc, and STAT3 (Delavaine and La Thangue, 1999; Coqueret and Gascan, 2000; Kitaura *et al.*, 2000). Paradoxically, studies have also reported that p21 participates in the assembly of cyclin D-CDK4/6 complexes, promoting CDK catalytic activity and sequestration of p21 into cyclin D-CDK4/6 complexes, thus allowing downstream activation of cyclin E-CDK2 and cell cycle progression (Figure 1.1) (Labaer *et al.*, 1997; Perez-Roger *et al.*, 1999). In addition, the p53/p21 pathway is also known to be important for triggering apoptosis. The mechanisms by which a cell decides whether to induce apoptosis or senescence in response to sustained p53/p21 signalling are currently unknown; however, it is thought that high levels of p53 and lysine 117 acetylation lead to transcription of apoptotic genes whereas low levels of p53 with transient kinetics and lysine 161/162 acetylation promotes senescence (reviewed in Childs *et al*. 2014). In addition, the apoptotic function of p53 is enhanced by binding of two members of the apoptosis stimulating protein of p53 (ASPP) family, ASPP1 and 2, to the p53 DNA binding domains, specifically stimulating the transactivation function of p53 at promoters of pro-apoptotic genes (Samuels-Lev *et al.*, 2001). Alterations to the p53/p21 signalling pathway during senescence, such as decreased ability to stabilise p53 to the levels required for apoptosis (Seluanov *et al*. 2001) and senescence-specific p53 post-translational modifications (Webley *et al*. 2000), together with senescence-associated up-regulation of pro-survival, anti-apoptotic genes, such as B-cell lymphoma 2 (BCL-2) (Wang, 1995), are thought to lead to resistance to p53-dependent apoptosis (Webley *et al*. 2000; Seluanov *et al*. 2001; Zhu *et al*. 2015; reviewed in Childs *et al*. 2014).

1.2 Fibroblast replicative senescence

Hayflick & Moorhead (1961) first discovered the limited replicative capacity of primary human foetal fibroblasts in culture. They found that early passage cells (hereafter known

as 'early proliferating' (EP)) proliferated *in vitro* for approximately 55 population doublings before succumbing to stable, G_1 cell cycle arrest. This replicative barrier, or 'Hayflick limit', is now known as replicative senescence (RS) (Figure 1.4). Recent evidence has suggested that replicative senescence is a multi-step, dynamic process throughout which senescent cells evolve and progress (Kim *et al.*, 2013). Deep senescence (DS), a stable, actively maintained senescent phenotype, takes over 7-10 days to develop post-senescence induction (Coppé *et al*. 2008; Rodier *et al*. 2009; Passos *et al*. 2010), and is characterised by additional markers of senescence such as a loss of lamin B1 and nuclear envelope integrity (Freund *et al*. 2012; reviewed in Baker & Sedivy 2013), as well as large scale chromatin changes (Narita *et al.*, 2003; Freund *et al.*, 2012; Shah *et al.*, 2013; Swanson *et al.*, 2013).

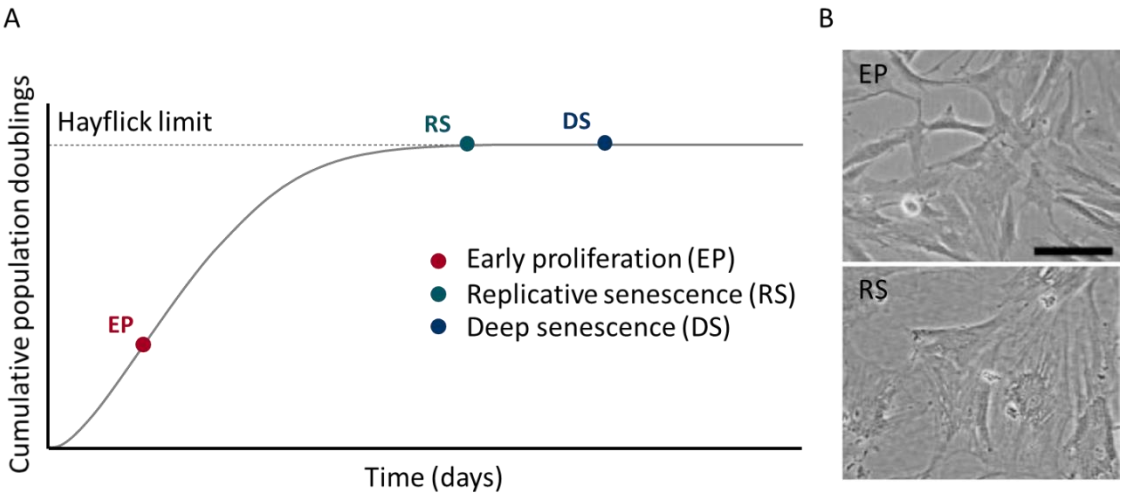

Figure 1.4 The Hayflick limit. (A) Early proliferating (EP, red) normal human fibroblasts undergo replicative senescence (RS, green) after a finite number of cell divisions in culture, as observed by Hayflick & Moorhead (1961). Deeply senescent (DS, blue) cells undergo no further expansion upon at least two serial passages. **(B)** Images depicting early proliferating (EP, top panel) and replicatively senescent (RS, bottom panel) normal adult human mammary fibroblasts (HMFs), adapted from Romanov *et al*. (2001). Scale bar denotes 100 micrometres (µm).

Telomere dysfunction is well-established as the main trigger of replicative senescence (Bodnar *et al.*, 1998). Telomeres are regions of repetitive nucleotide sequences (TTAGGG in vertebrates) that cap the ends of linear chromosomes and protect them from chromosomal fusion. Telomeres progressively shorten during each cell division due to a phenomenon known as the 'end replication problem'. In brief, the bi-directional DNA helix can be replicated in only one direction (5' to 3'), meaning that the 'lagging strand' (3' to 5') must be replicated in small fragments as the replication fork unwinds the DNA helix. DNA polymerase requires a primer for each fragment to initiate synthesis, thus the end sequence of the lagging strand serves as a primer and is not replicated. When the telomeres reach a critically short length, a DNA damage response (DDR) is rapidly triggered as described in Section 1.1.3 (Figure 1.3) leading to activation of p53, increased transcription of p21 and cell cycle arrest (Turenne *et al.*, 2001). This process is associated with the appearance of DDR foci which stain positive for phosphorylated histone variant H2AX (γ-H2AX) and the DNA damage checkpoint factor 53BP1, two widely accepted markers of replicative senescence (di Fagagna *et al.*, 2003).

The p16/pRB pathway is also activated by dysfunctional telomeres, albeit with slower kinetics than the p53/p21 pathway (Jacobs and De Lange, 2004). It is thought that rapid DDR-induction of p21 expression inhibits cyclin D1-CDK4, -CDK6, and cyclin E-CDK2 providing a primary halt to cell proliferation (Stein *et al.*, 1999). Subsequent activation of p16 then acts as an important secondary barrier to proliferation and contributes to maintenance of the senescent phenotype (Stein *et al.*, 1999). Consistent with this idea, p21 protein expression reaches a peak during the final two to three passages as the culture nears senescence (Alcorta *et al.*, 1996). p16 protein levels gradually rise in senescent fibroblasts, reaching a maximum after p21 levels have started to decline (Alcorta *et al*. 1996, Figure 1.5). Consequently, senescent fibroblast cultures can be positive for both p16 and/or p21 staining.

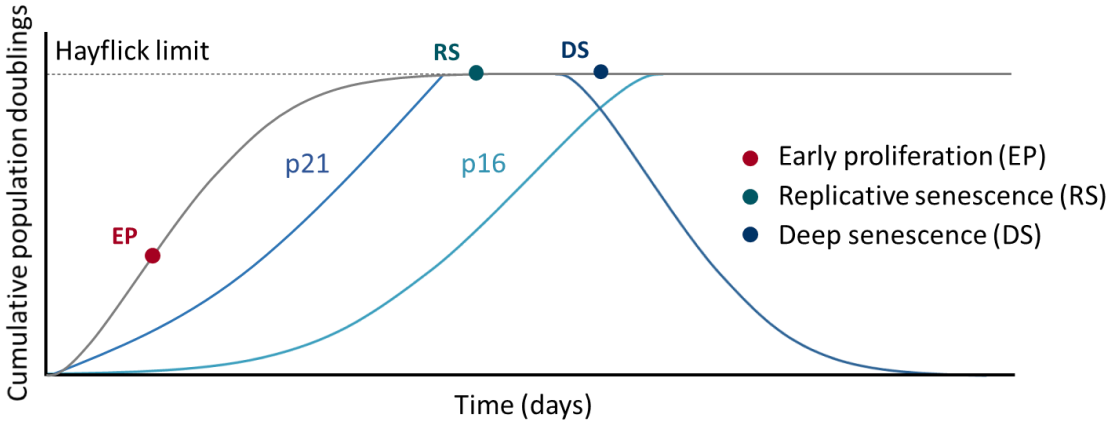

Figure 1.5 p16 and p21 kinetics and roles in replicative senescence. An early proliferating (EP) fibroblast population expresses a low level of p21 but not p16. Increased expression of p21 and p16 in senescence occurs with different kinetics in a fibroblast population. During the final two to three passages prior to senescence, p21 expression increases in the population due to telomere shortening triggering a DNA damage response. Telomere shortening then also triggers p16 activation with slower kinetics in the population. As senescence deepens, p21 expression declines in the population whereas p16 expression continues to gradually rise.

1.3 Other types of senescence

1.3.1 Epithelial cellular senescence

Unlike fibroblasts, epithelial cells exhibit a two-step pattern of senescence, where cells first undergo p16-dependent senescence in the absence of telomere erosion and p53 expression, referred to in this report as cellular senescence (Brenner, Stampfer and Aldaz, 1998). As mentioned previously, the exact mechanisms of p16 activation are currently unclear and occur heterogeneously within an EP HMEC proliferation; however, there is evidence to suggest that, in epithelial cells, this is induced by exposure to stress and a decline in polycomb proteins repressing transcription of the INK4/ARF locus (Ramirez *et al.*, 2001; Gil *et al.*, 2004; Garbe *et al.*, 2009). Evidence both *in vitro* and *in vivo* has shown that epithelial cells will typically bypass cellular senescence via p16 promoter methylation (Huschtscha *et al.*, 1998; Holst *et al.*, 2003). After p16 promoter methylation, epithelial cells will then continue on to divide until telomere-dependent senescence is triggered (Garbe *et al.*, 2009); thus, unlike fibroblasts, replicative senescence in these cells will be mediated solely by the p53/p21 axis (Figure 1.6).

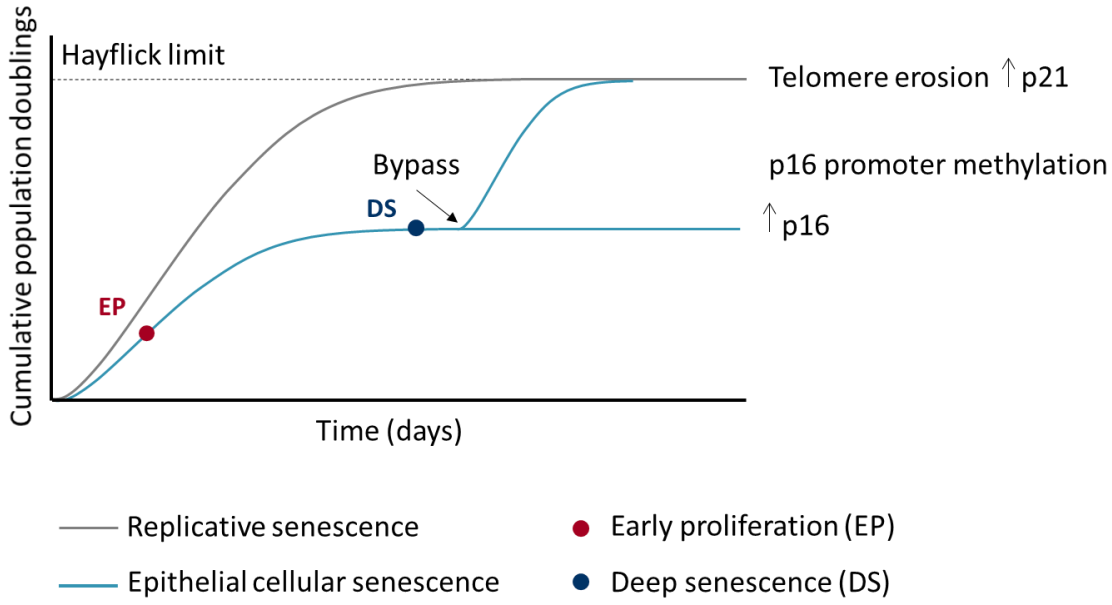

Figure 1.6 Schematic illustrating epithelial cellular senescence and replicative senescence. Early proliferating (EP) epithelial cells undergo p16-dependent cellular senescence after serial passaging reaching deep senescence (DS) after being kept in culture for three weeks. Epithelial cells can bypass cellular senescence via p16 promoter methylation and continue to proliferate until critically short telomeres trigger p53/p21 pathway activation inducing senescence.

1.3.2 Premature senescence

In addition to replicative senescence and cellular senescence, fibroblasts, epithelial cells and other cell types may also undergo premature senescence in response to a variety of triggers. Oncogene-induced senescence (OIS) is caused by activated oncogenes (RAS, MEK, BRAF) or loss of tumour suppressors (PTEN), involves both the p53/p21 and p16/pRB pathways (see Sections 1.1.2 and 1.1.3), and is thought to suppress tumourigenesis *in vivo* (Serrano *et al.*, 1997; Lin *et al.*, 1998; Zhu *et al.*, 1998; Dimri *et al.*, 2000). Oxidative stress or suboptimal cell culture can initiate stress-induced premature senescence (SIPS), engaging the p38 pathway and inducing either or both the p16/pRB and p53/p21 pathways, although the nature of this mechanism is poorly understood (Takahashi *et al*. 2006; reviewed in Muñoz-Espín & Serrano 2014). In addition, recent evidence has suggested that dysfunctional mitochondria can induce senescence (Wiley *et al.*, 2016). Little is known about the mechanisms which mediate this effect but studies implicate increased ROS, sustained activation of 5' AMP-activated protein kinase (AMPK), or interplay between the DDR and mTOR signalling (Moiseeva *et al.*, 2009; Correia-Melo *et al.*, 2016; Wiley *et al.*, 2016).

1.3.3 Senescence in other cell types

In addition to fibroblasts and epithelial cells, other cell types have been detected to undergo senescence, including endothelial cells (Erusalimsky, 2009), vascular smooth muscle cells (VSMC) (Matthews *et al.*, 2006), T lymphocytes (Brzezińska, Magalska and Sikora, 2003), glial cells (Chinta *et al.*, 2013), melanocytes (Michaloglou *et al.*, 2005), foam cells (fat-laden macrophages, VSMC-like, and endothelial-like cells present in atherosclerosis) (Childs *et al.*, 2016) and islet cells (Krishnamurthy *et al.*, 2006) (reviewed in Sikora 2013). Furthermore, recent studies reported that post-mitotic cells such as neurons (Geng *et al.*, 2010; Panossian *et al.*, 2011; Jurk *et al.*, 2012), and adipocytes (Tchkonia *et al.*, 2010) can also acquire features of senescence.

T cell senescence has been particularly well-characterised *in vitro*. Following multiple rounds of stimulation by antigen-presenting cells (APCs) and subsequent proliferation, senescence is triggered in T cells by critically short telomeres via p53/p21, p16/pRB and p38 signalling pathways (Liu *et al*. 2009; Lanna *et al*. 2015). Similar to fibroblasts, senescent CD8 T cells have shortened telomeres, increased expression of p16 and p21, and a pro-inflammatory secretory phenotype, including interleukin 6 (IL-6) and tumour necrosis factor alpha (TNF-α) (reviewed in Chou & Effros 2013). However, unlike fibroblasts, a crucial phenotype in T cell senescence is the permanent loss of the CD28 co-stimulatory molecule, an essential signalling receptor that activates T cells via the NF-κB pathway. As CD28 surface expression is necessary to mount effective T cell immune responses, down-regulation of CD28 fundamentally alters normal T cell function, survival and proliferation. For example, proliferating CD8 T cells possess the ability to up-regulate telomerase but CD28 down-regulation stimulates the loss of telomerase activity (Parish, Wu and Effros, 2010). In addition, consistent with observations in fibroblasts (see Section 1.2), senescent CD8 T cells are resistant to apoptosis (Spaulding, Guo and Effros, 1999). In support of *in vitro* evidence for T cell senescence, studies *in vivo* have shown that older persons have higher proportions of CD28-CD8+ T cells with shortened telomeres compared to younger adults (Fagnoni *et al*. 1996; reviewed in Chou & Effros 2013).

The majority of research exploring T cell senescence focuses on CD8 effector T cells. However, CD4 T cells, which normally function to co-ordinate signalling between T cells,

B cells, and APCs, have also been identified to undergo senescence characterised according to the same criteria as CD8 T cell senescence (reviewed in Chou & Effros 2013). However, upon senescence, CD4 T cells develop cytotoxic abilities normally reserved for CD8 cells and have been shown to kill endothelial cells *in vitro* (Nakajima *et al.*, 2002). Senescent CD4 T cells may play an important role in development of age-related autoimmune disorders as an increase in numbers of CD28-CD4+ T cells has been found in elderly patients with rheumatoid arthritis (Koetz *et al.*, 2000).

1.4 Markers of senescence

1.4.1 Commonly used markers of senescence

As described in Section 1.2 and Section 1.3, senescence can be induced by different triggers in multiple different cell types with subsequently varying senescent features, resulting in many markers of senescent phenotypes but no universal marker of the senescent state. Thus, multiple markers representing different characteristics of senescence should be used to clearly indicate the presence of senescence. A panel of markers should represent at least three of the following senescence-associated phenotypes: lack of proliferation; changes in nuclear and cellular morphology; expression of tumour suppressor genes; increased DNA damage; altered epigenetic landscape; expression of secretory factors; and senescence-associated β-galactosidase (SA-β-Gal) activity, as summarised in Appendix Table A.1.

Replicatively senescent fibroblasts adopt a complex phenotype characterised by an enlarged, flattened, and often vacuolated cellular morphology *in vitro* (reviewed in Sikora *et al*. 2011). Senescent fibroblasts possess enlarged nuclei which are irregularly shaped due to down-regulation of lamin B1, a structural protein of the nuclear envelope (Freund *et al.*, 2012). In addition, senescent fibroblasts up-regulate the p16/pRB and p53/p21 pathways; β-galactosidase activity detectable at pH 6.0 (SA-β-Gal) resulting from increased lysosomal biogenesis (Dimri *et al.*, 1995; Lee *et al.*, 2006); DDR foci characterised by γ-H2AX (di Fagagna *et al.*, 2003); and levels of oxidative DNA damage, measured using 8-oxoguanine (8-oxoG); Chen *et al*. 1995). Furthermore, activation of the p16/pRB pathway in replicative senescence can lead to the formation of distinct DAPI-dense foci known as senescence-associated heterochromatin foci (SAHF). In

fibroblasts, SAHF formation is variable between cell strains and is not considered a universal feature of replicative senescence (Kosar *et al.*, 2011). SAHFs play a role in sequestering and silencing E2F target genes essential for cell proliferation, and are associated with the presence of chromatin modifications (for example, methylation of histone 3 (H3) on lysine 9 (Lys9)), macroH2A, a histone variant known to contribute to gene silencing, and heterochromatin protein-1 (HP1), a common marker of heterochromatin (Narita *et al.*, 2003). In addition, promyelocytic leukaemia (PML) is known to promote the localisation of pRB/E2F complexes to PML nuclear bodies, a macromolecular structure associated with the nuclear matrix, which sequesters E2F and further inhibits its transcriptional activity (Vernier *et al.*, 2011).

It is well-established that total genomic DNA methylation decreases during ageing and replicative senescence (reviewed in Sedivy *et al*. 2008). Furthermore, recent work in replicatively senescent fibroblasts (Cruickshanks *et al.*, 2013; Hänzelmann *et al.*, 2015), as well as senescent mesenchymal stromal cells (Bork *et al.*, 2010), epithelial cells (Lowe *et al*. 2015) , and endothelial cells (Lowe, Horvath and Raj, 2016) has shown that senescent human cells possess a distinct DNA methylation signature from the proliferating culture, establishing this DNA modification as a novel marker of senescence. It has yet to be elucidated whether alterations in the global methylation state translates into specific gene expression changes, presenting an interesting topic for future research.

1.4.2 Senescence-associated secretory phenotype (SASP)

Senescent cells remain metabolically active and undergo widespread gene expression changes including increased expression of genes encoding secreted factors comprising the SASP. The SASP secretome is diverse and includes a range of 40-80 factors, such as inflammatory cytokines (IL-6, IL-8), growth factors, matrix metalloproteinases (MMPs) known to remodel the extracellular matrix, ROS which reinforce senescence in an autocrine fashion, and TGF-β family members which induce senescence in neighbouring cells (paracrine senescence) (Coppé *et al.*, 2008; Passos *et al.*, 2010; Nelson *et al.*, 2012; Acosta *et al.*, 2013). The SASP is a complex phenotype and develops slowly. From the point of triggering senescence, it can take seven to 10 days for the full pro-inflammatory SASP phenotype to appear in human fibroblasts (Coppé *et al.*, 2008; Rodier *et al.*, 2009;

Passos *et al.*, 2010), although an early peak in platelet-derived growth factor AA (PDGF-AA), a SASP factor which promotes myofibroblast differentiation, can be seen as early as two days post-senescence induction in wound-associated senescent cells (Demaria *et al.*, 2014). Interestingly, neither the p16/pRB or p53/p21 pathway is required for induction of the SASP (Coppé *et al*. 2008; reviewed in Coppé *et al*. 2010). Consequently, the pathways which regulate the SASP are distinct from those involved in initiating or enforcing cell cycle arrest. It is currently not clear how senescence stimuli trigger the downstream gene expression changes necessary for the SASP. However, recent work has suggested that redistribution of high mobility group box 1 (HMGB1), a protein capable of modulating gene expression when localised in the nucleus and, in a secreted form, stimulating cytokine secretion, is a possible mechanism linking the p53/p21 pathway and SASP induction. Prior to the development of the SASP, HMGB1 is relocalised from the nucleus to the extracellular milieu in a p53-dependent manner which is essential for senescence induction. Once secreted, HMGB1 can then stimulate cytokine secretion via toll like receptor 4 (TLR-4) and NF-κB signalling (Davalos *et al.*, 2013). Furthermore, HMGB2 has been found to potentially preferentially localise to SASP gene loci during senescence, thus excluding SASP loci from the surrounding repressive heterochromatin environment (Aird *et al*. 2016). Up-regulation of SASP factors is dependent on the increased activity of transcription factors NF-κB and C/EBPβ (Figure 1.7) (Coppé *et al*. 2008; reviewed in Freund *et al*. 2010). NF-κB, a downstream target of the DDR, is also thought to be gradually up-regulated by persistent low-level DDR signalling during senescence (Rodier *et al.*, 2009). Recent work suggests that the DDR induces the SASP by inhibiting autophagy of GATA binding protein 4 (GATA4), a transcription factor and upstream regulator of NF-κB via TRAF3 interacting protein 1 (TRAF3IP1) and IL-1α (Kang *et al.*, 2015). In addition, there is evidence to suggest that p38 MAPK activation plays a role in SASP activation, as inhibition reduced IL-8 expression in OIS neonatal foreskin IMR-90 fibroblasts (Acosta *et al.*, 2008), a range of SASP factors in SIPS neonatal foreskin HCA2 fibroblasts (Freund, Patil and Campisi, 2011), and IL-6 expression in replicatively senescent human dermal fibroblasts (Alimbetov *et al.*, 2016). IL-1α, a component of the SASP, has also been shown to participate in a positive feedback loop via NF-κB activation to stimulate IL-6 and IL-8 secretion (Orjalo *et al.*, 2009). Furthermore, two microRNAs, miR-146a and miR-146b, have been identified to negatively regulate the SASP via interleukin 1 receptor associated kinase 1 (IRAK1), a

positive regulator of NF-κB (Bhaumik *et al.*, 2009). However, inhibition of IL-1 signalling prevents up-regulation of miR-146a and miR-146b, indicating the important role of NF-κB in both positive and negative regulation of the SASP (Bhaumik *et al.*, 2009). In a recent screen, an extra layer of regulation was discovered as mTOR was identified to regulate SASP induction via down-regulation of mitogen-activated protein kinase-activated protein kinase 2 (MAPKAPK2) and IL-1α translation (Herranz *et al.*, 2015; Laberge *et al.*, 2015). MAPKAPK2 functions to phosphorylate and inhibit ZFP36 ring finger protein like 1 (ZFP36LI), a messenger RNA (mRNA)-binding protein which targets SASP components for decay (Herranz *et al.*, 2015). Further work has revealed that mitochondrial dysfunction-associated senescence (MiDAS) leads to a decreased nicotinamide adenine dinucleotide (NAD^+)/reduced NAD (NADH) ratio, activation of protein kinase AMP-activated catalytic subunit alpha 1 (AMPK) and the tumour suppressor p53, which modifies the SASP by preventing secretion of IL-1-dependent pro-inflammatory factors (Wiley *et al.*, 2016). Importantly, a recent study identified NOTCH1 as a key regulator of SASP composition, allowing senescent cells to switch between a pro-inflammatory secretome and a TGF-β-rich secretome driving paracrine senescence (Hoare *et al.*, 2016) (Figure 1.7).

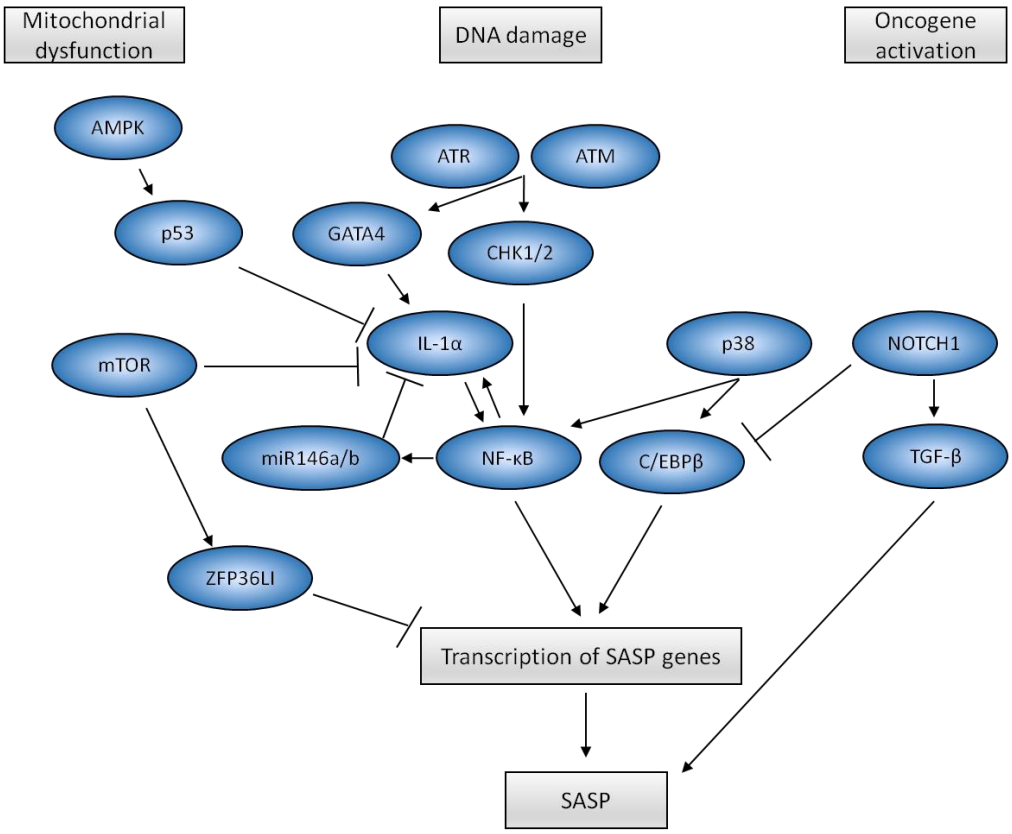

Figure 1.7 Pathways to SASP induction. As neither the p16/pRB nor p53/p21 pathway is required for SASP induction, the pathways which regulate the SASP are distinct from those enforcing cell cycle arrest. Regulation of the SASP involves co-ordination between transcription factors NF-κB and C/EBPβ, which are regulated by signalling pathways, including p38, NOTCH1, mTOR, and mitochondrial dysfunction, as well as feedback loops, including IL-1α, and miR-146a and -146b.

1.5 Senescence *in vivo*

1.5.1 Senescence, tissue dysfunction, and ageing

The world's population is rapidly ageing. In the UK, around one in six people is currently over 65, and this is predicted to rise to one in four within the next 30 years. Ageing is a major risk factor for developing most late-onset diseases (i.e. cardiovascular disease, neurodegenerative disease, and cancer). Furthermore, our ageing society presents considerable socio-economic challenges for individuals, families, and governments facing increased expenditure on health, social care, and pensions (reviewed in Tchkonia *et al*. 2013).

Several studies present convincing evidence of a correlation between ageing and senescence; for example, expression of p16 increases with age in human tissues (Krishnamurthy *et al.*, 2006). Senescent cells are present in sites of age-related diseases such as osteoarthritis, atherosclerosis, and Alzheimer's disease (Naylor, Baker and van Deursen, 2013). Furthermore, genome-wide associated studies (GWAS) repeatedly link the INK4/ARF locus with susceptibility to prevalent age-related disorders, such as coronary heart disease and type 2 diabetes (reviewed in Jeck *et al*. 2012).

In 2011, the first *in vivo* evidence for a causal link between p16-positive senescent cells and the development of age-related pathologies was presented (Baker *et al.*, 2011). In this study, a progeroid mouse model was used in combination with a transgene, INK-ATTAC, to selectively induce apoptosis in p16-positive senescent cells upon administration of a synthetic drug (AP20817). Late-life clearance of p16-positive senescent cells attenuated the progression of already-established age-related disorders in skeletal muscle, fat, and eyes. However, clearance of p16-positive senescent cells did not attenuate deterioration in the cardiovascular system and brain, as these dysfunctions developed independently of elevated p16 expression. Consequently, elimination of p16-positive senescent cells did not prolong lifespan in the BubR1 progeroid mice because of accelerated cardiovascular disease. Importantly, the authors recently demonstrated that use of the INK-ATTAC transgene in two genetic strains of wild-type (WT) mice significantly extended both the median health- and lifespan in male and female mice (Baker *et al.*, 2016), presenting exciting implications for the treatment of age-related diseases and improving healthspan in humans.

An important question that has yet to be addressed is how senescence in humans drives age-related dysfunction. The gradual accumulation of senescent cells in tissues with age is described as 'chronic senescence', and is thought to contribute to age-related disorders through a few key mechanisms (reviewed in van Deursen 2014). First, senescence can deplete the pools of cycling cells in an organism (including stem cells) subsequently disrupting tissue homeostasis and regeneration. For example, p16 expression increases with age in the stem and progenitor cells of the mouse brain (Molofsky *et al.*, 2006), bone marrow (Janzen *et al.*, 2006), and pancreas (Krishnamurthy *et al.*, 2006), where it suppresses stem cell proliferation and regeneration. Notably, the

age-related decline in stem/progenitor cell function and tissue regenerative capacity is substantially reduced in p16 knockout mice (Janzen *et al.*, 2006; Molofsky *et al.*, 2006). In addition, senescence is known to act as a barrier for efficient reprogramming of primary cells into pluripotent stem cells (Banito *et al.*, 2009). Secondly, senescent cells are thought to impair the function of the surrounding tissue through secretion of biologically active molecules in the SASP. For example, the fibroblast SASP contains components, such as extracellular matrix (ECM) remodelling proteins (e.g. MMP-3 and -10), which can disrupt tissue structure and organisation (Parrinello *et al.*, 2005). In addition, the SASP contains pro-inflammatory proteins, including IL-6 and IL-8, which may act as a source of chronic inflammation in tissues where senescent cells have accumulated (Coppé *et al.*, 2008). Low-level chronic tissue inflammation is a hallmark of ageing and plays an important role in the development and progression of several age-related diseases (reviewed in Freund *et al*. 2010). Together with MMPs, these inflammatory factors are thought to create a cancer permissive microenvironment. In line with this theory, the fibroblast SASP has been observed to promote the proliferation of premalignant or malignant epithelial cells in culture (Krtolica *et al.*, 2001) and *in vivo* (Liu and Hornsby, 2007). In addition, the fibroblast SASP may also intensify age-related dysfunction by spreading senescence to healthy neighbouring cells through secretion of TGF-β family members, chemokines and other factors (paracrine senescence) (Nelson *et al.*, 2012; Acosta *et al.*, 2013).

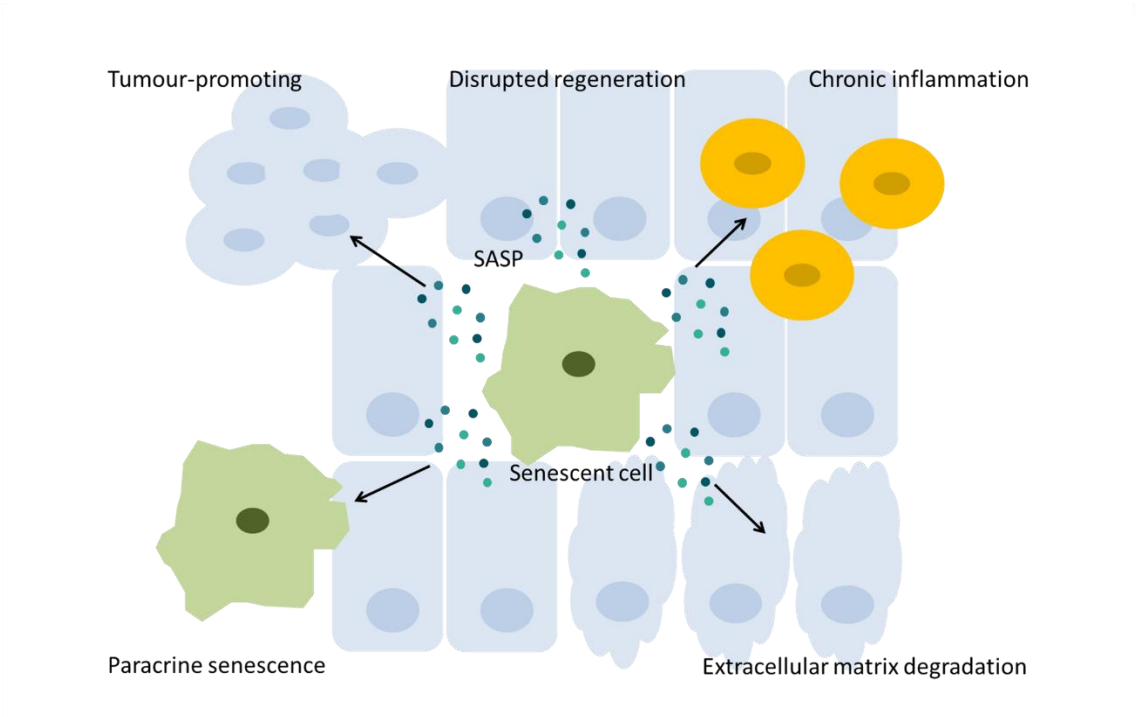

Figure 1.8 Mechanisms of senescence-induced tissue degeneration. There are a number of potential mechanisms by which senescence could drive age-related pathologies. The first mechanism proposes that senescent cells deplete pools of cycling cells in organisms, disrupting tissue homeostasis and rejuvenation (Janzen *et al.*, 2006; Krishnamurthy *et al.*, 2006; Molofsky *et al.*, 2006). Another mechanism suggests that senescent cells damage the tissue environment through chronic inflammation, extracellular matrix degradation, and tumour-inducing components of the SASP (Krtolica *et al*. 2001; Coppé *et al*. 2008; reviewed in Freund *et al*. 2010). Recently, the ability of senescent fibroblasts to spread senescence through their neighbouring environment (paracrine) was discovered (Acosta *et al.*, 2013), which may exacerbate the tissue damage.

Furthermore, why do these chronically senescent cells accumulate in tissues with age? There are currently two proposed mechanisms for senescent cell accumulation (reviewed in van Deursen 2014). The first is that senescent cell production increases with age *in vivo*. In line with this, several studies have demonstrated that stresses which induce senescence increase with age (reviewed in Garinis *et al*. 2008). Second, the ability of the body to efficiently clear senescent cells may decline with age. In support of this idea, senescent cells are known to attract immune cells through secretion of chemokines and activating cytokines present within the SASP (see Section 1.4.2) (Acosta *et al.*, 2013). In addition, recent evidence has convincingly shown that senescent cells can be eliminated by immune cells including T cells (Kang *et al.*, 2011), macrophages (Xue *et al.*,

2007; Lujambio *et al.*, 2013; Yun, Davaapil and Brockes, 2015), neutrophils (Xue *et al.*, 2007), and natural killer cells (Xue *et al.*, 2007; Krizhanovsky *et al.*, 2008; Iannello *et al.*, 2013; Sagiv *et al.*, 2016). Immune clearance of senescent cells may be affected by an age-dependent decline in immunological effectiveness, referred to as 'immunosenescence' (reviewed in Goronzy & Weyand 2013). Immunosenescence describes a complex and multi-faceted pattern of changes within the immune system with age. One of the most important changes is the loss of naïve T cells with age and subsequent loss of diversity in the T cell receptor (TCR) repertoire, thus impairing the ability of the immune system to respond to antigens (Yager *et al.*, 2008). Other major changes include an increase in the number of senescent T cells (see Section 1.3.3). Further stimulating chronic inflammation, senescent T cells have a lower production of anti-viral cytokines, increased secretion of pro-inflammatory cytokines and also secretion of a cytokine which may promote accelerated senescence in other non-senescent T cells (Lewis *et al*. 2004; reviewed in Chou & Effros 2013). Interestingly, senescent T cells have also been identified at sites of age-related disorders (Pietschmann *et al*. 2001; reviewed in Chou & Effros 2013). In addition, the efficiency and diversity of B cell antibody production is also reduced in immunosenescence (reviewed in Goronzy & Weyand 2013).

The recent awareness that senescence can drive ageing and age-related disorders (Baker *et al.*, 2011, 2016) has inspired efforts to further identify and understand the processes driving senescence in order to develop potential therapeutics. Thus, strategies that postpone senescence induction and delay senescent cell accumulation could exert a beneficial effect on healthspan by delaying or preventing multiple age-related diseases (reviewed in Tchkonia *et al*. 2013).

1.5.2 Other roles of senescence *in vivo*

Studies *in vitro* and *in vivo* present convincing evidence that senescence is a crucial tumour suppressor mechanism. For example, senescence induction depends on the tumour suppressor pathways (p16/pRB and p53/p21) (see Section 1.1.2 and Section 1.1.3) and most, if not all, cancers harbour mutations in one or both of these pathways (reviewed in Rodier & Campisi 2011). Furthermore, senescence may be activated in

response to oncogenic events *in vitro* and *in vivo* (see Section 1.3.2) (Serrano *et al.*, 1997).

Given that senescent cells are known to promote tumourigenesis, it seems paradoxical that senescence should also be an established anti-cancer mechanism. However, the evolutionary theory of antagonistic pleiotropy stipulates that a biological process selected as beneficial in young organisms can become deleterious in later life when selection is weak (Williams, 1957).

Beyond tumour suppression, recent discoveries have expanded our understanding of the beneficial roles of senescence *in vivo.* In contrast to 'chronic senescence' (i.e. accumulation of deleterious senescent cells with ageing), cells can undergo 'acute senescence' as part of tightly spatially and temporally controlled biological processes, which limits their ability to accumulate with age.

Senescence has been observed to occur during development in mouse, chicken, quail, and human embryos, suggesting conservation of the process across vertebrates (Nacher *et al.*, 2006; Muñoz-Espín *et al.*, 2013; Storer *et al.*, 2013). Senescence was detected in multiple embryonic structures including the mesonephros (transitory embryonic kidney), endolymphatic sac (a filtering tube regulating pressure in the inner ear), and the apical ectodermal ridge (AER) (a transient structure marking a limb bud) (Muñoz-Espín *et al.*, 2013; Storer *et al.*, 2013). Further analysis of the senescent cells in these structures revealed that p21 up-regulation and senescence induction is controlled by the TGF-β-SMAD and PI3K-FOXO developmental pathways. Interestingly, these pathways are already known to induce oncogene-induced and paracrine senescence (Figure 1.3) (see Section 1.1.3). As discussed in Section 1.5.1, there is now compelling evidence that senescent cells are removed via immune-mediated clearance (Xue *et al.*, 2007; Iannello *et al.*, 2013; Sagiv *et al.*, 2016). In line with this, senescent cells were found to be surrounded by macrophages in the mesonephros and AER during regression of these embryonic structures. Furthermore, there was a loss of macrophage recruitment to the mesonephros and AER in p21-null embryos resulting in delayed elimination of the structures, indicating a causal relationship between induction of senescence, macrophage recruitment and clearance of senescent cells (Muñoz-Espín *et al.*, 2013; Storer *et al.*, 2013). It is hypothesised that acute senescence during embryonic

development plays a compensatory role to apoptosis in morphogenesis (reviewed in Muñoz-Espín & Serrano 2014). To further support this idea, Yun *et al*. 2015 demonstrated that senescence occurs *in vivo* at sites of limb regeneration in salamanders using SA-β-Gal staining. Senescent cells are found transiently during the intermediate stages of regeneration and, in line with the findings described above, are subsequently cleared from the limb via macrophage-dependent immune clearance (Yun, Davaapil and Brockes, 2015).

In addition to embryonic development, acute senescence can also occur in adult organisms during tissue remodelling in response to damage. The matricellular protein, cysteine rich angiogenic inducer 61 (CCN1) expressed at cutaneous wound sites induces fibroblast senescence, leading to an accumulation of senescent fibroblasts promoting myofibroblast differentiation, anti-fibrosis, and wound healing through the SASP (Jun & Lau 2010; Demaria *et al*. 2014; reviewed in Muñoz-Espín & Serrano 2014). Recent work has also demonstrated that connective tissue growth factor (CCN2), a matricellular protein up-regulated during the inflammatory phase of wound healing, induces senescence in human foetal foreskin fibroblasts (BJ) *in vitro* and murine fibroblasts *in vivo* (Jun and Lau, 2016). In line with this literature, wound healing was shown to be delayed during drug treatment and senescent cell clearance in the INK-ATTAC WT mice, which was recovered following suspension of drug treatment (Baker *et al.*, 2016). Similarly, the accumulation of senescent activated stellate cells restricts liver fibrosis by secretion of MMPs present within the SASP (Krizhanovsky *et al.*, 2008). However, aged drug-treated INK-ATTAC WT mice did not show evidence of increased fibrosis in skin or other tissues (Baker *et al.*, 2016).

Importantly, given the role for acute senescence in embryonic and adult tissue remodelling, this thesis is focused on exploring the drivers of replicative senescence in normal adult human fibroblasts to further understanding of chronic senescence, ageing, and age-related diseases.

1.6 Senescence as a therapeutic target

As senescent cells are one of the causes of age-associated diseases and ageing, preventing or delaying the accumulation of senescent cells could be beneficial to health- and lifespan (see Section 1.5.1). Genetic elimination of senescent cells in a mouse model

of accelerated ageing delayed ageing and age-related diseases, indicating that targeting senescent cells is a promising strategy to improve healthspan (Baker *et al.*, 2011, 2016). However, p16/pRB or p53/p21 pathway inactivation is not a feasible therapeutic approach in humans as it would eliminate crucial tumour-suppressive mechanisms, thus increasing susceptibility to cancer.

A number of different anti-senescence strategies are currently being developed to address the deleterious effects of senescent cell accumulation with ageing. One option would be to target the pathways driving senescence (see Section 1.7). As mentioned previously, it is important not to interfere with tumour suppressor pathways that are likely to promote cancer. However, strategies that reduce the processes driving cells into chronic senescence, thus delaying age-related senescent cell accumulation could be beneficial. For example, short term dietary restriction in middle-aged mice, a treatment with known beneficial effects on health and lifespan, is associated with decreased abundance of senescent cells in the liver and intestine (Wang *et al.*, 2010). The authors speculate that dietary restriction delays accumulation of senescent cells via mTOR inhibition, improved mitochondrial function and decreased ROS. Interestingly, rapamycin (Demidenko *et al.*, 2009), a mTORC1 inhibitor, and AZD8055 (Walters, Deneka-Hannemann and Cox, 2016), a pan-mTOR inhibitor, have been identified to delay onset of replicative senescence *in vitro* (see Section 1.7). In addition, one recent study demonstrated that fast food diet (FFD) consumption in mice had a deleterious effect on health which was associated with an increase in senescent cells (Schafer *et al.*, 2016). Furthermore, exercise initiated in mice post-long-term FFD reduced senescent phenotype markers and attenuated physical deterioration, indicating that exercise could also play a role in delaying senescent cell accumulation *in vivo*. Thus, strategies designed to delay the onset of senescence and prevent senescent cell accumulation *in vivo* could potentially exert a beneficial effect on healthspan in humans. In order to achieve this, further understanding of the mechanisms driving senescence is required.

Another option would be to target pathways which can interfere with the adverse effects of the SASP. As discussed in Section 1.5.1, the SASP of accumulated senescent cells may act as a source of chronic inflammation and play an important role in the development and progression of several age-related diseases. Two recent studies have

identified key regulators of SASP composition in senescent cells, in particular NOTCH1 (Hoare *et al.*, 2016), and NAD+/NADH ratios (Wiley *et al.*, 2016) (see Section 1.4.2). Targeting these *in vivo* could manipulate senescent cells to either down-regulate the pro-inflammatory arm of the SASP to diminish chronic inflammation, or up-regulate the pro-inflammatory arm to facilitate elimination of senescent cells via immune clearance.

In addition, there is a growing body of literature identifying 'senolytics', compounds which selectively kill senescent cells. As discussed previously in Section 1.1.3, senescent cells are known to up-regulate pro-survival pathways that contribute to their resistance to apoptosis. An initial study employed gene expression analysis of non-senescent and senescent preadipocytes to identify up-regulated negative regulators of apoptosis and subsequent siRNA screening to discover potential senolytic targets (Zhu *et al.*, 2015). The senolytic targets included components of ephrin survival-regulating dependence receptor mechanisms, ephrin ligand (EFN) B1 and EFNB3, as well as the p21 plasminogen-activated inhibitor 2 (PAI-2), the PI3K delta catalytic subunit (PI3KCD), and BCL-XL, which regulates mitochondrial-dependent apoptosis. Screening of drugs known to target these genes identified dacatinib (a kinase inhibitor known to interfere with ephrin ligand B (EFNB)-dependent apoptosis suppression) and quercetin (a natural flavonol inhibiting PI3K and other kinases) (Zhu *et al.*, 2015; Roos *et al.*, 2016), and navitoclax (an inhibitor of pro-survival gene Bcl-2) as promising senolytics *in vitro* and *in vivo* (Zhu *et al.*, 2016). However, all three drugs were identified to eliminate senescent cells in a cell type-dependent manner and all are known to have side effects, including haematologic dysfunction such as transient thrombocytopenia and neutropenia (deficiency of platelets and neutrophils in the blood, respectively), fluid retention, skin rash, and QT prolongation. Therefore, further work needs to be performed to explore whether these drugs can be used to delay age-related diseases in humans.

In line with previous studies, recent compound screening in non-senescent and senescent foetal WI-38 fibroblasts has identified a potent senolytic drug, ABT263, which potentially targets BCL-XL and pro-apoptotic BAK (Chang *et al.*, 2016). Treatment of mice irradiated to stimulate senescence demonstrated that ABT263 is a potent and broad spectrum senolytic drug *in vivo*, eliminating both senescent bone marrow haematopoietic stem cells and senescent muscle stem cells. In addition, ABT-737 (a

small molecule inhibitor of BCL-2, BCL-XL, and BCL-W) has been identified to eliminate senescent foetal lung IMR-90 fibroblasts *in vitro* and senescent cells in lung and skin *in vivo*, leading to improved ageing-related phenotypes (Yosef *et al.*, 2016). Although ABT263 appears an exciting candidate for future therapeutics, it has some common toxic side effects in patients; namely, transient thrombocytopenia and neutropenia, leading to increased susceptibility to injury, bruising, and infection. Thus, similar to dacatanib and quercetin, further work needs to determine whether ABT263 treatment can be used to delay age-related diseases in humans, as well as explore potential adverse side-effects of ABT-737. Furthermore, there are a number of theoretical side effects caused by eliminating senescent cells which need to be tested in normally aged animal models, including impaired wound healing or fibrosis during liver regeneration (see Section 1.5.2) (Krizhanovsky *et al.*, 2008; Demaria *et al.*, 2014). In addition, clearance of senescent cells would not restore depleted pools of cycling cells or repair damage to non-senescent cells in tissues where senescent cells have accumulated. Thus, true rejuvenation would require a combination of senescent cell clearance and extensive replacement of depleted and damaged non-senescent cells. In order to restore depleted tissues, targeted reversal of senescent progenitor cells could potentially be employed. However, senescence has long been considered an irreversible process.

1.7 Reversal of senescence

Senescence is classically defined as an irreversible proliferative arrest. Over the past 20 years, only a few studies have challenged this dogma. An initial study retrovirally transduced mutant p53 into 'near-senescent' human neonatal foreskin fibroblasts (HCA2) and found that this stimulated bypass of senescence-induced growth arrest (Bond *et al.*, 1995). Later work then demonstrated that p53 antibody micro-injection in senescent HCA2 fibroblasts reinitiated DNA synthesis but with limited proliferation (Gire and Wynford-Thomas, 1998). However, as the study did not determine whether residual cycling cells were present in the population, no conclusion could be made as to whether senescent or slowly cycling cells were re-entering the cell cycle. In addition, ablation of p53 function in pre-senescent human fibroblasts delayed but did not prevent replicative senescence, indicating that p53 inactivation alone was not sufficient to mediate stable reversion of senescence in primary human fibroblasts (Gire and Wynford-Thomas, 1998). Further work identified that the senescent phenotype in MEFs can be rescued

using p53 or pRB inactivation (Dirac and Bernards, 2003; Sage *et al.*, 2003). It should be noted here that MEF replicative senescence is distinct from senescence in human cells (reviewed in Kuilman *et al*. 2010). MEFs express telomerase, possess long, stable telomeres, and undergo senescence after a limited number of passages in culture, despite retaining long telomeres. Furthermore, MEF senescence is dependent on p53 and $p19^{ARF}$, not p16 expression. Subsequently, a study investigating the consequences of p53 or pRB inactivation in replicatively senescent human foetal fibroblasts concluded that in some human cells, p16 provides a dominant, irreversible second barrier to proliferation which cannot be completely overcome (Beauséjour *et al.*, 2003).

Recent work has explored mTOR inhibition as a route to senescence reversal. AZD8055 delayed onset of replicative senescence in 'near-senescent' human neonatal fibroblasts (Walters, Deneka-Hannemann and Cox, 2016), and senescence induced by progerin, the truncated form of lamin A found in patients with Hutchinson-Gilford progeria (Cao *et al.*, 2011). However, a study investigating rapamycin treatment of human and rodent cell lines induced to senesce via exogenous p16 or p21 expression found that rapamycin prevents permanent loss of proliferative potential in arrested cells, but does not stimulate arrested cells to proliferate (Demidenko *et al.*, 2009). Importantly, epithelial cellular senescence has been shown to be reversible using p16 siRNA knockdown in normal adult DS HMECs (Lowe *et al.*, 2015); however, unlike fibroblast replicative senescence, epithelial cellular senescence occurs solely dependent on p16 expression (discussed further in Section 1.3.1). Thus, fibroblast replicative senescence is currently still viewed as an irreversible cell cycle arrest in the literature. Given that cells undergo acute senescence in development via a different mechanism (Muñoz-Espín *et al.*, 2013; Storer *et al.*, 2013) (see Section 1.5.2), it is important to note that none of the previous work on senescence reversal was performed in normal adult human fibroblasts. In this project, reversal of senescence is defined as the return of DS cells to a state similar to that of proliferating cells and distinct from cells which have overcome or bypassed senescence.

The ability to reverse replicative senescence in normal adult human fibroblasts would contribute to further understanding of the processes driving chronic senescence, potentially benefitting all of the anti-senescence strategies outlined in Section 1.6.

Therapeutically, it is important to recognise that senescence is known to occur as a tumour suppressor mechanism *in vivo*. As currently it is not possible to distinguish senescent cells *in vivo* by their senescence trigger, a method to identify and specifically target non-tumourigenic senescent cells would need to be developed prior to therapeutic use of senescence reversal.

1.8 Early growth response 2 (EGR2)

In this project, early growth response 2 (EGR2) was identified as the top hit for reversal of replicative senescence in HMFs. As such, a brief introduction to the gene is included below.

1.8.1 EGR2 gene locus, isoforms, and family

The early growth response 2 (EGR2) gene maps to human chromosome 10 at bands q21-22, with multiple transcript variants encoding isoform A and the slightly shorter isoform B (Figure 1.9) (O'Leary *et al.*, 2016). The protein encoded by this gene is a transcription factor with three tandem Cys_2His_2-type zinc fingers (Beckmann and Wilce, 1997). It is part of the immediate early gene EGR family encoding Cys_2His_2 zinc-finger transcription factors, comprising EGR1 (5q31), EGR2 (10q21), EGR3 (8p21), and EGR4 (2p13) (Figure 1.9) (Beckmann and Wilce 1997; reviewed in Poirier *et al*. 2008). The four EGR family members share three highly homologous DNA binding zinc finger domains that can bind to the same GC-rich consensus DNA binding motif. The zinc fingers each contain a nuclear localisation signal (Matheny, Day and Milbrandt, 1994), which might be involved in nuclear localisation of the EGR proteins (Beckmann and Wilce, 1997), as EGR2 is known to exist in both the cytoplasm and nucleus (Herdegen *et al.*, 1993). A few other conserved domains have also been identified including the R1 domain which is the site of interaction for NGFI-A binding (NAB) 1 and 2 proteins that can repress or activate transcriptional activity of EGR proteins (Russo, Sevetson and Milbrandt, 1995; Svaren *et al.*, 1996). In addition, the transactivity of EGR family members can be regulated by other co-modulators such as host cell factor C1 (Luciano and Wilson, 2003), and Ddx20 (Gillian and Svaren, 2004). Members of the EGR family have been implicated in a diverse array of processes including cell proliferation, differentiation, and apoptosis (Beckmann and Wilce, 1997).

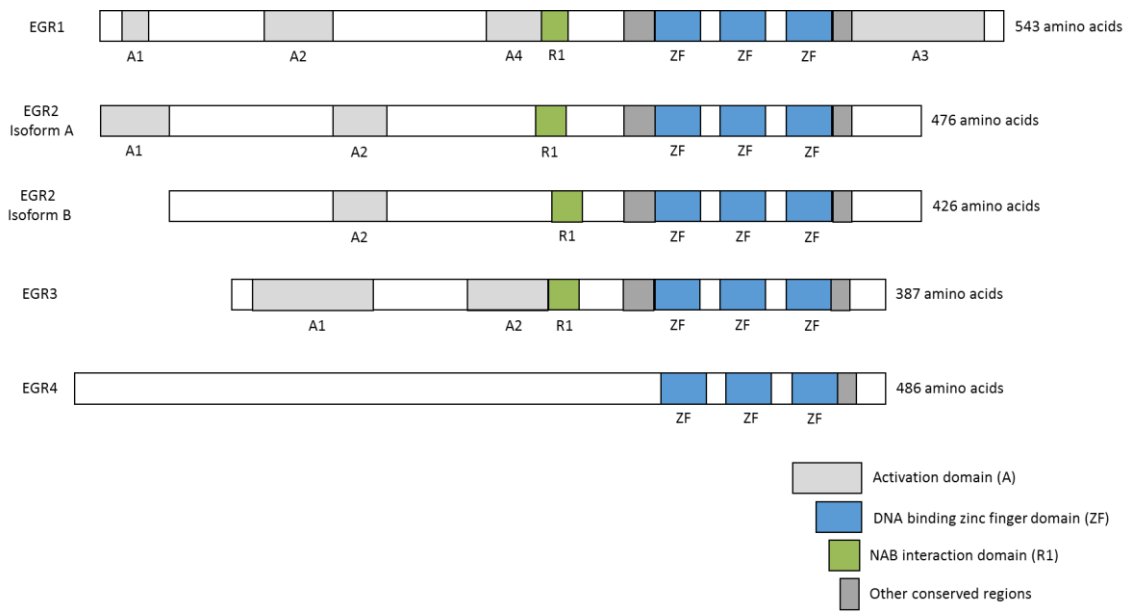

Figure 1.9 Schematic representation of the four members of the human EGR family, including the two EGR2 isoforms. There are several conserved regions between the EGR family members: the DNA binding zinc finger domains (blue); regions flanking the zinc finger domains (dark grey); NAB interaction domain (green); and transcriptional activation domains (light grey). Outside of these regions, the sequences of the EGR family members have less homology suggesting that they are differentially regulated by different pathways and may serve different functions. Adapted from (Poirier *et al.*, 2008).

Although these transcription factors show a high degree of homology within the DNA binding domains, it is clear that each individual member is regulated by distinct signalling pathways in a cell-type dependent manner, and this is highlighted by studies demonstrating that EGR1 homozygote knockout mice present a normal phenotype whereas EGR2 homozygote knockout results in post-natal lethality (Schneider-Maunoury *et al.*, 1993; Lee *et al.*, 1996).

1.8.2 EGR2 and development

Early work noted that homozygous EGR2 mouse knockouts were lethal in the early postnatal period (Schneider-Maunoury *et al.*, 1993). Initial analysis of EGR2 knockout embryos demonstrated a tightly controlled role for EGR2 in a number of sites, including hindbrain segmentation and development (Schneider-Maunoury *et al.*, 1993; Swiatek and Gridley, 1993), endochondral ossification (bone formation) (Levi *et al.*, 1996), and myelination of peripheral nerves (Zorick *et al.*, 1996). Fibroblast growth factor (FGF) signalling activates EGR2 expression specifically in rhombomere 3 and 5 in the hindbrain which is essential for the establishment of these developmental compartments. Within

these rhombomeres, cells undergo neuronal differentiation, nerve organisation, and neural crest differentiation into a range of cells including Schwann cells which play an important role in peripheral nerve myelination (Sham *et al.*, 1993; Labalette *et al.*, 2011). Despite early studies identifying the role of EGR2 in endochondral ossification, little is known about the role of EGR2 in bone formation. However, there is some evidence to suggest that EGR2 is responsible for regulating proliferation and terminal differentiation in chondrocytes and osteoclasts via PI3K-AKT and MEK-ERK signalling during embryogenesis and post-natal development (Levi *et al.*, 1996; Gabet *et al.*, 2010; Chen *et al.*, 2015).

1.8.3 EGR2 and the peripheral nervous system

As mutations in EGR2 were identified to result in inherited peripheral neuropathies, including Charcot-Marie-Tooth type 1 (Šafka Brožková *et al.*, 2012), Dejerine-Sottas syndrome (Gargaun *et al.*, 2016), congenital hypomyelinating neuropathy (Warner *et al.*, 1998), progressive scoliosis (Mikešová *et al.*, 2005), and Guillain-Barré Syndrome (Doncel-Perez *et al.*, 2015), the main focus of the literature to date has been on the role of EGR2 in the peripheral nervous system (PNS). Schwann cells, the principal glial cells of the vertebrate PNS, are essential for support and myelination of PNS axons. The development of Schwann cells into a final pro-myelinating form requires precise control of proliferation and cell cycle exit, with impaired control resulting in the inherited peripheral neuropathies as described above (Atanasoski *et al.*, 2006). Accumulating evidence suggests that EGR2 is a master regulator of proliferation and final differentiation in Schwann cells thus controlling onset of myelination in the PNS (Topilko *et al.*, 1994; Zorick *et al.*, 1996; Decker, 2006). Further studies elucidating the mechanism of EGR2-regulated Schwann cell myelination have identified p38 as an up-stream activator of EGR2 expression leading to strongly reduced proliferation, increased levels of the cell cycle inhibitor p27, inhibition of apoptosis via the JNK/c-Jun pathway, and altered expression of myelin-associated genes (Parkinson *et al.*, 2004; LeBlanc *et al.*, 2006; Hossain *et al.*, 2012). As both p21 and p16 are required for control of Schwann cell proliferation and differentiation (Atanasoski *et al.*, 2006), it seems likely that EGR2, a master regulator of the process, modulates the expression of these proteins. Using microarray expression analysis, EGR2 has been discovered to coordinate a diverse range of genes, including p21, in myelinating Schwann cells (Nagarajan *et al.*, 2001; Le *et al.*,

2005). Furthermore, in order to identify genes directly activated by EGR2 binding, *in vivo* chromatin immunoprecipitation sequencing (ChIP-Seq) has been performed on myelinating rat sciatic nerve, revealing peaks of EGR2 binding in the cell cycle regulators p21 and p27 (Srinivasan *et al.*, 2012).

1.8.4 EGR2 and the immune system

During T cell development, a population with a diverse range of TCRs is generated in the thymus through signals derived from the interaction of TCRs on thymocytes with their ligands, major histocompatibility complex (MHC) molecules bound with peptides. Thymocytes bearing a TCR able to interact with a self-MHC can receive signals that induce either differentiation into a mature T cell (positive selection) or apoptosis (negative selection). In mice with a conditional homozygote knockout of EGR2 in T cells, positively selected thymocytes fail to sustain expression of Bcl-2, a pro-survival gene, in the absence of EGR2 and are thus blocked from developing into mature T cells (Lauritsen *et al.*, 2008). Using EGR2-overexpressing mice, the effect of EGR2 on T cell development was confirmed, and EGR2 was also observed to promote maturation in B cell development (Li *et al.*, 2011). In addition, EGR2 was found to be expressed during the later stages of dendritic cell development in mouse bone marrow cells (Miah *et al.*, 2013).

In addition to thymocyte development, EGR2 expression can also regulate naïve T cell differentiation. Naïve CD4+ T cells can commit to a diverse range of helper cell subsets characterised by distinct cytokine profiles which are important for activation of B cells and cytotoxic T cells. Recent work has shown that overexpression of EGR2 in murine CD4+ T cells induced differentiation into regulatory T cells, whereas EGR2 deficiency rendered naïve murine CD4+ T cells prone to differentiation into T helper 17 cells (Okamura *et al.*, 2009; Miao *et al.*, 2013).

TCR engagement in the absence of proper co-stimulation, such as CD28/B7 signalling, leads to a hyporesponsive growth arrest state known as T cell anergy (reviewed in Schwartz 2003). Multiple studies have demonstrated that EGR2 expression is up-regulated in T cells in response to TCR stimulation without co-stimulatory signals (Harris *et al.*, 2004; Safford *et al.*, 2005; Anderson *et al.*, 2006). In normal mice under clean

conditions, conditional homozygote knockout of EGR2 in T cells led to the accumulation of effector T cells in response to self-antigens without proper co-stimulation. The EGR2 knockout T cells were hyperproliferative with decreased p21 expression, indicating that EGR2 functions to control anergy induction and proliferation of T cells *in vivo* (Zhu *et al.*, 2008; Zheng *et al.*, 2012). Furthermore, ChIP performed in EGR2 overexpressing T cells demonstrated that EGR2 directly binds to the p21 promoter (Zhu *et al.*, 2008). To further investigate the EGR2-regulated transcriptome, microarray and ChIP-Seq analyses were performed revealing 49 directly EGR2-regulated genes in murine T cell anergy, including BCL2L11, a protein known to interact with pro-survival protein BCL-2 (Zheng *et al.*, 2013). Interestingly, after one year, conditional EGR2 knockout mice exhibited features of lupus-like autoimmune disease compared with age-matched WT mice (Zhu *et al.*, 2008). Together, these data suggest that EGR2 may play an important role in T cell proliferation and development of autoimmune disease.

In support of this idea, dysregulation of EGR2 has been found in autoimmune conditions (reviewed in Zhang *et al*. 2015). The chromosome where EGR2 is located, 10q21, has been identified as a candidate locus for autoimmune diseases, such as Crohn's disease, in two GWAS (Rioux *et al.*, 2007; The Wellcome Trust Case Control Consortium, 2007). Furthermore, a single nucleotide polymorphism (SNP) in the 5' flanking region of EGR2 was associated with susceptibility to systemic lupus erythematosus, a systemic autoimmune disease, in a Japanese population (Myouzen *et al.*, 2010). Systemic sclerosis (SSc) or scleroderma is an autoimmune disease of the connective tissue disease of unknown aetiology associated with progressive fibrosis in the skin and internal organs. Examination of skin and lung biopsy specimens from SSc patients and a SSc mouse model indicated that expression of EGR2 is elevated in SSc (Fang *et al.*, 2011). Furthermore, TGF-β stimulated expression of EGR2 in explanted foreskin fibroblasts via SMAD3 signalling. Microarray analysis of EGR2-overexpressing human neonatal foreskin fibroblasts compared to the transduced control identified a greater than two-fold change in nearly 700 transcripts, indicating that EGR2 has a broad effect on human fibroblast gene expression. Interestingly, EGR1-overexpressing fibroblasts modulated 751 transcripts of which only nine overlapped with the EGR2-overexpressing profile, suggesting that EGR1 and EGR2 have divergent roles in human fibroblasts (Fang *et al.*, 2011).

1.8.5 EGR2, cancer, and senescence

As senescence is an important tumour suppressor mechanism (see Section 1.5.2), most cancer cells harbour mutations inactivating the senescence pathways in order to bypass senescence and induce proliferation. For example, the tumour suppressor p16 is typically down-regulated in cancer (Romagosa *et al.*, 2011). Studies *in vitro* and *ex vivo* present convincing evidence that EGR2 may function as a tumour suppressor. Microarray analysis has identified EGR2 as down-regulated in primary ovarian cancer, as well as up-regulated by exogeneous PTEN overexpression in endometrial cancer cells, indicating a potential role for EGR2 as a tumour suppressor downstream of PTEN (Ono *et al.*, 2000; Unoki and Nakamura, 2001). Further quantitative real time polymerase chain reaction (qRTPCR) analysis of endogenous EGR2 expression in 39 cancer cell lines, including colon, endometrial, gastric, lung, ovarian, and prostate cancer as well as glioblastoma and hepatoma, identified that expression of EGR2 was lower than the average normal adult tissue expression for 34 of the cancer cell lines (Unoki and Nakamura, 2003). In addition, there is a growing body of evidence to suggest that miRNA-mediated EGR2 suppression promotes *in vitro* proliferation of various human cancer cells including miR-20 in osteosarcoma (Zhuo *et al.*, 2015), miR-330-3p in non-small-cell lung cancer (Liu *et al.*, 2015), and miR-20 and -150 in gastric cancer (Wu *et al.*, 2010; Li *et al.*, 2013) (Figure 1.10). Interestingly, given that EGR2 is known to play a role in endochondral ossification, a recent GWAS has also identified SNPs within EGR2 which are strongly associated with susceptibility to Ewing sarcoma, an aggressive paediatric sarcoma (Postel-Vinay *et al.*, 2012). However, in contrast with the down-regulation of EGR2 observed in 34 other cancers (Unoki and Nakamura, 2003), EGR2 expression appeared to be up-regulated in Ewing sarcoma tissue, and EGR2 knockdown in Ewing sarcoma cell lines reduced proliferation and cell viability (Grunewald *et al.*, 2015). However, it should be noted that the tumour suppressor p16 has also been observed to be overexpressed in a rare subset of p16-positive human cancers (Romagosa *et al.*, 2011). Examination of the EGR2 gene and promoter sequence identified the presence of a 5'-C-phosphate-G-3' (CpG) island in intron 1 which tended to be hypermethylated in cancer cell lines where endogenous EGR2 expression was aberrantly high, leading the authors to postulate that methylation of intron 1 may function as an enhancer of EGR2 transcription during cancer (Unoki and Nakamura, 2003).

One study has identified EGR2 as a direct transcriptional target of the p53 family, as endogenous EGR2 mRNA and protein were up-regulated by ectopic p53 overexpression and in response to DNA damage in a p53-dependent manner in human oral, colorectal, osteosarcoma, and lung cancer cells (Yokota *et al.*, 2010) (Figure 1.10). Furthermore, a conserved p53-response element was identified in the EGR2 gene which was found to be transactivated by p53 in a luciferase reporter assay (Yokota *et al.*, 2010). In line with previous studies indicating that miRNA-mediated suppression of EGR2 induced proliferation (Wu *et al.*, 2010; Li *et al.*, 2013; Liu *et al.*, 2015; Zhuo *et al.*, 2015), overexpression of EGR2 in the human oral and cervical cancer cell lines was found to inhibit proliferation (Yokota *et al.*, 2010). In further support of a role for EGR2 in the p53 pathway, a number of studies have identified a role for EGR2 directly up-regulating expression of p21, a known target of p53 (Le *et al.*, 2005; Zhu *et al.*, 2008; Pospisil *et al.*, 2011; Srinivasan *et al.*, 2012) (Figure 1.10).

Interestingly, the EGR family member, EGR1, has been identified to be required for replicative senescence in MEFs (Krones-Herzig, Adamson and Mercola, 2003). EGR1-null MEFs bypass senescence and have decreased expression of p53, p21, and other known p53 target genes. Re-expression of EGR1 restores senescence in EGR1-null MEFs but not p53-null MEFs, indicating that EGR1 induces replicative senescence via the p53/p21 pathway (Krones-Herzig, Adamson and Mercola, 2003) (Figure 1.10). In line with this theory, EGR1 has been identified to transactivate the p53 promoter in MEFs (Das *et al.*, 2001). However, there are a number of significant differences between MEF and human fibroblast replicative senescence (see Section 1.7) including that senescence induction occurs independent of telomere length and p16 expression (reviewed in Kuilman *et al*. 2010). Given that the EGR family members share a transcription factor binding sequence but are known to possess distinct roles in a cell-type-dependent manner, it is plausible that the EGR family member important in human replicative senescence could be EGR2. In support of this, a recent whole-blood gene expression meta-analysis looking at over 7,000 human samples showed that EGR2 increases with age but EGR1 does not (Peters *et al.*, 2015).

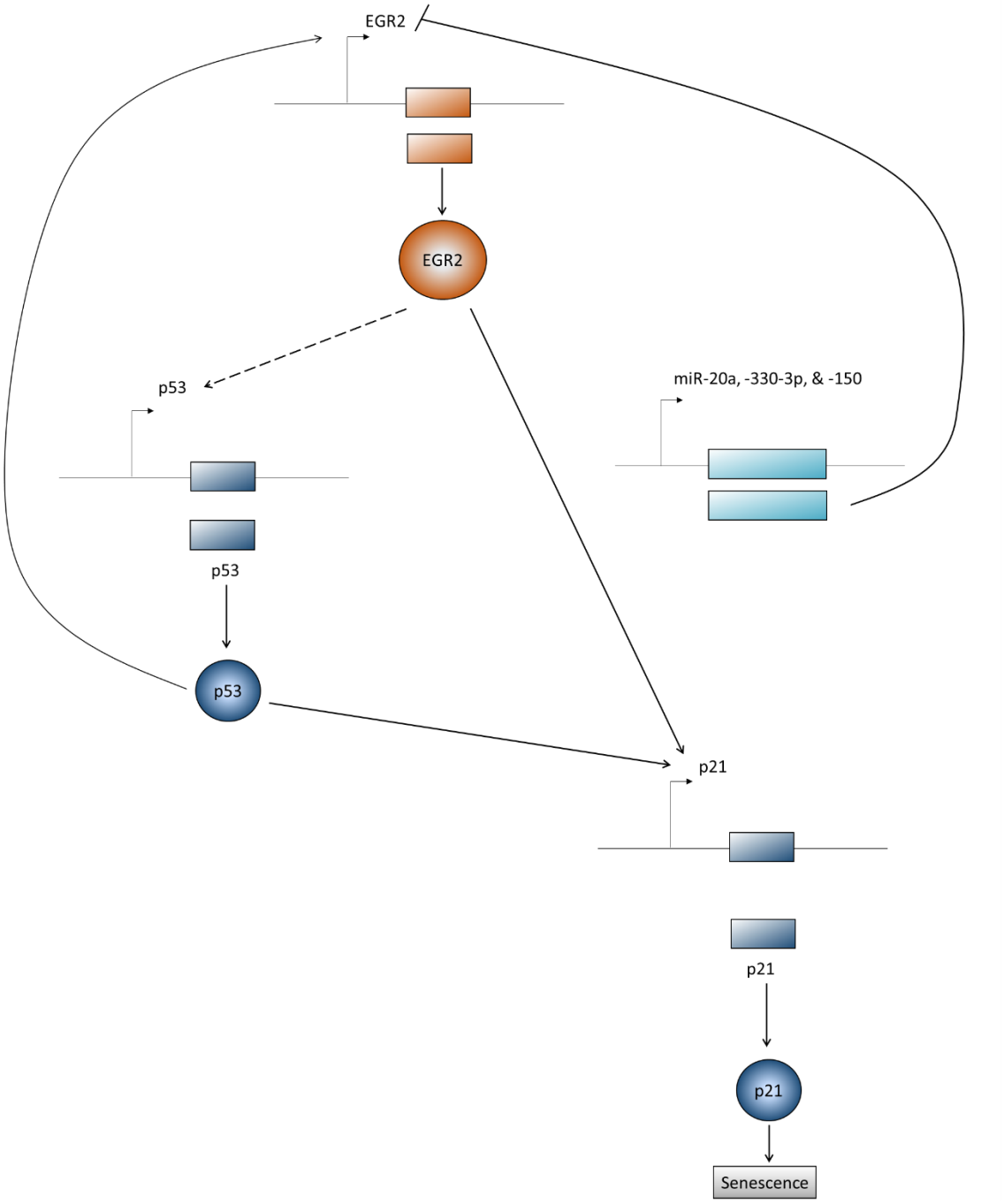

Figure 1.10 Schematic summarising potential relationship between EGR2, p53 and p21 in the literature. As EGR1, a close family member, up-regulates p53 expression in MEF senescence (Krones-Herzig, Adamson and Mercola, 2003), EGR2 (orange) potentially up-regulates p53 (blue) in human cell senescence as well as directly up-regulating expression of p21 (blue) (Le *et al.*, 2005; Zhu *et al.*, 2008; Pospisil *et al.*, 2011; Srinivasan *et al.*, 2012). Furthermore, EGR2 has been identified as a direct transcriptional target of p53, and multiple miRNAs (light green) have been found to suppress EGR2 expression in various human cancers (Wu *et al.*, 2010; Li *et al.*, 2013; Liu *et al.*, 2015; Zhuo *et al.*, 2015).

1.9 Small interfering RNA (siRNA) technology

Fire and Mello were awarded the Nobel Prize for their discovery that injection of double stranded RNA (dsRNA) triggers RNAi in *Caernohabditis elegans* (Fire *et al.*, 1998). RNAi is an endogenous pathway found in eukaryotic cells which silences specific mRNAs using targeted RNA sequences, either by suppressing transcription or by activating sequence-specific RNA degradation. The RNAi mechanism can be induced endogenously by dsRNA cleaved by the enzyme Dicer into fragments of 21-23 nucleotides known as small interfering RNAs (siRNAs), or by synthetic siRNAs artificially transfected into the cell using lipid reagents. The RNA-induced silencing complex (RISC) then incorporates the siRNA, and Argonaute 2, a protein within RISC, unwinds the siRNA and cleaves the sense (passenger) strand. The antisense (guide) strand remains bound to the now activated RISC complex which probes for and degrades mRNA complementary to the antisense strand (Whitehead, Langer and Anderson, 2009).

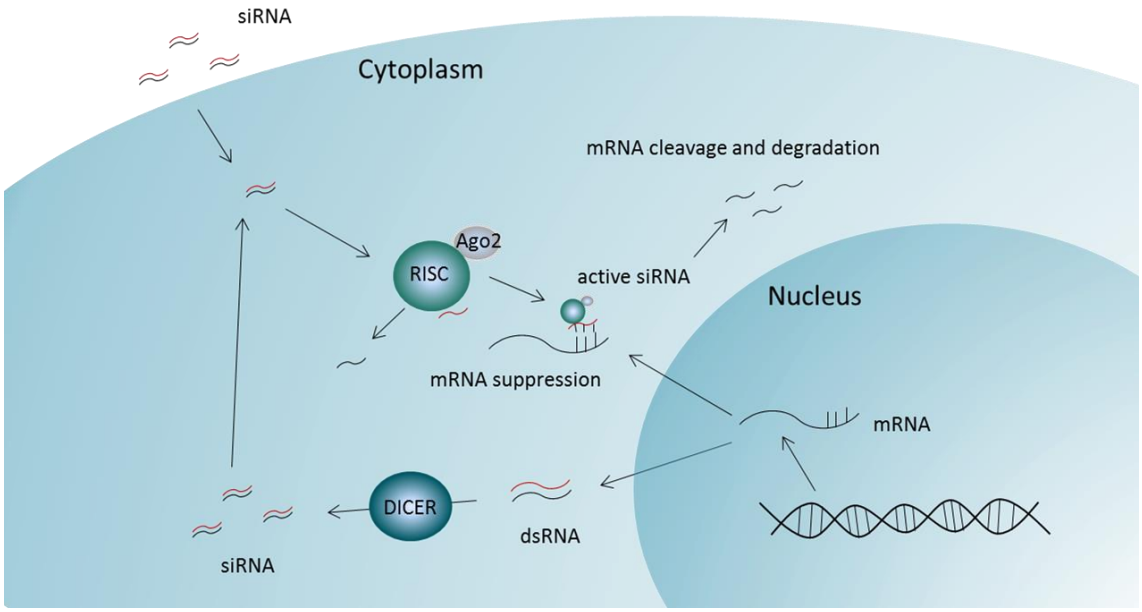

Figure 1.11 Schematic of the RNAi pathway. Endogenous dsRNA is cleaved by DICER into short sequences of RNA known as siRNA. Endogenous siRNA or synthetic siRNA transfected into the cell are incorporated into the RISC complex where Argonaute 2 (Ago2) cleaves the sense strand (passenger, black) from the antisense strand (guide, red). The activated siRNA-RISC complex then targets the complementary mRNA sequence for translational suppression or to induce cleavage and degradation.

The availability of genome-wide siRNA libraries has made it possible to carry out high-throughput, high-content large-scale RNAi screening experiments, leading to siRNA screening becoming a powerful tool for dissecting gene function in human cells *in vitro* (reviewed in Boutros & Ahringer 2008).

High-throughput, high-content siRNA screening allows the use of large sample sizes which generate statistically significant data with relative experimental ease. In addition, automated microscopy images provide morphological and immunofluorescence data that can be mined using independent, un-biased, multi-parameter analysis. Furthermore, the technology is cheaper than alternative techniques for studying gene knockdown (i.e. creation of transgenic models) and possesses the potential possibility of translation into human siRNA therapies.

However, siRNA screens have a number of limitations, namely the potential for false negatives, false positives and off-target effects (OTEs). False negatives can arise from incomplete knockdown of gene expression caused by inefficient siRNAs, insufficient siRNA dose, or too short an incubation period. Thus, false negatives can be minimised by pooling three to four independent non-overlapping siRNAs thus increasing knockdown efficiency, and by optimising the screen (i.e. seeding density, transfection reagent dose, siRNA concentration, and experimental protocol) to ensure maximum transfection efficiency and optimal detection of altered phenotypes (reviewed in Falschlehner *et al*. 2010).

False positives can occur as an indirect phenotypic response due to cell stress from the transfection protocol. In order to control for this, a negative siRNA control, such as siGLO, a siRNA targeting Cyclophilin B, a non-essential housekeeping gene, labelled with Dylight 547 (DY547) should be used. In addition, a poorly defined phenotypic read-out can allow one phenotype to appear similar to another, which if studied in more detail would emerge to be two different results (e.g. quiescence and senescence). Multi-parameter assessment can increase the selectivity of the phenotype and reduce false positives (reviewed in Echeverri *et al*. 2006).

OTEs can be caused by non-specific siRNA knockdown of an unknown gene (not the candidate gene) resulting in non-specific gene expression changes and phenotypes. To control for this, siRNA pools should be deconvoluted and each siRNA tested individually.

If at least two siRNAs from a given pool induce similar phenotypic changes characterised by multi-parameter analysis, it is unlikely that the phenotype is a result of OTEs. Additional replicates of the screen will also help to control for OTEs and reduce false positives. Lastly, effective siRNA knockdown at the message or protein level should be carefully validated for each hit using qRTPCR, immunofluorescence, or western blotting (reviewed in Echeverri *et al*. 2006).

1.10 Project aims

The overall aim of this project is to determine whether reversal of senescence in normal adult human mammary fibroblasts (HMFs) is achievable using siRNA transfection in order to subsequently employ siRNA screening as a tool to discover novel drivers of senescence.

Previously, our laboratory (lab.) has shown that cellular senescence in DS HMECs is reversible using siRNA transfection (Lowe *et al.*, 2015). Gene expression arrays subsequently identified genes with increased expression in DS HMECs compared to EP and reversed HMECs, and a siRNA screen of the top 200 hits in DS HMECs was performed. This revealed 28 siRNAs that strongly induced the reversal phenotype, as defined by a loss of a panel of senescence markers, including a significant increase in cell number, together with reduced cellular and nuclear area.

To determine whether senescence reversal is achievable in other cell types, this project will first aim to determine if siRNA reversal of deep senescence can be performed in fibroblasts. Secondly, the most potent rejuvenators in HMECs will be screened in the DS fibroblasts, in addition to potential candidates identified as known interactors in literature and database searches. Successful development of a novel technique to reverse senescence in fibroblasts will provide the opportunity to investigate the genes enforcing senescence (‘drivers’) in both HMECs and fibroblasts. Once validated, the top hit will be investigated to provide further insight into the mechanisms driving senescence, as well as potentially identifying a novel marker of senescence and future therapeutic target for delaying or reversing the onset of senescence.

Chapter 2 Materials and Methods

2.1 Mammalian cell culture

All reagents and chemicals used were purchased from Sigma (UK) unless otherwise stated. Cells were cultured as monolayers in T75 centimetre squared (cm^2) vented flasks (Corning, UK) at 37°C in the presence of 5% carbon dioxide (CO_2) and 95% humidity. Cells were passaged every seven days by aspirating the culture medium, washing the cells with 15 millilitres (mL) phosphate-buffered saline (PBS), and detaching them with 3 mL 1X trypsin-ethylenediaminetetraacetic acid (EDTA) (Life Technologies, UK) for 5-15 minutes at 37°C. Trypsin-EDTA was neutralised by adding 15 mL medium with supplements and cells were then centrifuged for five minutes at 1,200 revolutions per minute (rpm) (600 x *g)* (IEC CL10 centrifuge, Thermo Scientific, UK). Medium was aspirated and the cells were gently re-suspended in an appropriate volume of medium with supplements and cells were counted using a haemocytometer before re-seeding. Medium was changed every two to three days.

2.1.1 Culture of normal human mammary fibroblasts

Normal finite lifespan HMFs were kindly donated by Martha Stampfer (Lawrence Berkeley National Laboratory, Berkeley). These were obtained from reduction mammoplasty tissue of a 16-year-old individual, donor 48 (Stampfer *et al.*, 1981). The cells were seeded at 10,000 cells/cm^2 and maintained in Dulbecco's Modified Eagles Medium (DMEM) (Life Technologies, UK) supplemented with 10% foetal bovine serum (FBS) (Labtech.com, UK), L-glutamine (2 millimolar (mM) final concentration) (Life Technologies, UK) and insulin from bovine pancreas (10 microgram (µg)/mL final concentration). HMFs were serially passaged from passage (P) four (P4) until the population reached replicative senescence at P29 or 35 cumulative population doublings. The natural log of the cell numbers was plotted as a function of time and the number of population doublings determined from the slope of the line. Senescent HMFs were defined as being in deep senescence (DS) when no population expansion was observed after being kept in culture for three weeks beyond replicative senescence (P29+3).

Stocks of senescent HMFs were frozen down at P29 and thawed three weeks prior to each experiment involving DS cells.

2.1.2 Culture of wild-type and p21 double knockout human fibroblasts

Loxo26 wild-type (WT Loxo26) and Loxo26 p21 double knockout (Loxo26 $p21^{-/-}$) human fibroblasts were a kind gift from Prof. Ken Parkinson (Munro *et al.*, 2004). Loxo26 fibroblasts were cultured in T75 cm^2 vented flasks (Corning, UK) at 37°C in a 10% CO_2 atmosphere. The cells were maintained in DMEM (Life Technologies, UK) supplemented with 10% FBS (Labtech.com, UK), L-glutamine (2 mM final concentration) (Life Technologies, UK), and penicillin-streptomycin (50 units (U)/mL and 50 µg/mL final concentration, respectively) (Life Technologies, UK). The fibroblasts were passaged as outlined previously in Section 2.1.

2.1.3 Culture of normal human mammary epithelial cells

Normal HMECs were isolated from reduction mammoplasty tissue and kindly provided by Dr Martha Stampfer (Lawrence Berkeley National Laboratory, Berkeley, CA, USA) and kindly cultured by Dr Cleo Bishop. The cells were seeded at 5,000 cells/cm^2 and maintained in 'M87A' medium composed of 50% (v/v) Mammary Epithelial Basal Medium (MEBM, Lonza, UK) supplemented with MEGM SingleQuot Kit Supplements (excluding gentamycin) (Lonza, UK), 5 µg/mL transferrin, 5 µM isoproterenol, and 2 mM L-glutamine, together with 50% (v/v) DMEM nutrient mixture F-12 (DMEM/F-12) (Life Technologies, UK) supplemented with 10 µg/mL insulin, 5% (v/v) FBS (Labtech.com, UK), 100 nanograms (ng)/mL hydrocortisone, 10 nanomolar (nM) 3,3',5-triiodo-L-thyronine, 10 nM β-estradiol, 5 ng/mL epidermal growth factor (Life Technologies, UK), 0.1% (v/v) AlbuMAXTM (Life Technologies, UK), and 0.1 nM oxytocin (Bachem, Switzerland). HMECs were serially passaged as outlined previously from P4 until the population reached senescence at P11. Senescent HMECs were defined as being DS when no population expansion was observed after being kept in culture for three weeks beyond replicative senescence (P11+3).

2.2 Ultraviolet irradiation-induced senescence

In order to generate a p21 positive cell lysate to use alongside the Loxo26 $p21^{-/-}$ cell lysate in p21 antibody validation western blots, WT Loxo26 fibroblasts were irradiated by exposure to ultraviolet light (UV).

WT Loxo26 cells were seeded in 6-well plate format and sub-confluent cells were exposed to 10 millijoule (mJ)/cm^2 UV irradiation (Chen *et al.*, 2008). Cell lysates were collected 18-24 hours after UV irradiation according to Section 2.4.1.

2.3 Paracrine senescence

Conditioned medium was collected from proliferating (P15 and P16) HMFs and DS HMFs seeded in T25 flasks at 10,000 cells/cm^2 at two incubation time points: 48 hours, and 72 hours. The four conditioned medium samples were centrifuged in 50 mL falcon tubes at 5,000 x *g* for 10 minutes at room temperature (RT) to remove dead cells and subsequently filtered through a 0.2 μm^2 filter to remove cell debris. In order to supplement the nutrient-depleted conditioned medium, a solution of DMEM 40% FBS plus supplements (8 mM L-glutamine, 40 μg/mL insulin final concentrations) was prepared. To assess the effects of the conditioned medium, EP HMFs were seeded onto 96-well plates (Thermo Scientific, UK) at a density of 10,000 cells/cm^2 (3,200 cells/well) in two independent experiments, each performed in at least triplicate. The following day, a ratio of 3:1 conditioned medium to DMEM 40% was added to each well in order to generate 10% FBS conditioned medium. To achieve this, 90 μL of conditioned medium and 30 μL DMEM 40% FBS were added to each well. Control EP HMFs received 120 μL control medium as described in Section 2.1.1 (DMEM 10% FBS). Conditioned medium and control medium were replaced after 72 hours. Cells were fixed, stained, imaged and analysed after a further 48 hours according to Section 2.7 and Section 2.8.

2.4 Sodium dodecyl sulphate-polyacrylamide gel electrophoresis (SDS-PAGE) and Western Blotting

2.4.1 Protein lysate preparation

Cells were washed with PBS and lysed by the addition of radio-immunoprecipitation assay (RIPA) buffer with 2X protease cocktail inhibitor (Roche, UK) at RT for five minutes. 10X PhosSTOP, phosphatase inhibitor, was added to the RIPA and 2X protease cocktail inhibitor solution for lysates collected to assess dephosphorylation events on band resolution using western blotting. Protein lysate concentration was determined using the Bio-Rad Protein Assay kit (Bio-Rad, UK) according to manufacturer's instructions. This assay is based on the Bradford dye-binding method and relies on the shift in

absorbance of Coomassie brilliant blue G-250 dye when binding to protein (absorption maximum equals 595 nm). Once the protein concentration of the lysate was determined from its absorbance compared to a standard curve, an appropriate volume of 2X Laemmli Sample Buffer (0.1 molar (M) Tris pH 6.8, 20% (v/v) glycerol, 1% (v/v) β-mercaptoethanol, 1% (w/v) sodium dodecyl sulphate (SDS), 0.01% (v/v) Bromophenol blue) was added and the samples were heated to 95°C for five minutes. Samples were then centrifuged using a bench top centrifuge (Accuspin micro, Fisher Scientific, UK) at 13,000 rpm for five minutes. The protein samples were either used for SDS-PAGE and Western Blotting immediately or stored at -20°C until required. MDA-MB-468 cell lysate (p16-positive breast cancer cell line) was a kind gift from Dr Maddi Moore (Bishop Group).

2.4.2 SDS-PAGE

SDS-PAGE is a technique which separates proteins according to their electrophoretic mobility. SDS denatures and binds to the polypeptides imparting a negative charge. When the uniformly negatively charged polypeptides are loaded onto a polyacrylamide gel with an electric field, the proteins will migrate towards the positive electrode (anode) and separate by size due to the sieving nature of the gel matrix.

Gels were constructed and run using the Bio-Rad Mini-PROTEAN III system (Bio-Rad, UK). A sample volume of 20 microlitre (µL) was loaded in the wells of 5% stacking – 12% resolving gels (see Table 2.1) in a tank of running buffer (25 mM Tris (Fisher Scientific, UK), 192 mM Glycine, 0.1% SDS), and separated at 100 V for one to two hours. Proteins of known molecular weights (Precision Plus Protein All Blue Standards, Bio-Rad, UK) were loaded and used as reference.

2.4.3 Immunoblot analysis

Proteins were transferred onto a nitrocellulose membrane (Amersham Hybond ECL, GE, UK) using the Western transfer Mini-PROTEAN III system (Bio-Rad, UK) in transfer buffer (25 mM Tris, 192 mM Glycine, 20% (v/v) methanol (Fisher Chemical, UK)) for two hours at 350 milliamps (mA). The membrane was then washed in high-purity water and the protein temporarily visualised using Ponceau S stain (0.2% (w/v) Ponceau S in 1% acetic acid), which was removed by washing in PBS.

Non-specific binding sites on the membrane were then covered by blocking for one hour in 0.05% (v/v) Tween-20, 5% (w/v) Marvel skimmed milk in PBS (PBS-T-milk) at RT. The primary antibody was diluted in PBS-T-milk and incubated with the membrane under the appropriate conditions (see Table 2.2). The membrane was then washed in PBS-T-milk for 30 minutes with three changes to remove any unbound primary antibody. The appropriate secondary antibody was then diluted in PBS-T-milk and incubated with the membrane (see Table 2.2). The unbound secondary antibody was then removed by washing the membrane in PBS-T-milk for 30 minutes with three changes before washing for 20 minutes with two changes in 0.05% PBS-T.

Secondary antibodies are conjugated to horseradish peroxidase which converts a chemiluminescent substrate into a luminescent product. Enhanced-Chemiluminescence (ECL) (GE Healthcare, UK) was applied according to the manufacturer's protocol and the membrane exposed to a photographic film (Hyperfilm, GE Healthcare, UK) for visualisation of the protein of interest.

	5% Stacking gel	**12% Resolving gel**
Acrylamide (30%) / Bis Acrylamide (0.8%) solution (National Diagnostics, UK)	1.67 mL	4.15 mL
Tris pH 8.8 (1 M)	-	3.7 mL
Tris pH 6.8 (1 M)	1.25 mL	-
20% (w/v) SDS	50 µL	50 µL
20% (w/v) ammonium persulfate	50 µL	60 µL
Temed (Severn Biotech Ltd, UK)	10 µL	10 µL
Distilled water (dH_2O)	7.03 mL	2.05 mL

Table 2.1 Composition of the two polyacrylamide gels required for gel electrophoresis.

Antibody	Species	Manufacturer	Working dilution	Conditions
Anti-p16 JC8	Mouse	Prof. James Koh, Duke Cancer Institute (UK)	1:1,000	2 hours at RT
Anti-p21 (12D1)	Rabbit	Cell Signalling (UK)	1:1,000	Overnight at 4°C
Anti-p21 (ab7960)	Rabbit	Abcam (UK)	1:200	Overnight at 4°C
Anti-p21 (C-19) (sc397)	Rabbit	Santa Cruz Biotechnology (USA)	1:200	2 hours at RT
Anti-lamin B1 (ab16048)	Rabbit	Abcam (UK)	1:1,000	Overnight at 4°C
Anti-human EGR2 (OTI1B12)	Mouse	Origene (USA)	1:500	48 hours at 4°C
Anti-human EGR2 (H220)	Rabbit	Santa Cruz Biotechnology (USA)	1:1,000	Overnight at 4°C
Anti-mouse EGR2 (erongr2)	Rat	eBioscience (UK)	1:100	Overnight at 4°C
HRP-conjugated anti-mouse	Goat	Dako (UK)	1:2,000	1 hour at RT
HRP-conjugated anti-rabbit	Goat	Dako (UK)	1:5,000	1 hour at RT
HRP-conjugated anti-rat	Mouse	Abcam (UK)	1:10,000	1 hour at RT

Table 2.2 Antibodies used for immunoblotting, their working dilutions and conditions. All antibodies were diluted in PBS-T-milk with the exception of anti-human EGR2 (H220) which was diluted in 0.1% Tween in PBS supplemented with 5% (w/v) bovine serum albumin (BSA).

2.4.4 Densitometry

Protein quantification was performed using ImageJ software. Density levels were obtained and normalised against an appropriate loading control in order to calculate total protein levels. Protein levels were then normalised to the siGLO control and presented as a bar chart + standard deviation (SD) of two independent experiments.

2.4.5 Membrane stripping

Membranes were stripped for 30 minutes at RT in 25 mL stripping buffer (25 mM glycine with 1% (w/v) SDS) and washed twice for 10 minutes with 0.05% PBS-T at RT before being blocked for one hour at RT in PBS-T-milk and re-probed with additional antibodies.

2.5 siRNA forward-transfection optimisation

Before conducting the siRNA screens, a transfection reagent was identified, and the cell seeding density and volume of transfection reagent used to transfect the HMFs was optimised in order to produce a high level of transfection efficiency.

2.5.1 Identification of optimal transfection reagent

The uptake efficiency of two transfection reagents (Dharmafect 2 (Dh2) and 4 (Dh4)) (GE Healthcare, UK) previously identified to transfect DS HMECs (Bishop, unpublished) was tested in the HMFs in order to identify the optimal transfection reagent. HMFs were seeded at a range of densities in 384-well plate format and incubated at 37°C overnight. After incubating the siRNA/Dharmafect complexes at RT for 20 minutes, the cells were forward transfected with a range of Dh2 and Dh4 concentrations combined with 30 nM siGLO (Thermo Scientific, UK). Plates were incubated at 37°C and medium changed after 24 hours. Cells were fixed and stained five days later with 4',6-diamidino-2-phenylindole (DAPI), and then imaged and quantified according to Section 2.7 and Section 2.8. Visualisation of HMF siGLO uptake was used as a measure of transfection efficiency and subsequently the transfection reagent generating the highest siGLO uptake efficiency, Dh2, was chosen for use in further experiments.

2.5.2 Optimisation of cell seeding density in 384-well plate format

HMFs were seeded at 10,000-15,000 cells/cm^2 in 384-well plate format (Thermo Scientific Nunc, UK) and were incubated at 37°C. Cells were fixed and stained five days later with DAPI according to Section 2.7. Cells were then imaged and quantified according to Section 2.8.

2.5.3 Optimisation of transfection reagent dose

In order to identify a transfection reagent dose producing a high level of transfection efficiency with minimal toxicity, the volume of the chosen transfection reagent (Dh2) was optimised for the DS fibroblasts. DS HMFs were seeded at the optimised density of

15,000 cells/cm^2 in 384-well plates and incubated at 37°C overnight. Approximately 16 hours later, 10 µL siRNA/Dh2 complexes were incubated at RT for 20 minutes before cells were forward transfected with a range of Dh2 concentrations (0-0.6 µL/well) combined with 30 nM siGLO (in a total volume of 70 µL/well). Target sequences for the siRNAs are shown in Table 2.3. Plates were incubated at 37°C and medium changed after 24 hours and 48 hours. Cells were fixed and stained after a further 72 hours (i.e. five days post transfection) with DAPI and Cell Mask and then imaged and quantified according to Section 2.7 and Section 2.8.

siRNA name	siRNA target	Accession number	Supplier	siRNA target sequence
siGLO	Cyclophilin B (PPIB)	NM_000942	Dharmacon, UK	GAGCCCAGAUCAACCUUUA
p16	Cyclin-dependent kinase inhibitor 2A (CDKN2A) (p16)	NM_000077	QIAGEN, UK	TACCGTAAATGTCCATTTATA
p21	Cyclin-dependent kinase inhibitor 1A (CDKN1A) (p21)	(Pool of four siRNAs) NM_078467 NM_000389 NM_001220778 NM_001220777 NM_001291549	GE, UK	(Pool of four siRNAs) CTACCTTGAAGCTGAAACA CGCTACCTTGAAGCTGAAA GCTACCTTGAAGCTGAAAC GCTGACACTACGCGATTAC

Table 2.3 siRNA target sequences.

2.6 siRNA forward transfections

2.6.1 siRNA reversal of DS HMFs in 384-well plate format

DS HMFs were seeded at 15,000 cells/cm^2 and forward transfected with previously validated siRNAs targeting siGLO (Bishop *et al.*, 2010), Cyclin-dependent kinase inhibitor 2A (CDKN2A) (p16) (Bishop *et al.*, 2010), Cyclin-dependent kinase inhibitor 1A (CDKN1A) (p21) (Borgdorff *et al.*, 2010) and siRNA targeting p16 combined with siRNA targeting p21 siRNA (p16+p21) in 384-well plate format using 0.15 µL/well Dh2. Target sequences for the siRNAs are shown in Table 2.3. Plates were incubated at 37°C and medium

changed after 24 hours and 48 hours. Cells were fixed and stained after a further 72 hours (i.e. five days post transfection) with DAPI according to Section 2.7. Cells were then imaged and quantified according to Section 2.8.

2.6.2 siRNA screening in DS HMFs in 384-well plate format

Pools of three siRNAs (Ambion, UK) were used to target each specified gene in the screen alongside control siRNAs targeting siGLO, p16, p21, and p16+p21. DS HMFs were seeded at 15,000 cells/cm^2 and forward transfected with either 30 nM siRNA targeting the specified gene alone (Group 1), or 15 nM siRNA targeting the gene of interest in combination with 15 nM p16 siRNA (Group 2) or in combination with 15 nM p21 siRNA (Group 3) in 384-well plate format using 0.15 µL/well Dh2. Plates were incubated at 37°C and medium changed after 24 hours. Cells were fixed and stained five days later with DAPI according to Section 2.7. Cells were then imaged and quantified according to Section 2.8. After identifying the top hits from the initial screens, further screens were performed at both the five and seven day time point.

2.6.3 Validation of EGR2 top hit in DS HMFs

The EGR2 siRNA pool used in the siRNA screens was deconvoluted into three individual siRNAs. DS HMFs were subsequently forward transfected with the three EGR2 siRNAs (Ambion, UK) individually and pooled according to Section 2.6.2. siRNA target sequences for each of the individual EGR2 siRNAs are listed in Table 2.4.

siRNA name (siRNA ID)	siRNA target	Accession Number	siRNA target sequence (5'-3')
EGR2 1 (106082)	EGR2	NM_000399.3 NM_001136177.1 NM_001136178.1 NM_001136179.1	GGUUUUUGACCCUGGAUGU
EGR2 2 (115177)	EGR2	NM_000399.3 NM_001136177.1 NM_001136178.1 NM_001136179.1	CGCAAAACCACUAACUGAA
EGR2 3 (145568)	EGR2	NM_000399.3 NM_001136177.1 NM_001136178.1 NM_001136179.1	CCUUCACUUACAUGGGCAA

Table 2.4 Individual EGR2 siRNAs deconvoluted from the EGR2 siRNA pool used in the siRNA screens. All siRNAs were purchased from Ambion, UK.

2.6.4 siRNA forward transfection of DS HMFs in 6-well plate format

DS HMFs were seeded at 15,000 cells/cm^2 in 6-well plate format (Corning, UK) and forward transfected with 30 nM siRNA using 6.9 µL/well Dh2. siRNA/Dh2 complexes were incubated at RT for 20 minutes before cells were forward transfected. Cells were harvested for western blotting according to Section 2.4.1.

2.7 Immunofluorescence staining

Cells cultured on 384-well plates were washed with PBS and fixed using 3.7% paraformaldehyde (PFA) with 5% sucrose in PBS for 15 minutes at RT. After fixation, cells were washed with PBS and permeabilised with 0.1% Triton X-100 for 15 minutes at RT. Cells were washed with PBS and blocked with PBS supplemented with 0.25% (w/v) BSA (PBS/BSA) for 30 minutes before incubation with primary antibody diluted in PBS/BSA for two hours at RT. Cells were then washed with PBS/BSA for 30 minutes at RT and incubated with secondary antibody, DAPI (1:1,000), and Cell Mask Deep Red (1:10,000) (Life Technologies, UK) diluted in PBS/BSA for 2 hours at RT. Cells were washed with PBS/BSA for 30 minutes at RT before three final washes with PBS. Cells were then imaged and quantified according to Section 2.8. Details of the antibodies used for immunofluorescence staining and their dilutions are shown in Table 2.5.

2.7.1 Bromodeoxyuridine (BrdU) immunofluorescence staining

BrdU is a synthetic analogue for thymidine which is incorporated into DNA during the S phase of the cell cycle and is commonly used for detection of proliferating cells *in vitro*. For BrdU staining, cells were incubated with an optimised dose of 5 µM BrdU for an optimised incubation period of 16 hours. Cells were then washed with medium, PBS, and fixed with 3.7% PFA with 5% sucrose for 15 minutes at RT. After fixation, cells were washed with PBS and permeabilised with 0.1% Triton X-100 for 15 minutes at RT. Cells were washed with PBS and the DNA was denatured with 4 M hydrochloric acid (HCl) for 10 minutes. Cells were then washed with PBS (pH 8.5) for 10 minutes with two changes, and PBS (pH 7.4) for 20 minutes with four changes, before washing briefly with analytical grade dH_2O. After washing, the cells were incubated with the conjugated anti-BrdU mouse monoclonal antibody (clone MoBU-1) Alexa Fluor 488 conjugate (Life Technologies, UK) in 0.5% PBS-T supplemented with 1% BSA. Cells were washed with

PBS for 15 minutes with three changes. Cells were then imaged and quantified according to Section 2.8.

Antibody	Species	Source	Working dilution	Conditions
Anti-p16 JC8	Mouse	Prof. James Koh, Duke Cancer Institute (UK)	1:200	2 hours at RT
Anti-p21 (12D1)	Rabbit	Cell Signalling (UK)	1:1,000	Overnight at 4°C
Anti-8-oxoG	Mouse	Millipore (UK)	1:100	2 hours at RT
Anti-human EGR2 (H220)	Rabbit	Santa Cruz Biotechnology (USA)	1:250	Overnight at 4°C
Alexa Fluor 488 conjugated anti-mouse	Donkey	Life Technologies (UK)	1:500	2 hours at RT
Alexa Fluor 488 conjugated anti-rabbit	Goat	Life Technologies (UK)	1:500	2 hours at RT
Alexa Fluor 546 conjugated anti-rabbit	Goat	Life Technologies (UK)	1:500	2 hours at RT
Alexa Fluor 488 conjugated Anti-BrdU	Mouse	Life Technologies (UK)	1:100	2 hours at RT

Table 2.5 Working concentrations and incubation conditions of antibodies used for immunofluorescence staining. All antibodies were diluted in 0.25% (w/v) PBS/BSA.

2.8 High content image analysis

2.8.1 High content microscopy

Cells were seeded in 384-well plate format and were fixed and stained according to Section 2.7. Cells were then imaged using the IN Cell 1000 automated microscope (GE, UK) at 10X magnification (nine fields/well) using a polyChroic mirror (89100 bs*) (Chroma, US), unless otherwise stated. Nine fields of view at 10X magnification covers an area of 0.054 cm^2 out of the total area of a well of a 384-well plate (0.087 cm^2). Thus, for a 384-well plate seeded with 1,305 senescent cells per well, approximately 800 cells will be imaged and analysed for each well. All excitation and emission filters were from Chroma, US. The different staining and secondary antibodies used were visualised using

the excitation and emission filter sets outlined in Table 2.6. Image quantitation was then performed using the Developer software version 1.9.1 (GE, UK).

Immunofluorescence source	Excitation filter	Emission filter
DAPI (blue)	AT350_50X	ET455_50M
Alexa Fluor 488 (green)	ET490_20X	ET525_36M
Alexa Fluor 546 (red)	ET555_25X	ET605_52M
Cell Mask (far red)	ET645_30X	ET705_72M

Table 2.6 Excitation and emission filter sets for visualising different stains and antibodies.

2.8.2 Multi-parameter analysis and Z score generation

Multi-parameter analysis was performed using the Developer software version 1.9.1 (Figure 2.1) and a list of the measures used are displayed in Table 2.7. A full tabulation of the measures analysed for EP, DS, and siRNA treated DS HMFs is displayed in Appendix Table A.2.

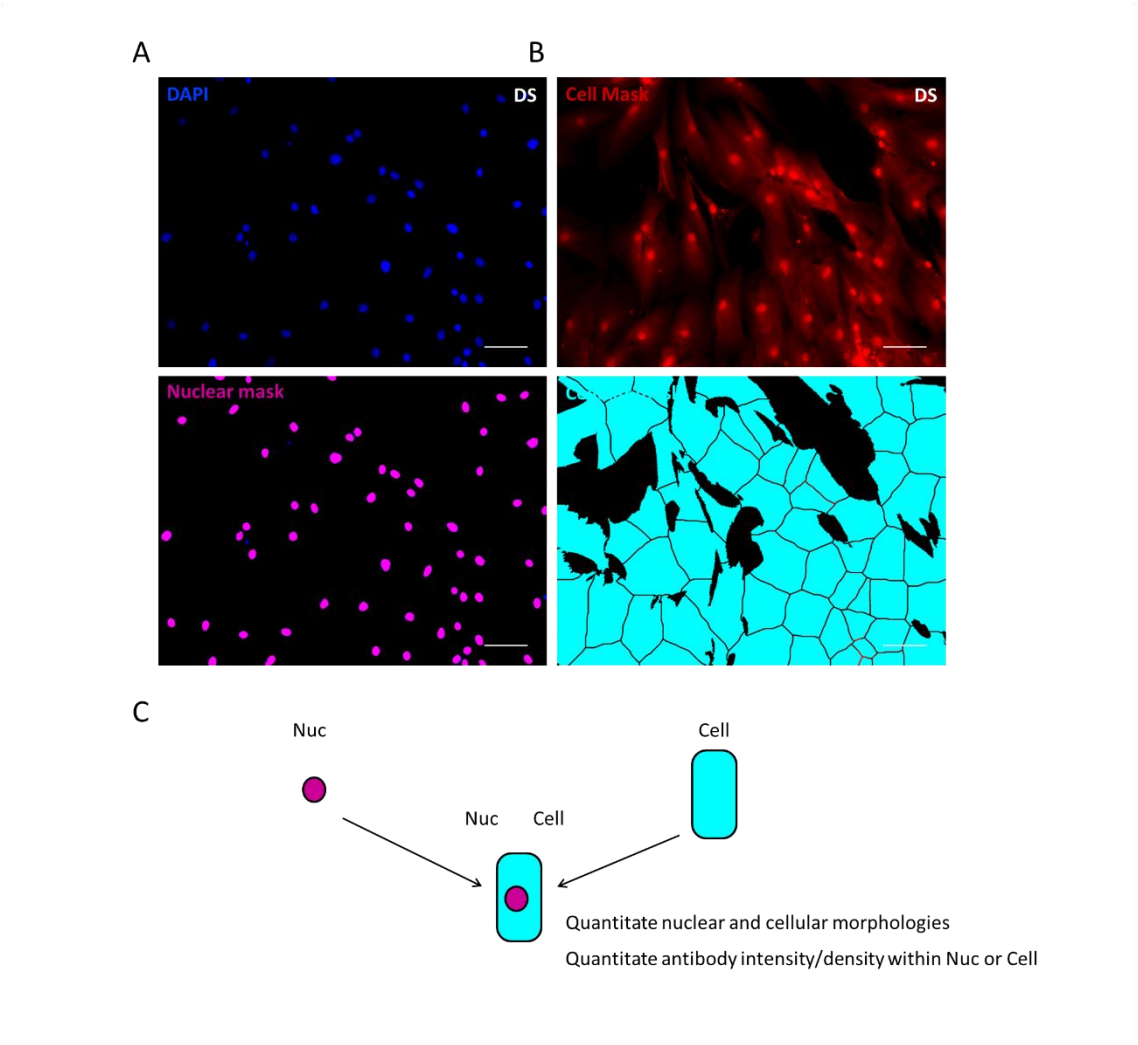

Figure 2.1 Representative images of DS fibroblasts and the Developer software image analysis and quantitation of nuclear and cellular phenotypes. DS HMFs were seeded at 15,000 cells/cm^2 in 384-well plate format, fixed after five days, stained with **(A)** DAPI (blue) to detect nuclei, with Developer software subsequently used to generate a nuclear mask (magenta); and **(B)** Cell Mask (red) to detect cell morphology, with Developer analysis software subsequently used to generate a cellular mask (cyan). Scale bar denotes 100 µm. **(C)** Schematic for quantitation of nuclear and cellular phenotypes using nuclear mask (Nuc, magenta) and cellular mask (Cell, cyan).

Name of parameter (used within heatmaps)	Name of the IN Cell 1000 Developer software measure	Description
Number	Count	Total number of targets per well
Area	Area	Target area (μm^2)
Roundness	Form Factor	Target circularity (expressed as a value from 0-1, 1 equals a perfect circle)
Elongation	Major/Minor axis ratio	Major axis length (the longest of two perpendicular axes of symmetry)/Minor axis length (the shortest of two perpendicular axes of symmetry)
Protein intensity	Dens Levels	Mean grey level of the pixels contained within a target (expressed as a value from 0-4,095 where 0 equals black and 4,095 equals white)
Protein density	Mass/Area	Mass (sum of all pixel values in a target)/target area (μm^2)

Table 2.7 A description of each of the parameters used within the multi-parameter analysis. Measures were obtained using the Developer software version 1.9.1. Thresholding for protein intensity or density was performed using overlap of frequency distributions.

Unless otherwise stated, Z scores were generated according to the formula below:

Z score = (mean value of two independent experiments for experimental siRNA - mean value of two independent experiments for siGLO)/SD for siGLO of two independent experiments.

For each of the parameters analysed, significance was defined as more than one Z score away from the siGLO mean in order to increase the window for hit detection and allow as many hits to be identified as possible. Z scores are given as a heatmap.

2.9 Scanning ion conductance microscopy (SICM)

In collaboration with Dr Pavel Novak's lab., SICM was used to perform high resolution mapping of proliferating, DS, and p16+p21 siRNA transfected DS HMF cell surface topographies.

SICM is a form of scanning probe microscopy which uses a capillary glass nanopipette in a conducting solution to image cell surface topography (Klenerman *et al.*, 2013). Application of voltage between an electrode in the pipette and an electrode in the bath creates a flow of sodium and chloride ions. This ion flow is limited by the small aperture in the pipette tip and is further reduced as the pipette tip approaches the ion-impermeable surface of the cell. The height of the nanopipette tip is adjusted to keep the ion flow constant as it scans the surface of the cell, which allows the topography of the cell surface to be recorded.

Proliferating HMFs (P11 to P15) were seeded in 35 mm x 10 mm dishes (Corning, UK) at an optimised seeding density of 7,000 cells/cm^2 in order to image individual HMF membranes in a sub-confluent population. Dishes were incubated at 37°C and medium changed after 48 hours and 96 hours. Cells were imaged live at 48 hours and 96 hours using SICM.

DS HMFs were seeded at the optimised density of 7,000 cells/cm^2 in 35 mm x 10 mm dishes and incubated at 37°C overnight. Approximately 16 hours later, siRNA/Dh2 complexes were incubated at RT for 20 minutes before cells were forward transfected with 3.45 µL Dh2 combined with either 30 nM siGLO or 15 nM p16 siRNA in combination with 15 nM p21 siRNA. Dishes were incubated at 37°C and medium changed after 24 hours and 48 hours. Cells were imaged live 72 hours later using SICM.

2.10 Database searches

Protein interaction datasets for each hit were generated using the BioGRID bioinformatics database (http://www.thebiogrid.org). These interactions were then overlaid to generate a network requiring that each interactor generated a chain with at least two other drivers, revealing a total of 33 protein interactions. Using this method, only one protein interaction network was generated.

To further explore the relationships between drivers and interactors, GeneMANIA (http://www.genemania.org) was used to generate an interaction network using data from a variety of sources, including physical interactions, co-expression, genetic interactions, co-localisation, predicted interactions, pathways, and shared protein domains.

KEGG PATHWAY (http://www.genome.jp/kegg/pathway.html) and PANTHER (http://www.pantherdb.org) databases were searched to assign functional annotations to the 28 hits that strongly induced the reversal phenotype ('drivers') in the previous DS HMEC siRNA screen as well as the 33 interactors identified using bioinformatics.

2.11 Bioinformatics analysis of binding site enrichment

The genomic location for each gene measured on the array was extracted using biomart (Durinck *et al.*, 2009) in R with Ensembl version 75. The promoter for each of these genes was calculated as ranging from 2 kilobase pairs (kbp) upstream of the transcription start site and 50 base pairs (bp) downstream and the genomic sequence was then obtained from the hg19 reference sequence. Transcription factor motifs for EGR2 were obtained from TRANSFAC (Matys *et al.*, 2006). CountPWM function was used from the Biostrings package (Pagès *et al.*, 2016) with default parameters to calculate the number of potential binding targets for the motifs. To calculate the enrichment of the potential binding targets for the differential gene expression lists generated by the HMEC gene expression array, a background set of genes of the same number as the original differential expression list was created by randomly sampling from the remaining genes. This was performed 1,000 times to create 1,000 random gene lists and subsequently compared with the potential binding targets of these lists to our original differential expression list. This analysis was performed by Dr Rob Lowe.

2.12 Statistical analysis

An un-paired, two-tailed t-test was performed to compare the means of two groups using the Microsoft Office Excel Analysis ToolPak (Microsoft, USA). A one-way analysis of variance (ANOVA) was used to analyse the differences between the means of three or more independent groups using Prism 7 (GraphPad Software Inc., USA). A two-way ANOVA was used to analyse the differences between multiple subgroups within multiple independent groups using Prism 7. Post-hoc statistical analysis was performed using

either a Dunnett's or Tukey's multiple comparison test. The Dunnett's test was used to compare every mean to a control mean, whereas the Tukey test was used to compare every mean with every other mean. Unless otherwise stated, at least two independent experiments were performed each in triplicate.

Chapter 3 Reversal of deep senescence in adult human mammary fibroblasts.

3.1 Introduction

The limited replicative capacity of primary human fibroblasts in culture was first discovered by Hayflick & Moorhead (1961). This replicative barrier, or 'Hayflick limit' is now known as replicative senescence; a state of stable cell cycle arrest in response to telomere erosion which is frequently referred to in the literature as an irreversible process (see Section 1.2). There is now compelling evidence that senescent cells accumulate in human tissues with age (Dimri *et al.*, 1995; Krishnamurthy *et al.*, 2004). Furthermore, senescent cells can be found at the sites of age-related diseases such as osteoarthritis, atherosclerosis, and Alzheimer's disease (Naylor, Baker and van Deursen, 2012). In addition, GWAS have repeatedly linked the INK4/ARF locus (encoding p16, see Section 1.1.2) with numerous age-related diseases (Jeck, Siebold and Sharpless, 2012). Importantly, clearance of senescent cells using a transgenic approach (Baker *et al*. 2011) or senolytic pharmacological agents (Chang *et al.*, 2015; Zhu *et al.*, 2016) has been shown in mice to extend healthspan and recently, lifespan (Baker *et al.*, 2016), demonstrating a direct relationship between senescence, age-related diseases, and ageing (see Section 1.5.1).

In order to explore the mechanism of replicative senescence, a model will be established in this Chapter using normal adult HMFs serially passaged to senescence. Recent evidence has suggested that senescence is a multi-step, dynamic process, with a fully senescent phenotype taking over 10 days to develop post-senescence induction (see Section 1.2). Given this, HMFs will be kept in culture for three weeks post-senescence induction to ensure a stable, long-term, fully senescent phenotype defined as deep senescence (DS). Subsequently, DS HMFs will be validated and characterised using immunofluorescence staining, high-content imaging, and multi-parameter analysis.

Previous work in our lab. has shown that cellular senescence in adult DS HMECs is reversible using siRNA transfection (Lowe *et al.*, 2015). To investigate whether reversal of senescence is achievable in other cell types, this Chapter also aims to develop a protocol for the introduction of siRNA into adult DS HMFs in order to determine whether siRNA reversal of deep senescence can be performed in fibroblasts (Figure 3.1).

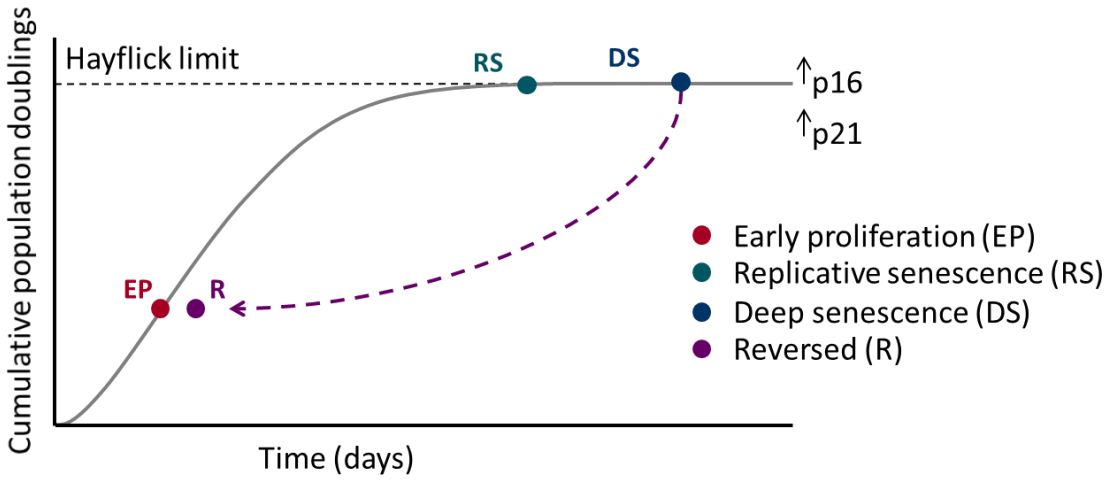

Figure 3.1 Schematic of senescence reversal strategy. Early proliferating (EP) fibroblasts (red) will be serially passaged until reaching replicative senescence (RS, green) after a finite number of cell divisions, as observed by Hayflick & Moorhead (1961). RS fibroblasts will be kept in culture for three further weeks to ensure a stable, long-term, fully senescent phenotype defined as deep senescence (DS, blue), which will be validated and characterised using multi-parameter analysis and immunofluorescence staining for well-established markers of senescence. Subsequently, a siRNA transfection protocol will be developed for DS HMFs in order to investigate whether deep senescence can be reversed (R, purple) in adult human fibroblasts.

3.1.1 Chapter aims

1. To culture adult HMFs to deep senescence using serial passaging.
2. To conduct multi-parameter analysis of EP and DS fibroblasts in order to validate and characterise the DS phenotype.
3. To further validate and define the DS phenotype using staining for markers of senescence including BrdU, p16, p21, SAHF, and 8-oxoG.
4. To optimise siRNA transfection of DS HMFs.
5. To investigate whether reversal of deep senescence can be achieved in HMFs.

3.2 Replicative senescence in adult human mammary fibroblasts

3.2.1 Culturing adult human mammary fibroblasts to replicative senescence

Normal, finite lifespan HMFs will be used to model replicative senescence throughout this thesis. These cells were obtained from reduction mammoplasty tissue of a healthy 16-year old female donor (048R) (Stampfer *et al.*, 1981).

To establish a model for replicative senescence in the lab., adult HMFs were serially passaged from P4 until proliferation ceased at P29 after 35 population doublings, which is equivalent to 175 days in culture (Figure 3.2). This is in line with previous work which showed that these fibroblasts reached replicative senescence after approximately 40 population doublings when cultured from P1 (Romanov *et al.*, 2001; Garbe *et al.*, 2009).

Fibroblasts at P11 were defined as EP. Recent evidence has suggested that senescence is a dynamic, multi-step process throughout which senescent cells evolve and progress into deep senescence (Freund *et al.*, 2012; De Cecco *et al.*, 2013; Shah *et al.*, 2013; Swanson *et al.*, 2013) (see Section 1.2). Thus, senescent fibroblasts were defined as DS (P29+3) when no further expansion was observed after being kept three weeks in culture beyond replicative senescence (P29). To examine the long-term stability of DS fibroblasts in culture, cells were kept up to 130 days after reaching deep senescence with standard medium changes. No further expansion was observed during this period, indicating a stable, long-term arrest of the population (Figure 3.2).

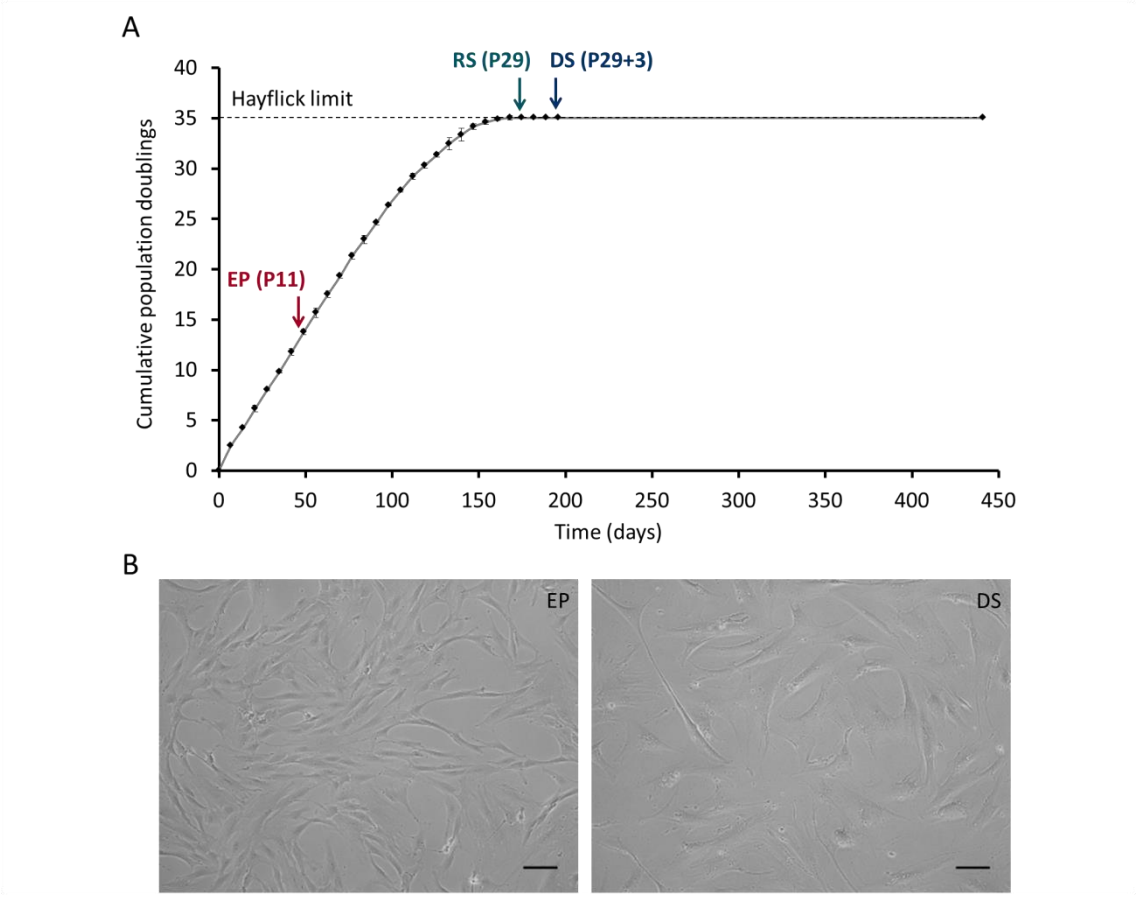

Figure 3.2 Cumulative population doublings of normal adult human mammary fibroblasts. **(A)** Early proliferating (EP) fibroblasts at P11 were serially passaged until they reached replicative senescence at P29. Deeply senescent (DS) fibroblasts were defined as a population which did not expand when kept in culture for three weeks post-replicative senescence (P29+3). No expansion was observed in DS fibroblasts kept in culture for a further 130 days. N=1 between P4 and P6; N=2 or more between P7 and P29+3; N=1 P29+3 + 130 days. Error bars=SD of at least two independent experiments. **(B)** Representative brightfield images of EP and DS fibroblasts taken on the Nikon Eclipse TE2000-S. Scale bar denotes 100 µm.

3.2.2 A panel of morphological markers to validate and characterise the DS phenotype

It is important to note that senescence can be induced by multiple different triggers, causing subsequent heterogeneity in senescent cell morphology. As such, there are many markers of senescent phenotypes but no universal marker of the senescent state (Sharpless and Sherr, 2015) (see Section 1.4). Thus, a panel of markers is commonly used to validate the presence of senescence. Well-established markers of replicative senescence *in vitro* include a stable growth arrest (Hayflick and Moorhead, 1961), enlarged, and flattened cell morphology, an enlarged nucleus with an irregular nuclear envelope (Mehta *et al.*, 2007; Freund *et al.*, 2012), increased staining for p16 and p21 (Alcorta *et al.*, 1996), and increased staining for oxidative DNA damage (Chen *et al.*, 1995) (see Section 1.4.1).

In order to validate the DS phenotype and identify a panel of senescence-associated markers in adult HMFs, morphological changes between EP and DS fibroblasts were quantified using multi-parameter analysis (see Section 2.8.2). Fibroblasts were seeded at 15,000 cells/cm^2 (1,305 cells/well) and after five days, the cells were fixed, stained, and imaged according to Sections 2.7 and 2.8. Using this approach, a significant difference in cell number was observed between the EP and DS fibroblast phenotypes (2,739 ± 189 cells/well compared to 1,182 ± 156 cells/well, respectively; p=0.0004) (Figure 3.3), as measured by the cell number per well after five days. No increase in cell number compared to the original seeded cell number was observed in the DS fibroblasts over the five days (1,182 ± 156 cells/well versus 1,305 cells/well), indicating stable cell cycle arrest in the DS fibroblasts. A slight decrease in cell number was consistently observed when seeding senescent HMFs due to a small proportion of the population which did not re-attach. Furthermore, the DS fibroblast phenotype displayed significant changes in multiple nuclear measures compared to EP fibroblasts, including increased nuclear area (280 ± 5 µm^2 versus 215 ± 5 µm^2, respectively; p=0.0001), increased nuclear elongation (1.42 ± 0.03 arbitrary unit (AU) versus 1.37 ± 0.01 AU, respectively; p=0.049), and decreased nuclear roundness (0.91 ± 0.009 AU versus 0.94 ± 0.003 AU, respectively; p=0.004) (Figure 3.3).

In some cell types, regions of highly condensed chromatin called SAHF are a marker of senescence (Narita *et al.*, 2003) (see Section 1.4). However, SAHF formation in fibroblast strains is variable and is not considered a universal feature of replicative senescence

(Kosar *et al.*, 2011). In line with this finding, DS nuclei examined three weeks post-replicative senescence did not display SAHF (Figure 3.3E). Furthermore, DS nuclei kept in culture for 130 days further did not display SAHF (data not shown). Thus, the DS HMFs were determined to be SAHF negative.

In addition, cellular morphological changes were quantified for EP and DS fibroblast phenotypes using multi-parameter analysis. The DS fibroblast phenotype displayed significant changes in cell morphology compared to the EP fibroblasts, including increased cell area (5,832 ± 424 μm^2 versus 2,110 ± 280 μm^2, respectively; p=0.0002) and decreased cell elongation (1.77 ± 0.013 AU versus 1.82 ± 0.003 AU, respectively; p=0.02) (Figure 3.4).

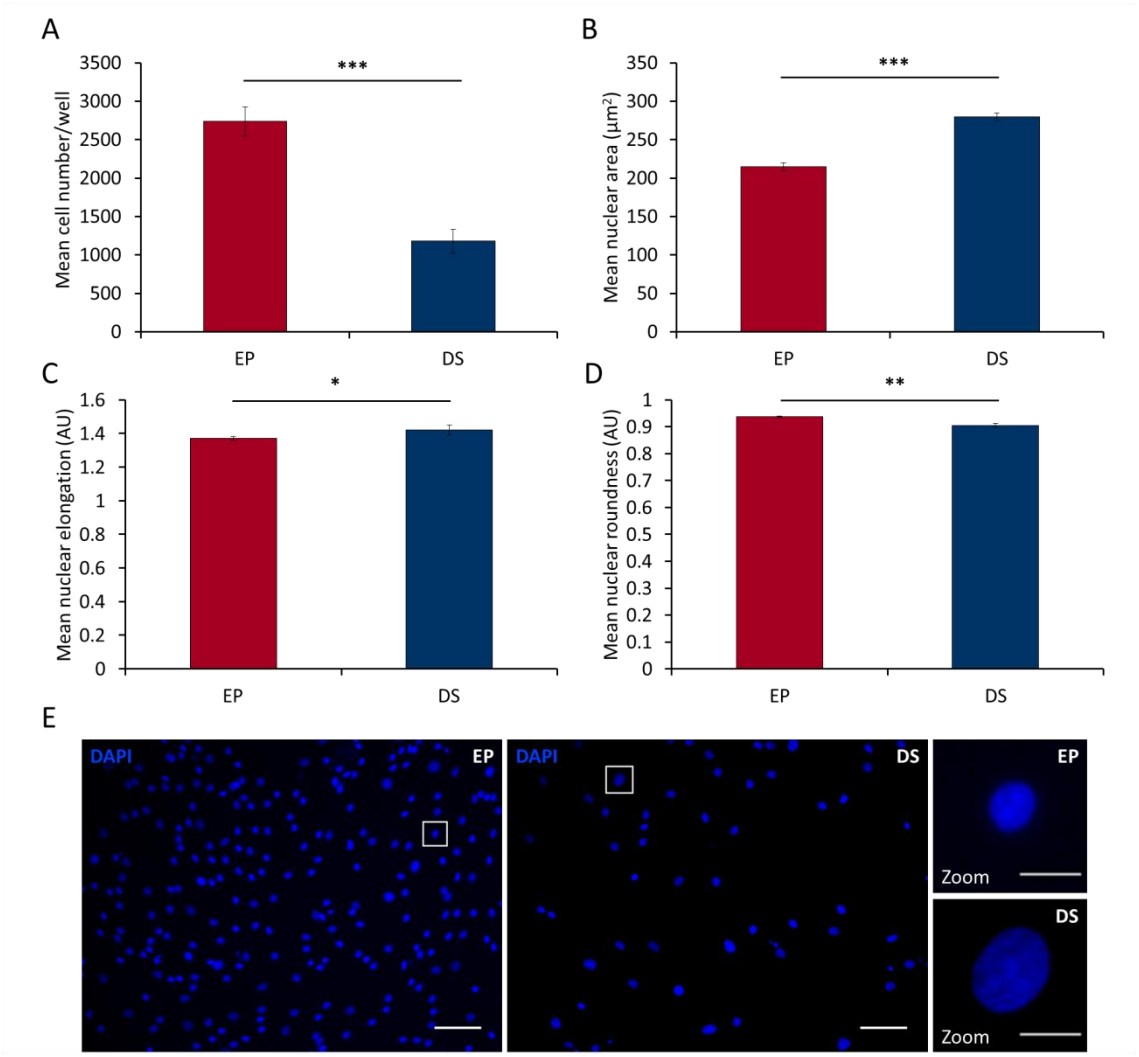

Figure 3.3 Multi-parameter analysis of nuclear morphological measures in EP and DS fibroblasts. EP and DS cells were seeded at 15,000 cells/cm^2 in 384-well plate format, fixed after five days, stained with DAPI, and nuclear phenotypes quantitated according to Section 2.7 and Section 2.8. **(A)** Mean cell number per well. **(B)** Mean nuclear area (µm^2). **(C)** Mean nuclear elongation (AU). **(D)** Mean nuclear roundness (AU). Un-paired two-tailed t-test * p<0.05, ** p<0.01, *** p<0.001. N=3 throughout. Error bars=SD of three independent experiments, each performed with six replicates. **(E)** Representative images of EP and DS fibroblast nuclei. DAPI (blue). Scale bar denotes 100 µm. Right panels=digital zoom, scale bar denotes 20 µm.

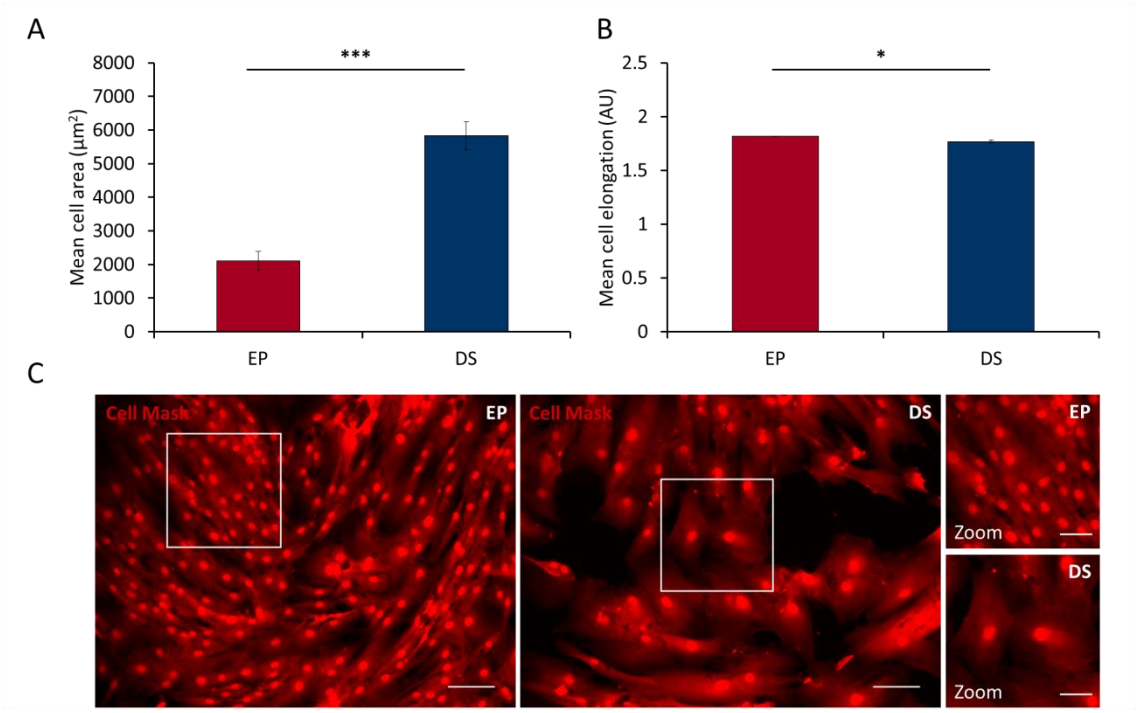

Figure 3.4 Multi-parameter analysis of cell morphological measures in EP and DS fibroblasts. EP and DS cells were seeded at 15,000 cells/cm^2 in 384-well plate format, fixed after five days, stained with Cell Mask, and cell phenotypes quantitated according to Section 2.7 and Section 2.8. **(A)** Mean cell area (µm^2). **(B)** Mean cell elongation (AU). Un-paired two-tailed t-test * $p<0.05$, *** $p<0.001$. N=3 throughout. Error bars=SD of three independent experiments, each performed with six replicates. **(C)** Representative images of EP and DS fibroblasts. Cell Mask (red). Scale bar denotes 100 µm. Right panels=digital zoom, scale bar denotes 50 µm.

In summary, multi-parameter analysis identified a panel of six well-established morphological senescence markers which both validate and define the DS fibroblast phenotype. In subsequent work, this panel will be used to identify siRNA-induced morphological changes in the DS fibroblasts.

3.2.3 Immunofluorescence staining further validates and characterises the DS fibroblast phenotype

To further investigate the proliferative status of EP and DS cells, progression through S phase of the cell cycle was examined using immunofluorescence staining for BrdU incorporation. Following optimisation (data not shown), EP and DS fibroblasts were pulsed with BrdU for 16 hours then immediately fixed and stained with DAPI and mouse anti-BrdU Alexa Fluor 488 according to Sections 2.7.1. Cells were then imaged and BrdU positive nuclei quantified according to Section 2.8. Supporting the previous analysis which showed that DS HMFs did not increase in cell number (see Section 3.2.2), DS nuclei did not incorporate BrdU and therefore presented a significantly reduced percentage of BrdU positive nuclei (0% ± 0%) in comparison to EP nuclei (15% ± 1%; p=0.003) (Figure 3.7). It is important to note that as fixation occurred immediately after the 16 hour BrdU pulse, the data generated here is representative only of the BrdU-incorporating cells, not the resulting daughter progeny. Thus, given the 16 hour BrdU incubation, 15% ± 1% BrdU incorporation in EP nuclei is in line with the data presented previously within this Chapter, as EP fibroblasts seeded at 15,000 cells/cm^2 in 384-well plate format have a doubling time of approximately 100 hours, meaning that approximately 16% of cells should incorporate BrdU in a 16 hour incubation (see Section 3.2.2, and Figure 3.3).

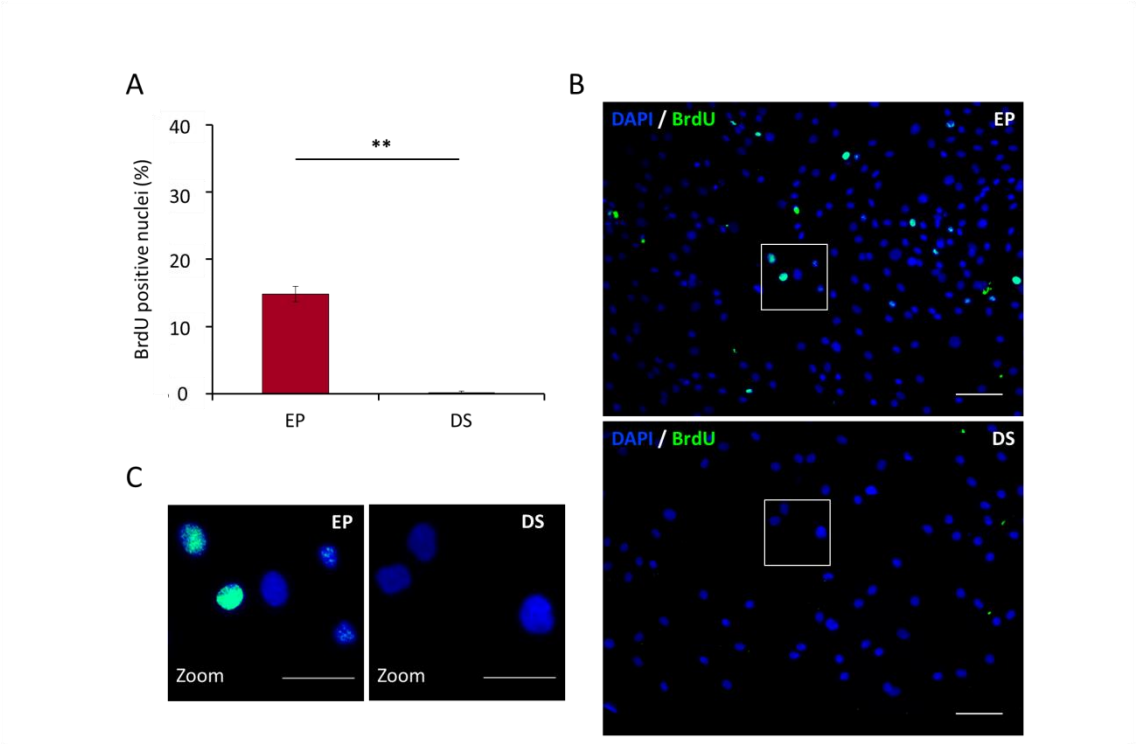

Figure 3.5 Percentage of nuclei positive for BrdU incorporation in EP and DS fibroblasts. EP and DS cells were seeded at 15,000 cells/cm^2 in 384-well plate format, fixed after five days, and stained with DAPI and mouse anti-BrdU Alexa Fluor 488 according to Section 2.7.1. Using the secondary only control, a nuclear intensity threshold was established to define BrdU positive or negative nuclei. **(A)** Bars denote mean percentage of BrdU positive nuclei. Un-paired two-tailed t-test ** $p<0.01$. N=2 throughout. Error bars=SD of two independent experiments, each performed with three replicates. **(B)** Representative immunofluorescence images and **(C)** digitally zoomed images of EP and DS fibroblasts. DAPI (blue), BrdU (green). Scale bar denotes 100 µm on original images and 50 µm on zoomed images.

Up-regulation of p16 and p21 expression is a hallmark of replicative senescence in fibroblasts. However, the increase of p16 and p21 expression levels during senescence occurs with different kinetics (Alcorta *et al.*, 1996; Stein *et al.*, 1999). Proliferating fibroblasts possess a basal endogenous level of p21 expression which increases sharply as the culture nears replicative senescence before declining (reviewed in Sherr & Roberts 1999). By contrast, p16 levels gradually accumulate, reaching a maximum in deep senescence after p21 levels have started to decline (Alcorta *et al.*, 1996) (see Section 1.2). Consequently, a deeply senescent fibroblast culture may contain cells positive for p16, p21, or both.

In order to further validate and explore the DS phenotype, p16 and p21 levels were investigated in EP and DS fibroblasts. To achieve this, multiple rabbit anti-p21 antibodies were validated via western blotting for the presence of a single band at the expected molecular weight. Subsequently, rabbit anti-p21 (12D1) and mouse anti-p16 (JC8) were identified as suitable antibodies and optimised for immunofluorescence staining (Appendix Figure A.1). Following this, p16 and p21 expression levels were quantified in the EP and DS fibroblasts using western blot (Appendix Figure A.2A-C) and immunofluorescence staining according to Section 2.4 and Section 2.8, respectively (Figure 3.6). Using the secondary only control, p16 and p21 nuclear intensity thresholds were established to define negative and positive nuclei, and analysis was performed to categorise the population into four subgroups: double negative; double positive; and positive for either p16 or p21. In line with the literature, a significantly increased percentage of DS nuclei were double positive (62% ± 18%) in comparison to EP nuclei (5% ± 1%; p=0.02), indicating up-regulation of both p16 and p21 expression. Correspondingly, a significantly decreased percentage of DS nuclei were identified as double negative (5% ± 6%) in comparison to EP nuclei (53% ± 9%; p=0.03). Unsurprisingly, given the heterogeneity of p16 and p21 expression in the senescent fibroblast population, 11% ± 8% of DS nuclei were positive for only p16 expression and 23% ± 4% were positive for only p21 expression. Furthermore, in line with the literature demonstrating that proliferating fibroblasts possess a basal level of p21 expression, 37% ± 8% of EP nuclei were positive for only p21 expression only. However, 6% ± 1% of EP nuclei were also positive for p16 expression only, perhaps indicating an early onset in the gradual accumulation of p16 levels. Further investigation revealed that EP HMFs

defined as positive for p16 or p21 possess lower average nuclear p16 or p21 intensity levels relative to positive DS HMFs (Figure 3.6C-D). This indicated that positive EP HMFs express each of these senescence markers at a lower level than positive DS HMFs, potentially at a level below the threshold level which is necessary for senescence induction.

In summary, increased expression of p16 and p21 expression in the DS population further validated the senescent phenotype of the HMFs. Thresholding of p16 and p21 nuclear intensities allowed subsequent categorisation into four subgroups, which further characterised the EP and DS populations, and demonstrated the variation in p16 and p21 positivity for both the EP and DS populations.

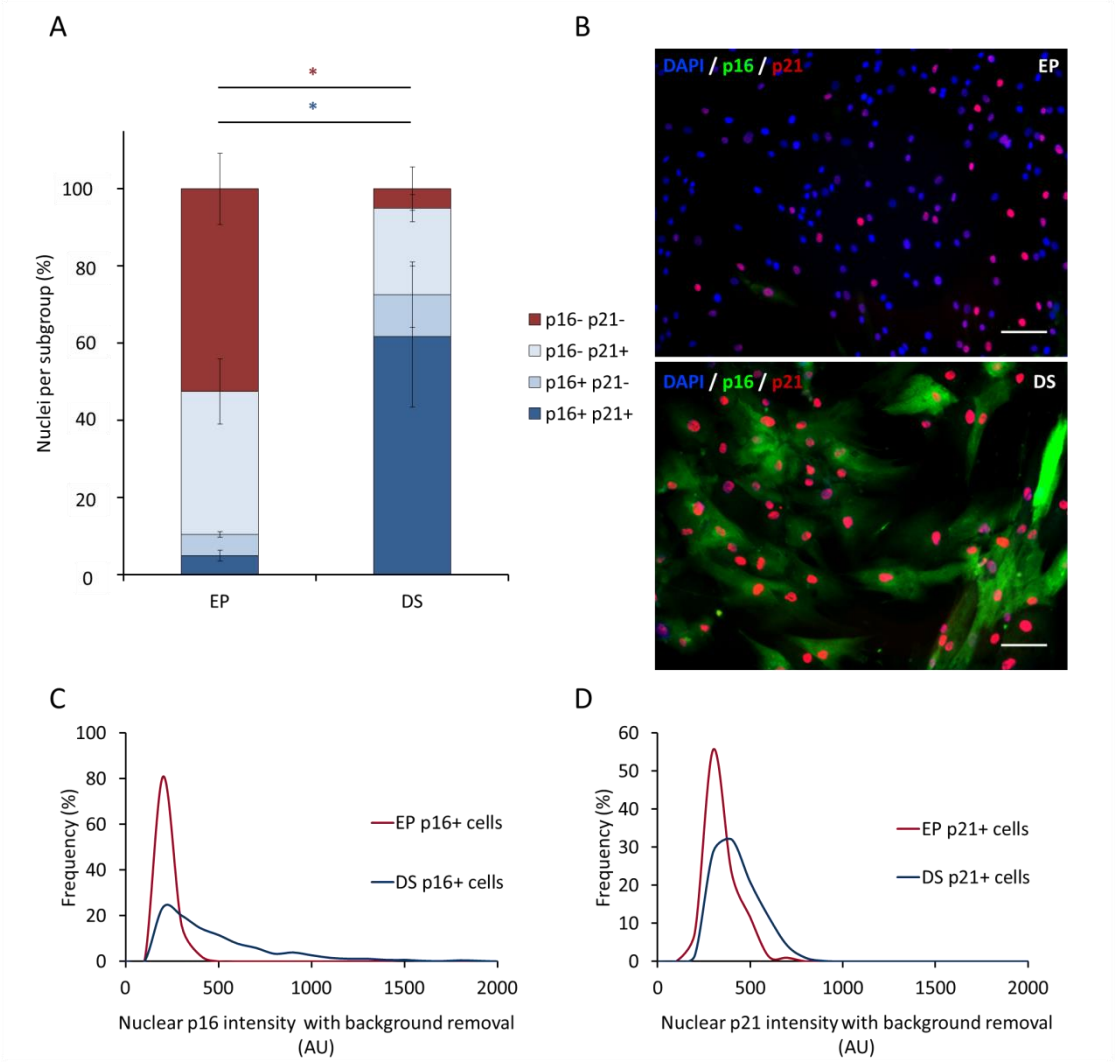

Figure 3.6 p16 and p21 expression in EP and DS fibroblasts. EP and DS cells were seeded at 15,000 cells/cm^2 in 384-well plate format, fixed after five days, stained with DAPI, mouse anti-p16 (JC8), rabbit anti-p21 (12D1), donkey anti-mouse Alexa Fluor 488, goat anti-rabbit Alexa Fluor 546, and nuclear intensities were quantitated according to Section 2.7 and Section 2.8. Nuclear intensity thresholds were established for p16 and p21 to define positive or negative nuclei. Nuclei were classified into four subgroups: p16 and p21 negative (p16- p21-); p16 negative and p21 positive (p16- p21+); p16 positive and p21 negative (p16+ p21-); and p16 and p21 positive (p16+ p21+). **(A)** Bars denote mean percentage of nuclei per subgroup. Two-way ANOVA and Tukey's test * $p<0.05$. Significance colours match nuclei subgroup. N=2 throughout. Error bars=SD of two independent experiments, each performed with three replicates. **(B)** Representative immunofluorescence images of EP and DS fibroblasts. DAPI (blue), p16 (green), p21 (red). Scale bar denotes 100 µm. **(C)** Representative frequency distribution of nuclear p16 intensities in EP and DS p16 positive (p16+) HMFs. **(D)** Representative frequency distribution of nuclear p21 intensities in EP and DS p21 positive (p21+) HMFs.

Fibroblasts which have undergone replicative senescence have also been shown to have elevated levels of oxidative DNA damage in response to ROS. Oxidative DNA damage can be visualised by increased staining for 8-oxoG, an oxidatively damaged nucleotide excised from DNA and present within the cytoplasm (Chen *et al.*, 1995) (see Section 1.4.1). Using a previously validated mouse anti-8-oxoG antibody (Lowe *et al.*, 2015) (data not shown), the levels of oxidative damage in EP and DS fibroblasts were examined (Figure 3.7). Following thresholding of 8-oxoG levels, a significant percentage of DS cells were defined as positive for 8-oxoG staining (71% ± 3%) versus EP cells (16% ± 4%; p=0.005). In addition, further investigation of the 8-oxoG positive (8-oxo+) subgroup in EP and DS HMFs revealed that 8-oxo+ DS HMFs possessed increased levels of 8-oxoG in comparison to EP HMFs (Figure 3.7C). Interestingly, there was a similar proportion of double positive (p16+ p21+) DS HMFs (62% ± 18%) in the population (Figure 3.6) as 8-oxoG positive DS HMFs, potentially indicating a relationship between the kinetics of p16 and p21 up-regulation and accumulation of 8-oxoG levels during the deepening of the senescence phenotype. Together, these data indicate the presence of elevated levels of oxidative DNA damage in the DS fibroblasts, providing further confirmation of the DS phenotype.

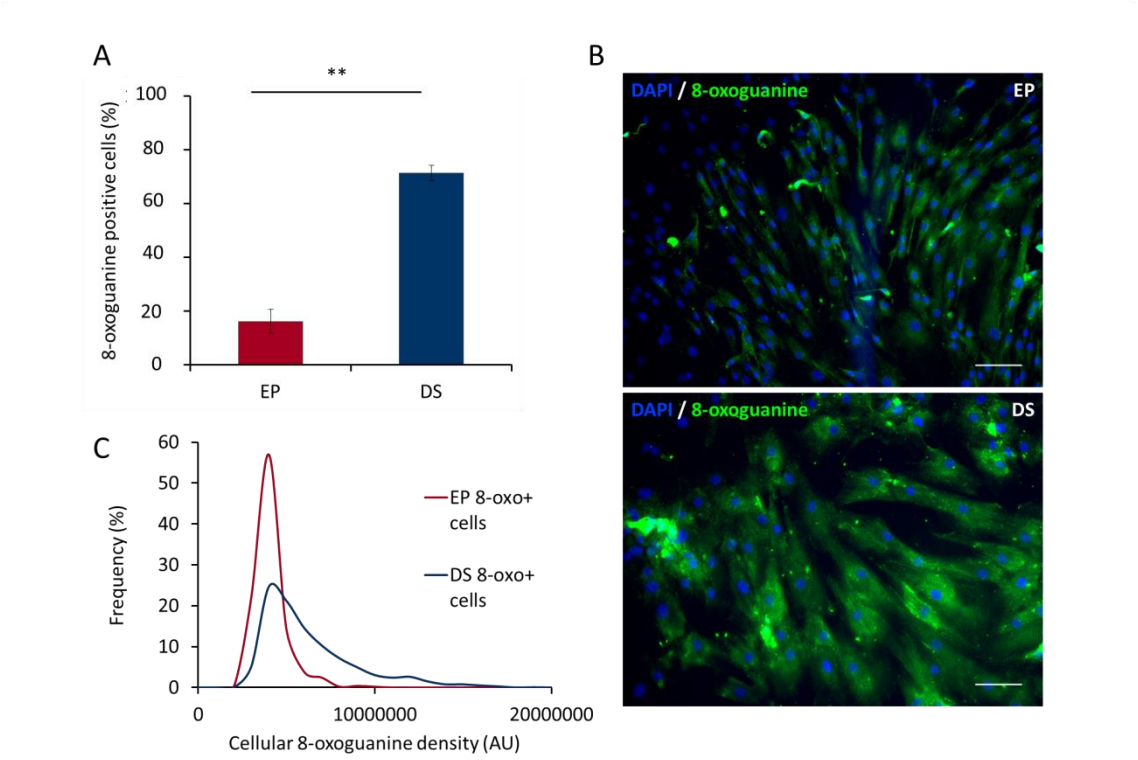

Figure 3.7 Percentage of EP and DS nuclei positive for 8-oxoG. EP and DS cells were seeded at 15,000 cells/cm^2 in 384-well plate format, fixed after five days, stained with DAPI, mouse anti-8-oxoG, donkey anti-mouse Alexa Fluor 488, and 8-oxoG cellular density was quantitated according to Section 2.7 and Section 2.8. A cellular density threshold was established to define 8-oxoG positive or negative cells. **(A)** Bars denote mean percentage of 8-oxoG positive cells. Un-paired two-tailed t-test ** $p<0.01$. N=2 throughout. Error bars=SD of two independent experiments, each performed with three replicates. **(B)** Representative immunofluorescence images of EP and DS fibroblasts. DAPI (blue), 8-oxoG (green). Scale bar denotes 100 µm. **(C)** Representative frequency distribution of cellular 8-oxoG densities in EP and DS 8-oxoG positive (8-oxo+) HMFs.

3.2.4 Further markers of senescence to characterise the DS phenotype

Acosta *et al*. (2013) recently demonstrated that OIS fibroblasts induce paracrine senescence in neighbouring proliferating fibroblasts via the SASP (see Section 1.4.2). In order to explore whether DS HMFs transmit senescence in a paracrine manner, EP HMFs were seeded at an optimised density of 10,000 cells/cm^2 (data not shown) and exposed to conditioned medium which was incubated for 48 or 72 hours on DS HMFs seeded at 10,000 cells/cm^2 or on EP HMFs as a negative control, according to Section 2.3. After five days, EP fibroblasts were fixed and stained with DAPI and Cell Mask according to Section 2.7. Cell number was quantitated according to Section 2.8.2. This work was performed by Arturo Robles Tenorio (an MSc student in the Bishop lab., May 2015-September 2015).

Using this approach, no difference in cell number was detected for EP HMFs exposed to conditioned medium which was incubated on EP HMFs (EP48, 5,379 ± 1,011 cells/well; EP72, 4,553 ± 239 cells/well), or conditioned medium incubated on DS HMFs for 48 hours (DS48, 4,725 ± 794 cells/well) in comparison to the un-conditioned medium control (CTRL, 4,969 ± 241 cells/well). However, EP HMFs treated with conditioned medium which was incubated on DS HMFs for 72 hours (DS72) showed a significant decrease in mean cell number (3,518 ± 380 cells/well; p=0.0001) (Figure 3.8). Further preliminary data investigating nuclear and cellular morphology indicated a trend towards increased nuclear and cellular area in the DS72-treated EP HMFs as well as increased cellular 8-oxoG intensity compared to CTRL-treated EP HMFs (data not shown). These data demonstrate that conditioned medium incubated on DS HMFs can decrease cell number, nuclear and cellular area, and increase cellular 8-oxoG intensity of EP HMFs, which may indicate transmission of senescence to EP HMFs in a paracrine manner, potentially via the SASP.

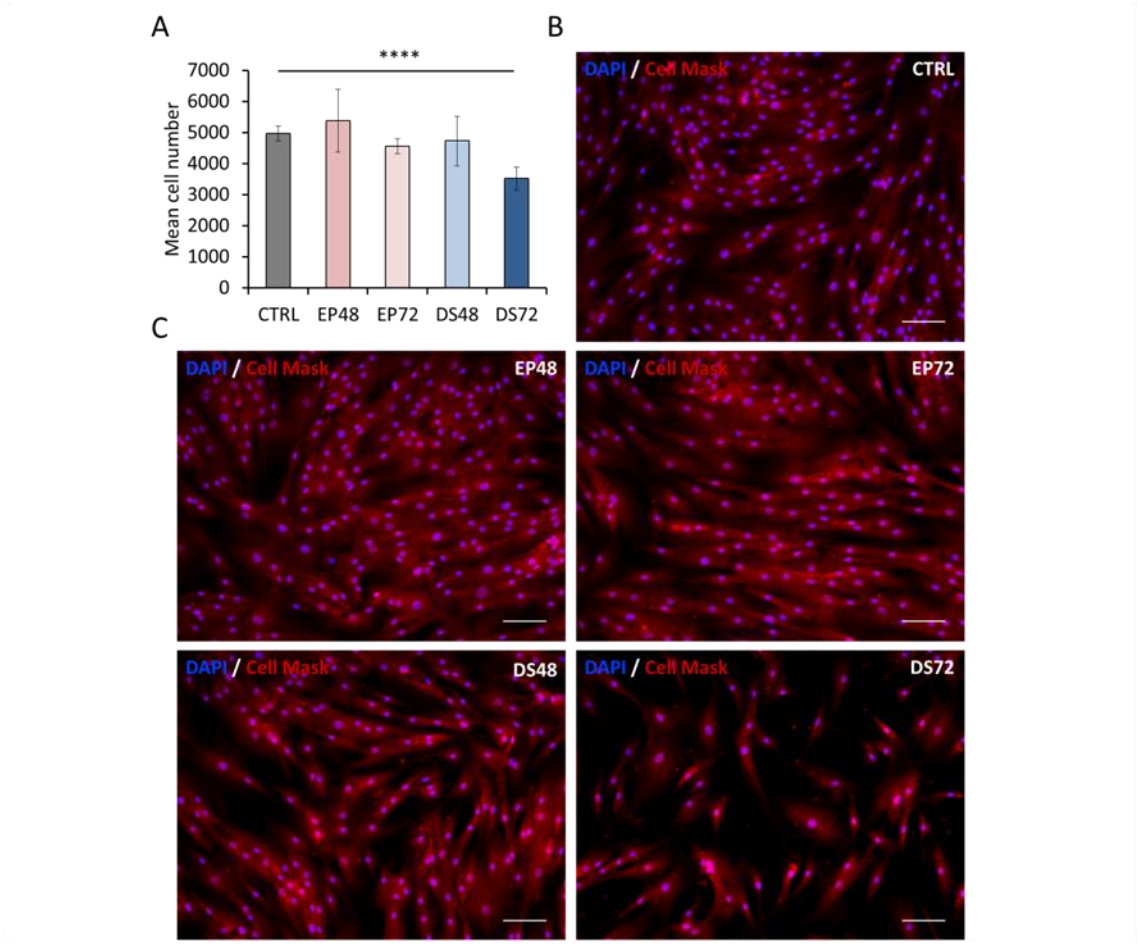

Figure 3.8 Analysis of cell number for EP HMFs exposed to DS HMF conditioned medium. EP cells were seeded at 10,000 cells/cm^2 in a 96-well plate format, fixed, and stained with DAPI and Cell Mask after five days of exposure to either unconditioned control medium (CTRL) or conditioned medium collected under four conditions: 48 hour incubation on EP fibroblasts (EP48); 72 hour incubation on EP fibroblasts (EP72); 48 hour incubation on DS fibroblasts (DS48); or 72 hour incubation on DS fibroblasts (DS72); according to Section 2.3, 2.7, and 2.8. Cell number was quantitated according to Section 2.8.2. **(A)** Mean cell number of EP fibroblasts exposed to medium from five conditions. One-way ANOVA and Dunnett's test **** $p<0.0001$. N=2 throughout. Error bars=SD of two independent experiments, each performed with six replicates. **(B-C)** Representative images of the five different conditions: **(B)** CTRL; **(C)** EP48; EP72; DS48; and DS72. DAPI (blue), Cell Mask (red). Scale bar denotes 100 µm. The data displayed within this figure were generated by Arturo Robles Tenorio, MSc student within the Bishop lab. under supervision of ET.

As the progression from early to deep senescence is mediated by the down-regulation of lamin B1 (see Section 1.2), it was hypothesised that lamin B1 levels would be decreased in DS fibroblasts in comparison to EP HMFs. To explore this, lamin B1 levels were investigated in EP and DS HMFs using western blotting. Using this approach, DS HMFs displayed decreased lamin B1 levels in comparison to EP HMFs (N=1, representative experiment, Appendix Figure A.2A, D), indicating progression of the senescent HMFs into a deeply senescent phenotype.

3.3 Reversal of deep senescence in fibroblasts

3.3.1 Transfection optimisation of DS HMFs in 384-well plate format

Senescent primary cells are notoriously difficult to transfect. Therefore, before reversal of deep senescence in fibroblasts could be tested, a transfection reagent with a high transfection efficiency and low cytotoxicity was sought to efficiently deliver siRNA to DS HMFs.

In order to identify the optimal transfection reagent, the uptake efficiency of two different transfection reagents (Dh2 and Dh4), which had previously been shown to transfect DS epithelial cells (Lowe *et al.*, 2015), were tested in the DS fibroblasts. Dh2 demonstrated greater uptake efficiency than Dh4 and was accordingly selected as the optimal transfection reagent (data not shown). Subsequently, the cell seeding density and Dh2 dose were optimised in order to produce a high level of transfection efficiency with minimal toxicity. As senescent cells do not proliferate, an optimal seeding density to detect senescence reversal is one with enough cells to maximise the exponential increase in cell number, without reaching confluency by the experimental endpoint. Accordingly, an optimised seeding density of 15,000 cells/cm^2 was chosen for the DS fibroblasts (data not shown).

To identify a Dh2 dose with maximum transfection efficiency and minimal toxicity, siGLO, a fluorescently labelled control siRNA targeting a non-essential housekeeping gene, was used as a negative control for transfections. siGLO transfection enables quantification of the uptake of this DY547-labelled transfection reagent/siRNA mix (see Section 2.5). Using the optimised seeding density of 15,000 cells/cm^2, DS fibroblasts were forward transfected with 30 nM siGLO using 0-0.6 µL/well Dh2 according to Section

2.5.3 (N=1, representative experiment, performed multiple times in different contexts). In order to identify the optimal Dh2 dose to be used in future experiments, two measures were investigated: average cell number per well to ensure minimal toxicity, as well as average siGLO uptake per cell to identify maximum transfection efficiency. No noticeable decrease in mean cell number/well was observed in Dh2 doses from 0 µL/well (1,230 ± 66 cells/well) to 0.6 µL/well (1,206 ± 39 cells/well), indicating minimal toxicity even at 0.6 µL (N=1, Figure 3.9A). Further, 0.15 µL/well was identified as the lowest dose inducing effective siGLO uptake (32 ± 3 foci/cell) relative to the 0.15 µL Dh2 only control (2 ± 0 foci/cell), and Dh2 doses higher than 0.15 µL/well did not produce a further increase in siGLO foci, indicating that 0.15 µL is the minimum effective dose. Accordingly, 0.15 µL/well was selected as the optimal Dh2 dose to be used in future experiments (Figure 3.9B-D). In addition, it was confirmed that siGLO was an appropriate negative control as there were no changes in proliferation, morphology, BrdU incorporation, or protein expression compared to untransfected (UTC) cells and cells treated with Dh2 alone (Appendix Figure A.3). Subsequently, siGLO was used throughout this thesis as a negative control for the siRNA reversal transfections.

Polo-like kinase 1 (PLK1), a serine-threonine kinase that is essential for mitosis, is often used as a positive 'killer' control in siRNA transfections, as cells transfected with PLK1 siRNA undergo apoptosis during cell division. PLK1 siRNA transfection in DS HMFs provided further confirmation that the culture was fully arrested as no significant decrease in cell number was observed at 0.15 µL Dh2 (data not shown).

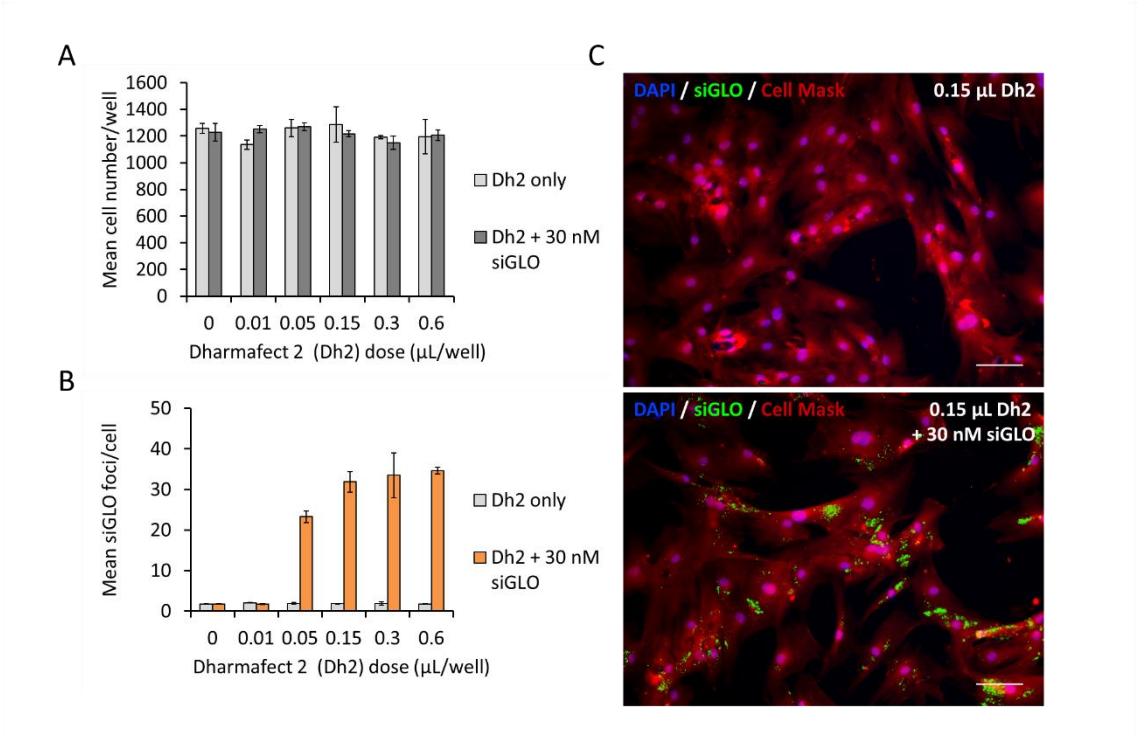

Figure 3.9 Optimisation of Dh2 dose in DS fibroblasts. DS fibroblasts were seeded at 15,000 cells/cm^2 and forward transfected with either 0-0.6 µL/well Dh2 alone, or with 30 nM siRNA targeting cyclophilin B labelled with DY547 (siGLO) according to Section 2.5.3. After five days, cells were fixed, stained with DAPI and Cell Mask, imaged, and quantified according to Sections 2.7 and 2.8. **(A)** Mean cell number/well of cells transfected with either 0-0.6 µL/well Dh2 alone or with 30 nM siGLO. **(B)** Mean cellular siGLO foci number of cells transfected with either 0-0.6 µL/well Dh2 alone or with 30 nM siGLO. N=1 throughout. Single representative experiment which has been performed multiple times in different contexts. Error bars=SD of a single experiment containing three replicates. **(C)** Representative immunofluorescence images of DS HMFs transfected with 0.15 µL Dh2 alone or with 30 nM siGLO using 0.15 µL Dh2. DAPI (blue), siGLO (green), Cell Mask (red). Scale bar denotes 100 µm.

3.3.2 Reversal of deep senescence in HMFs

Previously, Lowe *et al*. (2015) demonstrated that p16 siRNA knockdown in DS HMECs transiently reverses epithelial cellular senescence creating a 'reversed' phenotype, as characterised by the loss of multiple senescence-associated features (see Section 1.7).

Unlike replicative senescence in fibroblasts, which activates both the p53/p21 and p16/pRB pathways, HMECs exhibit a two-step pattern of senescence, where cells first undergo p16-dependent epithelial cellular senescence in the absence of telomere erosion and p53 or p21 expression (Brenner, Stampfer and Aldaz, 1998). With this in mind, it was hypothesised that transient knockdown using previously validated p16 (Bishop *et al.*, 2010) and p21 (Borgdorff *et al.*, 2010) siRNAs together in DS fibroblasts would induce a 'reversed phenotype', as characterised by the previously defined panel of senescence-associated markers (see Section 3.2.3). Accordingly, DS fibroblasts were seeded at a previously optimised seeding density of 15,000 cells/cm^2 and forward transfected with 30 nM p16 siRNA, 30 nM p21 siRNA, or 15 nM p16 siRNA combined with 15 nM p21 siRNA (p16+p21 siRNA) using the optimised dose of 0.15 µL Dh2 (see Section 2.6.1). After five days, cells were stained with DAPI and Cell Mask and senescence-associated markers quantified according to Section 2.7 and 2.8.

DS fibroblasts transfected with p16 siRNA had no change in proliferation, nuclear or cellular morphology compared with cells transfected with siGLO (Figure 3.10A). DS fibroblasts transfected with p21 siRNA consistently increased cell number (1,476 ± 238 cells/well) compared to siGLO transfected cells (1,017 ± 106 cells/well), and consistently altered multiple senescent morphologies, including reduced nuclear area (203 ± 8 µm^2 versus 281 ± 9 µm^2), and reduced cell area (3,407 ± 661 µm^2 versus 6,341 ± 800 µm^2). There was also a trend towards altered nuclear elongation (1.36 ± 0.04 AU), nuclear roundness (0.92 ± 0.01 AU), or cell elongation (1.98 ± 0.09 AU) in the p21 siRNA transfected DS fibroblasts compared to the siGLO control (1.42 ± 0.03 AU; 0.90 ± 0.01 AU; 1.80 ± 0.03 AU, respectively). Strikingly, siRNA knockdown of both p16 and p21 in DS fibroblasts consistently induced an increase in cell number (1,657 ± 214 cells/well) compared to the siGLO transfected cells. It is also interesting to note that in all four experiments presented in Figure 3.10, the combined knockdown of p16 and p21 generated a greater cell number than the corresponding p21 siRNA transfected cells. Moreover, in all experiments, the p16+p21 transfected DS fibroblasts displayed altered

nuclear and cellular morphology in comparison to both the siGLO transfected and p21 siRNA transfected cells, with reduced nuclear area (187 ± 9 μm^2), reduced nuclear elongation (1.35 ± 0.03 AU), increased nuclear roundness (0.92 ± 0.007 AU), and decreased cell area (2,908 ± 676 μm^2). There was also a trend towards increased cell elongation in p16+p21 siRNA knockdown HMFs in comparison to the siGLO transfected DS HMFs (2.02 ± 0.13 AU), although this was not as consistent as other measures, potentially due to the limitations of the IN Cell developer software segmentation of fibroblast cellular shape.

In conclusion, p16 siRNA knockdown in DS HMFs did not increase cell number or alter DS HMF morphology. However, p21 siRNA knockdown in DS HMFs increased the cell number and altered senescent morphologies. In all experiments, knockdown of both p16 and p21 consistently induced an increase in cell number in comparison to both siGLO and p21 siRNA knockdown alone, as well as consistently inducing further changes towards a reversal phenotype in multiple senescent morphologies, including nuclear area, cell area, nuclear elongation, and roundness, indicating that knockdown of both p16 and p21 is necessary and sufficient to induce DS fibroblasts to a reversed phenotype.

In order to determine the re-entry into the cell cycle of the reversed fibroblasts, immunostaining for BrdU incorporation was performed according to Section 2.7.1 and 2.8. In line with cell number data previously presented in this Section (Figure 3.10), DS fibroblasts transfected with p16 siRNA did not increase the proportion of cycling cells (4% ± 2%) compared to cells transfected with siGLO (1% ± 1%). Importantly, in line with previous cell number data (Figure 3.10), p21 siRNA (17% ± 6%; p=0.03) and p16+p21 siRNA (32% ± 10%; p=0.001) transfected DS HMFs had a significantly increased proportion of BrdU positive cells in comparison to the siGLO transfected DS HMF control. Furthermore, p16+p21 siRNA knockdown in DS HMFs induced an increase in BrdU incorporation greater than that observed in EP cells (15% ± 1%) (Figure 3.5). Together with the cell number data generated previously (Figure 3.10), this data further indicates that p16+p21 siRNA knockdown induced the DS HMF population to re-enter the cell cycle and proliferate.

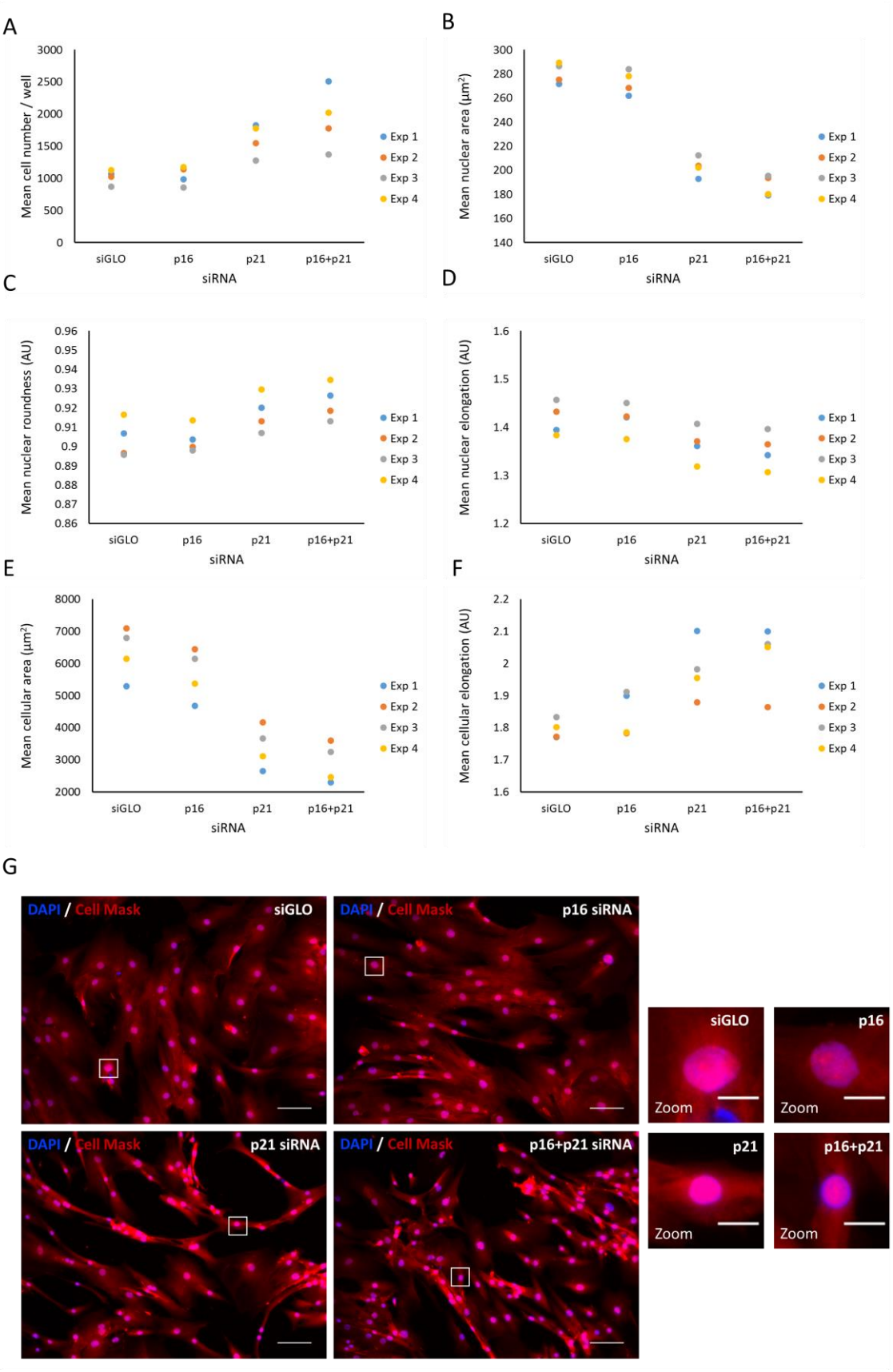

Figure 3.10 Transfection of DS fibroblasts with p16 siRNA, p21 siRNA, or p16 siRNA together with p21 siRNA. DS cells were seeded at 15,000 cells/cm^2 in 384-well plate format and forward transfected with 30 nM siGLO (siGLO), 30 nM p16 siRNA (p16), 30 nM p21 siRNA (p21), and 15

nM p16 together with 15 nM p21 siRNA (p16+p21) using 0.15 µL Dh2 according to Section 2.6.1. After five days, cells were fixed, stained with DAPI and Cell Mask, imaged, and quantified according to Sections 2.7 and 2.8. Data points denote four independent experiments (Exp 1 (blue), Exp 2 (orange), Exp 3 (grey), Exp 4 (yellow)), each performed with at least three replicates, for the following measures: **(A)** mean cell number/well, **(B)** mean nuclear area (μm^2), **(C)** mean nuclear elongation (AU), **(D)** mean nuclear roundness (AU), **(E)** mean cell area (μm^2), **(F)** mean cell elongation (AU). **(G)** Representative immunofluorescence images of siGLO, p16, p21, and p16+p21 transfected DS HMFs. DAPI (blue), Cell Mask (red). Scale bar denotes 100 µm. Right panels=digital zoom, scale bar denotes 20 µm.

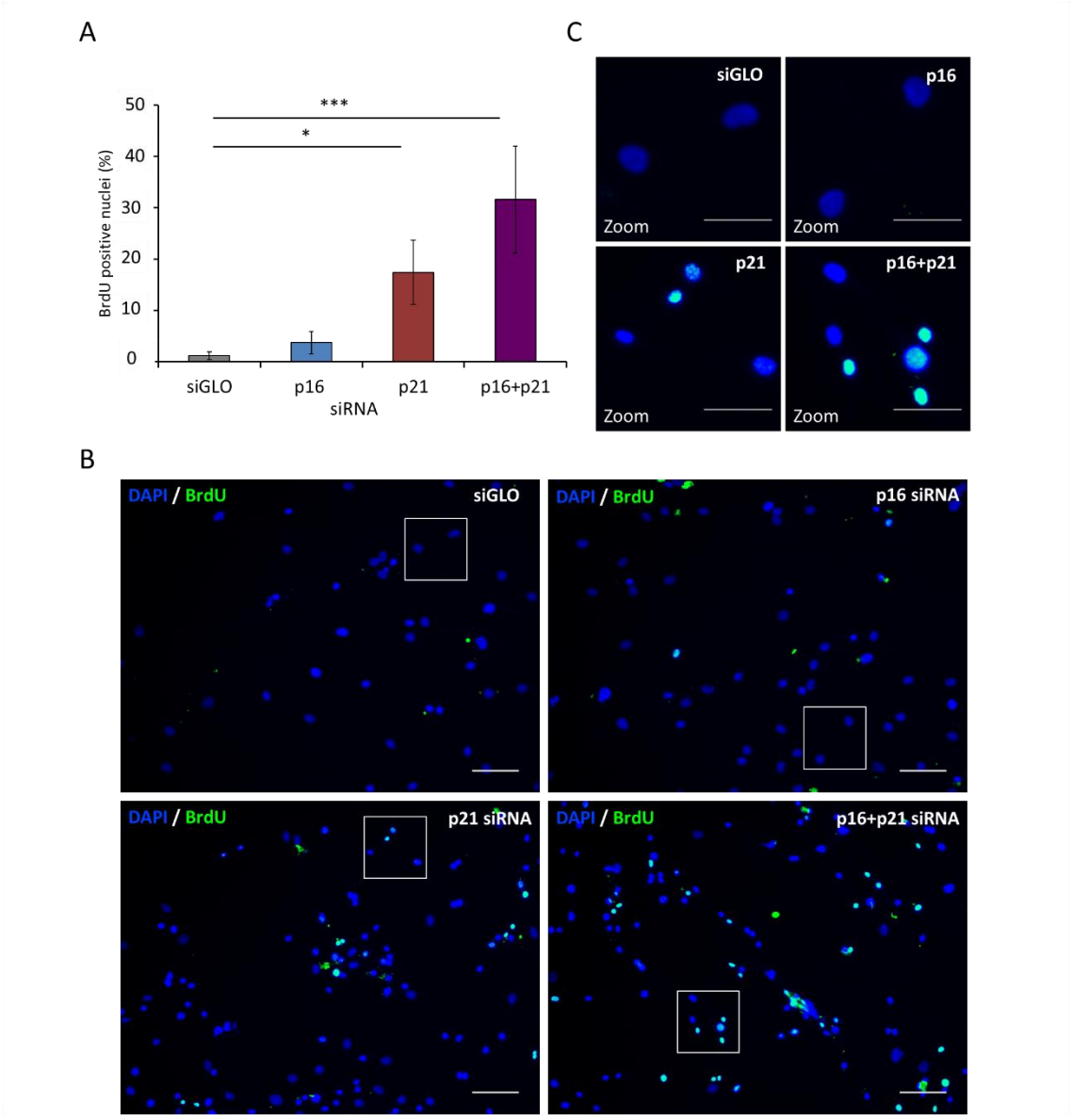

Figure 3.11 Percentage of nuclei positive for BrdU incorporation in siRNA transfected DS fibroblasts. DS cells were seeded at 15,000 cells/cm^2 in 384-well plate format and forward transfected with 30 nM siGLO (siGLO), 30 nM p16 siRNA (p16), 30 nM p21 siRNA (p21), and 15 nM p16 together with 15 nM p21 siRNA (p16+p21) using 0.15 µL Dh2 according to Section 2.6.1. After five days, cells were fixed, stained with DAPI, mouse anti-BrdU Alexa Fluor 488, and nuclear intensity was quantitated according to Section 2.7.1 and 2.8. Using the secondary only control, a nuclear intensity threshold was established to define BrdU positive or negative nuclei. **(A)** Bars denote mean percentage of BrdU positive nuclei. One-way ANOVA and Dunnett's test * $p<0.05$, *** $p<0.001$. N=3 throughout. Error bars=SD of three independent experiments, each performed with three replicates. **(B)** Representative immunofluorescence images and **(C)** digitally zoomed images of siGLO, p16, p21, and p16+p21 siRNA transfected DS HMFs. DAPI (blue), BrdU (green). Scale bar denotes 100 µm and 50 µm on zoomed images.

To further characterise the reversed phenotype, additional markers of senescence, such as p16 and p21 expression, were examined in the siRNA transfected DS population. First, p16 and p21 protein knockdown following p16 or p21 siRNA transfection in DS HMFs was assessed via western blotting. For both antibodies, western blot analysis revealed one clean band at the appropriate molecular weight (approximately 16 kilodalton (KDa) and 21 KDa) within the siGLO knockdown DS HMFs (Figure 3.12A). Importantly, quantification revealed a statistically significant reduction in p16 levels following p16 siRNA knockdown (91% ± 7%; p=0.03) and p21 levels following p21 siRNA knockdown (48% ± 5%; p=0.03) relative to the siGLO knockdown control (Figure 3.12B). Interestingly, although not statistically significant, there was a trend towards increased p16 levels following p21 siRNA knockdown and increased p21 levels following p16 siRNA knockdown, indicating a potential compensatory feedback system between these two proteins.

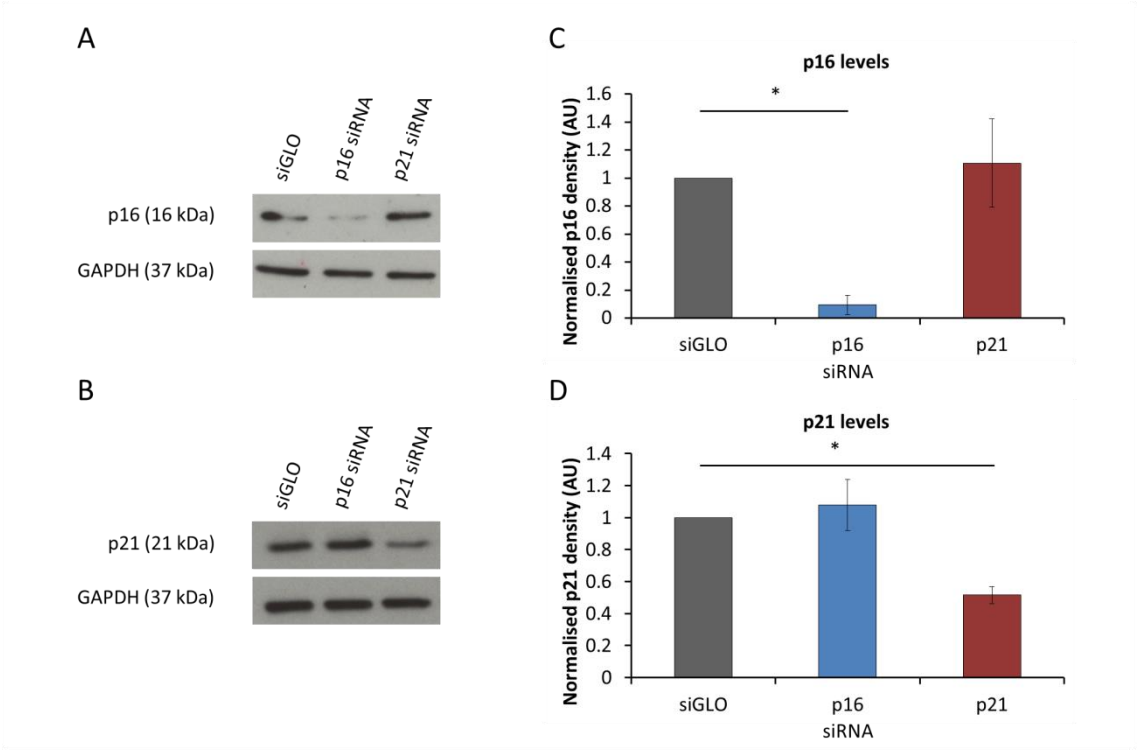

Figure 3.12 Western blot analysis of p21 and p16 levels in siGLO, p16, p21, and p16+p21 transfected DS HMFs loaded by total protein concentration. (A) Representative western blots depicting p16 and **(B)** p21 levels in 30 nM siGLO, 30 nM p16 siRNA, or 30 nM p21 siRNA transfected DS HMFs. Cell lysates were harvested for western blotting according to Section 2.4.1. Lysates were probed for rabbit anti-p21 (12D1), mouse anti-p16 (JC8), and the rabbit anti-GAPDH antibody was used as a loading control. Antibody dilutions and conditions may be found in Section 2.4.3. **(C)** Densitometry analysis of p16 and **(D)** p21 levels in transfected DS HMFs. Analysis was performed using ImageJ software. Bars denote mean density levels. One-way ANOVA and Dunnett's test * $p<0.05$. N=2 throughout. Error bars=SD normalised to GAPDH siRNA of two independent experiments.

Subsequently, p16 and p21 levels were investigated in the siGLO, p16, p21, and p16+p21 transfected DS HMFs using immunofluorescence staining according to Section 2.7 and Section 2.8. In line with the western blotting data presented previously (Figure 3.12), immunofluorescence staining showed a reduction in p16 and p21 protein levels following p16 or p21 siRNA knockdown, respectively (Figure 3.13A-B). In addition, p16 levels were increased following p21 siRNA knockdown and, to a lesser extent, p21 levels were increased following p16 siRNA knockdown in comparison to the siGLO transfected control, further suggesting the presence of a compensatory feedback loop upregulating p16 or p21, respectively, by the five day time point (Figure 3.13A-B).

Using the immunofluorescence secondary only control, thresholds for positivity were determined for p16 and p21 nuclear intensities, and the population was fractioned into four subgroups: double negative; double positive; and positive for either p16 or p21 expression. The proportion of each subgroup in the siGLO transfected DS HMFs is comparable to previous DS HMFs (Figure 3.6) and to the UTC and Dh2 only transfected DS HMF controls in this experiment (Appendix Figure A.3). In line with the finding that p16 levels decreased following p16 knockdown in DS HMFs (Figure 3.13A-B), this analysis revealed a significant increase in the p21 positive only population (59% ± 14%; p=0.0007) and significant decrease in the double positive population (35% ± 12%; p=0.0005) in the p16 siRNA transfected DS HMFs compared to the siGLO transfected cells (31% ± 10% and 64% ± 9%, respectively). In the p21 siRNA knockdown DS HMFs, the proportion of cells in the p16 positive only subgroup significantly increased (57% ± 6%; p<0.0001), the double positive subgroup significantly decreased (23% ± 2%; p<0.0001), and the p21 positive only subgroup significantly decreased (4% ± 2%; p=0.001) compared to the siGLO transfected cells (2% ± 1%, 64% ± 9%, and 31% ± 10% respectively). Interestingly, there was a trend towards an increase in the double negative subgroup of p21 siRNA transfected DS HMFs (16% ± 2%; p=0.0958) compared to the siGLO transfected DS HMFs (3% ± 0%), potentially indicating a proportion of the population which have reversed senescence upon p21 siRNA knockdown. Importantly, following knockdown of both p16 and p21 in DS HMFs, there was a significant increase in the double negative subgroup (22% ± 0%; p=0.01) in comparison to the siGLO transfected cells (3% ± 0%), indicating a significant proportion of cells in which knockdown was successful. Interestingly, the increase in the double negative subgroup

was proportional to the increase in BrdU positive cells (32% ± 10%; p=0.001) (Figure 3.11) following p16+p21 siRNA knockdown, potentially indicating that the double negative knockdown HMFs are progressing through the cell cycle at this 5 day post-knockdown time-point. Furthermore, p16+p21 siRNA knockdown in DS HMFs significantly decreased the p21 positive only subgroup (6% ± 0%; p=0.002) and significantly decreased the double positive subgroup (30% ± 1%; p=0.0001), leading to a shift towards a significantly increased p16 positive only subgroup (42% ± 2%; p=0.0001) compared to the siGLO transfected cells.

In summary, p16 siRNA knockdown alone did not increase the proportion of the double negative subgroup in DS HMFs, but p21 siRNA alone induced a trend towards an increased double negative subgroup, and p16+p21 siRNA significantly increased the proportion of the double negative subgroup. This suggests that p16 or p21 siRNA alone was not sufficient to significantly increase the proportion of reversed, double negative cells in the population, but that knockdown of both p16 and p21 together functions co-ordinately to significantly increase the proportion of the double negative knockdown cells. Therefore, the data generated here indicates that p16+p21 siRNA double knockdown is required for significant knockdown of p16 and p21 in the population.

Levels of oxidative damage were also investigated for the siRNA transfected DS HMFs according to Sections 2.7 and 2.8. Using this approach, the proportion of cells positive for 8-oxoG did not significantly change following p16 siRNA knockdown (84% ± 2%) compared to the siGLO transfected cells (89% ± 1%) (Figure 3.14). However, the percentage of 8-oxoG positive cells in the p21 siRNA transfected DS HMFs and p16+p21 siRNA transfected DS HMFs (62% ± 7% and 55% ± 10%, respectively) decreased significantly compared to siGLO transfected DS HMFs (p=0.02 and p=0.01, respectively). In addition, further investigation of the 8-oxoG positive subpopulation revealed a decrease in 8-oxoG cellular density in the p21 and p16+p21 siRNA transfected cells compared to the siGLO transfected DS HMFs (Figure 3.14B). Together, these data indicate a decrease in oxidative damage upon p16 and p21 knockdown in DS HMFs.

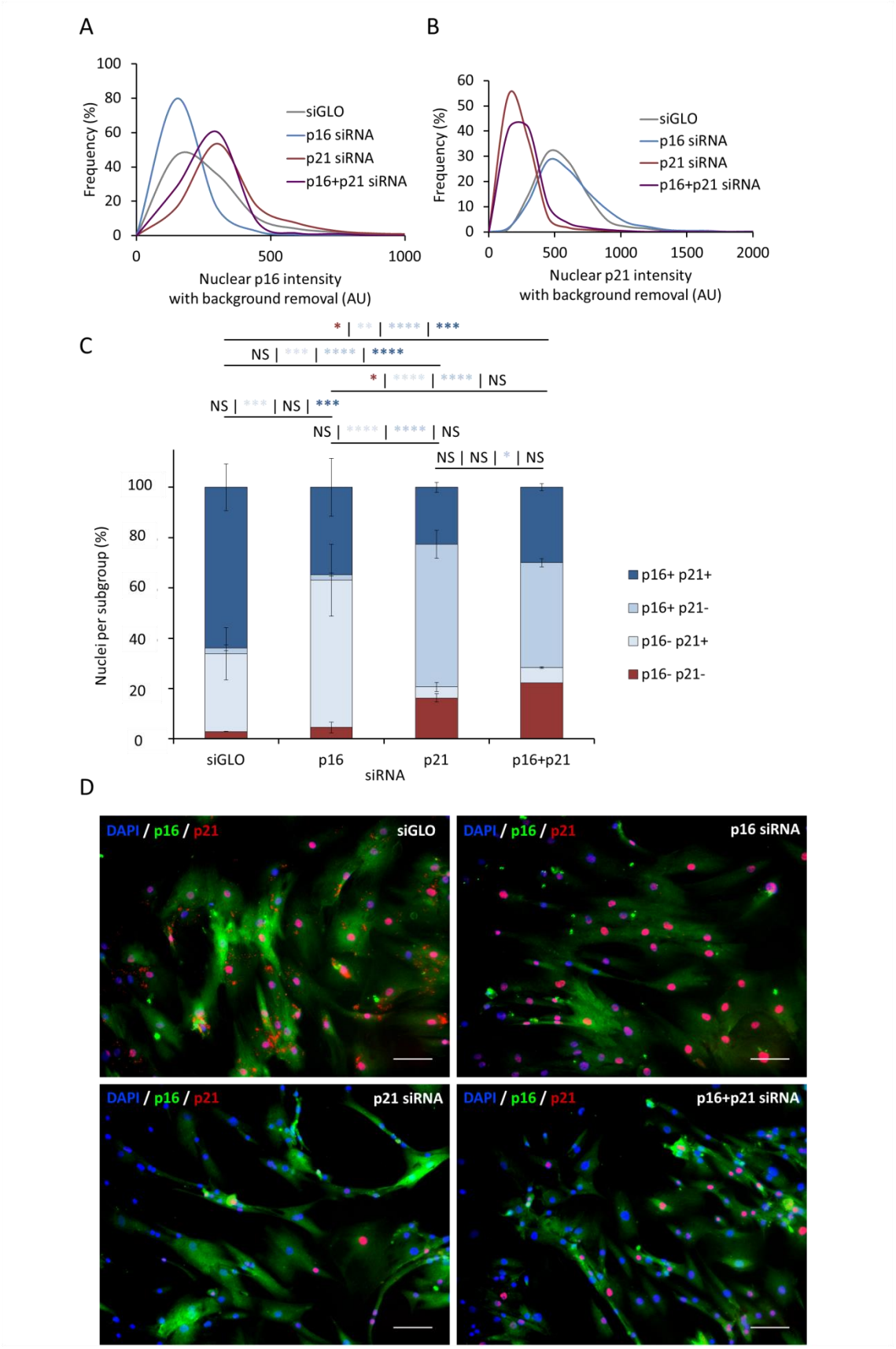

Figure 3.13 p16 and p21 expression in siRNA transfected DS fibroblasts. DS cells were seeded at 15,000 cells/cm^2 in 384-well plate format and forward transfected with 30 nM siGLO (siGLO), 30 nM p16 siRNA (p16), 30 nM p21 siRNA (p21), or 15 nM p16 together with 15 nM p21 siRNA

(p16+p21) using 0.15 µL Dh2 according to Section 2.6.1. Cells were fixed at day five, stained with DAPI, mouse anti-p16 (JC8), rabbit anti-p21 (12D1), donkey anti-mouse Alexa Fluor 488, and goat anti-rabbit Alexa Fluor 546, and nuclear intensities were quantitated according to Section 2.7 and 2.8. **(A)** Representative frequency distribution of nuclear p16 intensities after background removal in siGLO, p16, p21, and p16+p21 siRNA transfected HMFs. **(B)** Representative frequency distribution of nuclear p21 intensities after background removal in siGLO, p16, p21, and p16+p21 siRNA transfected HMFs. **(C)** Nuclear intensity thresholds were established for p16 and p21 to define positive or negative nuclei. Nuclei were classified into four subgroups: p16 and p21 positive (p16+ p21+); p16 positive and p21 negative (p16+ p21-); p16 negative and p21 positive (p16- p21+); and p16 and p21 negative (p16- p21-). Bars denote mean percentage of nuclei per subgroup. Two-way ANOVA and Tukey's test * $p<0.05$, ** $p<0.01$, *** $p<0.001$, **** $p<0.0001$. NS=not significant. Significance colours match nuclei subgroup and are ordered left to right in the following order: p16- p21-; p16- p21+; p16+ p21-; p16+ p21+. N=2 throughout. Error bars=SD of two independent experiments, each performed with three replicates. **(D)** Representative immunofluorescence images of siGLO, p16, p21, and p16+p21 siRNA transfected DS HMFs. DAPI (blue), p16 (green), p21 (red). Scale bar denotes 100 µm.

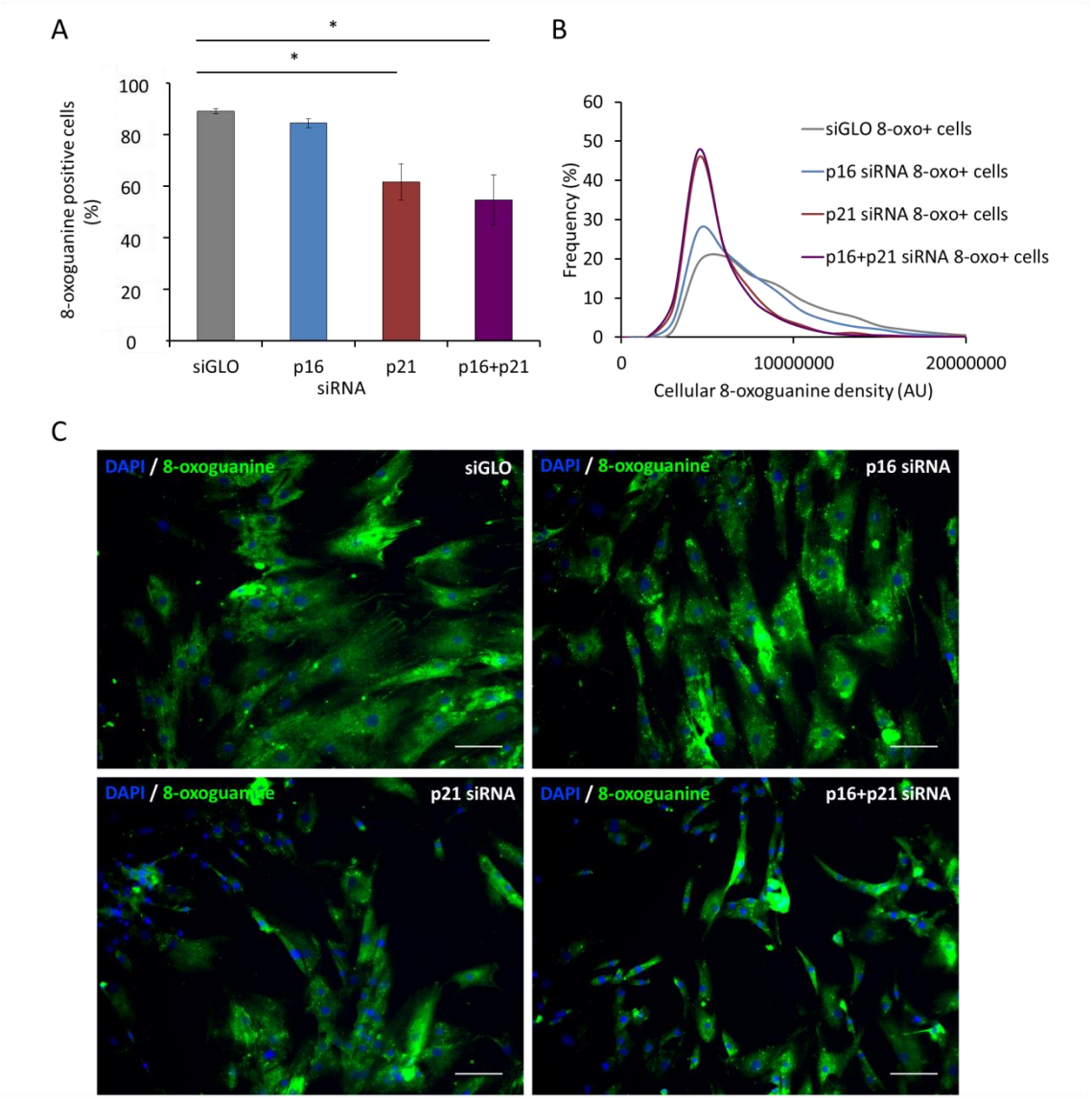

Figure 3.14 Percentage of cells positive for 8-oxoG in siRNA transfected DS fibroblasts. DS cells were seeded at 15,000 cells/cm^2 in 384-well plate format and forward transfected with 30 nM siGLO (siGLO), 30 nM p16 siRNA (p16), 30 nM p21 siRNA (p21), or 15 nM p16 together with 15 nM p21 siRNA (p16+p21) using 0.15 µL Dh2 according to Section 2.6.1. After five days, cells were fixed, stained with DAPI, mouse anti-8-oxoG, donkey anti-mouse Alexa Fluor 488, and 8-oxoG cellular density was quantitated according to Section 2.7 and Section 2.8. A cellular density threshold was established to define 8-oxoG positive or negative cells. **(A)** Bars denote mean percentage of 8-oxoG positive cells. One-way ANOVA and Dunnett's test * $p<0.05$. N=2 throughout. Error bars=SD of two independent experiments, each performed with three replicates. **(B)** Representative frequency distribution of cellular 8-oxoG density in siGLO, p16, p21, and p16+p21 siRNA transfected 8-oxoG positive HMFs. **(C)** Representative immunofluorescence images of siGLO, p16, p21, and p16+p21 transfected DS HMFs. DAPI (blue), 8-oxoG (green). Scale bar denotes 100 µm.

3.3.3 Identification of membrane stiffness as a novel potential marker of senescence

Recent evidence has suggested that dermal fibroblasts (Kim *et al.*, 2015) and epithelial cells (Berdyyeva, Woodworth and Sokolov, 2005) exhibit increasing membrane stiffness *in vitro* during serial passaging. In addition, dermal fibroblasts isolated from healthy older donors have been shown to exhibit increased membrane stiffness *ex vivo* (Schulze *et al.*, 2012). However, the relationship between cell membrane stiffness and senescence remains currently unexplored. To investigate the relationship between cell membrane stiffness and senescence, SICM was used to map the topography and stiffness of EP, DS, and reversed HMF membranes at high resolution according to Section 2.9 (Appendix Figure A.10). This work was performed in collaboration with BSc and MSc students within Dr Pavel Novak's lab., and part of this work formed the basis of a manuscript recently published in Soft Matter (Clarke *et al.*, 2016). Analysis of Young's modulus, a measure of the stiffness of a solid material, showed that DS fibroblasts had significantly stiffer membranes (6,311 ± 2,214 Pa; p=0.05) than EP HMFs (2,916 ± 2,465 Pa), and that p16 and p21 double knockdown enabled reversal of the membrane to a stiffness similar to that of EP HMFs and significantly softer than DS HMFs (3,132 ± 1,737 Pa; p=0.05), potentially revealing membrane stiffness as a novel marker of senescence.

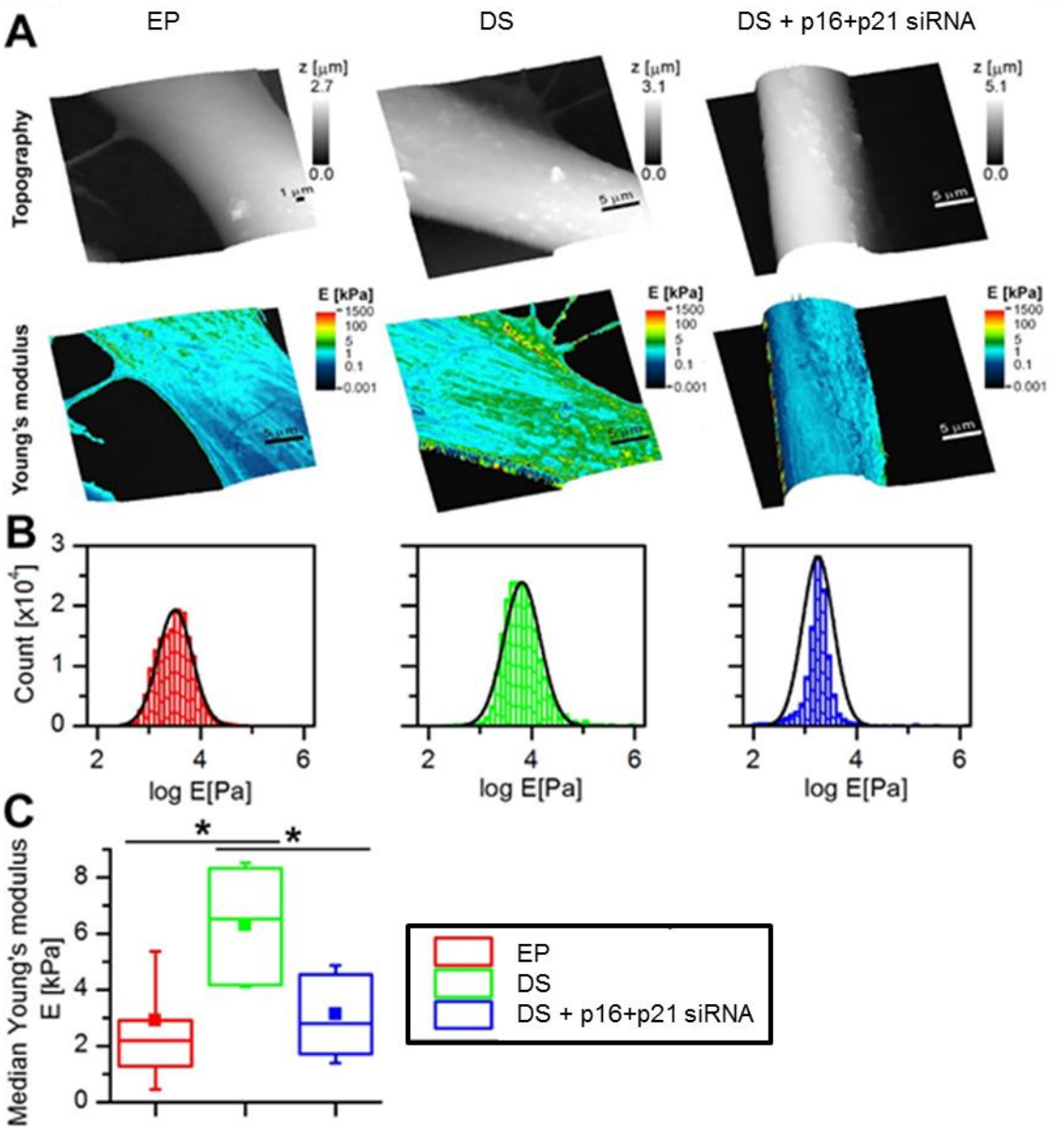

Figure 3.15 High resolution mapping of EP, DS, and reversed HMF membranes using scanning ion conductance microscopy. (A) Representative images of the topography and Young's modulus of EP, DS, and DS HMFS transfected with 15 nM p16 and 15 nM p21 (p16+p21) siRNA HMFs. **(B)** Distribution of local Young's modulus E in the EP (left), DS (middle), and DS HMF transfected with p16+p21 siRNA (right). **(C)** The mean of median Young's moduli of DS cells (N=6) is significantly different from both the EP (N=17) and DS cells transfected with p16+p21 siRNA (N=22). One-way ANOVA and Tukey's test * $p<0.05$. The data displayed within this figure was generated in collaboration with Ashna Gopal, Devesh Dillum, Jeswy Thankam Shaji, and Ho Ting Au, BSc and MSc students within Dr Pavel Novak's lab.

3.4 Discussion and future work

3.4.1 Validation and characterisation of the DS HMF phenotype

Within this Chapter, a model of fibroblast replicative senescence was established by serially passaging EP HMFs to deep senescence. Recent literature has suggested that senescence is a dynamic, multi-step process through which senescent cells continue to evolve during extended periods in culture (Freund *et al.*, 2012; De Cecco *et al.*, 2013; Shah *et al.*, 2013; Swanson *et al.*, 2013, Kim *et al.*, 2013) (see Section 1.2). In order to ensure that the senescent population had progressed into a permanent senescence phenotype from an initial senescence arrest, fibroblasts were passaged to replicative senescence then kept in culture for three weeks further to the state defined here as 'deep senescence'. Furthermore, DS fibroblasts kept in culture for 150 days beyond replicative senescence remained stably arrested, demonstrating the development of a permanent senescence phenotype (Figure 3.2). Subsequently, the EP and DS phenotypes were characterised using morphological multi-parameter analysis as well as immunofluorescence staining for multiple well-established senescence markers. This analysis identified a panel of senescence-associated markers which validated and defined the DS phenotype, enabling subsequent experiments to identify changes to the DS phenotype induced by siRNA knockdown.

In summary, the DS phenotype includes a stable cell cycle arrest, characterised by both a stable cell number (see Section 3.2.2) and a lack of BrdU incorporation (see Section 3.2.3). In line with the literature, DS fibroblasts possessed an enlarged nucleus with an elongated and less round nuclear morphology, as well as an enlarged and less elongated cellular morphology (see Section 3.2.2) (Sharpless and Sherr, 2015). In addition, DS fibroblasts displayed an increased expression of the tumour suppressors, p16 and p21, indicating activation of the p16/pRB and p53/p21 pathways (see Section 3.2.3) (Alcorta *et al.*, 1996). Furthermore, DS fibroblasts accumulated the products of oxidative DNA damage as characterised by an increase in 8-oxoG (see Section 3.2.3) (Chen *et al.*, 1995).

Further markers of the senescence phenotype were also investigated (see Section 1.4). DS fibroblasts induced paracrine senescence in EP fibroblasts (Figure 3.8) (work performed by an MSc student, AR under supervision of ET), indicating the presence of the SASP (Acosta *et al.*, 2013). Furthermore, DS fibroblasts have decreased lamin B1

expression in comparison to EP cells (Appendix Figure A.2), indicating deepening of the senescence phenotype (Freund *et al.*, 2012). In the future, it would be interesting to explore the DS phenotype further, including investigating telomere length using qRTPCR; the presence of telomere associated foci (TAF) using confocal microscopy (Hewitt *et al.*, 2012), and telomerase activity using the telomeric repeat amplification protocol (TRAP) assay. In addition, DDR markers such as 53BP1 or γ-H2AX; and the presence of SASP components, such as IL-6 and IL-8, could be explored using immunofluorescence microscopy. Furthermore, enzyme-linked immunosorbent assay (ELISA) or Luminex-based assays could be used to detect secretion of SASP components into the surrounding medium. In addition, replicatively senescent fibroblasts possess extensive changes to DNA methylation in comparison with proliferating cells (Cruickshanks *et al.*, 2013). To investigate DNA methylation dynamics between EP and DS fibroblasts and define a senescence-associated methylation signature in these cells, an Illumina EPIC array could be performed to assess methylation at >900,000 different cytosine residues.

3.4.2 siRNA transfection targeting p16 and p21 reverses deep senescence in normal adult HMFs

Fibroblast replicative senescence is commonly referred to as an irreversible cell cycle arrest in the literature. Previous work has demonstrated that knockdown of p53 in senescent human neonatal fibroblasts reinitiates DNA synthesis but with only limited proliferation (Gire and Wynford-Thomas, 1998) (see Section 1.7). In addition, Beauséjour *et al*. (2003) demonstrated that the reversibility of fibroblast senescence was dependent on their p16 expression levels. For example, senescent BJ fibroblasts (neonatal foreskin), which had low levels of p16 expression, were reversible by inactivating pRB or p53, but senescent WI38 fibroblasts (foetal lung), with higher p16 expression levels, were not. In order to further explore the p16 reversal block, Beauséjour *et al*. (2003) inactivated p53 in senescent WI38 cells following p16 knockdown, and found that DNA synthesis was stimulated but not proliferation, leading the authors to suggest that neither p53 nor pRB inactivation is sufficient to allow cell proliferation once the p16/pRB pathway is engaged.

As the previous work on senescence reversal in human cells has been performed on fibroblasts derived from foetal or neonatal tissues, it is important to note that recent

evidence has suggested that during normal embryonic development, cells undergo acute senescence via a different mechanism to cells which undergo age-related chronic senescence (Muñoz-Espín *et al.*, 2013; Storer *et al.*, 2013) (see Section 1.5.2). Ultimately, the aim of this project is to further our understanding of the drivers of age-related chronic senescence, thus, adult DS HMFs were used throughout this project.

Previous work in our lab. has demonstrated that p16 siRNA knockdown in DS HMECs reverses p16-dependent cellular senescence (Lowe *et al.*, 2015). Given this, it was hypothesised in this Chapter that reversal of p16- and p21-dependent replicative senescence would require knockdown of p16 and p21 together in DS HMFs. In support of this hypothesis, p16 siRNA knockdown alone in DS HMFs did not increase cell number or alter the senescence markers examined in this Chapter (see Section 3.3.2, Figure 3.10). Interestingly, p21 siRNA knockdown in DS HMFs consistently increased cell number and altered morphological markers which defined the DS phenotype (see Section 3.3.2, Figure 3.10). However, in comparison to p21 siRNA transfected DS HMFs, knockdown of both p16 and p21 together further increased cell number and altered four morphological markers of senescence, including decreased nuclear and cellular area, decreased nuclear elongation and increased nuclear roundness (see Section 3.3.2, Figure 3.10). Further investigation of the siRNA transfected DS HMFs revealed that BrdU incorporation was significantly increased in the p21 siRNA knockdown DS HMFs, and further significantly increased in the p16+p21 siRNA knockdown DS HMFs compared to the siGLO transfected DS HMFs, indicating the presence of cycling cells in the population (see Section 3.3.2, Figure 3.11). Strikingly, BrdU incorporation in the p16+p21 siRNA knockdown DS HMFs was higher than in the EP population, potentially as a result of an increased number of cells entering the cell cycle at the same time due to synchronisation of cell cycle re-entry in the p16+p21 siRNA transfected DS population. Examination of p16 and p21 levels revealed that only p16+p21 siRNA knockdown significantly increased the proportion of the double negative subgroup in the DS population compared to siGLO transfected cells, indicating a potential subpopulation of reversed cells (see Section 3.3.2, Figure 3.13). Furthermore, investigation of 8-oxoG revealed that the percentage of cells positive for 8-oxoG significantly decreased in p21 siRNA and further significantly decreased in p16+p21 siRNA knockdown DS HMFs compared to siGLO transfected cells, indicating that oxidative damage levels were also reduced following siRNA knockdown

(see Section 3.3.2, Figure 3.14A). Further interrogation revealed that the p21 siRNA and p16+p21 siRNA knockdown DS HMFs defined as positive for 8-oxoG possessed lower levels of 8-oxoG than the 8-oxo+ siGLO transfected DS HMFs, providing further confirmation that oxidative damage levels were reduced upon reversal (see Section 3.3.2, Figure 3.14B). Taken together, these findings indicate that knockdown of both p16 and p21 in adult DS HMFs is necessary to reverse deep senescence. In addition, a novel marker of senescence, membrane stiffness, was identified in this Chapter, which further confirmed the p16+p21 siRNA knockdown DS HMF reversed phenotype (see Section 3.3.3). In future, it would be interesting to determine whether membrane stiffness is a universal feature of senescence and determine whether membrane stiffening plays a role driving senescence. This is explored in more detail in Chapter 6 Section 6.1.3.

Interestingly, p16 and p21 levels were identified to increase following knockdown of p21 or p16 in DS HMFs, respectively, indicating the presence of a potential compensatory feedback mechanism. To explore the kinetics of this potential compensatory mechanism, a time course experiment could be performed to explore p16 and p21 levels using immunofluorescence at one, three, and five days post-transfection. Interestingly, previous evidence has suggested that p16 transcription may be regulated by a negative feedback loop via pRB (Hara *et al.*, 1996). In order to explore the presence of this pRB-dependent negative feedback mechanism in DS HMFs, it would be interesting to determine whether pRB siRNA knockdown prevents p21 or p16 overexpression following p16 or p21 siRNA knockdown, respectively.

To further validate the reversed phenotype of the p16+p21 siRNA transfected DS HMFs, analysis of the p16+p21 knockdown DS HMF phenotype could be expanded to encompass other markers, including telomere length, DDR markers 53BP1 or γ-H2AX, and SASP components, such as IL-6 and IL-8, as described in Section 3.4.1 and explored in more detail in Chapter 6 Section 6.1.1. Furthermore, previous work in our lab. has defined senescence-associated differentially methylated positions (senDMPs) in DS HMECs relative to EP cells, and demonstrated that reversal of senescence in DS HMECs using p16 siRNA knockdown effectively reversed the senDMP signature (Lowe *et al.*, 2015). In order to further validate the reversed DS fibroblast phenotype, the methylation dynamics following p16+p21 siRNA transfection in DS HMFs could be examined and compared to the EP and DS HMF methylation signatures. Importantly, the

senescence-associated methylation signature has been associated with bypass of senescence, a process which is potentially required for tumour progression to malignancy (Cruickshanks *et al.*, 2013). Thus, investigation of the p16+p21 siRNA transfected DS HMF methylation signature in comparison to EP and DS HMFs would further test whether p16+p21 siRNA knockdown induces reversal of senescence, and this is discussed in more detail in Chapter 6 Section 6.1.2.

Given the previous work on senescence reversal performed in foetal and neonatal fibroblasts (Gire and Wynford-Thomas, 1998; Beauséjour *et al.*, 2003) (see Section 1.7), future analysis could be expanded to encompass reversal of senescence in other primary cells, including foetal and neonatal fibroblasts. Narita *et al*. (2003) previously noted that SAHF formation is less pronounced in senescent BJ fibroblasts than senescent WI38 cells, leading the authors to suggest that the presence of SAHF indicates an irreversible cell cycle arrest. Consistent with this hypothesis, the DS fibroblasts used throughout this project did not display SAHF (see Section 3.2.2). However, the authors also noted that SAHF-forming senescent WI38 fibroblasts had increased p16 expression in comparison to senescent BJ fibroblasts, implying that p16 up-regulation induces SAHF formation, thus altering chromatin structure and enforcing permanent arrest. The DS fibroblasts used in this project exhibited robust p16 expression (see Section 3.2.3) and remained arrested for over 150 days in culture (see Section 3.2.1), indicating a stable and permanent cell cycle arrest despite the lack of SAHF formation. In light of this, it would be of interest to investigate whether senescence reversal is also achievable in WI38 fibroblasts. It would also be of interest to explore senescence reversal in HMFs which have undergone senescence in response to alternative triggers including OIS and SIPS (see Section 1.3.2).

In summary, the data presented in this Chapter has demonstrated for the first time that deep senescence can be effectively reversed in normal adult HMFs using siRNA transfection targeting p16 and p21 (see Section 3.3.2). The successful reversal of deep senescence in adult HMFs subsequently provided the opportunity to screen novel siRNAs that induce reversal in both DS HMECs and DS HMFs, as will be explored in Chapter 4.

Chapter 4 siRNA screening to identify unknown drivers of senescence in fibroblasts

4.1 Introduction

In this Chapter, siRNA screening in DS HMFs will be employed as a route to identifying novel genes driving the senescent phenotype. Our lab. has previously shown that reversal of cellular senescence in DS HMECs is achievable using p16 siRNA knockdown (Lowe *et al.*, 2015) (Figure 4.1A) (see Section 1.7). Using gene expression arrays, previous work identified genes with expression changes between EP, DS, and reversed DS HMECs (Bishop, unpublished). In order to distinguish between genes driving the senescent phenotype and downstream 'passenger' genes, a siRNA screen of the top 200 genes identified to have increased expression in DS HMECs compared to the EP and reversed cells was previously performed in the DS HMECs (see schematic in Figure 4.1B). From this, 28 siRNAs were identified to strongly induce reversal in the DS HMECs, as defined by the loss of a panel of senescence markers, including reduced cellular area and nuclear area, and the resumption of the cell cycle (as measured by increased cell number). Accordingly, these 28 genes were classified as potential 'drivers' of senescence in DS HMECs.

Unlike replicative senescence in fibroblasts, HMECs undergo p16-dependent cellular senescence in the absence of telomere erosion and p53/p21 expression. In order to determine whether genes driving cellular senescence in HMECs also play a role in driving replicative senescence in other cell types, siRNA screening in DS HMFs will be employed in this Chapter. Ultimately, by identifying genes that enable senescence reversal in both HMECs and HMFs, this project aims to discover novel drivers of senescence in humans.

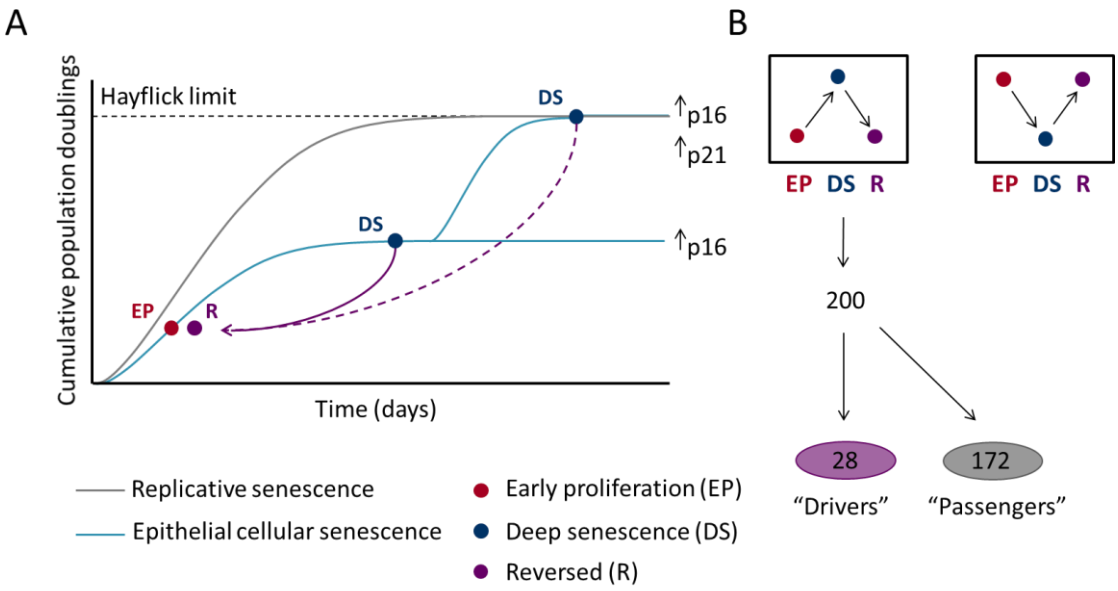

Figure 4.1 Schematic of senescence reversal strategy in both HMECs and HMFs, and mRNA expression profiling as a route to identifying new 'drivers' of senescence. (A) Our lab. has previously achieved reversal of p16-dependent epithelial cellular senescence (blue line) using siRNA targeting p16 in DS HMECs. **(B)** mRNA microarray data identified genes with expression changes between early proliferating (EP, red), deep senescence (DS, blue), and reversed (R, purple) HMECs. The top 200 genes with increased expression in the DS versus the EP and reversed HMECs were investigated in a siRNA screen, and 28 siRNAs were identified to strongly induce reversal in DS HMECs. These 28 hits are classified as potential 'drivers' of senescence (purple).

4.1.1 Chapter aims

1. To use bioinformatics to construct an interaction network between the 28 previously identified drivers of senescence in HMECs (including p16) in order to expand the pool of genes to be screened in the adult DS HMFs.
2. To perform a siRNA screen of 60 siRNAs in adult DS HMFs comprising the 27 siRNAs (i.e. the 28 drivers not including p16) identified to strongly induce reversal in adult DS HMECs and 33 siRNAs targeting interactors identified through bioinformatics, in order to identify novel drivers of senescence in both cell types.
3. To conduct multi-parameter analysis of top hits selected from the siRNA screen in order to explore the reversal phenotypes in more detail and to select a candidate for validation and further investigation.

4.2 Bioinformatics interaction network of previously identified hits

To investigate the potential relationships between the 28 previously identified drivers and to expand the pool of genes to be screened in the DS HMFs, a bioinformatics interaction network was constructed. In summary, each of the 28 hits was probed for protein interactors using the BioGRID database (http://www.thebiogrid.org) in order to generate protein interaction datasets (see Section 2.10). The hit protein interaction datasets were then overlaid to reveal a total of 33 protein interactors, which were defined as proteins which generated a chain with at least two other drivers. Using this method, only one protein interaction network was generated (Figure 4.2). Of the 28 previously identified drivers, 13 were not found to be present in this stringently generated network.

To further explore the relationships between drivers and interactors, a less stringent interaction network was built using GeneMANIA, a bioinformatics database with genomic and proteomic data collated from a variety of sources, including co-expression data, genetic interactions, co-localisation, predicted interactions, pathways, and shared protein domains. Remarkably, using these criteria, the network identified interactions between all of the drivers and interactors except for one driver, zona pellucida-like domain containing 1 (ZPLD1), an understudied gene for which there are only six citations in NCBI PubMed (Appendix Figure A.4).

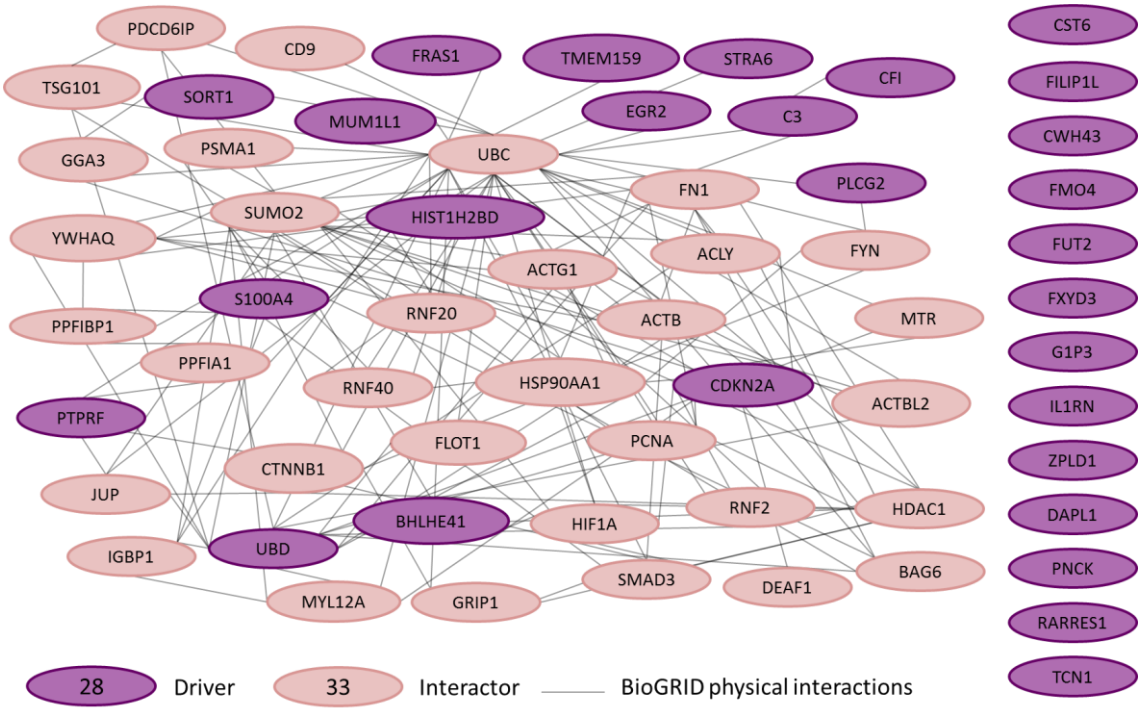

Figure 4.2 Protein interaction network of drivers and interactors. Twenty-eight potential drivers of senescence (purple) were identified in the previous DS HMEC screen. Using bioinformatics, 33 interactors (pink) were identified to generate a chain with at least two other drivers. Lines represent physical interactions determined by the BioGRID database. Thirteen drivers were not found to be present in this network (listed on right).

It is important to note that ubiquitin C (UBC), a highly-connected protein in the BioGRID database (1,435 interactors), has the potential to create false positive connections in a bioinformatics network. In order to ensure that the previous interactors were not falsely identified, UBC was removed and the protein interaction network regenerated. Using BioGRID physical interactions as the most stringent criteria to identify interactors, one interactor, known as CD9 molecule (CD9) was lost from the re-generated interaction network (Appendix Figure A.5). However, a re-generated interaction network using GeneMANIA demonstrated that CD9 remains present in the network through both co-expression and co-localisation relationships with multiple drivers and interactors (Appendix Figure A.6). In summary, the removal of the highly-connected protein UBC from the network does not cause the loss of previously identified interactors, except CD9, which remains present in the less stringently generated GeneMANIA network.

4.2.1 Pathway analysis identifies functional categories of hits and interactors

Using Panther, KEGG pathways, and Gene Ontology (GO) bioinformatics tools, these 61 genes (28 previously identified drivers (including p16) and 33 interactors) were grouped into six functional categories: immune response; cell adhesion/cytoskeleton; metabolism; transcription; growth/proliferation; and protein/vesicle trafficking (Figure 4.3). Strikingly, the cell adhesion/cytoskeleton subgroup contained the largest number of proteins (four drivers and 12 interactors), indicating a potential role for extracellular interactions in driving senescence. The metabolism subgroup contained the second largest number of proteins (seven drivers and two interactors) and, perhaps unsurprisingly, the growth/proliferation subgroup contained the third largest number of proteins (one driver, CDKN2A (p16), and six interactors). Interestingly, the six main functional categories identified here showed overlap with the spectrum of cell processes altered during human ageing (immunity, focal adhesion/cytoskeleton, metabolism, and cell cycle) (Peters *et al*. 2015).

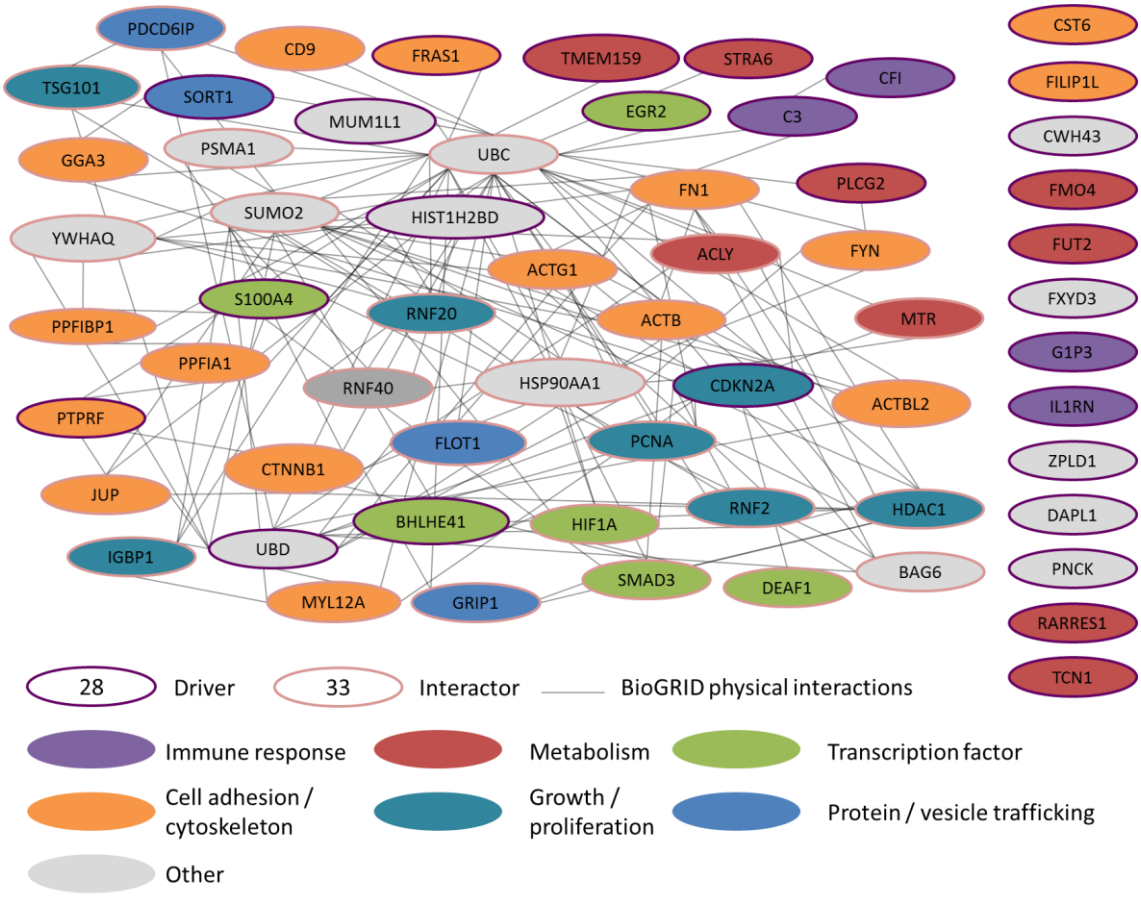

Figure 4.3 Functional subgrouping of protein interaction network. Using PANTHER, KEGG pathways, and GO bioinformatics tools, potential drivers (outlined in purple) and interactors (outlined in pink) were subgrouped into functional categories: immune response (purple), metabolism (red), transcription factor (green), cell adhesion/cytoskeleton (orange), growth/proliferation (teal), protein/vesicle trafficking (blue), other (grey). Lines represent BioGRID physical interactions.

4.3 siRNA screening to identify unknown drivers of senescence in adult DS HMFs

4.3.1 Identification of 45 hits for senescence reversal in DS HMFs

In the DS HMEC screen, p16 siRNA was amongst the 28 'driver' siRNAs identified to reverse HMEC p16-dependent cellular senescence (Lowe *et al.*, 2015). However, in DS HMFs, p16 siRNA alone was found to not be sufficient to reverse replicative senescence (see Section 3.3.2). With this in mind, p16 siRNA was not included as a target siRNA in the DS HMF screen, bringing the total number to 60 target siRNAs (27 drivers and 33 interactors). Furthermore, as DS HMF reversal was found to require siRNA knockdown of both p16 and p21 (see Section 3.3.2), it was hypothesised that the hits identified in the DS HMEC screen may additionally require knockdown of either the p16/pRB or the p53/p21 pathway to induce reversal in the DS HMFs. Accordingly, DS HMFs were screened with 60 target siRNAs in three conditions: 30 nM siRNA individually (Group 1); 15 nM siRNA in combination with 15 nM p16 siRNA (Group 2); or 15 nM siRNA in combination with 15 nM p21 siRNA (Group 3) (Figure 4.3).

To perform the siRNA screen, DS fibroblasts were seeded at a previously optimised seeding density of 15,000 cells/cm^2 (see Section 2.5.2) and forward transfected with 30 nM siRNA according to the above listed conditions (Group 1, 2, and 3) using the previously optimised dose of 0.15 µL Dh2 (see Section 2.6.2). After five days, cells were stained with DAPI and cell number quantified according to Section 2.7 and 2.8.

There was no significant change in proliferation for DS fibroblasts transfected with siGLO compared with the UTC DS HMF control, indicating an acceptable level of siRNA transfection cytotoxcity in the experiment (Appendix Figure A.3). As such, the data generated by the siGLO transfected control was used as a baseline for Z score generation (see Section 2.8.2) in order to determine the effects on proliferation of each of the 60 siRNAs in each of the three conditions.

Using this approach, a hit list was generated for each of the three conditions. In order to increase the window for hit detection and allow as many hits to be identified as possible, significance was defined as at least one Z score greater than the respective

A

Drivers		Interactors	
BHLHE41	ZPLD1	ACLY	JUP
C3	TMEM159	ACTB	MTR
CDKN2A	DAPL1	ACTBL2	MYL12A
CST6	PLCG2	ACTG1	PCNA
FILIP1L	PNCK	BAG6	PDCD6IP
EGR2	PTPRF	CD9	PPFIA1
STRA6	RARRES1	CTNNB1	PPFIBP1
CWH43	S100A4	DEAF1	PSMA1
MUM1L1	SORT1	FLOT1	RNF2
FMO4	TCN1	FN1	RNF20
FRAS1	UBD	FYN	RNF40
FUT2		GGA1	SMAD3
FXYD3		GRIP1	SUMO2
G1P3		HDAC1	TSG101
HIST1H2BD		HIF1A	UBC
CFI		HSP90AA1	YWHAQ
IL1RN		IGBP1	

B

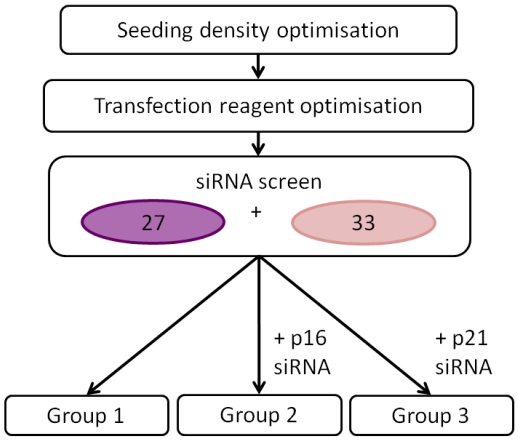

Figure 4.4 Gene list and siRNA screening workflow. (A) In the DS HMF screen, the following gene lists were investigated: 27 drivers (purple; 28 minus p16 siRNA) identified to reverse senescence in a previous DS HMEC siRNA screen, and 33 interactors (pink) identified using bioinformatics. **(B)** Schematic illustrating the experimental design of the siRNA screen. Using a previously optimised seeding density and transfection reagent dose (see Section 2.6.2), DS HMFs were forward transfected with the 60 target siRNAs in three conditions: 30 nM siRNA individually (Group 1); 15 nM siRNA in combination with 15 nM siRNA (Group 2); and 15 nM siRNA in combination with p21 siRNA (Group 3).

control for each condition (see Section 2.8.2). DS HMFs transfected with Group 1 (siRNAs individually) were compared to 30 nM siGLO control; Group 2 (siRNAs in combination with p16 siRNA) were compared to 30 nM p16 siRNA control; and Group 3 (siRNAs in combination with p21 siRNA) were compared to cells transfected with 30 nM p21 siRNA (Figure 4.4).

Using this hit identification criteria, only one Group 1 member (30 nM siRNA individually) was defined as a hit (one Z score), which was early growth response 2 (EGR2), a transcription factor involved in several cellular processes, including cell cycle and proliferation (Parkinson *et al.*, 2004; Atanasoski *et al.*, 2006; Srinivasan *et al.*, 2012) (Figure 4.4). Interestingly, the identification of a siRNA which did not require additional knockdown of p16 or p21 potentially indicates a hit which is essential for driving senescence upstream of both the p16/pRB and p53/p21 pathways. Two Group 2 siRNAs (in combination with p16 siRNA), fraser extracellular matrix complex subunit 1 (FRAS1),

an extracellular matrix protein, and ring finger protein 20 (RNF20), an E3 ubiquitin ligase, were defined as hits (one Z score) (Figure 4.4). Potentially, this may indicate that these hits sit upstream of the p53/p21 pathway and interact with the p16/pRB pathway to drive senescence. Importantly, FRAS1 is a driver identified to reverse p16-dependent HMEC cellular senescence, suggesting a role for FRAS1 upstream of the p16/pRB pathway in HMECs and potentially upstream of p53/p21 in the DS HMFs. This may indicate an interplay between the p16/pRB and p21/p53 pathways which is dictated in a cell-type dependent manner. Remarkably, 45 of the 60 siRNAs in Group 3 (in combination with p21 siRNA) were defined as hits (Figure 4.4). Of these, eight Group 3 siRNAs increased cell number greater than 10 Z scores, including EGR2, basic helix-loop-helix family member e41 (BHLHE41), fibronectin (FN1), and actin gamma 1 (ACTG1) siRNA, similar to the p16+p21 reversed HMFs (12 Z scores). As the 28 'driver' siRNAs in the screen were identified as hits for senescence reversal in p16-dependent HMEC cellular senescence, it is perhaps unsurprising that 21 of these were identified as hits requiring additional knockdown of the p53/p21 pathway to reverse senescence in DS HMFs, thus indicating potential roles for these genes upstream of the p16/pRB pathway. However, 24 of the 33 'interactors' investigated in this screen were also identified as Group 3 hits (in combination with p21 siRNA), which highlights the utility of the bioinformatics approach and provides phenotypic validation of the bioinformatics-generated network. Interestingly, there were also two siRNAs, histone deacetylase 1 (HDAC1) and UBC, which were identified to eliminate senescent cells in all three conditions, indicating potential senolytic targets.

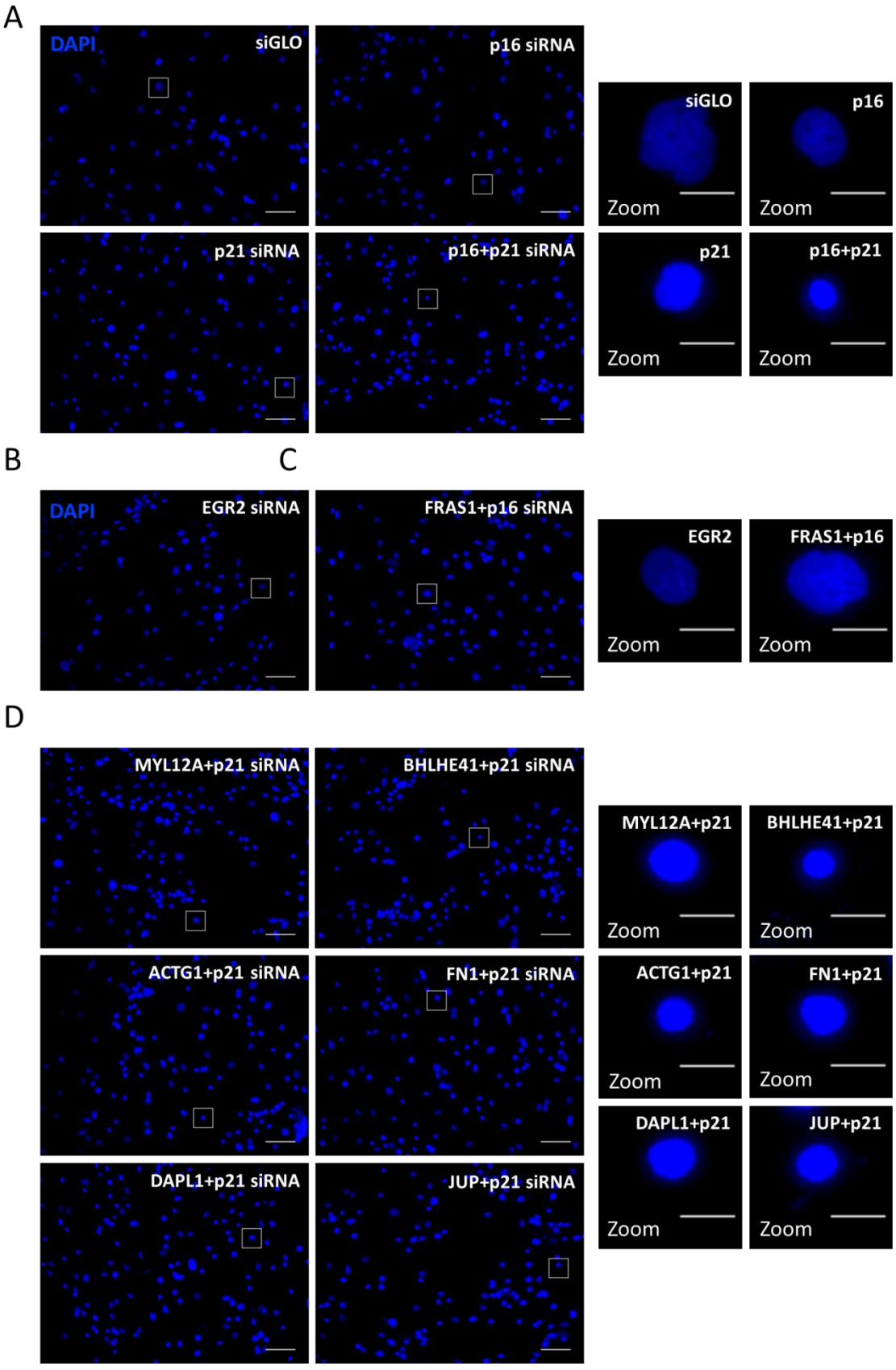

Figure 4.5 Representative images of a siRNA screen conducted to identify the top siRNAs inducing a reversal phenotype in DS HMFs using analysis of cell number and nuclear morphologies. Two independent siRNA screens, each in triplicate, were performed in DS HMFs

according to Section 2.6.2. Cells were fixed, stained with DAPI, imaged and cell number quantified according to Section 2.7 and 2.8. **(A)** Representative nuclei of 30 nM siGLO (siGLO), 30 nM p16 siRNA (p16), 30 nM p21 siRNA (p21), and 15 nM p16 siRNA together with 15 nM p21 siRNA (p16+p21) transfected DS HMFs. **(B)** Representative nuclei of top hits in Group 1, **(C)** Group 2 and **(D)** Group 3 identified in the siRNA screen. DAPI (blue). Scale bar denotes 100 μM. Right panels=digital zoom. Scale bar denotes 20 μM.

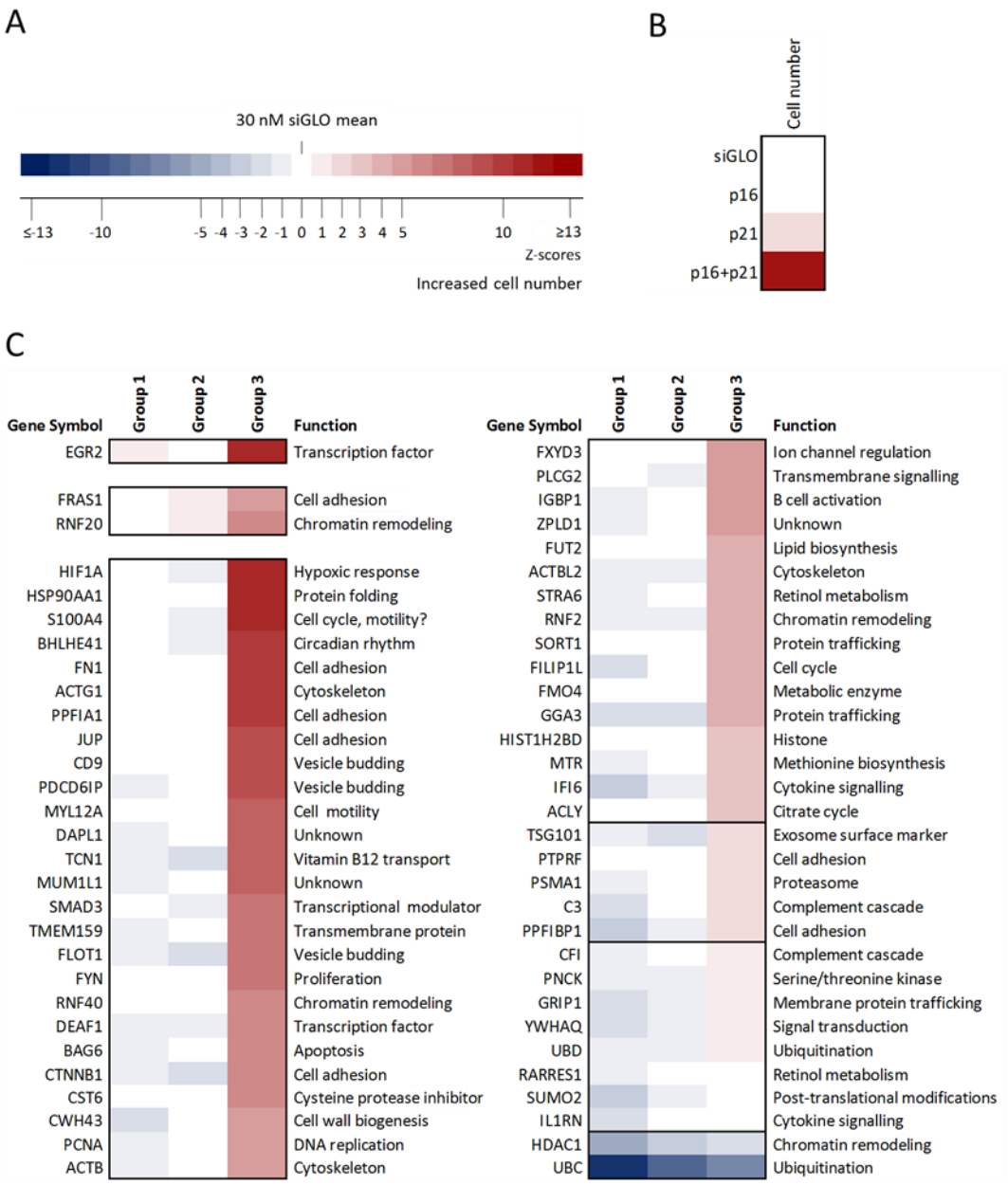

Figure 4.6 Identification of the top siRNAs which induced an increase in cell number in DS HMFs using analysis of cell number. Two independent siRNA screens, each in triplicate, were performed in DS HMFs according to Sections 2.6.2. Cells were fixed, stained with DAPI, imaged and cell number quantified according to Section 2.7 and 2.8. Z scores were then generated according to Section 2.8.2. **(A)** Key. The colour saturation reflects the number of Z scores from the control mean. Scores highlighted in red denote an increase in cell number significantly greater than the siGLO control mean indicating a release of cell cycle arrest. White denotes no significant change from the siGLO control mean. Blue denotes a significant decrease in cell number compared to the siGLO control mean. **(B)** Heatmap depicting significant changes in cell number from the 30 nM siGLO control mean for 30 nM p16 siRNA (p16), 30 nM p21 siRNA (p21),

and 15 nM p16 together with 15 nM p21 siRNA (p16+p21) controls. **(C)** Heatmap depicting significant changes in cell number for each of the 60 siRNAs in three different conditions: 30 nM siRNA individually (Group 1); 15 nM siRNA in combination with 15 nM siRNA (Group 2); and 15 nM siRNA in combination with p21 siRNA (Group 3).

In order to explore the nuclear phenotype of DS HMFs transfected with the 60 target siRNAs, multi-parameter analysis was performed using the previously defined panel of senescence-associated nuclear morphologies, including nuclear area, roundness, and elongation. To determine the effects on nuclear morphology of each of the 60 siRNAs in each of the three conditions, the data generated by the siGLO transfected control was used as a baseline for Z score generation (see Section 2.8.2). This analysis showed that in addition to increasing cell number (one Z score) (Figure 4.6), EGR2 siRNA in Group 1, also decreased nuclear area (one Z score) compared to the siGLO control (Figure 4.7). In Group 2, FRAS1 and RNF20 siRNA were previously defined as hits using cell number (Figure 4.6) but did not significantly alter nuclear phenotype for the three nuclear morphologies examined. Previously, 45 Group 3 siRNAs were scored as hits using cell number (Figure 4.6). Of these, 35 siRNAs also significantly decreased nuclear area and elongation, and increased nuclear roundness (Figure 4.7). Together, these findings suggest that one siRNA individually, EGR2, and 35 siRNAs in combination with p21 siRNA can induce proliferation and alter nuclear morphologies towards a reversal phenotype.

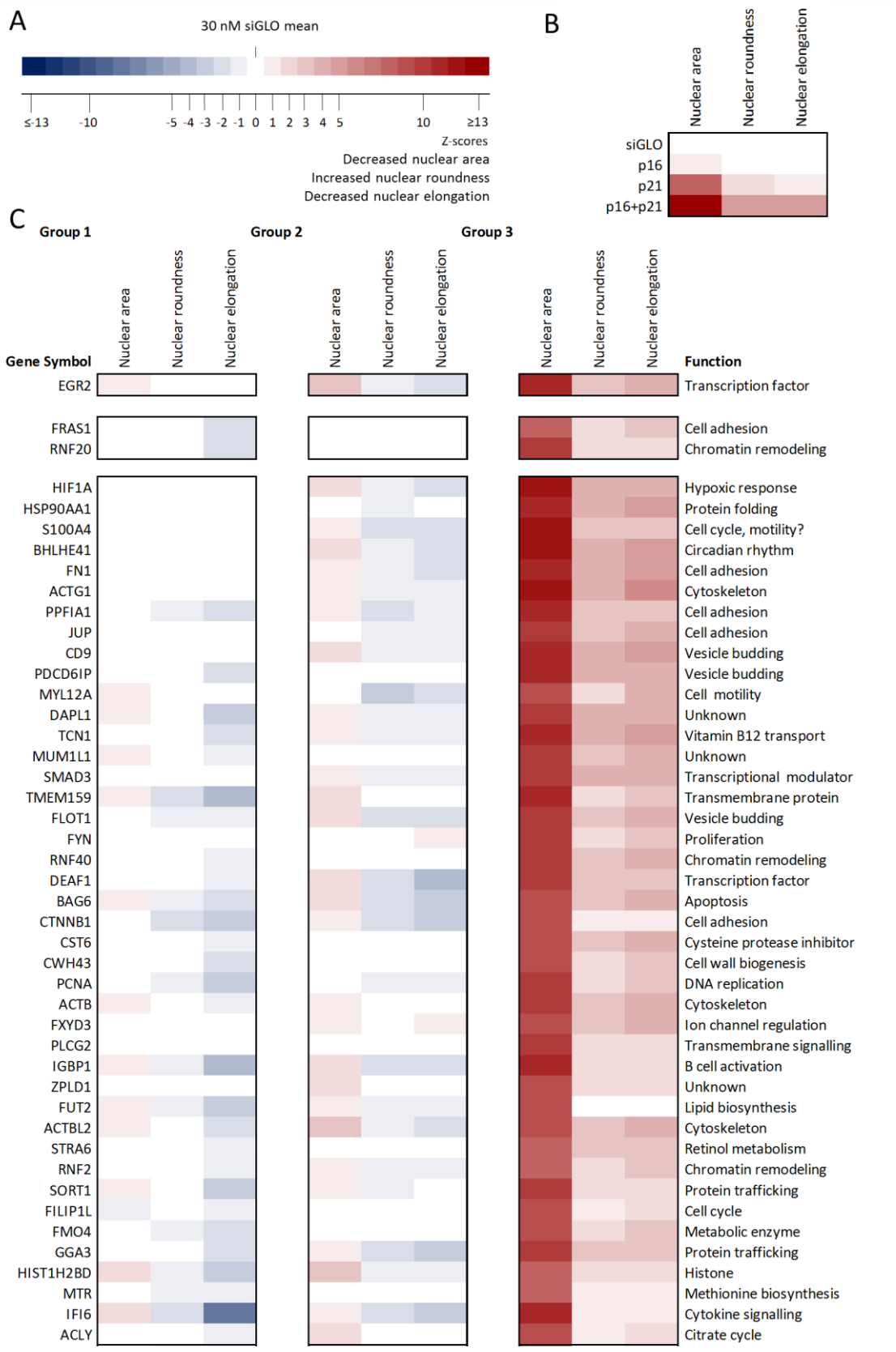
A
30 nM siGLO mean
≤-13
-10
-5 -4 -3 -2 -1 0 1 2 3 4 5
10
≥13
Z-scores
Decreased nuclear area
Increased nuclear roundness
Decreased nuclear elongation
B
Nuclear area
Nuclear roundness
Nuclear elongation
siGLO
p16
p21
p16+p21
C
Group 1
Group 2
Group 3
Nuclear area
Nuclear roundness
Nuclear elongation
Gene Symbol
Function
EGR2
Transcription factor
FRAS1
Cell adhesion
RNF20
Chromatin remodeling
HIF1A
Hypoxic response
HSP90AA1
Protein folding
S100A4
Cell cycle, motility?
BHLHE41
Circadian rhythm
FN1
Cell adhesion
ACTG1
Cytoskeleton
PPFIA1
Cell adhesion
JUP
Cell adhesion
CD9
Vesicle budding
PDCD6IP
Vesicle budding
MYL12A
Cell motility
DAPL1
Unknown
TCN1
Vitamin B12 transport
MUM1L1
Unknown
SMAD3
Transcriptional modulator
TMEM159
Transmembrane protein
FLOT1
Vesicle budding
FYN
Proliferation
RNF40
Chromatin remodeling
DEAF1
Transcription factor
BAG6
Apoptosis
CTNNB1
Cell adhesion
CST6
Cysteine protease inhibitor
CWH43
Cell wall biogenesis
PCNA
DNA replication
ACTB
Cytoskeleton
FXYD3
Ion channel regulation
PLCG2
Transmembrane signalling
IGBP1
B cell activation
ZPLD1
Unknown
FUT2
Lipid biosynthesis
ACTBL2
Cytoskeleton
STRA6
Retinol metabolism
RNF2
Chromatin remodeling
SORT1
Protein trafficking
FILIP1L
Cell cycle
FMO4
Metabolic enzyme
GGA3
Protein trafficking
HIST1H2BD
Histone
MTR
Methionine biosynthesis
IFI6
Cytokine signalling
ACLY
Citrate cycle

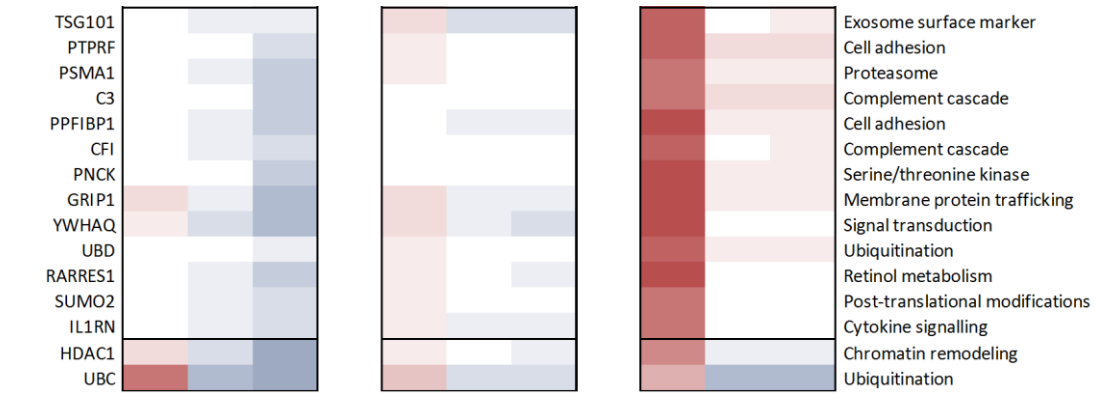

Figure 4.7 Identification of the top siRNAs which induced a reversal phenotype in DS HMFs using multi-parameter analysis of nuclear morphology. Two independent siRNA screens, each in triplicate, were performed in DS HMFs according to Section 2.6.2. Cells were then fixed, stained with DAPI, imaged and nuclear morphologies quantified according to Section 2.7 and 2.8. Z scores were then generated according to Section 2.8.2. **(A)** Key. The colour saturation reflects the number of Z scores from the control mean. Scores highlighted in red denote a significant change in nuclear area, roundness, or elongation towards the reversed phenotype compared to the siGLO control mean. White denotes no significant change from the siGLO control mean. Blue denotes a significant change in nuclear area, roundness, or elongation away from the reversed phenotype compared to the siGLO control mean. **(B)** Heatmap depicting significant changes in nuclear area, roundness and elongation from the siGLO control mean for p16 siRNA (p16), p21 siRNA (p21), and p16 together with p21 siRNA (p16+p21) controls. **(C)** Heatmap depicting significant changes in nuclear area, roundness and elongation for each of the 60 siRNAs in three different conditions: 30 nM siRNA individually (Group 1); 15 nM siRNA in combination with 15 nM siRNA (Group 2); and 15 nM siRNA in combination with p21 siRNA (Group 3).

In summary, 45 potential novel drivers of senescence were identified in the siRNA screen, including 21 'drivers' identified in both DS HMECs and HMFs and 24 'interactors' identified as hits in DS HMFs. The top siRNA in Group 1 (EGR2) and Group 2 (FRAS1) were selected for further investigation and characterisation of senescence-associated parameters. In addition, the top 12 siRNAs in Group 3 were classified as 'strong' hits for senescence reversal as they induced an increase in proliferation greater than eight Z scores from the siGLO control. Subsequently, these 14 siRNAs were chosen for inclusion in a siRNA screen to find the most potent reversal phenotype by investigating dose effect, time point extension, and further characterisation of morphological senescence-associated parameters.

4.4 Further investigation of the top siRNA hits

4.4.1 Investigation of dose effect, time point extension, and multi-parameter analysis for the top hits

Following the siRNA screen, the 14 top siRNAs were selected for further investigation. In order to identify the most potent reversal protocol and therefore the strongest hits for senescence reversal, siRNA dose effect and time point extension were investigated for the 14 top siRNAs: EGR2; FRAS1; hypoxia inducible factor 1-alpha (HIF1A); heat shock protein 90 alpha family class A member 1 (HSP90AA1); S100 calcium-binding protein A4 (S100A4); BHLHE41; FN1; ACTG1; PTPRF interacting protein alpha 1 (PPFIA1); junction plakoglobin (JUP); CD9; programmed cell death 6 interacting protein (PDCD6IP); myosin light chain 12A (MYL12A); death associated protein like 1 (DAPL1). Potentially, weakly specific or non-specific siRNAs in the pool may not provide sufficient knockdown to induce the most potent reversed phenotype at the 30 nM dose. To investigate this, an increased dose of 60 nM was compared to the original 30 nM dose. In addition, to determine whether the kinetics to generate the most potent phenotype required a longer incubation period, these experiments were harvested at five days or a later seven day time point.

To perform the siRNA screen, DS fibroblasts were seeded at a previously optimised seeding density of 15,000 cells/cm^2 (see Section 2.5.2). After ensuring that the transfection reagent dose (0.15 µL/well) plus 60 nM siGLO produced minimal toxicity in the DS fibroblasts (data not shown), the cells were forward transfected with 30 nM

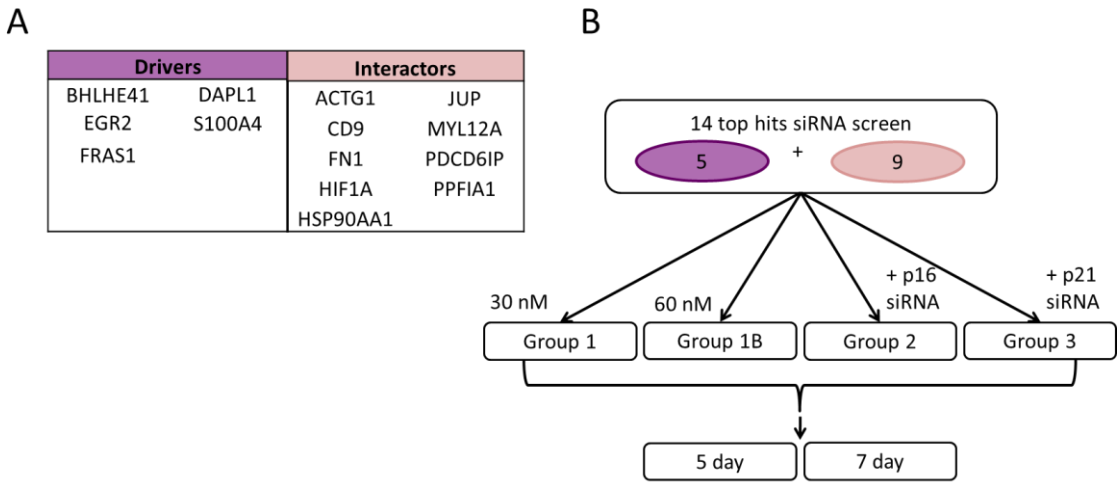

Figure 4.8 Gene list of the 14 top hits and siRNA screening workflow for investigation of dose effect and time point extension. (A) Following the large scale DS HMF screen, the 14 top hits were selected for further investigation: five drivers (purple), and nine interactors (pink). **(B)** Schematic illustrating the experimental design of the smaller siRNA screen investigating dose effect and time point extension in the top 14 hits. Using a previously optimised seeding density and transfection reagent dose (see Section 2.6.2), DS HMFs were forward transfected with the 14 siRNAs in four conditions: 30 nM siRNA individually (Group 1); 60 nM siRNA individually (Group 1B); 15 nM siRNA in combination with 15 nM siRNA (Group 2); and 15 nM siRNA in combination with p21 siRNA (Group 3). After five or seven days, cells were fixed and stained with DAPI and Cell Mask, and quantified according to Section 2.7 and 2.8.

siRNA (Group 1), 60 nM siRNA (Group 1B), and 15 nM siRNA in combination with 15 nM p16 (Group 2) or 15 nM p21 siRNA (Group 3) (see Section 2.6.2) (Figure 4.8). After five or seven days, cells were fixed and stained with DAPI and Cell Mask, and quantified according to Section 2.7 and 2.8. Three independent siRNA screens were performed for both the five day and seven day incubation, each in triplicate.

To explore morphological changes in the DS HMFs following siRNA knockdown, multi-parameter analysis of the previously defined panel of senescence-associated morphological markers was combined with the increased dose and time-course (see Section 3.2.2). Thus, each condition was analysed for cell area, nuclear area, nuclear elongation, nuclear roundness, and cell elongation, with the data generated by the 30 nM siGLO used as the baseline for Z score generation (see Section 2.8.2). These measures are ranked in order of their effectiveness at discriminating senescence from reversal (i.e. the magnitude of difference in Z scores between the p16+p21 siRNA

reversed DS HMFs and the 30 nM siGLO transfected control cells) with cell area ranking highest. Using this approach, a hit list was generated for each of the four conditions. In order to increase the window for hit detection and allow as many hits to be identified as possible, significance was defined as at least one Z score greater than the respective control for each condition (see Section 2.8.2). DS HMFs transfected with Group 1 (30 nM siRNAs individually) were compared to 30 nM siGLO control; Group 1B (60 nM siRNA individually) were compared to 60 nM siGLO control; Group 2 (siRNAs in combination with p16 siRNA) were compared to 30 nM p16 siRNA control; and Group 3 (siRNAs in combination with p21 siRNA) were compared to cells transfected with 30 nM p21 siRNA.

In line with findings from previous experiments (see Section 3.3.2 and Section 4.3.1), p21 siRNA knockdown altered nuclear and cellular morphology, but siRNA knockdown of p16 and p21 together induced a greater shift in nuclear and cellular morphology (Figure 4.9A, Figure 4.10B).

Interestingly, at the 30 nM dose, four siRNAs (EGR2, MYL12A, BHLHE41, and DAPL1) induced a reduction in cell area relative to the 30 nM siGLO control mean (three Z scores for EGR2 and MYL12A siRNA, one Z score for BHLHE41 and DAPL1 siRNA) (Figure 4.9B, Figure 4.10C). Furthermore, 30 nM EGR2, BHLHE41, and DAPL1 siRNA induced an increase in cell elongation greater than the siGLO control mean. Five siRNAs, HIF1A, S100A4, CD9, PDC6IP, and ACTG1 increased cell elongation at the 30 nM dose relative to the 30 nM siGLO control mean but did not alter the other five senescence-associated morphologies. Strikingly, 13 siRNAs induced nuclear and cellular morphological changes towards a reversed phenotype in a dose dependent manner. Of the four siRNAs which altered cellular morphology at the 30 nM dose, all four siRNAs, EGR2, MYL12A, BHLHE41, and DAPL1, further significantly decreased cell area (five, four, four, and two Z scores, respectively) relative to the 60 nM siGLO control mean. In addition, 60 nM EGR2 further increased cell elongation (two Z scores) relative to the 60 nM siGLO control mean but BHLHE41 and DAPL1 siRNA did not. Furthermore, at the 60 nM dose, EGR2, MYL12A, BHLHE41, DAPL1, HIF1A, and PPFIA1 siRNA also decreased nuclear area (one Z score) compared to the 60 nM siGLO control. Nuclear elongation and nuclear roundness were not significantly altered towards the reversed phenotype by any Group 1 or Group 1B siRNA.

At the seven day time point, the reversed morphologies of the p21 and p16+p21 controls are weaker in comparison to the five day time point, potentially demonstrating the transient nature of siRNA knockdown which has allowed the cells to begin reverting to a senescent morphology. However, the dose dependent effect was still present (Figure 4.11, Figure 4.12), but the decrease in cell area induced by EGR2, MYL12A, BHLHE41, and DAPL1 siRNA was reduced in comparison to the five day screen. Interestingly, at the later time point, seven siRNAs, including EGR2, MYL12A, BHLHE41, and DAPL1, induced a dose dependent effect on nuclear area morphology which was not present at the five day time point. Furthermore, it is interesting to note that although the Group 3 siRNA (in combination with p21) reversal morphology was weaker at seven days when compared to the five day time point, there were multiple siRNAs in combination with p21 siRNA which induced a greater reversed morphology than the controls at the seven day time point.

In summary, in both the five day and seven day screens, these analyses showed that many of the top siRNAs induced significant changes towards a reversal phenotype in multiple senescence-associated parameters in a dose dependent manner. This approach allowed the top siRNAs to be ranked by the strength of the reversal phenotype induced in a dose dependent manner. Accordingly, EGR2 siRNA ranked highest, followed by MYL12A, BHLHE41, and DAPL1 siRNA.

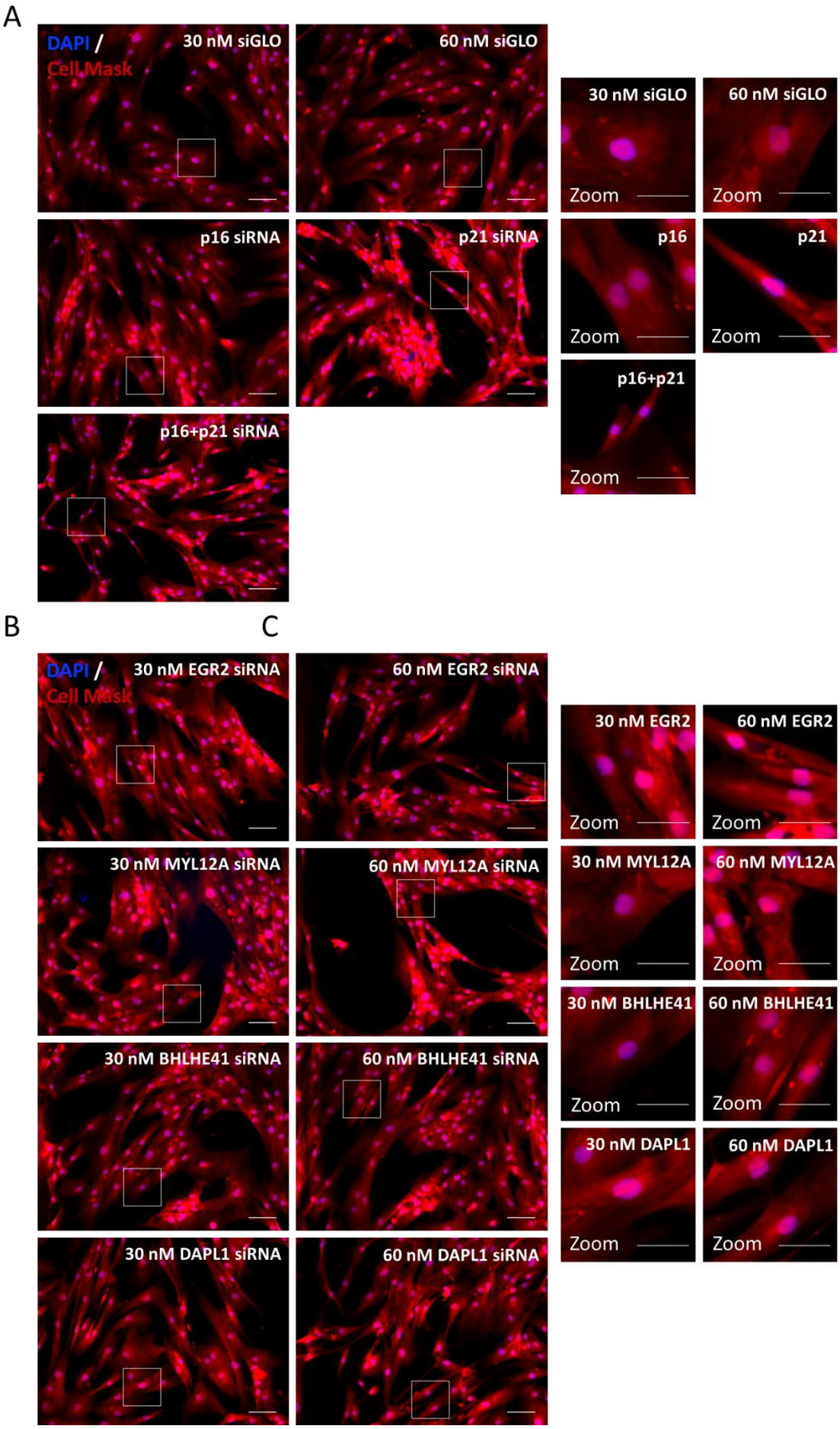
A
DAPI /
Cell Mask
30 nM siGLO
60 nM siGLO
p16 siRNA
p21 siRNA
p16+p21 siRNA
Zoom
p16
p21
p16+p21
B
C
30 nM EGR2 siRNA
60 nM EGR2 siRNA
30 nM MYL12A siRNA
60 nM MYL12A siRNA
30 nM BHLHE41 siRNA
60 nM BHLHE41 siRNA
30 nM DAPL1 siRNA
60 nM DAPL1 siRNA
30 nM EGR2
60 nM EGR2
30 nM MYL12A
60 nM MYL12A
30 nM BHLHE41
60 nM BHLHE41
30 nM DAPL1
60 nM DAPL1

Figure 4.9 Representative images of a siRNA screen conducted to further investigate the top siRNAs inducing a reversal phenotype in DS HMFs at day five using analysis of nuclear and cellular morphologies. Three independent siRNA screens, each in triplicate, were performed for the five day time point in DS HMFs according to Section 2.6.2. Cells were fixed, stained with DAPI and Cell Mask, imaged and nuclear and cellular morphologies quantified according to Section 2.7 and 2.8. **(A)** Representative images of 30 nM siGLO, 60 nM siGLO, 30 nM p16 siRNA (p16), 30 nM p21 siRNA (p21), and 15 nM p16 siRNA together with 15 nM p21 siRNA (p16+p21) transfected DS HMFs. **(B)** Representative images of top hits in Group 1 (30 nM individually) and **(C)** Group 1B (60 nM individually) identified in the siRNA screen. DAPI (blue), Cell Mask (red). Scale bar denotes 100 μM. Right panels=digital zoom. Scale bar denotes 50 μM.

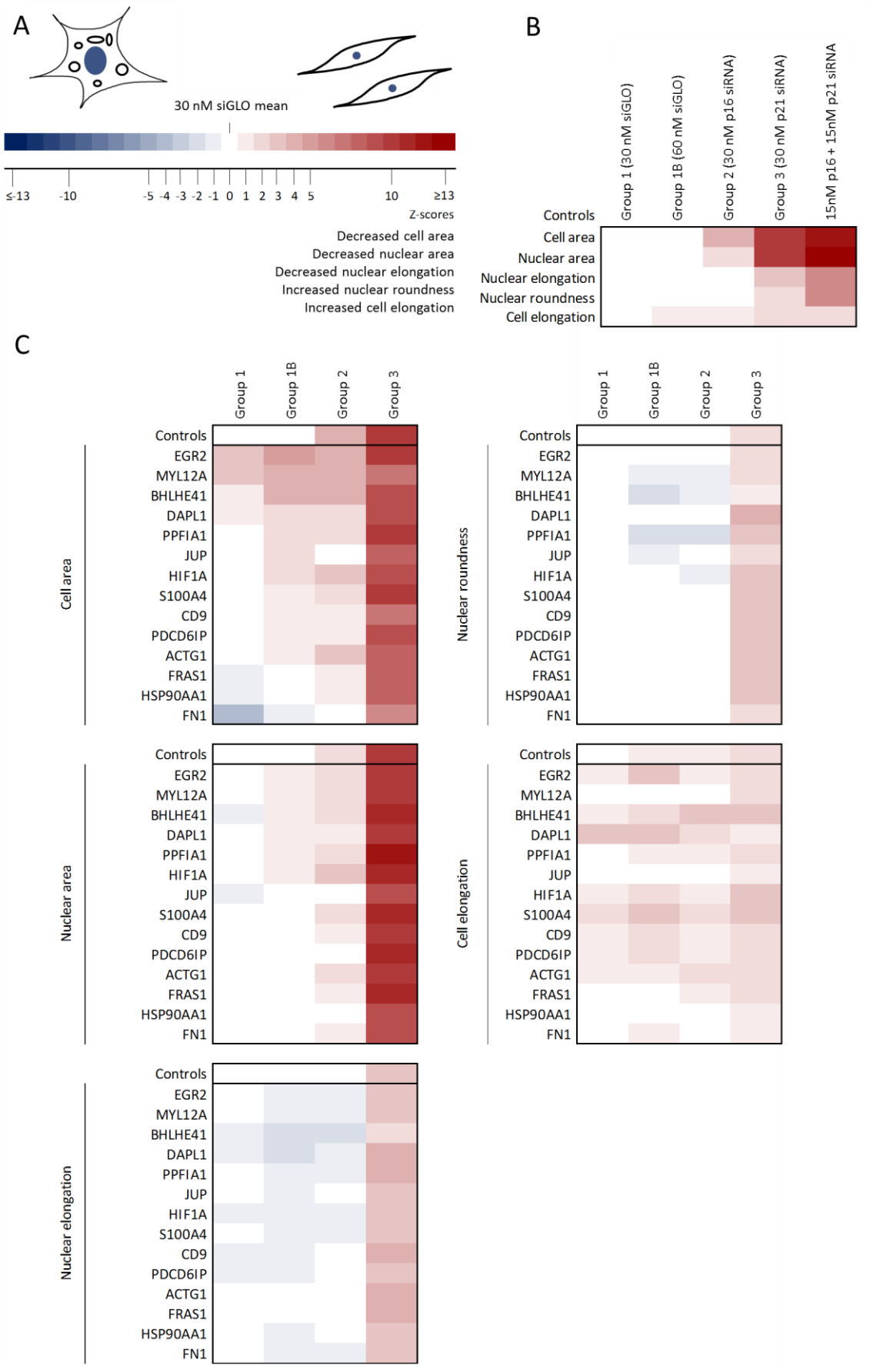

Figure 4.10 Multi-parameter analysis of the top siRNAs identified to reverse senescence in the DS HMFs at day five. Three independent siRNA screens, each in triplicate, were performed for

the five day time point in DS HMFs according to Section 2.6.2. Cells were fixed, stained with DAPI and Cell Mask, imaged and nuclear and cellular morphologies quantified according to Section 2.7 and 2.8. Z scores were then generated according to Section 2.8.2. **(A)** Key. The colour saturation reflects the number of Z scores from the siGLO control mean. Scores highlighted in red denote a shift towards the reversed phenotype and blue denotes a shift away from the reversed phenotype. **(B)** Heatmap depicting significant changes in each of the panel of five morphological senescence-associated markers from the 30 nM siGLO control mean (Group 1 control) for 60 nM siGLO (Group 1B control), 30 nM p16 siRNA (p16) (Group 2 control), 30 nM p21 siRNA (p21) (Group 3 control), and 15 nM p16 together with 15 nM p21 siRNA (p16+p21) transfected DS HMFs. **(C)** Heatmap depicting significant changes in each of the panel of five morphological senescence-associated markers for the hit siRNAs selected from the previous screen in four different conditions: 30 nM siRNA individually (Group 1); 60 nM siRNA individually (Group 1B); 15 nM siRNA in combination with 15 nM siRNA (Group 2); and 15 nM siRNA in combination with p21 siRNA (Group 3), compared to 30 nM siGLO control mean.

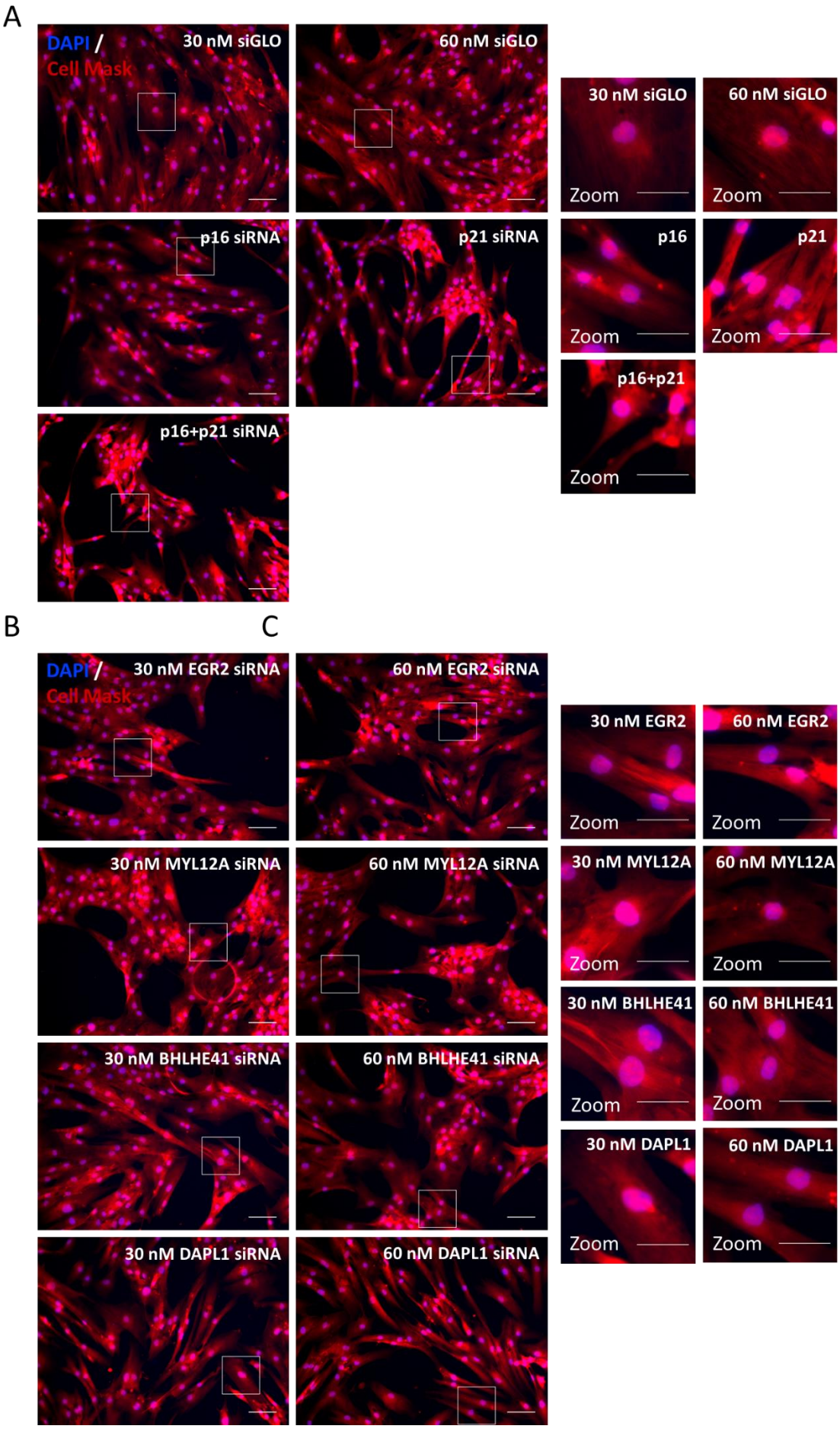
A
DAPI /
Cell Mask
30 nM siGLO
60 nM siGLO
p16 siRNA
p21 siRNA
p16+p21 siRNA
Zoom
p16
p21
p16+p21
B
C
30 nM EGR2 siRNA
60 nM EGR2 siRNA
30 nM MYL12A siRNA
60 nM MYL12A siRNA
30 nM BHLHE41 siRNA
60 nM BHLHE41 siRNA
30 nM DAPL1 siRNA
60 nM DAPL1 siRNA
30 nM EGR2
60 nM EGR2
30 nM MYL12A
60 nM MYL12A
30 nM BHLHE41
60 nM BHLHE41
30 nM DAPL1
60 nM DAPL1

Figure 4.11 Representative images of a siRNA screen conducted to further investigate the top siRNAs inducing a reversal phenotype in DS HMFs at day seven using analysis of nuclear and cellular morphologies. Three independent siRNA screens, each in triplicate, were performed for the seven day time point in DS HMFs according to Section 2.6.2. Cells were fixed, stained with DAPI and Cell Mask, imaged and quantified according to Section 2.7 and 2.8. **(A)** Representative images of 30 nM siGLO, 60 nM siGLO, 30 nM p16 siRNA (p16), 30 nM p21 siRNA (p21), and 15 nM p16 siRNA together with 15 nM p21 siRNA (p16+p21) transfected DS HMFs. **(B)** Representative images of top hits in Group 1 (30 nM individually) and **(C)** Group 1B (60 nM individually) hits identified in the siRNA screen. DAPI (blue), Cell Mask (red). Scale bar denotes 100 μM. Right panels=digital zoom. Scale bar denotes 50 μM.

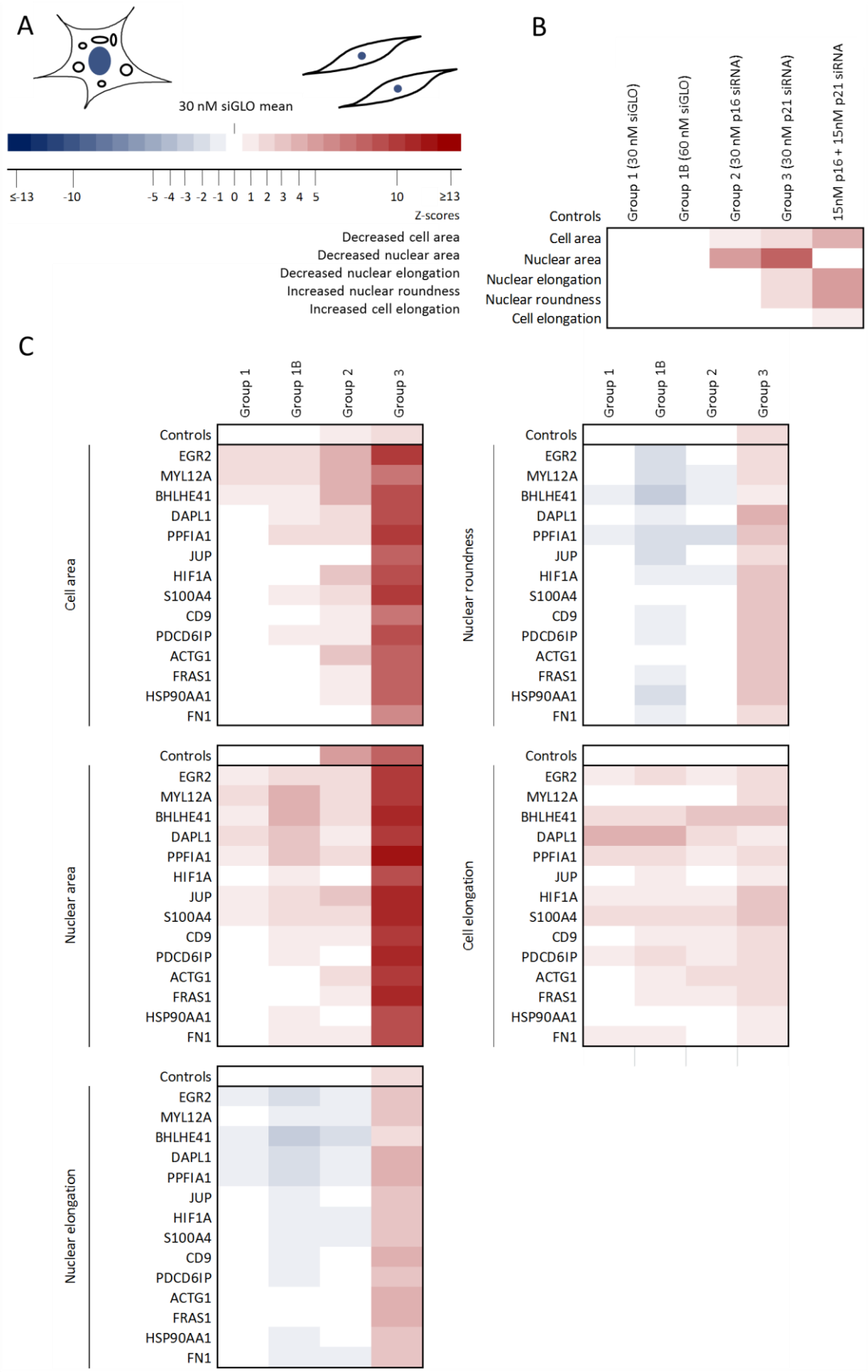
A
30 nM siGLO mean
≤-13
-10
-5 -4 -3 -2 -1 0 1 2 3 4 5
10
≥13
Z-scores
Decreased cell area
Decreased nuclear area
Decreased nuclear elongation
Increased nuclear roundness
Increased cell elongation
B
Group 1 (30 nM siGLO)
Group 1B (60 nM siGLO)
Group 2 (30 nM p16 siRNA)
Group 3 (30 nM p21 siRNA)
15nM p16 + 15nM p21 siRNA
Controls
Cell area
Nuclear area
Nuclear elongation
Nuclear roundness
Cell elongation
C
Group 1
Group 1B
Group 2
Group 3
Cell area
Nuclear roundness
Nuclear area
Cell elongation
Nuclear elongation
Controls
EGR2
MYL12A
BHLHE41
DAPL1
PPFIA1
JUP
HIF1A
S100A4
CD9
PDCD6IP
ACTG1
FRAS1
HSP90AA1
FN1

Figure 4.12 Multi-parameter analysis of the top siRNAs identified to reverse senescence in the DS HMFs at day seven. Three independent siRNA screens, each in triplicate, were performed for the seven day time point in DS HMFs according to Section 2.6.2. Cells were fixed, stained with DAPI and Cell Mask, imaged and quantified according to Section 2.7 and 2.8. Z scores were then generated according to Section 2.8.2. **(A)** Key. The colour saturation reflects the number of Z scores from the siGLO control mean. Scores highlighted in red denote a shift towards the reversed phenotype and blue denotes a shift away from the reversed phenotype. **(B)** Heatmap depicting significant changes in each of the panel of five morphological senescence-associated markers from the 30 nM siGLO control mean (Group 1 control) for 60 nM siGLO (Group 1B control), 30 nM p16 siRNA (p16) (Group 2 control), 30 nM p21 siRNA (p21) (Group 3 control), and 15 nM p16 together with 15 nM p21 siRNA (p16+p21) transfected DS HMFs. **(C)** Heatmap depicting significant changes in each of the panel of five morphological senescence-associated markers for the hit siRNAs selected from the previous screen in four different conditions: 30 nM siRNA individually (Group 1); 60 nM siRNA individually (Group 1B); 15 nM siRNA in combination with 15 nM siRNA (Group 2); and 15 nM siRNA in combination with p21 siRNA (Group 3), compared to 30 nM siGLO control mean.

4.4.2 Immunofluorescence staining for p16 and p21 expression to further rank the top hits

In order to further characterise and rank the top hits, p16 and p21 nuclear intensities were examined for each siRNA condition using mouse anti-p16 (JC8) and rabbit anti-p21 (12D1) double immunofluorescence staining according to Section 2.7. Using the secondary only control, thresholds for positivity were determined for p16 and p21 which enabled the cell population for each siRNA condition to be fractioned into four subgroups: double negative; double positive; and positive for either p16 or p21.

In order to further rank the top hits on the strength of their reversal phenotype, the double negative subgroup was used as a measure to identify the subpopulation of 'reversed' cells. In line with the findings from previous experiments (see Section 3.3.2), the proportion of cells in the double negative subgroup was not significantly increased following p16 (5% ± 1%) or p21 (12% ± 1%) siRNA knockdown; however, the proportion of cells in the double negative subgroup was significantly increased following p16+p21 siRNA knockdown (19% ± 4%; p=0.005) compared to the siGLO control (2% ± 1%) (Appendix Figure A.7).

Given that EGR2 siRNA induced a modest but significant increase in cell number at the 30 nM dose as well as induced nuclear and cellular morphological changes towards a reversed phenotype in a dose dependent manner, it was hypothesised that an increase in the double negative subgroup would be observed at the 30 nM and 60 nM EGR2 siRNA dose. At the 30 nM (Group 1) and 60 nM (Group 1B) doses, as well as in combination with p16 siRNA (Group 2), no siRNA significantly increased the double negative subgroup (Figure 4.14A-C). However, it is important to note here that p21 siRNA knockdown increased cell number (see Section 4.3.1) and BrdU incorporation (see Section 3.3.2) but did not significantly increase the double negative subgroup, indicating that a small pool of ‘reversed’ cycling cells captured at the five day time-point can increase cell number over the time-course of the experiment.

In line with previous data which demonstrated a significantly increased cell number (Figure 4.6) as well as significantly altered nuclear and cellular morphologies towards a reversed phenotype (Figure 4.10) following Group 3 siRNA knockdown, eight Group 3 siRNAs significantly increased the double negative subgroup relative to the 30 nM siGLO

control, namely FN1, JUP, EGR2, HSP90AA1, FRAS1, PDCD6IP, ACTG1, and MYL12A (Figure 4.13D), indicating a significant increase in the 'reversed' subpopulation. However, six Group 3 siRNAs did not significantly increase the double negative subgroup relative to the 30 nM siGLO control: HIF1A; S100A4; PPFIA1; CD9; BHLHE41; and DAPL1. As previous data have demonstrated that these Group 3 siRNAs significantly increased cell number and altered nuclear and cellular morphology towards a reversed phenotype, these data potentially implicate these as oncogenic siRNAs which induce senescence bypass, not senescence reversal.

Interestingly, the double positive subgroup was significantly increased and the p21+p16- subgroup significantly decreased for two Group 1 siRNAs, BHLHE41 and PPFIA1, relative to the 30 nM siGLO control. Together, these data revealed an increase in p16 levels following BHLHE41 or PPFIA1 siRNA knockdown. Furthermore, 14 Group 1B siRNAs significantly increased the double positive subgroup as well as significantly decreased the p21+p16- subgroup (Figure 4.14B), indicating that siRNA knockdown of these genes increased p16 levels in a dose dependent manner. Importantly, 60 nM siGLO did not significantly alter the subgroup proportions relative to 30 nM siGLO (Figure 4.14B). Thus, the increased double positive subgroup and decreased p21+p16- subgroup following Group 2 (60 nM) siRNA knockdown was not a consequence of siRNA dose toxicity. Previous data has suggested the presence of a p21-dependent compensatory feedback loop which regulates p16 levels (see Section 3.3.2). Potentially, siRNA knockdown of these genes may induce the p21-dependent compensatory feedback mechanism, resulting in an increase in p16 levels.

It should be noted that an ANOVA and post-hoc Dunnett's test generate a unique adjusted p value for each comparison dependent on the entire family of comparisons, resulting in p values which are interpretable only within the context of the entire family of comparisons. Thus, the p values generated for each condition (30 nM siRNA, 60 nM siRNA, + 15 nM p16 siRNA, + 15 nM p21 siRNA) cannot be directly compared here.

In conclusion, these analyses allowed the top 14 hit siRNAs to be further ranked, with FN1 (34% ± 7%; p=0.001), JUP (31% ± 25%; p=0.005), EGR2 (30% ± 7%; p=0.008) ranked as the top three siRNAs inducing the greatest increase in the double negative subgroup. Notably, EGR2 siRNA, the strongest scorer in the 60 siRNA screen (Figure 4.6, Figure 4.7),

and strongest scorer in the multi-parameter analysis of the subsequent top hit screen (Figure 4.10), was ranked highly in this analysis. Taken together, the morphological and double negative subgroup data revealed three hits scoring highly in both analyses, EGR2, JUP, and MYL12A siRNA.

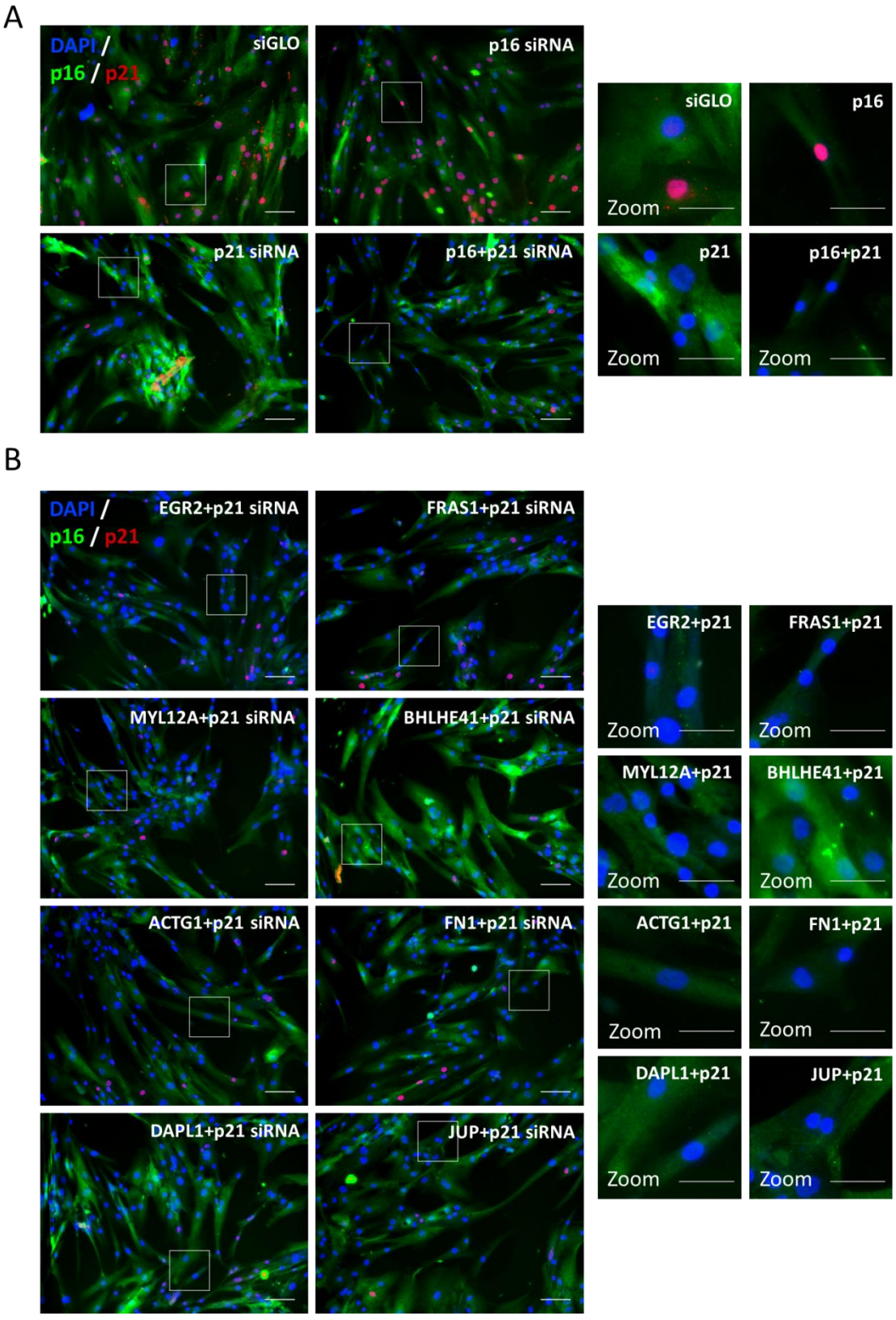

Figure 4.13 Representative images of a siRNA screen conducted to further investigate the top siRNAs inducing a reversal phenotype in DS HMFs at day five using analysis of p16 and p21 nuclear expression. Three independent siRNA screens, each in triplicate, were performed for the five day time point in DS HMFs according to Section 2.6.2. Cells were fixed, stained with

DAPI, p16, and p21, imaged and quantified according to Section 2.7 and 2.8. **(A)** Representative images of 30 nM siGLO, 60 nM siGLO, 30 nM p16 siRNA (p16), 30 nM p21 siRNA (p21), and 15 nM p16 siRNA together with 15 nM p21 siRNA (p16+p21) transfected DS HMFs. **(B)** Representative images of Group 3 top hits (15 nM siRNA in combination with p21 siRNA) identified in the siRNA screen. DAPI (blue), p16 (green), p21 (red). Scale bar denotes 100 μM. Right panels=digital zoom. Scale bar denotes 50 μM.

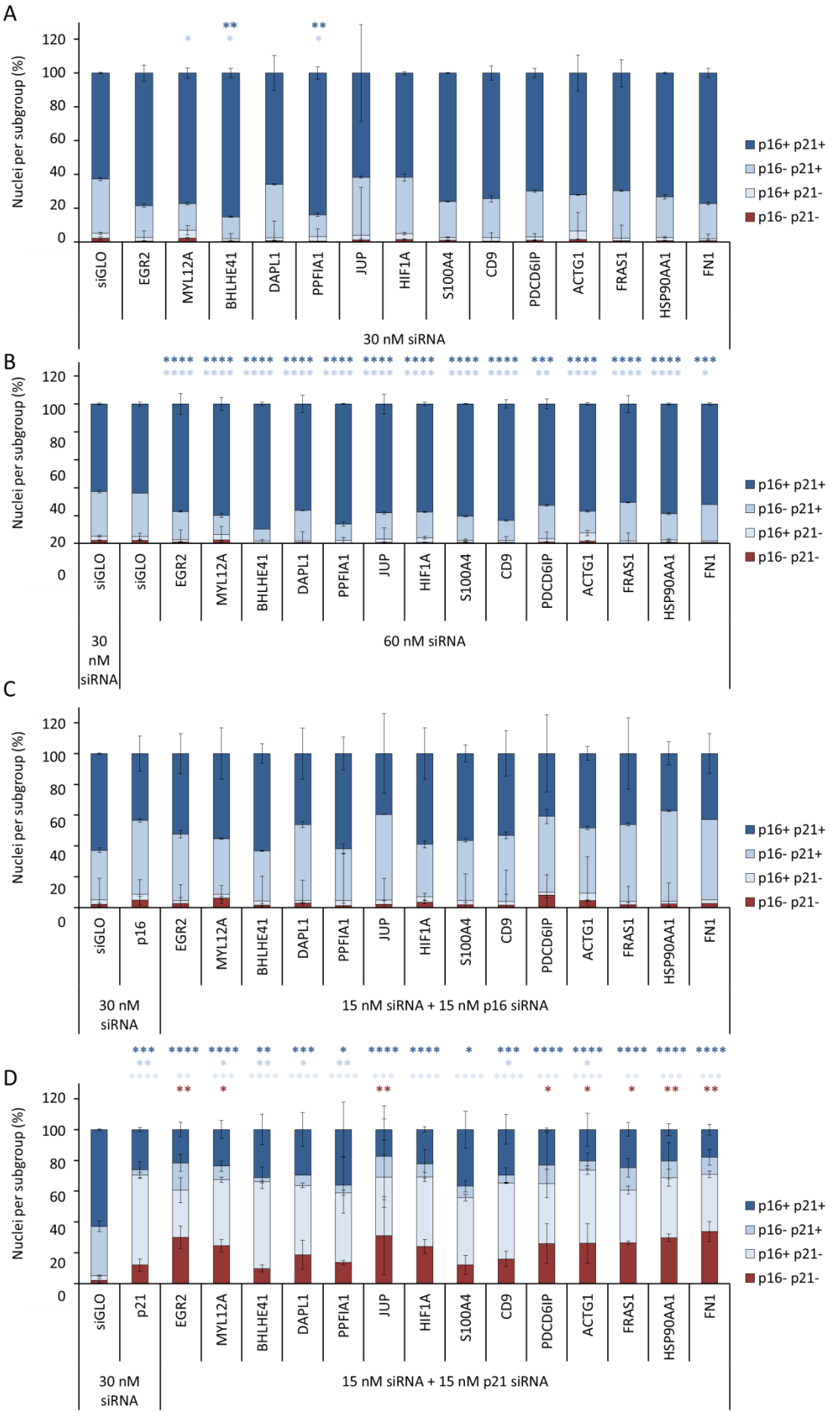
A
Nuclei per subgroup (%)
120
100
80
60
40
20
0
siGLO
EGR2
MYL12A
BHLHE41
DAPL1
PPFIA1
JUP
HIF1A
S100A4
CD9
PDCD6IP
ACTG1
FRAS1
HSP90AA1
FN1
30 nM siRNA
p16+ p21+
p16- p21+
p16+ p21-
p16- p21-
B
Nuclei per subgroup (%)
siGLO
siGLO
EGR2
MYL12A
BHLHE41
DAPL1
PPFIA1
JUP
HIF1A
S100A4
CD9
PDCD6IP
ACTG1
FRAS1
HSP90AA1
FN1
30 nM siRNA
60 nM siRNA
p16+ p21+
p16- p21+
p16+ p21-
p16- p21-
C
Nuclei per subgroup (%)
siGLO
p16
EGR2
MYL12A
BHLHE41
DAPL1
PPFIA1
JUP
HIF1A
S100A4
CD9
PDCD6IP
ACTG1
FRAS1
HSP90AA1
FN1
30 nM siRNA
15 nM siRNA + 15 nM p16 siRNA
p16+ p21+
p16- p21+
p16+ p21-
p16- p21-
D
Nuclei per subgroup (%)
siGLO
p21
EGR2
MYL12A
BHLHE41
DAPL1
PPFIA1
JUP
HIF1A
S100A4
CD9
PDCD6IP
ACTG1
FRAS1
HSP90AA1
FN1
30 nM siRNA
15 nM siRNA + 15 nM p21 siRNA
p16+ p21+
p16- p21+
p16+ p21-
p16- p21-

Figure 4.14 Ranking top siRNAs according to p16 and p21 double negative subgroup frequency at day five. Two independent siRNA screens, each in triplicate, were performed for the five day time point in DS HMFs according to Section 2.6.2. Cells were then fixed and stained with DAPI, mouse anti-p16 (JC8), rabbit anti-p21 (12D1), donkey anti-mouse Alexa Fluor 488, and goat anti-rabbit Alexa Fluor 546. Cells were imaged and intensities were quantitated according to Section 2.7 and 2.8. Nuclear intensity thresholds were established for p16 and p21 to define positive or negative nuclei. Nuclei were classified into four subgroups: p16 and p21 positive (p16+ p21+); p16 negative and p21 positive (p16- p21+); p16 positive and p21 negative (p16+ p21-); and p16 and p21 negative (p16- p21-). Bars denote nuclei per subgroup. Two-way ANOVA and Dunnett's test * $p<0.05$, ** $p<0.01$, *** $p<0.001$, **** $p<0.0001$. N=2 throughout. Error bars=SD of two independent experiments, each performed with three replicates. **(A)** 30 nM hit siRNA (Group 1) relative to 30 nM siGLO control. **(B)** 60 nM hit siRNA (Group 1B) and 60 nM siGLO control relative to the 30 nM siGLO control. **(C)** 15 nM hit siRNA + 15 nM p16 siRNA (Group 2) and 30 nM p16 siRNA control relative to the 30 nM siGLO control. **(D)** 15 nM hit siRNA + 15 nM p21 siRNA (Group 3) and 30 nM p21 siRNA control relative to the 30 nM siGLO control.

At the seven day time point, there was an increase in the double positive subgroup and decrease in the double negative subgroup for the p21 siRNA and p16+p21 siRNA transfected DS HMFs compared to the five day time point, indicating that p16 and p21 expression levels were beginning to increase following the transient siRNA knockdown (N=1, Figure 4.15, Figure 4.16). Furthermore, only two siRNAs in combination with p21 siRNA, MYL12A, and FN1, demonstrated an increased double negative subgroup at seven days, in comparison to 11 siRNAs at the five day time point.

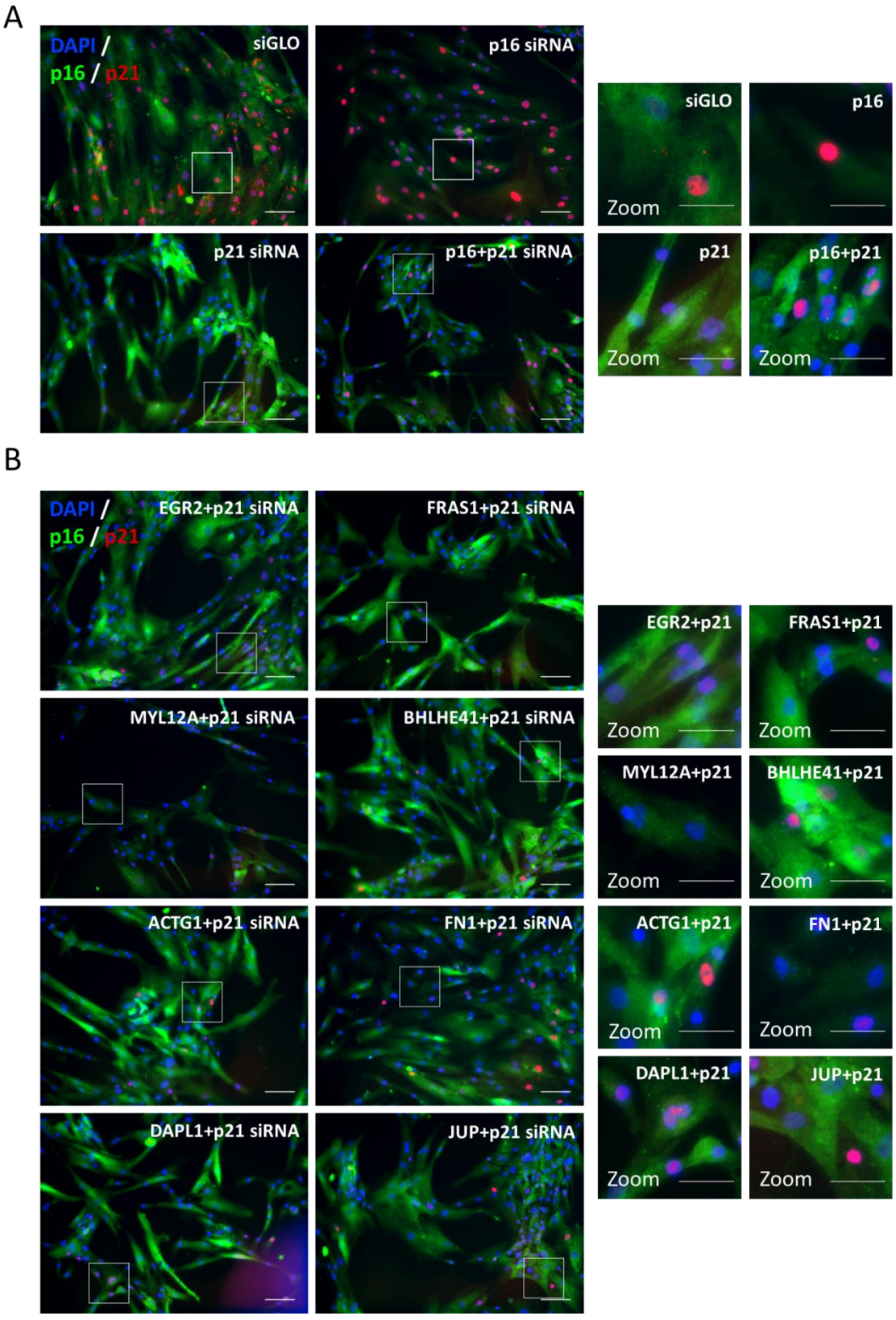

Figure 4.15 Representative images of a siRNA screen conducted to further investigate the top siRNAs inducing a reversal phenotype in DS HMFs at day seven using analysis of p16 and p21 nuclear expression. One independent siRNA screen, in triplicate, was performed for the seven day time point in DS HMFs according to Section 2.6.2. Cells were fixed, stained with DAPI, mouse

anti-p16 (JC8), and rabbit anti-p21 (12D1), donkey anti-mouse Alexa Fluor 488, and goat anti-rabbit Alexa Fluor 546, imaged and quantified according to Section 2.7 and 2.8. **(A)** Representative images of 30 nM siGLO, 60 nM siGLO, 30 nM p16 siRNA (p16), 30 nM p21 siRNA (p21), and 15 nM p16 siRNA together with 15 nM p21 siRNA (p16+p21) transfected DS HMFs. **(B)** Representative images of Group 3 top hits identified in the siRNA screen. DAPI (blue), p16 (green), Cell Mask (red). Scale bar denotes 100 μM. Right panels=digital zoom. Scale bar denotes 50 μM.

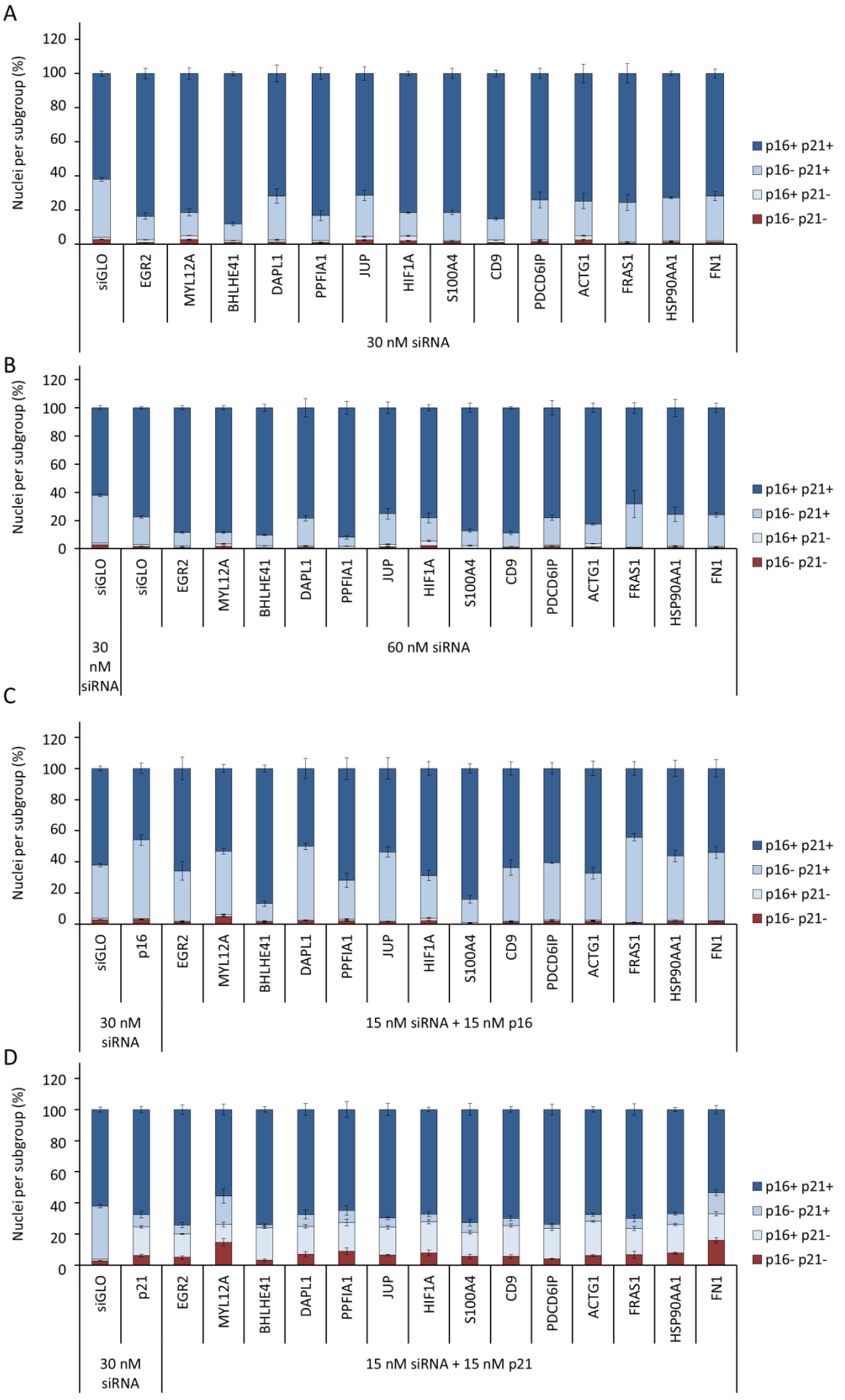
A
Nuclei per subgroup (%)
120
100
80
60
40
20
0
siGLO
EGR2
MYL12A
BHLHE41
DAPL1
PPFIA1
JUP
HIF1A
S100A4
CD9
PDCD6IP
ACTG1
FRAS1
HSP90AA1
FN1
30 nM siRNA
p16+ p21+
p16- p21+
p16+ p21-
p16- p21-
B
Nuclei per subgroup (%)
siGLO
siGLO
EGR2
MYL12A
BHLHE41
DAPL1
PPFIA1
JUP
HIF1A
S100A4
CD9
PDCD6IP
ACTG1
FRAS1
HSP90AA1
FN1
30 nM siRNA
60 nM siRNA
C
Nuclei per subgroup (%)
siGLO
p16
EGR2
MYL12A
BHLHE41
DAPL1
PPFIA1
JUP
HIF1A
S100A4
CD9
PDCD6IP
ACTG1
FRAS1
HSP90AA1
FN1
30 nM siRNA
15 nM siRNA + 15 nM p16
D
Nuclei per subgroup (%)
siGLO
p21
EGR2
MYL12A
BHLHE41
DAPL1
PPFIA1
JUP
HIF1A
S100A4
CD9
PDCD6IP
ACTG1
FRAS1
HSP90AA1
FN1
30 nM siRNA
15 nM siRNA + 15 nM p21

Figure 4.16 Ranking top siRNAs according to p16 and p21 double negative subgroup frequency at day seven. A single siRNA screen, in triplicate, performed for the seven day time point in DS HMFs according to Section 2.6.2. Cells were then fixed and stained with DAPI, mouse anti-p16 (JC8), rabbit anti-p21 (12D1), donkey anti-mouse Alexa Fluor 488, and goat anti-rabbit Alexa Fluor 546. Cells were imaged and intensities were quantitated according to Section 2.7 and 2.8. Nuclear intensity thresholds were established for p16 and p21 to define positive or negative nuclei. Nuclei were classified into four subgroups: p16 and p21 positive (p16+ p21+); p16 negative and p21 positive (p16- p21+); p16 positive and p21 negative (p16+ p21-); and p16 and p21 negative (p16- p21-). Bars denote nuclei per subgroup. N=1 throughout. No statistical test performed. Error bars=SD of one independent experiment, performed with three replicates. **(A)** 30 nM hit siRNA (Group 1) relative to 30 nM siGLO control. **(B)** 60 nM hit siRNA (Group 1B) and 60 nM siGLO control relative to the 30 nM siGLO control. **(C)** 15 nM hit siRNA + 15 nM p16 siRNA (Group 2) and 30 nM p16 siRNA control relative to the 30 nM siGLO control. **(D)** 15 nM hit siRNA + 15 nM p21 siRNA (Group 3) and 30 nM p21 siRNA control relative to the 30 nM siGLO control.

In order to explore EGR2, the top hit from the morphological and double staining analysis, in more detail, the morphologies of the different p16 and p21 subgroups were examined (Figure 4.17). This analysis showed a clear shift towards a reversal phenotype in nuclear and cellular morphology for all of the subgroups between 30 nM EGR2, 60 nM EGR2, EGR2+p21 siRNA and their controls (30 nM siGLO, 60 nM siGLO, 30 nM p21 siRNA, respectively), indicating that EGR2 knockdown affects DS HMF morphology towards a reversal phenotype even in the presence of p16 or p21, potentially indicating a role for the transcription factor in control of the senescence phenotype through either pathway.

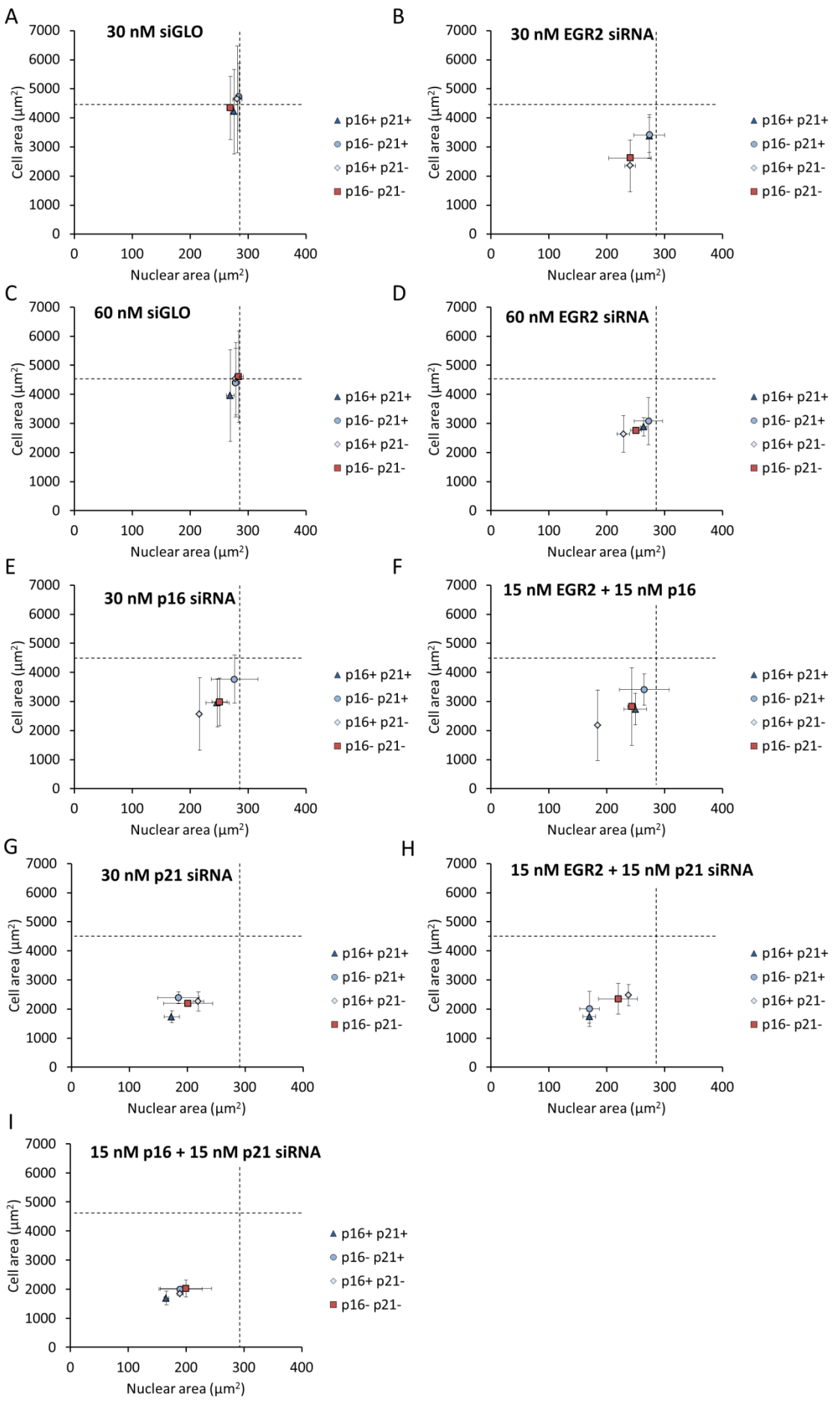
A
30 nM siGLO
B
30 nM EGR2 siRNA
C
60 nM siGLO
D
60 nM EGR2 siRNA
E
30 nM p16 siRNA
F
15 nM EGR2 + 15 nM p16
G
30 nM p21 siRNA
H
15 nM EGR2 + 15 nM p21 siRNA
I
15 nM p16 + 15 nM p21 siRNA
Cell area (µm²)
Nuclear area (µm²)
p16+ p21+
p16- p21+
p16+ p21-
p16- p21-

Figure 4.17 Interrogation of p16 and p21 subgroup morphologies at day five following transfection with EGR2 siRNA in three different conditions, and the respective controls. Two independent siRNA screens, each in triplicate, were performed for the five day time point in DS HMFs according to Section 2.6.2. Cells were then fixed and stained with DAPI, mouse anti-p16 (JC8), rabbit anti-p21 (12D1), donkey anti-mouse Alexa Fluor 488, and goat anti-rabbit Alexa Fluor 546. Cells were imaged and intensities were quantitated according to Section 2.7 and 2.8. Nuclear intensity thresholds were established for p16 and p21 to define positive or negative nuclei. Nuclei were classified into four subgroups: p16 and p21 positive (p16+ p21+); p16 negative and p21 positive (p16- p21+); p16 positive and p21 negative (p16+ p21-); and p16 and p21 negative (p16- p21-). Scatter points denote the average median values per subgroup. Dashed lines indicate the 30 nM siGLO mean. N=2 throughout. Error bars=SD of two independent experiments, each performed with three replicates. **(A)** 30 nM siGLO. **(B)** 30 nM EGR2 siRNA. **(C)** 60 nM siGLO **(D)** 60 nM EGR2 siRNA. **(E)** 30 nM p16 siRNA. **(F)** 15 nM EGR2 + 15 nM p16 siRNA. **(G)** 30 nM p21 siRNA. **(H)** 15 nM EGR2 + 15 nM p21 siRNA. **(I)** 15 nM p16 + 15 nM p21 siRNA.

4.5 Discussion and future work

4.5.1 siRNA screening identified 45 siRNAs that drive senescence in both HMECs and HMFs and two siRNAs which eliminate DS HMFs

In summary, siRNA screening identified 45 siRNAs that induced a significant increase in cell number in comparison to the 30 nM siGLO control; one siRNA individually (EGR2 siRNA), two siRNAs in combination with p16 siRNA (FRAS1 and RNF20 siRNA), and 42 siRNAs in combination with p21 siRNA. Subsequently, EGR2 siRNA, FRAS1 siRNA, and the top 12 siRNAs in combination with p21 siRNA which induced an increase in proliferation greater than eight Z scores from the siGLO control were chosen as the top 14 siRNAs to investigate further.

Interestingly, siRNA screening also identified two genes, knockdown of which eliminated senescent cells, HDAC1 and UBC. Senescent cell accumulation is thought to cause progressive harm to the surrounding microenvironment. Targeted destruction of senescent cells is a promising therapy to treat age-related diseases, but senescent fibroblasts show reduced sensitivity to apoptosis making them a difficult target to clear (reviewed in Childs *et al*. 2014) (see Section 1.6). HDAC1 and UBC represent novel targets for senescent cell clearance, and act as a proof of principle that it is possible to shift human adult fibroblasts from a senescent state to apoptosis. However, a major limitation of these genes is that they are likely to be essential for normal cell growth and proliferation. HDAC1 is a component of the histone deacetylase complex, which interacts with pRB, deacetylates p53, and is a key element in control of cell proliferation and apoptosis. UBC is a polyubiquitin precursor associated with numerous cellular processes such as protein degradation, DNA repair, and cell cycle regulation. To investigate the potential role for HDAC1 and UBC in targeted senescent cell clearance, siRNA knockdown of these genes could be performed in normal EP HMFs and HMECs.

4.5.2 Ranking of top hits using multi-parameter analysis identifies candidates for future work

In order to identify the most potent reversal protocol, dose effect and time point extension were investigated in the top 14 siRNAs. Multi-parameter analysis revealed 11 siRNAs that shifted DS fibroblast cell morphology towards a reversed phenotype in a dose dependent manner at the five day time point. This analysis allowed ranking of the

top 14 hit siRNAs, with EGR2 siRNA inducing the strongest dose dependent shift in cellular phenotype and thus ranking highest, followed by MYL12A, BHLHE41, and DAPL1 siRNA. By the seven day time point, fewer siRNAs induced a dose dependent shift in cell morphology, but 12 siRNAs induced a shift in DS fibroblast nuclear morphology towards a reversed phenotype in a dose dependent manner, including EGR2, MYL12A, BHLHE41, and DAPL1 siRNA. Furthermore, double immunofluorescence staining using p16 and p21 antibodies identified eight siRNAs which, in combination with p21 siRNA, significantly increased the double negative subgroup of cells when compared to the 30 nM siGLO control. Of these, EGR2 siRNA had the third greatest increase in the double negative subgroup, after FN1 and JUP siRNA. By the seven day time point, two siRNAs had an increased double negative subgroup compared to the 30 nM siGLO control: MYL12A and FN1 siRNA, indicating that the kinetics of the siRNA knockdown of these genes impacts the cells over a longer time-course than the other siRNAs investigated. Interestingly, this increase in the p16 and p21 double negative subgroup was observed upon knockdown of these genes in combination with p21 and not p16, suggesting that the reversal of senescence via silencing of these genes may be mediated by p16. Given this, it is hypothesised that these genes may act upstream of p16.

In summary, these analyses revealed two siRNAs, EGR2 and MYL12A, which altered cellular and nuclear morphology in a dose dependent manner when transfected alone, and, increased the double negative subgroup in combination with p21 siRNA. BHLHE41 and DAPL1 siRNA transfected alone altered cellular and nuclear morphology in a dose dependent manner but did not significantly increase the double negative subgroup in any condition. FRAS1, JUP, PDCD6IP, HSP90AA1, ACTG1, and FN1 siRNA in combination with p21 siRNA significantly increased the double negative subgroup, but when transfected individually did not rank highly for altered cellular and nuclear morphology at five days or seven days.

Notably, of the 10 siRNAs ranked highly in either one or both analyses, MYL12A, FRAS1, JUP, ACTG1, and FN1 all encode proteins involved with cytoskeleton and cell adhesion; EGR2 and BHLHE41 both encode transcription factors; and DAPL1, PDCD6IP, and HSP90AA1 encode proteins with disparate functions and are thus grouped as ‘other’ (Figure 4.18A). DAPL1, an understudied gene with only six citations in PubMed, has been identified as a susceptibility locus for age-related macular degeneration and human

longevity (Flachsbart *et al.*, 2010; Grassmann *et al.*, 2015), and it has been proposed to play a role in epithelial differentiation (Sun *et al.*, 2006). PDCD6IP encodes an endosome sorting complexes required for transport (ESCRT) protein which is a key player in membrane budding (Sun *et al.*, 2016) and also thought to participate in apoptosis (Strappazzon *et al.*, 2010). HSP90AA1, a stress inducible isoform of the molecular chaperone Hsp90, functions to promote proper protein maturation and structural maintenance (Zuehlke *et al.*, 2015).

The most enriched functional group identified in the top 10 hits siRNAs was genes involved in the cytoskeleton and cell adhesion. MYL12A encodes a myosin regulatory light chain, which regulates the activity of myosins, including non-muscle myosin II (NM II) (Park *et al.*, 2011). NM II is an actin-binding protein which can regulate the actin cytoskeleton to play an important role in cell structure, adhesion, and migration. Notably, ACTG1, a cytoplasmic actin found in non-muscle cells (Baranwal *et al.*, 2012), was also identified as one of the 10 siRNAs ranking highly in this Chapter. Two current theories exist for how NM II mediates cell adhesion through regulation of the actin cytoskeleton (Vicente-Manzanares *et al.*, 2009). Potentially, NM II mediates adhesion maturation either through clustering of actin filaments, therefore increasing molecular interactions between adhesion proteins and increasing their strength, or through the generation of force which activates adhesion components by mechanical stretching. For example, fibronectin is known to undergo conformational changes induced by an integrin-transmitted mechanical force which allows self-assembly into aggregates and fibrils. Furthermore, MYL12A mRNA has been previously identified to increase in premature senescent human colon cancer cells (Dabrowska and Skoneczny, 2011).

FRAS1, a transmembrane protein, appears to function in the regulation of epidermal adhesion during embryogenesis and may be an important regulator of ECM remodeling (Short, Wiradjaja and Smyth, 2007). FRAS1 contains a motif structurally similar to a cadherin fold, which is capable of binding to ECM proteins such as FN1 and collagen, as well as furin motifs which bind and activate TGF-β, potentially allowing regulation of TGF-β signaling (Short, Wiradjaja and Smyth, 2007).

JUP is a member of the catenin family and a cytoplasmic protein which provides a mechanical link between desmosomal cadherins and the cytoskeleton. Interestingly, JUP

has previously been shown to regulate FN1 mRNA stability in murine keratinocytes (Todorović *et al.*, 2010). In addition, JUP and β-catenin are known to up-regulate PML, a marker of senescence (Ferbeyre *et al.*, 2000) (see Section 1.4), which then forms a complex with β-catenin, transactivating a subset of genes including ARF (Shtutman *et al.*, 2002).

FN1 is a major ECM component and plays an important role in cell adhesion, spreading and migration. Fibronectin mRNA increases significantly during replicative senescence in at least two fibroblast strains as well as vascular endothelial cells (Kumazaki, 1992; Kumazaki, Kobayashi and Mitsui, 1993). Integrin-linked kinase (ILK), an integrin-binding cytoplasmic protein, mediates interactions between multiple cytoskeletal proteins, and is involved in the regulation of adhesion, proliferation, and ECM accumulation. A previous study has shown that ILK, fibronectin, and other extracellular matrix components, such as smooth muscle alpha actin (α-SMA) and vimentin, accumulate with age in rat cardiac fibroblasts (Chen *et al.*, 2006). Interestingly, in the cardiac fibroblasts isolated from old rats, ILK siRNA knockdown significantly reduced fibronectin protein expression, as well as α-SMA and vimentin, and prevented fibroblasts from entering senescence, as indicated by down-regulated p21 and p53 expression and decreased SA-β-Gal staining (Chen *et al.*, 2006).

Currently, the relationship between ECM composition, cellular mechanical forces, and senescence remains unclear. Potentially, alterations to ECM composition either through changes in gene expression or induction of conformational changes by internal or external mechanical forces could impact integrin signalling and cytoskeleton dynamics, subsequently affecting nuclear and cellular morphology and inducing expression of genes driving senescence. In support of this, ECM from young cells is sufficient to restore multiple features of the youthful, proliferative phenotype in senescent human fibroblasts, including lower SA-β-Gal activity and increased BrdU incorporation (Choi *et al.*, 2011).

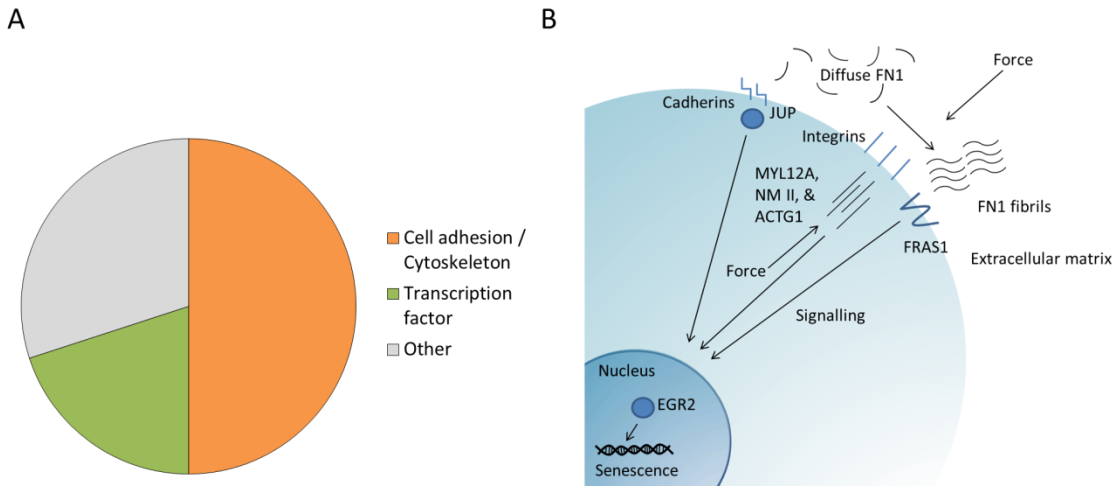

Figure 4.18 Functional analysis of 10 hit siRNAs and theoretical network of siRNAs with cell adhesion/cytoskeleton function. (A) Functional analysis of 10 hit siRNAs revealed five siRNAs targeting genes involved in cell adhesion/cytoskeleton processes, two transcription factors and three defined as 'other'. **(B)** Theoretical network of mechanical force, extracellular matrix, and intracellular signalling. Internal or external forces via MYL12A, NMII, and ACTG1 stretch diffuse FN1 into fibrils, activating signal propagation to the nucleus and potential activation of transcription factors such as EGR2 from outside the cell, potentially via integrin signalling, FRAS1, or cadherin signalling and JUP.

Together, the cytoskeletal and cell adhesion hit siRNAs identified in this Chapter could form a theoretical model for the relationship between ECM, mechanical forces and senescence (Figure 4.18B). Potentially, external mechanical forces or internal forces generated by NMII and MYL12A via ACTG1 could stretch diffuse FN1 in the extracellular matrix into fibrils, thus activating signal propagation to the nucleus and activation of transcription factors such as EGR2 via integrins and integrin-like kinases, cadherin signalling and JUP or other transmembrane proteins such as FRAS1, subsequently altering gene expression and driving senescence induction.

The second largest functional group identified in the top 10 hit siRNAs was transcription factors. BHLHE41 is a transcription factor that represses the clock gene, PER1, through E-box promoter binding and interaction with the transcription factor Sp1, leading to regulation of the circadian rhythm (Li *et al.*, 2004). There is some evidence to suggest a link between senescence and the circadian rhythm; for example, NONO, a multi-functional nuclear protein and partner of PER proteins, binds to p16, thus coupling the cell cycle to the circadian clock (Kowalska *et al.*, 2013). In addition, age-dependent

changes in circadian rhythm have been observed using *in vitro* bioluminescence recordings of Per1 (circadian clock gene) -luciferase at different ages in primary rat dermal fibroblast cultures (Sandu *et al.*, 2015). However, previous work has demonstrated that overexpression of BHLHE41 inhibits proliferation of lung cancer cells via down-regulation of cyclin D1 expression (Falvella *et al.*, 2008). In line with this, BHLHE41 siRNA did not significantly increase the double negative subgroup in combination with p21 siRNA despite inducing an increase in cell number, potentially indicating a role in senescence via an alternate mechanism to the p16/pRB and p53/p21 pathways, as well as suggesting BHLHE41 may act as a tumour suppressor inducing senescence bypass following siRNA knockdown (Figure 4.14). There is also growing support for a connection between disruption of circadian clock function, long interspersed element-1 (LINE-1; L1) retrotransposon-associated genomic instability and ageing. Melatonin, a neuro-hormone produced during the dark phase of the light/dark cycle, suppresses expression of L1 retrotransposons, preventing DNA damage via insertions and DNA double-strand breaks, thereby preventing senescence (Belancio *et al.*, 2014). Consistent with this theory, transient L1 overexpression in primary normal human fibroblasts and stem cells leads to senescence (Belancio *et al.*, 2010).

In an earlier screen, EGR2 was identified as one of the most potent inducers of senescence reversal in DS HMECs. EGR2 is a transcription factor and putative tumour suppressor; and expression of EGR2 is often decreased in human tumours and cancer cell lines (Unoki and Nakamura, 2001) (see Section 1.8.5). Defects in this gene are associated with diseases such as Charcot-Marie-Tooth syndrome, a demyelinating neuropathy of the PNS (Šafka Brožková *et al.*, 2012) (see Section 1.8.3). In PNS glial cells (Schwann cells), EGR2 is required to initiate myelin formation and to control exit from the cell cycle in a manner potentially involving p16 and p21 (Atanasoski *et al.*, 2006; Srinivasan *et al.*, 2012). One study determined that EGR2 over-expression blocks proliferation in both rat Schwann cells and mouse fibroblasts (Parkinson *et al.*, 2004). In a ChIP-Seq study of EGR2 in myelinating rat sciatic nerve, peaks of EGR2 binding were identified in the p21 gene (Srinivasan *et al.*, 2012). In addition, analysis of EGR2-deficient mice has identified decreased expression of p21 (Le *et al.*, 2005). The wider role of EGR2 was explored in more detail in Chapter 1 Section 1.8, and further discussion of EGR2 will be presented in Chapter 5 Section 5.7, and Chapter 6 Sections 6.3 and 6.4.

Once validated, these hits represent potential drivers of senescence and future novel therapeutic targets. In summary, this data reveals EGR2 siRNA as the strongest scorer for senescence reversal in the DS fibroblasts, followed by MYL12A, FRAS1, BHLHE41, DAPL1, JUP, PDCD6IP, HSP90AA1, ACTG1, and FN1 siRNA. Subsequently, EGR2 was selected for further validation and investigation as a potential driver senescence, and as such will be explored in more detail in Chapter 5.

Chapter 5 Validation of EGR2 as a driver of senescence

5.1 Introduction

In Chapter 4, siRNA screening revealed EGR2 siRNA as the top hit for senescence reversal in both DS HMECs and HMFs, potentially identifying a novel driver of senescence. Within this Chapter, the mechanism by which EGR2 drives senescence will be explored and EGR2 will be validated as a hit for senescence reversal. In order to achieve this, bioinformatics analysis will be performed identifying genes containing predicted EGR2 binding sites which are associated with HMEC senescence, thus revealing potential EGR2-regulated genes driving senescence. Furthermore, genes which are known to be directly regulated by EGR2 in the literature will be compared to genes up-regulated in HMEC senescence in order to further identify potential EGR2-regulated genes in senescence. EGR2 protein levels will be investigated to determine whether an increase is observed during senescence in HMECs and HMFs, and EGR2 siRNA knockdown will be validated using phenotypic analysis and immunofluorescence staining of the deconvoluted siRNA pool. The interplay between the p16/pRB and p53/p21 pathways and EGR2 levels will also be explored using immunofluorescence staining following siRNA knockdown of p16 or p21 in DS HMFs.

5.1.1 Chapter aims

1. To investigate the potential mechanism of EGR2 driving senescence using bioinformatics.
2. To determine whether EGR2 expression increases in HMF and HMEC senescence.
3. To validate EGR2 as a driver of senescence in DS HMFs using three individual siRNAs targeting EGR2.
4. To investigate the interplay between siRNA knockdown of p16 and p21, and EGR2 protein levels.

5.2 Bioinformatics to decipher the mechanism of EGR2 driving senescence

5.2.1 Re-mining the HMEC gene expression array for EGR2 binding sites

To explore the potential mechanisms through which EGR2 may be driving senescence and identify a panel of genes that might be regulated by EGR2 during senescence, bioinformatics was used to re-mine the senescence-associated genes identified in the

HMEC gene expression array (Bishop, unpublished) (see Section 4.1) for EGR2 transcription factor binding sites in collaboration with Dr Rob Lowe.

MethylCap-seq, a method based on affinity purification of methylated DNA using the methyl-CpG-binding domain (MBD) of the methyl-CpG-binding protein 2 (MeCP2) and subsequent next-generation sequencing, has revealed differentially methylated regions (DMRs) during long-term culture of adult human dermal fibroblasts (Hänzelmann *et al.*, 2015). To correlate senescence-associated DMR changes with gene expression changes, the transcriptome of early and late passage fibroblasts was sequenced (Hänzelmann *et al.*, 2015). Following this, analysis of transcription factor binding sites in genes found to be differentially expressed in senescence revealed that the EGR2 transcription factor binding site is significantly enriched in the promoter regions of both up- and down-regulated genes. Interestingly, GO analysis of the differentially expressed genes revealed a highly significant enrichment for cell division and DNA repair in down-regulated genes, and for cell adhesion and extracellular matrix organisation in up-regulated genes. Further investigation of the differentially expressed genes identified two hits for senescence reversal in the DS HMF siRNA screen, sortilin 1 (SORT1), proliferating cell nuclear antigen (PCNA), as well as actin, gamma 2 (ACTG2), a cytoplasmic actin similar to the highly-ranking reversal hit, ACTG1 (see Section 4.3.1).

Given this, it was hypothesised that EGR2 could selectively bind to promoters driving expression of genes important for the initiation and/or maintenance of senescence in DS HMECs. In order to investigate this, the senescence-associated differentially expressed genes identified in the HMEC gene expression array (Bishop, unpublished) were analysed for the previously published EGR2 consensus binding sequences (ACGCCCACGCA) (Jolma *et al.*, 2013; Mathelier *et al.*, 2016) (Figure 5.1A) and compared to randomly sampled background gene sets, according to Section 2.11. In line with the literature, there was a small but significant enrichment for EGR2 binding sites at the promoters of genes dynamic in HMEC senescence relative to random sampling (1.03 fold enrichment; p=0.04) (Figure 5.1B). Strikingly, 13 of the genes differentially expressed during HMEC senescence identified to contain an EGR2 binding site were also identified as drivers of senescence in the DS HMEC screen (Figure 5.1C). Furthermore, nine of these genes were identified as hits for senescence reversal in the DS HMF siRNA screen (S100A4, MUM1 like 1 (MUM1L1), cystatin E/M (CST6), FXYD domain containing ion

transport regulator 3 (FXYD3), phospholipase C gamma 2 (PLCG2), ZPLD1, fucosyltransferase 2 (FUT2), SORT1, and flavin containing monooxygenase 4 (FMO4)) (see Section 4.3.1). This suggests that EGR2 may drive senescence by altering the expression of these genes. S100A4, for example, was classified as a top hit in the DS HMF screen (see Section 4.4), and in combination with p21 siRNA knockdown induced a reversed phenotype in the DS HMFs similar to EGR2 siRNA knockdown (see Section 4.4.1). Interestingly, no interactors were identified to contain predicted EGR2 transcription factor binding sites in the dataset of genes dynamically expressed during HMEC senescence (Figure 5.1C). However, closer examination of the dataset revealed that no interactor met the stringent threshold used to define dynamic expression during HMEC senescence (q value<0.01), and thus all were excluded from the analysis. Consequently, these interactors may potentially contain predicted EGR2 binding sites that were not identified here.

Interestingly, both p16 and p15 were also identified to contain EGR2 transcription binding sites in this analysis. p21 expression increased in HMEC senescence but did not meet the stringent threshold (q value<0.01) used in this analysis, therefore it was excluded from this analysis. However, post-hoc examination of the p21 promoter identified the presence of EGR2 binding sites, in line with the literature (Zhu *et al*. 2008; Srinivasan *et al*. 2012). These data suggest a direct role for EGR2 up-regulation of p16 and p21 expression during senescence, supporting the previous observation that p16 and p21 protein levels decreased in DS HMFs following EGR2 siRNA knockdown (see Section 4.4.1). It is also important to note that the EGR2 promoter did not contain EGR2 transcription factor binding sites, indicating that EGR2 does not auto-regulate its expression in humans.

A

B

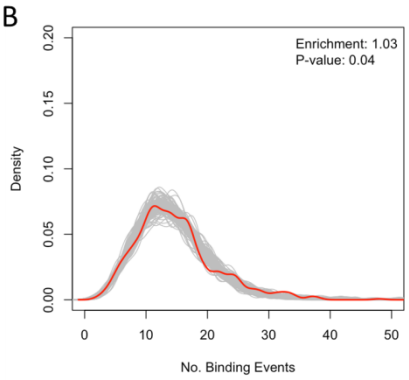

C

Drivers		Interactors	
BHLHE41	**ZPLD1**	ACLY	JUP
C3	TMEM159	ACTB	MTR
CDKN2A	DAPL1	ACTBL2	MYL12A
CST6	**PLCG2**	ACTG1	PCNA
FILIP1L	**PNCK**	BAG6	PDCD6IP
EGR2	**PTPRF**	CD9	PPFIA1
STRA6	RARRES1	CTNNB1	PPFIBP1
CWH43	**S100A4**	DEAF1	PSMA1
MUM1L1	SORT1	FLOT1	RNF2
FMO4	TCN1	FN1	RNF20
FRAS1	**UBD**	FYN	RNF40
FUT2		GGA1	SMAD3
FXYD3		GRIP1	SUMO2
G1P3		HDAC1	TSG101
HIST1H2BD		HIF1A	UBC
CFI		HSP90AA1	YWHAQ
IL1RN		IGBP1	

Figure 5.1 Identifying EGR2 binding sites in drivers of senescence using bioinformatics. (A) EGR2 DNA binding motif (Jolma *et al.*, 2013; Mathelier *et al.*, 2016). **(B)** The EGR2 DNA binding motif was investigated in the promoters of genes up-regulated in HMEC senescence (red) relative to random sampling (grey). Analysis performed by Dr Rob Lowe. **(C)** The gene promoters predicted to contain EGR2 DNA binding motifs in the DS HMF siRNA screen are presented here in bold.

5.2.2 Cross comparison of genes up-regulated in HMEC senescence with genes regulated by EGR2 in the literature

To further identify potential EGR2-regulated genes driving senescence, the genes found to increase during senescence in the HMEC gene expression array were cross-referenced with genes known to be directly regulated by EGR2 in the literature.

As the current literature focuses on the role of EGR2 in myelinating Schwann cells and T cell anergy (see Section 1.8), previous work identifying targets directly regulated by EGR2 has been performed in rat myelinating nerve and mouse T cell anergy models (Srinivasan *et al.*, 2012; Zheng *et al.*, 2013). Genome-wide ChIP-Seq has been performed using pooled rat myelinating sciatic nerve to reveal 153 genes with EGR2 binding peaks within 100 kb which were previously identified to be down-regulated by EGR2 deficiency in microarray analyses (Srinivasan *et al.*, 2012). This identified peaks of EGR2 binding within genes involved in neurogenesis, myelination, and cell cycle exit, including p21 and p27 (Srinivasan *et al.*, 2012). Using a T cell anergy model, microarray analysis of anergised CD4+ T helper 1 (Th1) cells harvested from an $EGR2^{flox/flox}$ mouse model compared with or without prior EGR2 Cre-mediated deletion revealed 90 probes up-regulated upon anergy induction in an EGR2-dependent manner (Zheng *et al.*, 2013). Subsequent ChIP-Seq for EGR2 binding sites comparing anergised Th1 cells to untreated Th1 cells identified 47 genes which were directly up-regulated by EGR2 in T cell anergy (Zheng *et al.*, 2013). Given that the aim of this Chapter is to investigate the mechanism of EGR2 in adult human fibroblast and epithelial senescence, these data sets are used for cross-comparison with the senescence-associated HMEC gene expression array with the caveat that many of the EGR2 gene targets identified in these data may be species- or cell-type specific.

As EGR2 is thought to act as a transcriptional activator (Fang *et al.*, 2011; Srinivasan *et al.*, 2012; Zheng *et al.*, 2013), the genes identified to be up-regulated during HMEC senescence (q value<0.05) were cross-compared with the 153 gene targets identified in pooled rat sciatic nerve and the 47 gene targets identified in murine T cell anergy (Figure 5.2A). This analysis revealed 30 genes up-regulated in HMEC senescence which are known to be directly regulated by EGR2 in the literature, including 17 genes identified as EGR2 targets in pooled rat sciatic nerve (Figure 5.2B) and 13 in murine T cell anergy (Figure 5.2C). Of these 30 genes, further interrogation revealed five genes which were

predicted to possess EGR2 transcription factor binding sites in the HMEC array analysis performed in Section 5.2.1: regulator of cell cycle (C13ORF15); MTSS1, I-BAR domain containing (MTSS1); Kruppel like factor 9 (KLF9); protocadherin 7 (PCDH7); and ferritin heavy chain 1 (FTH1). Fascinatingly, GO analysis of these five genes identified a significant enrichment for 'negative regulation of epithelial cell proliferation' (>100 fold enrichment; p=0.0015), indicating that the genes potentially directly regulated by EGR2 in HMEC senescence (RGCC, KLF9, MTSS1, and FTH1) function to inhibit proliferation. Furthermore, as the q value for the increase in p21 (CDKN1A) expression in HMEC senescence was below the threshold used in this analysis (q value<0.05), it was included in this comparison and thus identified as a direct target of EGR2 which was up-regulated in both HMEC senescence and rat nerve myelination. Interestingly, EGR2 was identified as an auto-regulatory target in murine T cell anergy, although EGR2 was not identified to possess EGR2 transcription factor binding sites in the analysis performed in Section 2.11, indicating potential species and/or cell type-specific auto-regulation.

In addition, genome-wide transcriptional profiling of EGR2 overexpressing human foreskin fibroblasts has revealed 348 genes which showed a greater than twofold expression increase in response to EGR2 overexpression (Fang *et al.*, 2011). Cross-comparison of these 348 genes with those found to be up-regulated during HMEC senescence identified 46 genes which were present in both datasets. Interestingly, five of these genes were also identified in the DS HMF siRNA screen as potential drivers of senescence: actin beta (ACTB); ACTG1; CTNNB1; HIF1A; and FYN proto-oncogene, Src family tyrosine kinase (FYN) (see Section 4.3.1). Further interrogation of the 46 genes up-regulated in HMEC senescence and in EGR2-overexpressing fibroblasts revealed nine genes which were predicted to contain EGR2 transcription factor binding sites in the HMEC array analysis (TSC22 domain family member 2 (TSC22D2), SPARC/osteonectin, cwcv and kazal like domains proteoglycan 1 (SPOCK1), unc-51 like autophagy activating kinase 1 (ULK1), membrane metalloendopeptidase (MME), lysyl oxidase like 4 (LOXL4), monooxygenase DBH like 1 (MOXD1), ankyrin repeat and FYVE domain containing 1 (ANKFY1), reversion inducing cysteine rich protein with kazal motifs (RECK), and fibroblast growth factor 2 (FGF2)) (Figure 5.2D). However, these were not found to be significantly enriched for a biological process using GO analysis. Interestingly, the pro-inflammatory protein, protein S (alpha) (PROS1), was identified as a transcriptional

target of EGR2 in both rat myelinating nerve and murine T cell anergy. In addition, caveolin 2 (CAV2) was identified as a direct target of EGR2 in both rat myelinating nerve and human foreskin fibroblasts (Figure 5.2E). Fascinatingly, caveolins function to form specialised invaginations of the plasma membrane called caveolae, which are thought to play vital roles in diverse cellular processes, including cell signalling, cell adhesion and mechanosensing (reviewed in Pat-Horenczyk & Brom 2007). Together with the drivers identified to be putative EGR2 transcriptional targets in the HMEC gene expression array (see Section 5.2.1), these genes could form the basis for future work investigating downstream EGR2-regulated genes and potential pathways driving senescence, which will be further explored in Section 5.7.1

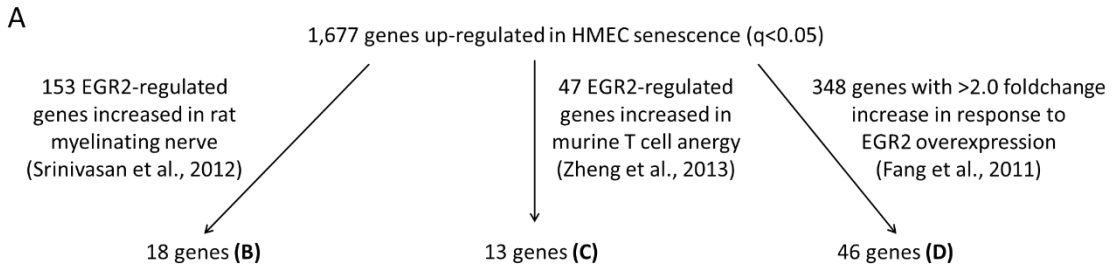
A
1,677 genes up-regulated in HMEC senescence (q<0.05)
153 EGR2-regulated genes increased in rat myelinating nerve (Srinivasan et al., 2012)
47 EGR2-regulated genes increased in murine T cell anergy (Zheng et al., 2013)
348 genes with >2.0 foldchange increase in response to EGR2 overexpression (Fang et al., 2011)
18 genes (B)
13 genes (C)
46 genes (D)

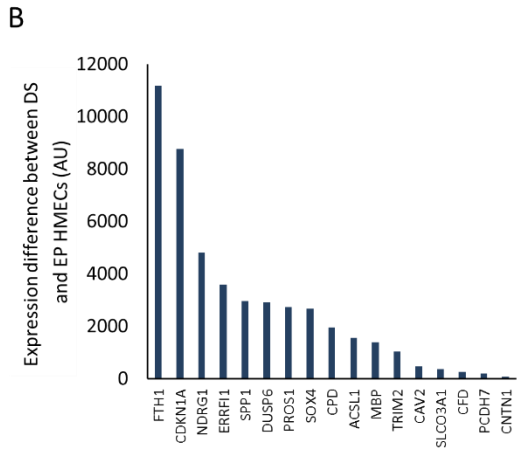
B
Expression difference between DS and EP HMECs (AU)
12000
10000
8000
6000
4000
2000
0
FTH1
CDKN1A
NDRG1
ERRFI1
SPP1
DUSP6
PROS1
SOX4
CPD
ACSL1
MBP
TRIM2
CAV2
SLCO3A1
CFD
PCDH7
CNTN1

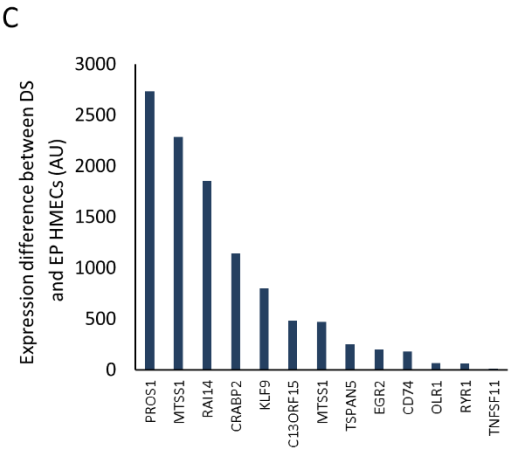
C
Expression difference between DS and EP HMECs (AU)
3000
2500
2000
1500
1000
500
0
PROS1
MTSS1
RAI14
CRABP2
KLF9
C13ORF15
MTSS1
TSPAN5
EGR2
CD74
OLR1
RYR1
TNFSF11

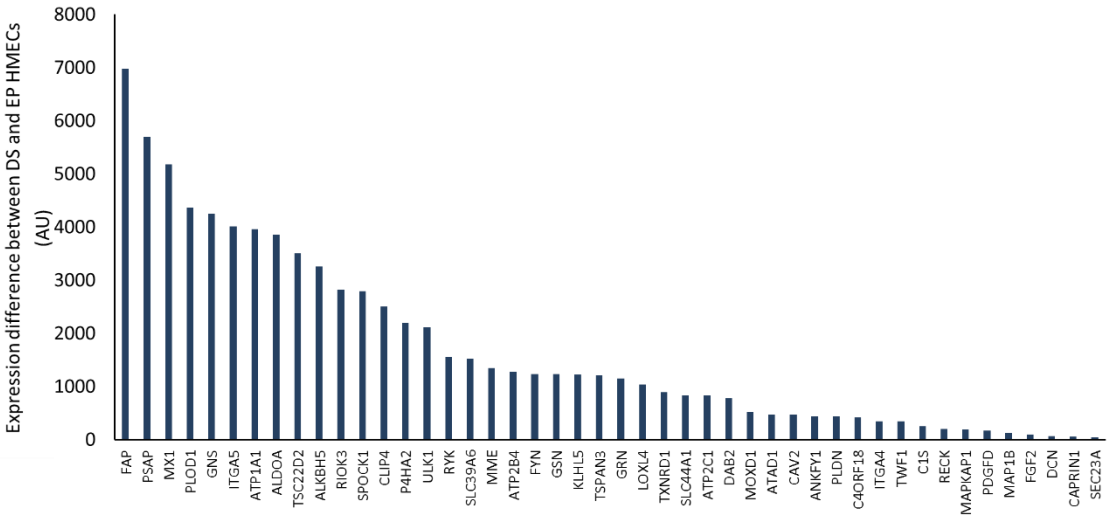
D
Expression difference between DS and EP HMECs (AU)
8000
7000
6000
5000
4000
3000
2000
1000
0
FAP
PSAP
MX1
PLOD1
GNS
ITGA5
ATP1A1
ALDOA
TSC22D2
ALKBH5
RIOK3
SPOCK1
CLIP4
P4HA2
ULK1
RYK
SLC39A6
MME
ATP2B4
FYN
GSN
KLHL5
TSPAN3
GRN
LOXL4
TXNRD1
SLC44A1
ATP2C1
DAB2
MOXD1
ATAD1
CAV2
ANKFY1
PLDN
C4ORF18
ITGA4
TWF1
C1S
RECK
MAPKAP1
PDGFD
MAP1B
FGF2
DCN
CAPRIN1
SEC23A

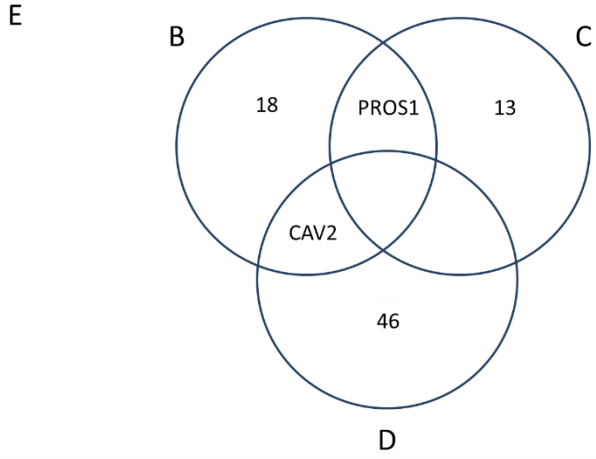
E
B
C
18
PROS1
13
CAV2
46
D

Figure 5.2 Cross comparison of genes up-regulated in HMEC senescence with the literature. **(A)** Schematic depicting methodology for comparison of the HMEC senescence-associated up-regulated genes (Bishop, unpublished) with three published datasets of EGR2-regulated genes. **(B-D)** Genes with increased expression in HMEC senescence (q value<0.05) were cross compared with genes identified to be directly up-regulated by EGR2 in **(B)** pooled rat sciatic nerve (Srinivasan *et al.*, 2012) **(C)** mouse T cell anergy (Zheng *et al.*, 2013) or **(D)** up-regulated in EGR2 overexpressing human foreskin fibroblasts by a greater than twofold change (Fang *et al.*, 2011).**(E)** Overlap between the genes identified in the cross-comparison as directly up-regulated by EGR2 in one of the three published datasets (B, C, D) and up-regulated during HMEC senescence.

5.3 Investigating EGR2 protein levels in senescence

As reversal of senescence can be achieved in both HMECs and HMFs following EGR2 siRNA knockdown, EGR2 has been implicated as a driver of senescence in both cell types (see Section 4.5.1). In support of this, previous work in the lab. has shown that EGR2 gene expression increases in HMEC senescence (Bishop, unpublished). Given this, it was hypothesised that both HMECs and HMFs would possess elevated EGR2 protein levels during senescence. As EGR2 is a member of the EGR family (see Section 1.8.1), it is important to note that although both EGR2 and EGR3 had significantly increased gene expression in DS HMECs, EGR2 was the only member of the EGR2 family whose gene expression significantly decreased in reversed HMECs (Bishop, unpublished), indicating that EGR2 may act to drive senescence, whilst EGR3 may simply be a passenger in the process.

5.3.1 Identification of a suitable anti-EGR2 antibody for quantification of EGR2 protein levels

In order to investigate EGR2 protein levels in HMECs and HMFs, the literature was mined to identify a suitable anti-EGR2 antibody, revealing rabbit anti-human EGR2 (PRB-236P) (BioLegend, UK (formerly Covance)) as the gold standard anti-EGR2 antibody for western blotting (Grunewald *et al.*, 2015; Nafez *et al.*, 2015; Salotti *et al.*, 2015), immunofluorescence staining (Gomez-Sanchez *et al.*, 2013; Wu *et al.*, 2016), and ChIP experiments (Srinivasan *et al.*, 2012; Zheng *et al.*, 2013). Interestingly, EGR2 has a predicted molecular weight 53 KDa; however, rabbit anti-human EGR2 (PRB-236P) has been shown to identify multiple bands between 75 and 50 KDa using western blotting (Grunewald *et al.*, 2015; Nafez *et al.*, 2015; Salotti *et al.*, 2015) . These multiple EGR2 bands may be generated as a result of multiple isoforms and/or post-translational modifications altering the molecular weight or proper migration of the protein. Investigation of the EGR2 gene and protein sequence identified multiple EGR2 transcripts encoding two isoforms: isoform A (predicted molecular weight, 50.31 KDa), and a slightly shorter isoform B (predicted molecular weight, 44.97 KDa), with both isoforms containing three phosphorylation sites, which could result in proteins of varying molecular weights due to de-phosphorylation events during lysate collection (Figure 5.3). Furthermore, both isoforms contain 14 cysteines capable of forming covalent di-sulphide bonds, potentially increasing the stability of the folded protein

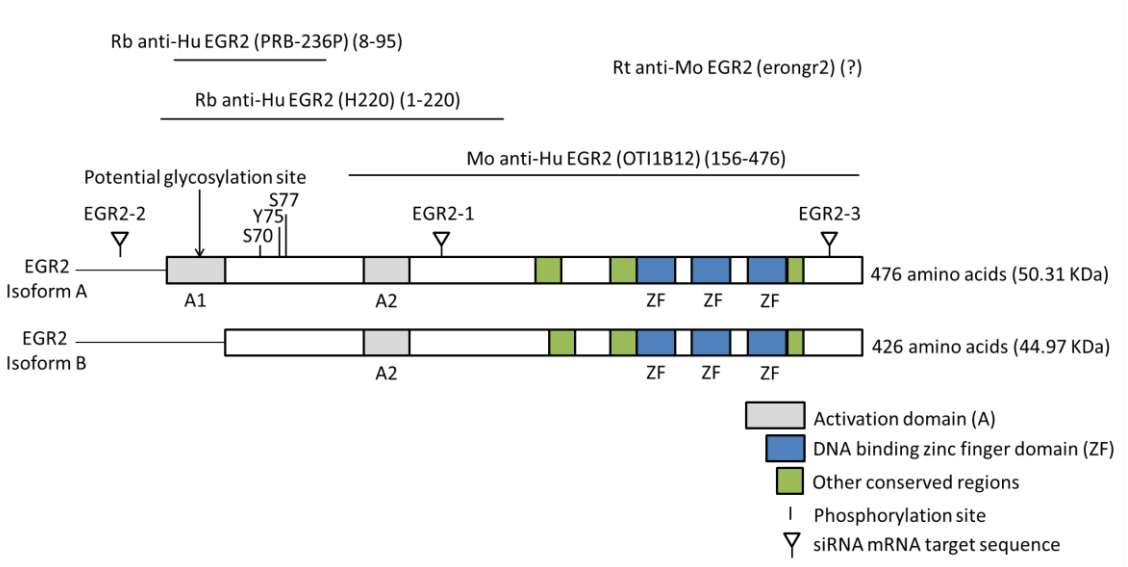

Figure 5.3 Schematic representation of the two human EGR2 isoforms, EGR2 family conserved regions, post-translational modification sites, EGR2 siRNA target sequences and anti-EGR2 antibody binding sites. There are several conserved regions between the EGR family members: the DNA binding zinc finger domains (blue), regions flanking the zinc finger domains and NAB interaction domain (green), and transcriptional activation domains (grey). Three phosphorylation sites have been identified in both EGR2 isoforms (http://www.phosphosite.org) as well as a potential glycosylation site present in isoform A. The siRNA mRNA target sequence translated into its location on the protein is also indicated for the three individual EGR2 siRNAs used in this project. Anti-EGR2 antibody binding sites are indicated: rabbit anti-human EGR2 (PRB-236P) which binds to the N-terminus between amino acids 8 and 95; rabbit anti-human EGR2 (H220) which binds to the N-terminus between amino acids 1 and 220; and mouse anti-human EGR2 (OTI1B12) which binds to the C-terminus between amino acids 156 and 476. There is no information provided on the binding site of rat anti-mouse EGR2 (erongr2).

conformation, preventing complete denaturation and monomeric migration of the protein. In addition, O-N-Acetylglucosamine (O-GlcNAc) glycosylation, the covalent attachment of β-N-acetylglucosamine to serine or threonine residues, has been shown to occur at the N-terminal A1 activation domain of family member EGR1, a domain which is shared with EGR2 isoform A (Khidekel *et al.*, 2007) (see Section 1.8.1; Figure 5.3).

Unfortunately, the rabbit anti-human EGR2 antibody (PRB-236P) was discontinued in October 2015 due to batch variability. Subsequently, multiple commercially available EGR2 antibodies were tested in multiple conditions in an attempt to identify a suitable

EGR2 antibody for investigation of EGR2 protein levels (see Appendix Table A.3). It should be noted that validation was focused at the protein level as this is the functional unit of the EGR2 transcription factor. As mouse EGR2 and human EGR2 proteins are highly homologous (89% identical and 95% similar sequences), anti-EGR2 antibodies were tested using WT and conditional EGR2 knockout murine T cell ($EGR^{-/-}$) lysates harvested from hCD2-Cre x $EGR2^{flox/flox}$ mice, kindly donated by Prof. Wang and Dr Miao (see Appendix Figure A.8). Antibodies tested included mouse anti-human EGR2 (OTI1B12), rat anti-mouse EGR2 (erongr2), and rabbit anti-human EGR2 (H220) antibodies (binding sites indicated in Figure 5.3). However, mouse anti-human EGR2 (OTI1B12) recognised numerous non-specific bands (approximate molecular weights: 25; 30; 50; 70; and 80 KDa) (see Appendix Figure A.8), and rat anti-mouse EGR2 (erongr2) generated a poor signal, thus requiring a high antibody concentration and long incubation period which resulted in irreproducible results via western blotting (see Appendix Figure A.8 and Appendix Table A.3). Only one antibody, rabbit anti-human EGR2 (H220), consistently produced a smeary band between 50 and 75 KDa, in line with the molecular weight of the multiple bands present in the literature (Grunewald *et al.*, 2015; Nafez *et al.*, 2015; Salotti *et al.*, 2015). Importantly, this smeary band was of stronger intensity than the non-specific bands (Appendix Figure A.9). Accordingly, rabbit anti-human EGR2 (H220) was selected for future optimisation.

In order to enable investigation of EGR2 protein levels using western blotting, multiple attempts were undertaken to improve the resolution of the rabbit anti-human EGR2 (H220) band. As previous inspection of the EGR2 gene and protein sequence had identified three phosphorylation sites, phosphatase inhibitors were added to the lysis buffer according to Section 2.4.1 in order to maintain the phosphorylated protein state and prevent potential de-phosphorylation events which may generate EGR2 proteins of varying molecular weights. In addition, as both EGR2 isoforms possess 14 cysteines capable of forming covalent di-sulphide bonds, the concentrations of β-mercaptoethanol and SDS in the Laemmli sample buffer were increased to 10% and 4%, respectively, in order to ensure complete denaturation of the protein and proper migration of the protein through the gel. Furthermore, lysate fractionation was performed to isolate the nuclear extract, potentially enriching the lysate for nuclear EGR2 transcription factor and maximising antibody binding specificity. Despite these

attempts to improve the resolution (see Appendix Table A.3), the EGR2 band between 50 and 75 KDa remained a smear, preventing accurate quantitation of EGR2 protein levels. In future, as EGR2 may possess O-GlcNAc glycosylation at the N-terminus (Figure 5.3), and protein glycosylation is known to impact protein folding, stability, and molecular weight, de-glycosylation of EGR2 could be investigated in order to attempt to improve resolution of the EGR2 band and allow future investigation of EGR2 protein levels using western blotting, as explored in more detail in Chapter 6 Section 6.3.1.

Although the smeary band generated by rabbit anti-human EGR2 (H220) antibody was not quantifiable via western blotting, the band was at the appropriate molecular weight (between 50 and 75 KDa) in EP and DS HMFs in line with the literature (Grunewald *et al.*, 2015; Nafez *et al.*, 2015; Salotti *et al.*, 2015), and was identified to be significantly stronger than the few non-specific bands present (see Appendix Figure A.9). As such, EGR2 protein levels were not interrogated via western blotting in this Chapter and the rabbit anti-human EGR2 (H220) antibody was subsequently optimised for immunofluorescence staining which was then used as the primary method for EGR2 protein level investigation.

5.3.2 Immunofluorescence staining for EGR2 protein levels in EP and DS HMFs and HMECs

Following optimisation of rabbit anti-human EGR2 (H220) antibody for immunofluorescence, EGR2 protein expression was quantified in the EP and DS fibroblasts using immunofluorescence staining. EP and DS HMFs were seeded at the previously optimised density of 15,000 cells/cm^2 (see Section 2.6.3). After five days, cells were stained with DAPI, rabbit anti-EGR2, and Cell Mask according to Section 2.7 and Section 2.8.

As a transcription factor, EGR2 possesses a nuclear localisation signal and functions to regulate gene transcription within the nucleus (see Section 1.8.1), thus it is hypothesised that functional EGR2 would be localised within the nucleus during senescence. In support of this, immunofluorescence staining of EGR2 in EP and DS HMFs showed a trend towards increased nuclear density in the DS population (Figure 5.4, Figure 5.5A), and a significant increase in the number of nuclear EGR2 foci in DS HMFs (Figure 5.5B). Importantly, transcription occurs at discrete sites in the nucleus known as ‘transcription

factories' (Jackson *et al.*, 1993). Thus, a significant increase in EGR2 nuclear foci may demonstrate an increase in the functional transcriptional foci of EGR2 during senescence, indicating a role for EGR2 in senescence. Interestingly, the number of cytoplasmic EGR2 foci was not significantly increased in DS compared to EP HMFs (Figure 5.4, Figure 5.5CD), potentially indicating an increase in cytoplasmic to nuclear translocation.

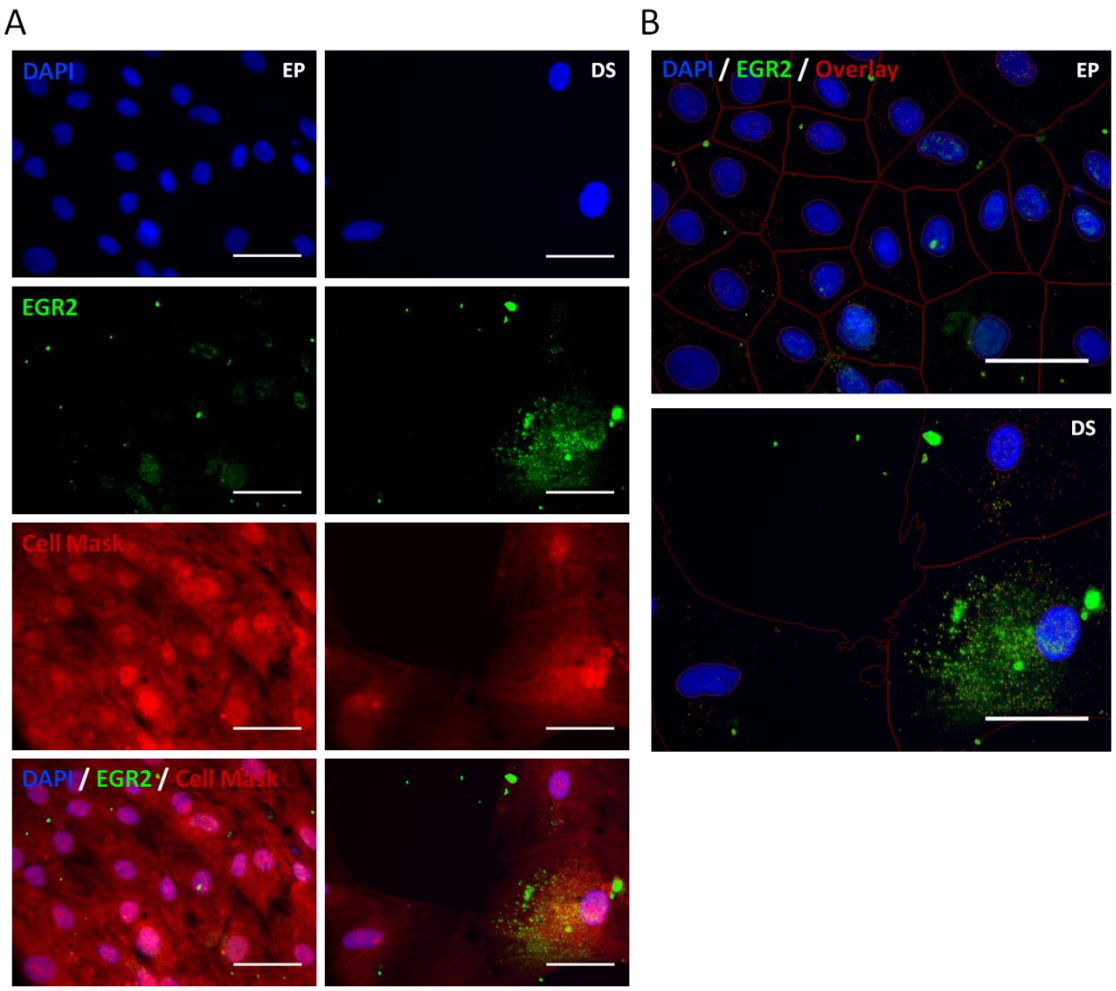

Figure 5.4 Representative images of EGR2 expression in EP and DS HMFs using immunofluorescence. EP and DS HMFs were seeded at 15,000 cells/cm^2 in 384-well plate format, fixed at day five, stained with DAPI, rabbit anti-human EGR2 (H220), goat anti-rabbit Alexa Fluor 488, and Cell Mask. EGR2 cellular and nuclear density and foci were quantitated according to Section 2.7 and Section 2.8. **(A)** Representative immunofluorescence images of EP and DS fibroblasts. DAPI (blue), EGR2 (green), Cell Mask (red). Scale bar denotes 50 µm. **(B)** Enlarged representative immunofluorescence images stained with DAPI, EGR2, and Cell Mask with the nuclear, cellular, and foci segmentation overlay. Scale bar denotes 50 µm.

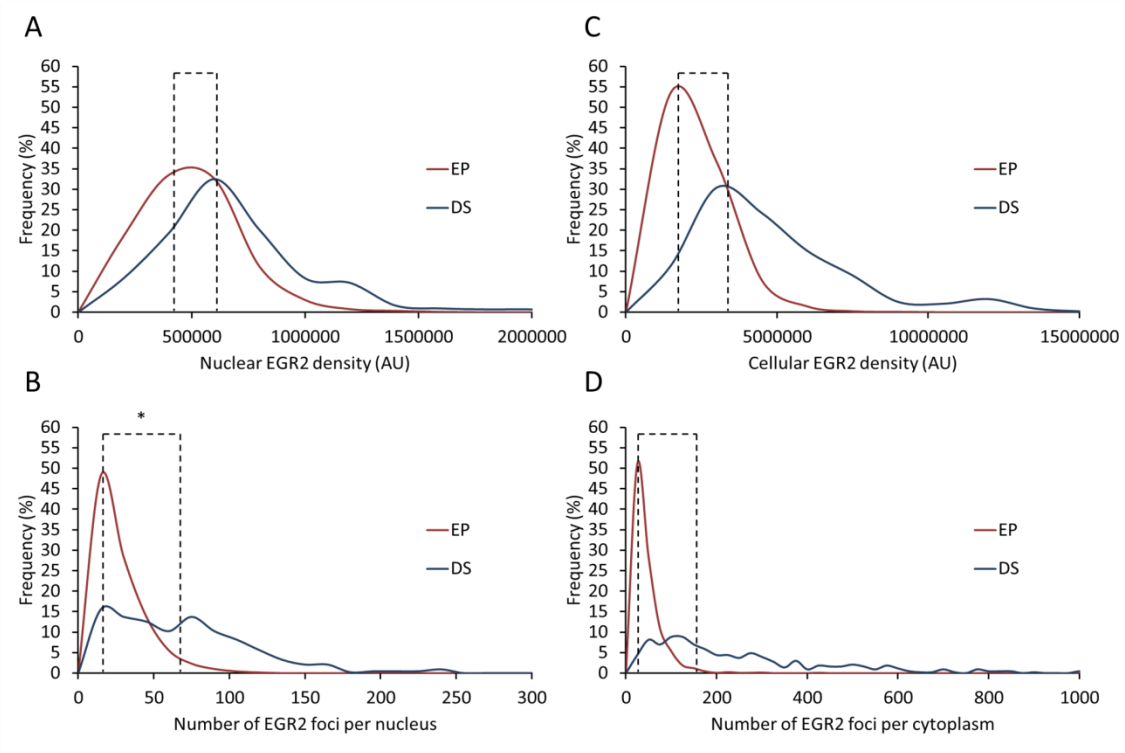

Figure 5.5 EGR2 expression in EP and DS HMFs using immunofluorescence. EP and DS HMFs were seeded at 15,000 cells/cm^2 in 384-well plate format, fixed at day five, stained with DAPI, rabbit anti-human EGR2 (H220), goat anti-rabbit Alexa Fluor 488, and Cell Mask. EGR2 cellular and nuclear density and foci were quantitated according to Section 2.7 and Section 2.8. Frequency distribution plots for **(A)** nuclear EGR2 density levels and **(B)** number of nuclear EGR2 foci, and **(C)** cellular EGR2 protein density levels and **(D)** number of cytoplasmic EGR2 foci for EP and DS HMFs. Un-paired two-tailed t-test of the medians * $p<0.05$. Two independent experiments, each containing three technical repeats were performed.

Given that EGR2 was first identified as a driver of senescence in HMECs (see Section 4.5.2), it was hypothesised that EGR2 nuclear levels should also increase during HMEC senescence. EP (P6) and DS (P11+3) HMECs were seeded at the previously optimised density of 7,500 or 10,000 cells/cm^2, respectively. HMEC cell culture and seeding was performed by Dr Cleo Bishop. After five days, cells were stained with DAPI, rabbit anti-EGR2, and Cell Mask according to Section 2.7 and Section 2.8.

Similar to the trend in DS HMFs towards increased nuclear EGR2 density, DS HMECs had significantly increased EGR2 nuclear density levels (Figure 5.6, Figure 5.7A). Furthermore, a trend towards increased nuclear foci was also observed, but this did not appear to be statistically significant in HMECs (Figure 5.6, Figure 5.7B). However, HMEC populations are known to undergo p16-dependent senescence heterogeneously, leading to the presence of approximately 20% p16-positive senescent HMECs within the EP population (see Section 1.3.1) (Bishop *et al.*, 2010). Accordingly, senescent HMECs were observed in the EP population which displayed nuclear EGR2 foci (Figure 5.6), indicating up-regulation of EGR2 nuclear foci during HMEC senescence in the EP population. Subsequent removal of senescent HMECs from the EP dataset by thresholding for increased cell area, a marker of senescence and a measure previously validated to correlate p16-positive status (Bishop *et al.*, 2010), revealed a significant increase in nuclear foci in DS HMECs compared to the solely EP population (Figure 5.6, Figure 5.7C). In addition, EGR2 cellular density was significantly increased in the DS HMECs (Figure 5.6, Figure 5.7D), and, in line with the DS HMFs, a trend towards increased cytoplasmic foci was observed in DS HMECs (Figure 5.6, Figure 5.7E). However, unlike EGR2 nuclear foci, subsequent removal of senescent HMECs from the EP dataset did not reveal a significant increase in cytoplasmic foci in DS HMECs compared to the solely EP population (Figure 5.6, Figure 5.7F), suggesting that the significantly increased nuclear foci represent the important functional unit of EGR2 in HMEC senescence. In conclusion, both HMFs and HMECs have significantly increased EGR2 nuclear foci in senescence, potentially indicating the presence of EGR2 'transcription factories' driving expression of the genes enforcing senescence.

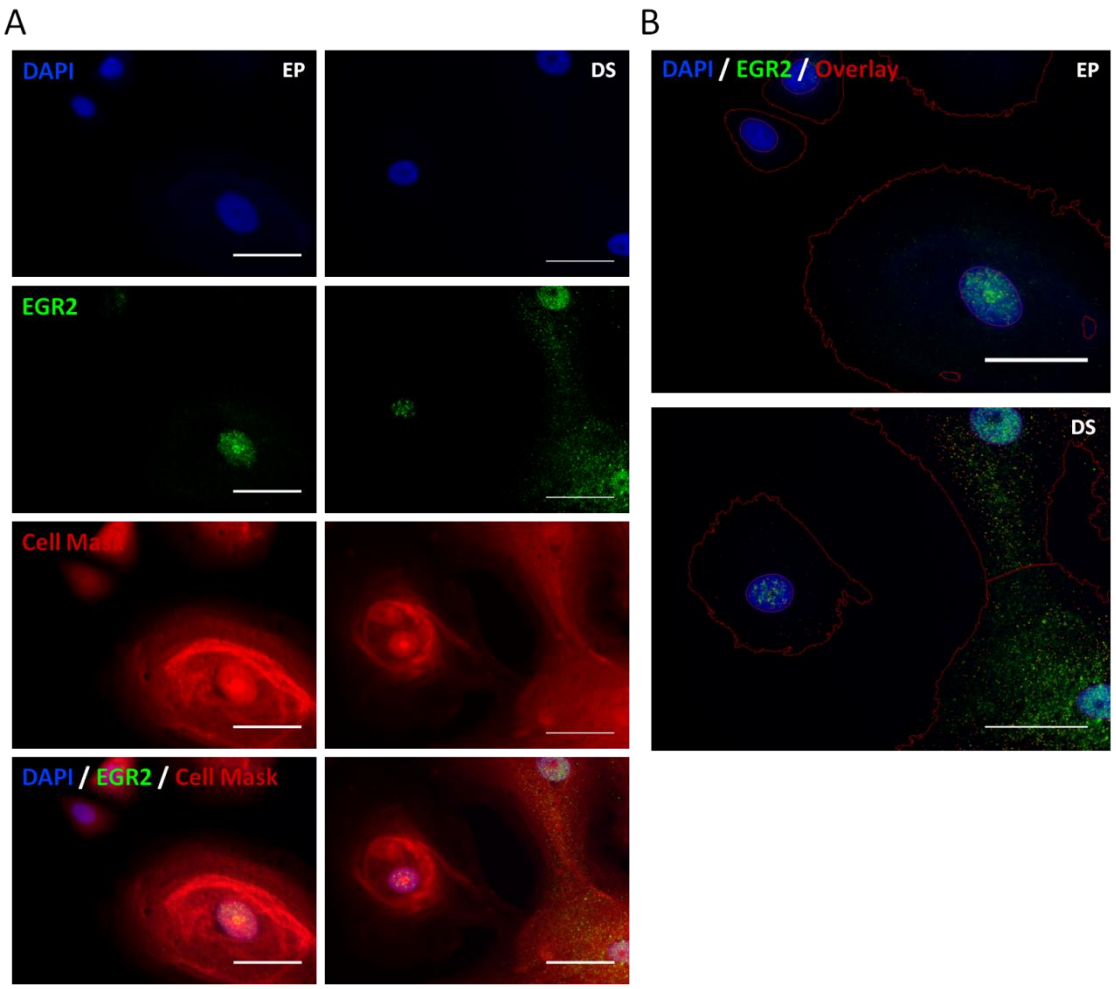

Figure 5.6 Representative images of EGR2 expression in EP and DS HMECs using immunofluorescence. EP and DS HMECs were seeded at 7,500 or 10,000 cells/cm^2, respectively in 384-well plate format, fixed at day five, stained with DAPI, rabbit anti-human EGR2 (H220), goat anti-rabbit Alexa Fluor 488, and Cell Mask. EGR2 cellular and nuclear density and foci were quantitated according to Section 2.7 and Section 2.8. HMEC cell culture and seeding was performed by Dr Cleo Bishop. **(A)** Representative immunofluorescence images of EP and DS HMECs. DAPI (blue), EGR2 (green), Cell Mask (red). Scale bar denotes 50 µm. **(B)** Enlarged representative immunofluorescence images stained with DAPI, EGR2 and Cell Mask with the nuclear, cellular, and foci segmentation overlay. Scale bar denotes 50 µm.

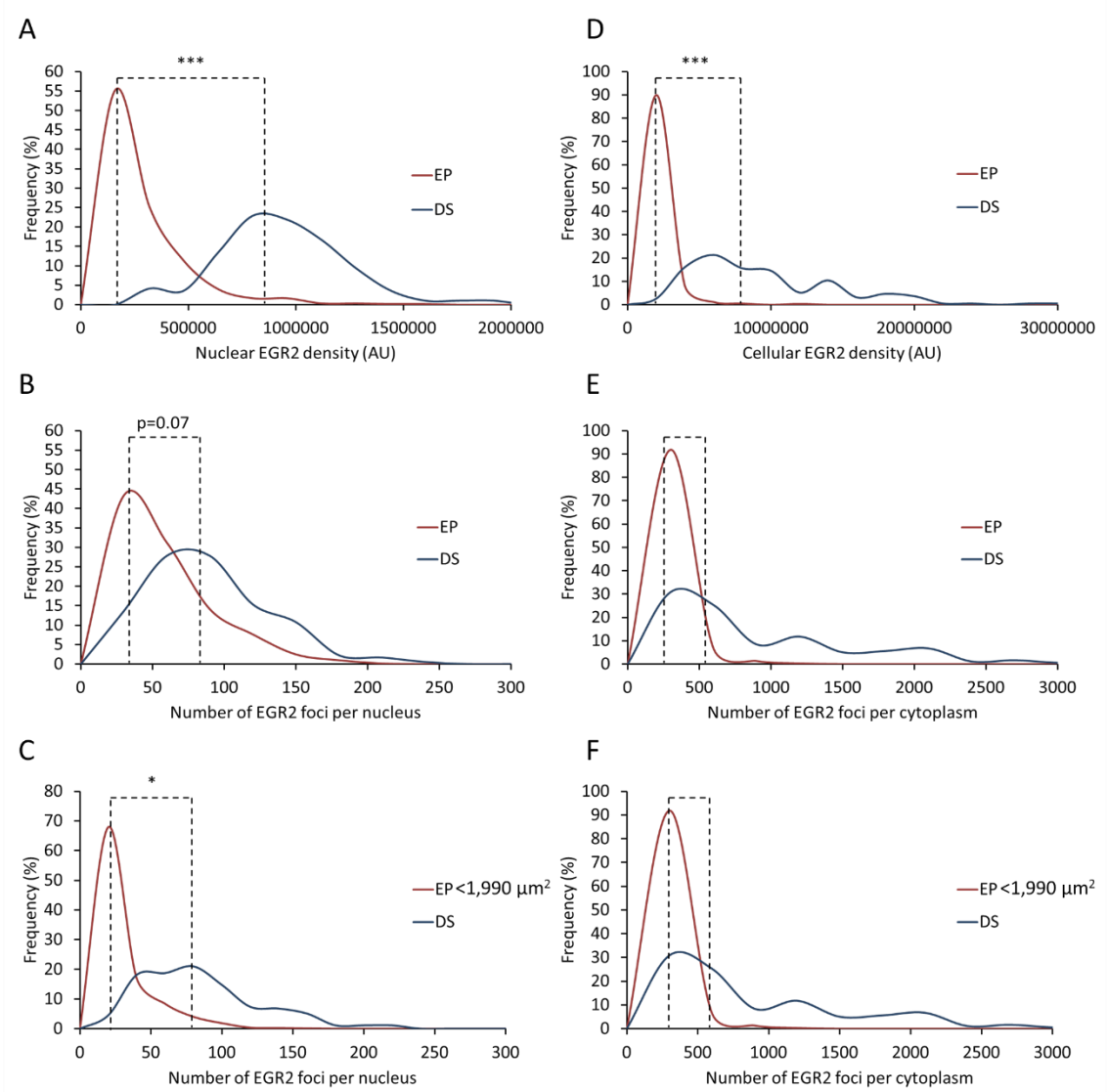

Figure 5.7 EGR2 expression in EP and DS HMECs using immunofluorescence. EP and DS HMECs were seeded at 7,500 and 10,000 cells/cm^2, respectively, in 384-well plate format, fixed at day five, stained with DAPI, rabbit anti-human EGR2 (H220), goat anti-rabbit Alexa Fluor 488, and Cell Mask. EGR2 cellular and nuclear density and foci were quantitated according to Section 2.7 and Section 2.8. HMEC cell culture and seeding was performed by Dr Cleo Bishop. Frequency distribution plots for: **(A)** nuclear EGR2 density levels for EP and DS HMECs; **(B)** the number of nuclear EGR2 foci for EP and DS HMECs; **(C)** the number of nuclear EGR2 foci for EP HMECs with a cellular area smaller than 1,990 µm^2, a proxy measure to remove senescent HMECs from the EP population, and DS HMECs; **(D)** cellular EGR2 protein density levels for EP and DS HMECs; **(E)** the number of cytoplasmic EGR2 foci for EP and DS HMECs; and **(F)** the number of cytoplasmic EGR2 foci for EP HMECs with a cellular area smaller than 1,990 µm^2, a proxy measure to remove senescent HMECs from the EP population, and DS HMECs. Un-paired two-tailed t-test of the medians * $p<0.05$, *** $p<0.001$. Two independent experiments, each containing three technical repeats were performed.

5.4 Phenotypic validation of three individual siRNAs targeting EGR2

As described in Chapter 4, EGR2 was selected as the top hit for validation and further investigation. An important post-screening validation step is to establish whether or not knockdown of the specific protein is occurring post-siRNA transfection. De-convolution of the siRNA pool helps to control for OTEs, as it is highly unlikely that an OTE generated by two unique siRNA sequences would induce a similar phenotype characterised by four different phenotypic parameters. Thus, in order to determine whether EGR2 siRNA knockdown was specific, the siRNA pool used in the DS HMF screen was deconvoluted (see Section 2.6.3) and the three individual siRNAs targeting EGR2 were first validated phenotypically in the DS HMFs. Given that EGR2 is known to encode two isoforms, it is important to note that all three individual siRNAs are designed to target both EGR2 isoforms (Figure 5.3).

DS HMFs were seeded at an optimised density of 15,000 cells/cm^2 and forward transfected with an optimised dose of 0.3 µL Dh2 and the three individual siRNAs targeting EGR2 in two conditions: 30 nM siRNA, and 15 nM siRNA in combination with 15 nM p21 siRNA. The appropriate controls were also performed: 30 nM siGLO; 30 nM p16 siRNA; 30 nM p21 siRNA; and 15 nM p16 siRNA together with 15 nM p21 siRNA. After five days, cells were stained with DAPI and Cell Mask, and cellular and nuclear phenotypes quantified according to Section 2.7 and 2.8. Two independent experiments were performed, each in triplicate.

In line with previous experiments (see Section 3.3.2 and 4.3.1), p16+p21 siRNA reversed the DS HMFs, as demonstrated by an increased cell number, decreased cell and nuclear area, and increased cell elongation (Figure 5.8). Importantly, all three individual EGR2 siRNAs also altered nuclear and cellular morphologies towards a reversed phenotype in comparison to the siGLO control mean: EGR2-1 siRNA increased cell elongation (three Z scores); EGR2-2 siRNA increased cell elongation (six Z scores) and decreased nuclear area (one Z score); and EGR2-3 siRNA increased cell elongation (five Z scores), as well as decreased nuclear and cell area (three and one Z scores, respectively). Furthermore, EGR2-3 significantly increased cell number (one Z score) in comparison to the siGLO control mean (Figure 5.8), echoing the increase in cell number observed in the original

screen (Section 4.3.1, Figure 4.6). In addition, both EGR2-2 siRNA and EGR2-3 siRNA significantly increased cell number (seven Z scores each) in combination with p21 siRNA, relative to the p21 siRNA control (five Z scores); however, EGR2-1 siRNA did not. These data indicate that EGR2-2 and EGR2-3 are both functional siRNAs, with EGR2-3 siRNA being the most potent siRNA, and EGR2-1 siRNA potentially acts as a weak or minimally functional siRNA in the pool. Importantly, the presence of two siRNAs in the pool which generated the same reversal phenotype indicates that the results observed following EGR2 siRNA transfection are not the consequence of an OTE.

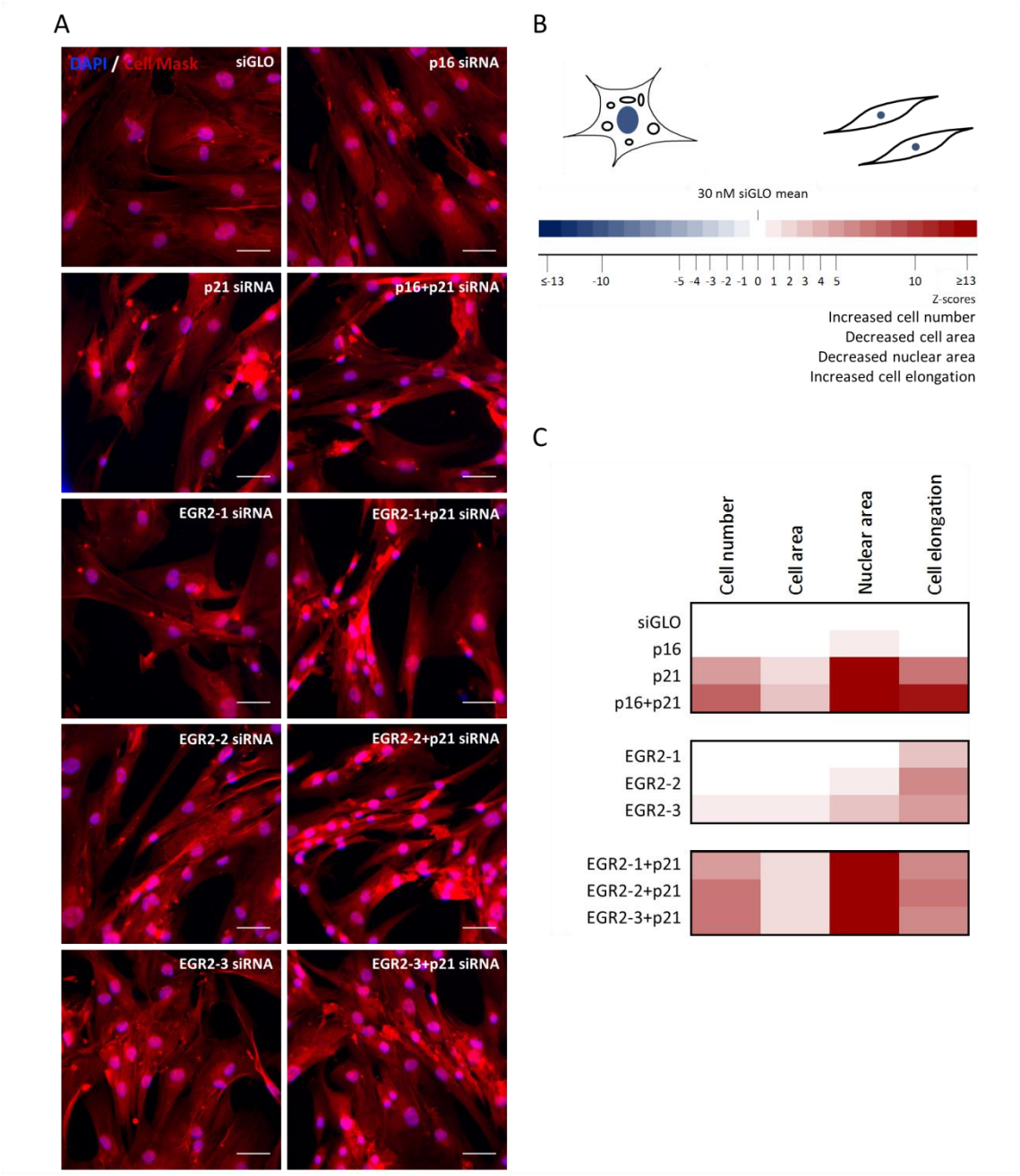

Figure 5.8 Phenotypic validation of three individual siRNAs targeting EGR2 in adult DS HMFs. DS HMFs were seeded at 15,000 cells/cm^2 in 384-well plate format, fixed at day five, stained with DAPI and Cell Mask, imaged, and nuclear and cellular morphologies quantified according to Section 2.7 and 2.8. **(A)** Representative images of 30 nM siGLO (siGLO), 30 nM p16 (p16), 30 nM p21 (p21), 15 nM p16 siRNA together with p21 siRNA (p16+p21), 30 nM EGR2-1 siRNA (EGR2-1), 30 nM EGR2-2 siRNA (EGR2-2), 30 nM EGR2-3 siRNA (EGR2-3), 15 nM EGR2-1 + 15 nM p21 siRNA (EGR2-1+p21), 15 nM EGR2-2 + 15 nM p21 siRNA (EGR2-2+p21), 15 nM EGR2-3 + 15 nM p21 siRNA (EGR2-3+p21) transfected DS HMFs. DAPI (blue), Cell Mask (red). Scale bar denotes 50 µm. **(B)** Key. Z scores were generated according to Section 2.8.2. The colour saturation reflects the number of Z scores from the control mean. Scores highlighted in red denote an

increase in cell number significantly greater than the siGLO control mean indicating a shift towards the reversed phenotype. White denotes no significant changes from the siGLO control mean. Blue denotes a significant decrease in cell number compared to the siGLO control mean. **(C)** Heatmap depicting significant changes in cell number, cell area, nuclear area, and nuclear elongation from the siGLO control mean for p16, p21, and p16+p21 controls, as well as the individual EGR2 siRNAs (EGR2-1, EGR2-2, EGR2-3), and individual EGR2 siRNAs in combination with p21 siRNA (EGR2-1+p21, EGR2-2+p21, and EGR2-3+p21). Two independent experiments were performed, each in triplicate.

5.5 Immunofluorescence validation of three individual siRNAs targeting EGR2

In addition to phenotypic validation of the individual siRNAs targeting EGR2, protein knockdown following siRNA knockdown of EGR2 was also assessed using immunofluorescence, as described in Section 5.4. After five days, the cells were fixed and stained with DAPI, rabbit anti-human EGR2 (H220), and Cell Mask according to Section 2.7 and quantified according to Section 2.8. Two independent experiments were performed, each in triplicate.

In line with the phenotypic data presented previously (Figure 5.5), EGR2-2 and EGR2-3 siRNA transfection induced a greater reduction in nuclear and cellular EGR2 density levels and the number of nuclear or cytoplasmic foci than EGR2-1 siRNA, further indicating that EGR2-1 is a weak or minimally functional siRNA (Figure 5.9, Figure 5.10A-D). Importantly, as EGR2 nuclear foci were identified to significantly increase during both HMF and HMEC senescence in Section 5.3.2, EGR2-2 and EGR2-3 siRNA significantly reduced nuclear EGR2 foci (0.70 ± 0.01 fold change; p=0.0004; 0.74 ± 0.01 fold change; p=0.0007, respectively) relative to the siGLO control (Figure 5.9, Figure 5.10B). Furthermore, EGR2-3 siRNA reduced nuclear density (0.88 ± 0.07 fold change; p=0.06) and EGR2-2 siRNA significantly reduced nuclear density (0.85 ± 0.08 fold change; p=0.004) relative to the siGLO control (Figure 5.9, Figure 5.10A). In addition, both EGR2-2 and EGR2-3 siRNA significantly reduced EGR2 cellular density (0.74 ± 0.006 fold change; p=0.005; 0.73 ± 0.02 fold change; p=0.004, respectively) and cytoplasmic foci (0.64 ± 0.03 fold change; p=0.003; 0.73 ± 0.08 fold change; p=0.0098, respectively) relative to the siGLO control (Figure 5.9, Figure 5.10C-D). Attempts to validate individual EGR2 siRNA knockdown using western blotting generated inconsistent results; however, multiple blots suggested that EGR2-1 did not decrease EGR2 levels, and that EGR2-3 siRNA resulted in the greatest EGR2 knockdown, followed by EGR2-2 siRNA, thus mirroring the immunofluorescence analysis (Appendix Figure A.10). In summary, together with the phenotypic validation data, the immunofluorescence analysis indicates that the siRNA pool targeting EGR2 contains two functional siRNAs which are specific for EGR2.

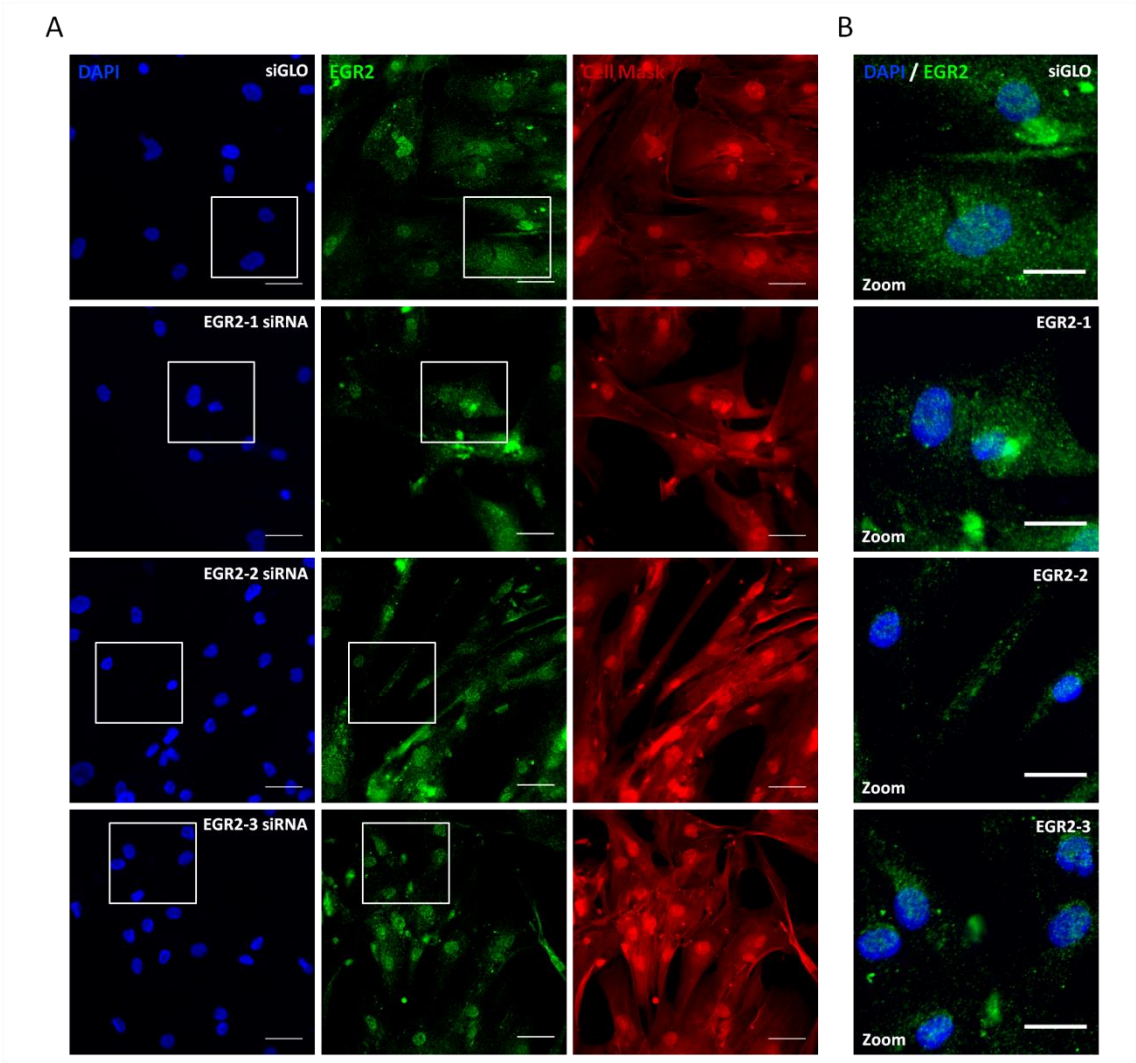

Figure 5.9 Representative images of three individual siRNAs targeting EGR2 using immunofluorescence in adult DS HMFs. DS HMFs were seeded at 15,000 cells/cm^2 in 384-well plate format, fixed at day five, stained with DAPI, rabbit anti-human EGR2 (H220), goat anti-rabbit Alexa Fluor 488, and Cell Mask according to Section 2.7. **(A)** Representative images of 30 nM siGLO (siGLO), 30 nM EGR2-1 siRNA (EGR2-1), 30 nM EGR2-2 siRNA (EGR2-2), and 30 nM EGR2-3 (EGR2-3) siRNA transfected DS HMFs. DAPI (blue), EGR2 (green), Cell Mask (red). Scale bar denotes 50 µm. **(B)** Right panels=digital zoom. Scale bar denotes 30 µm.

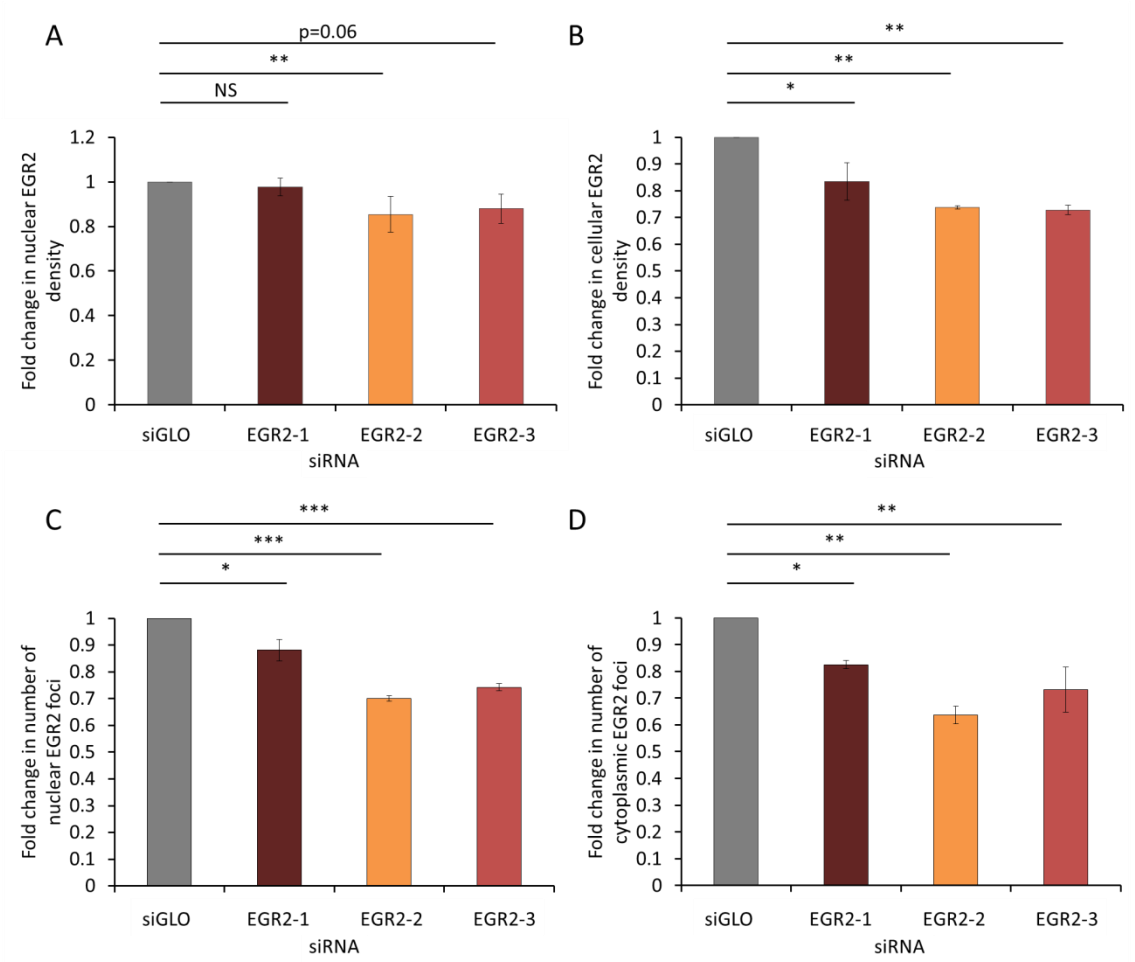

Figure 5.10 Protein knockdown validation of three individual siRNAs targeting EGR2 using immunofluorescence in adult DS HMFs. DS HMFs were seeded at 15,000 cells/cm^2 in 384-well plate format, fixed at day five, stained with DAPI, rabbit anti-human EGR2 (H220), goat anti-rabbit Alexa Fluor 488, and Cell Mask. EGR2 cellular and nuclear density and foci were quantitated according to Section 2.7 and Section 2.8. **(A-D)** Bars denote mean fold change of the **(A)** median nuclear EGR2 density, **(B)** median number of nuclear EGR2 foci, **(C)** median cellular EGR2 density, and **(D)** median number of cytoplasmic EGR2 foci relative to the siGLO median control for 30 nM siGLO (siGLO), 30 nM EGR2-1 siRNA (EGR2-1), 30 nM EGR2-2 siRNA (EGR2-2), and 30 nM EGR2-3 (EGR2-3) siRNA transfected DS HMFs. One-way ANOVA and Dunnett's test Non-significant (NS), * $p<0.05$, ** $p<0.01$, *** $p<0.001$. N=2 throughout. Error bars=SD of two independent experiments, each performed with three replicates.

5.6 Immunofluorescence investigation of the relationship between p16, p21, and EGR2

Previous analysis showed that EGR2 siRNA knockdown significantly increased the proportion of cells negative for both p16 and p21 in the transfected DS HMF population (see Section 4.4.1), indicating that the presence of EGR2 during senescence may be important for driving expression of p16 and p21.

As the presence of EGR2 potentially drives senescence and p16+p21 knockdown reverses senescence, it was hypothesised that p16 or p21 may modulate EGR2 protein levels through a feedback loop. In order to explore this, DS HMFs were seeded at an optimised density of 15,000 cells/cm^2 and forward transfected with 30 nM siGLO, 30 nM p16 siRNA, 30 nM p21 siRNA, and 15 nM p16 together with 15 nM p21 siRNA at an optimised dose of 30 nM with 0.3 µL Dh2. After five days, the cells were fixed and stained with DAPI, rabbit anti-human EGR2 (H220), and Cell Mask according to Section 2.7, and quantified according to Section 2.8.

Interestingly, p16 siRNA alone, which did not reverse senescence (data not shown), did not significantly alter nuclear or cellular EGR2 density or the number of nuclear or cytoplasmic EGR2 foci (Figure 5.11, Figure 5.12A-D). However, p21 siRNA significantly decreased the number of nuclear EGR2 foci (0.49 ± 0.07 fold change; p=0.03) and cellular EGR2 density (0.60 ± 0.007 fold change; p=0.02) relative to the siGLO control (Figure 5.11, Figure 5.12B-C). Furthermore, p16+p21 siRNA reversed some phenotypes of senescence (data not shown) and significantly decreased the number of nuclear EGR2 foci (0.42±0.20 fold change; p=0.01) as well as cellular EGR2 density (0.41 ± 0.02 fold change; p=0.004) and the number of cytoplasmic EGR2 foci (0.48 ± 0.06 fold change; p=0.04) relative to the siGLO control (Figure 5.11, Figure 5.12B-D).

The reduction in nuclear EGR2 foci and EGR2 cellular density levels in the p21 siRNA transfected DS HMFs suggests that there is a feedback or feed-forward mechanism between p21 expression and EGR2 protein levels, with the presence of p21 driving up-regulation and/or maintenance of EGR2 levels. Although there is a trend towards a further decrease in EGR2 nuclear foci and cellular density following double knockdown of p16 and p21 siRNA, this was not statistically significant, suggesting that the mechanism driving up-regulation of EGR2 is dependent on p21, not p16. In future, it

would be interesting to investigate p16 and p21 levels in the individual EGR2 siRNA transfected DS HMFs. Further exploration of the relationship between p16, p21, and EGR2 is discussed in Section 5.7.1.

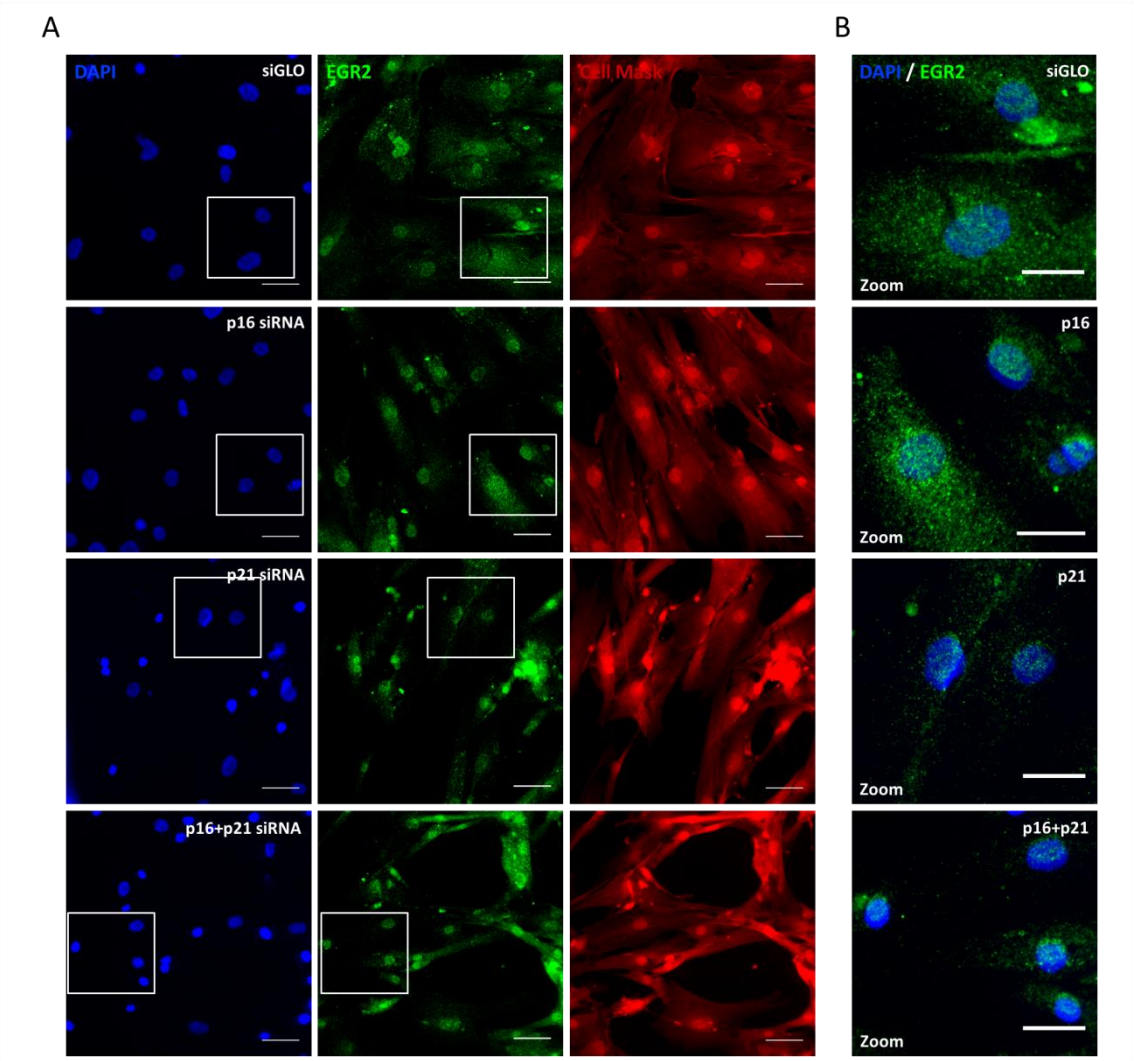

Figure 5.11 Representative images of EGR2 expression in p16 and/or p21 knockdown in adult DS HMFs using immunofluorescence. DS HMFs were seeded at 15,000 cells/cm^2 in 384-well plate format, fixed at day five, stained with DAPI, rabbit anti-human EGR2 (H220), goat anti-rabbit Alexa Fluor 488, and Cell Mask. EGR2 cellular and nuclear density and foci were quantitated according to Section 2.7 and Section 2.8. **(A)** Representative images of 30 nM siGLO (siGLO), 30 nM p16 siRNA (p16), 30 nM p21 siRNA (p21), and 15 nM p16 siRNA together with 15 nM p21 siRNA (p16+p21) transfected DS HMFs. DAPI (blue), EGR2 (green), Cell Mask (red). Scale bar denotes 50 µm. **(B)** Right panels=digital zoom. Scale bar denotes 30 µm.

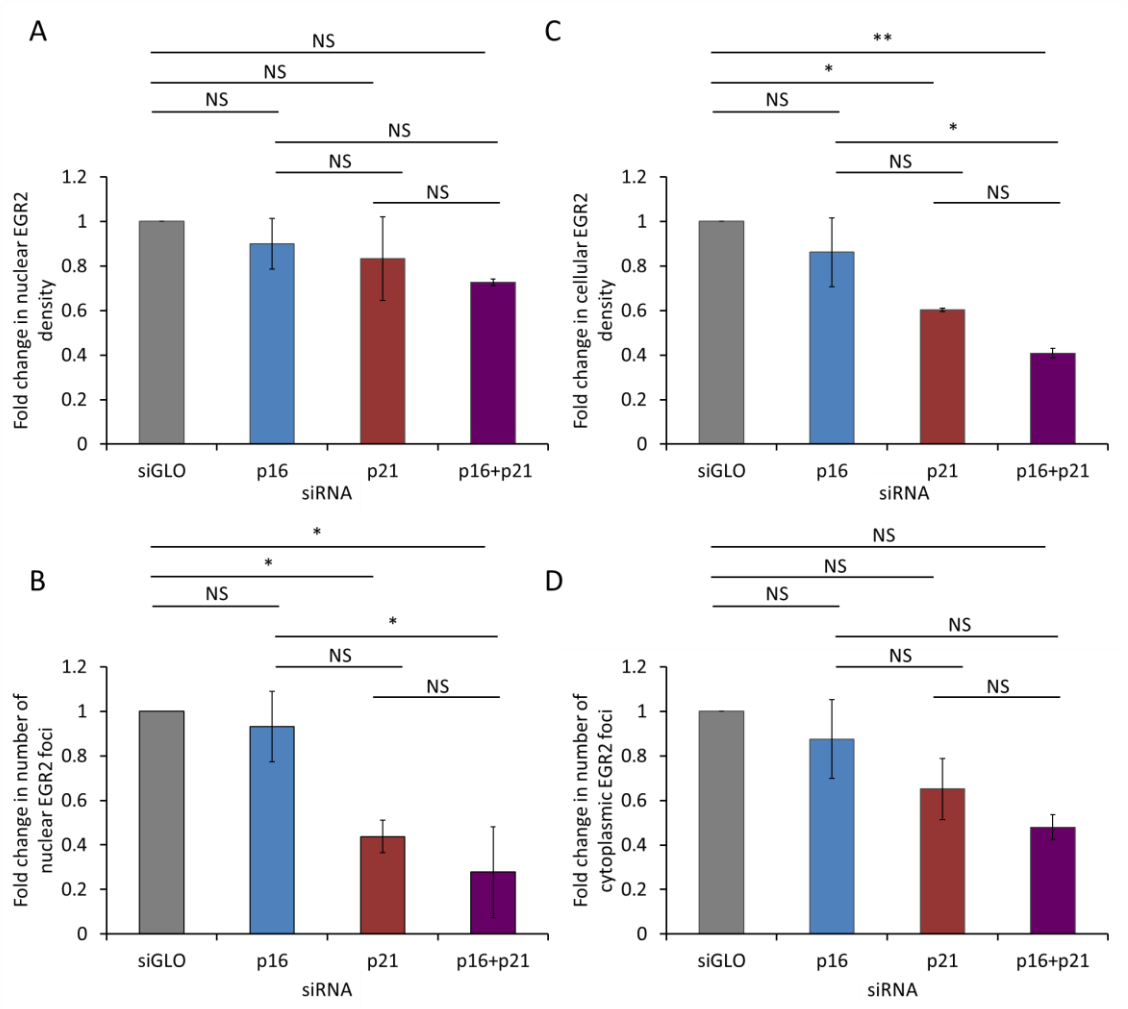

Figure 5.12 Relationship between p16 and/or p21 knockdown and EGR2 protein levels in DS HMFs using immunofluorescence staining. DS HMFs were seeded at 15,000 cells/cm^2 in 384-well plate format, fixed at day five, stained with DAPI, rabbit anti-human EGR2 (H220), goat anti-rabbit Alexa Fluor 488, and Cell Mask. EGR2 cellular and nuclear density and foci were quantitated according to Section 2.7 and Section 2.8. **(A-D)** Bars denote mean fold change of the **(A)** median nuclear EGR2 density, **(B)** median number of nuclear EGR2 foci, **(C)** median cellular EGR2 density, and **(D)** median number of cytoplasmic EGR2 foci relative to the siGLO median control for 30 nM siGLO (siGLO), 30 nM p16 (p16), 30 nM p21 (p21), and 15 nM p16 siRNA together with p21 siRNA (p16+p21) transfected DS HMFs. One-way ANOVA and Tukey's test Non-significant (NS), * $p<0.05$, ** $p<0.01$. N=2 throughout. Error bars=SD of two independent experiments, each performed with three replicates.

5.7 Discussion and future work

Within this Chapter the protein levels of EGR2 during senescence have been investigated using immunofluorescence revealing an increase in EGR2 nuclear foci during HMF replicative senescence and HMEC cellular senescence. Following this, phenotypic and immunofluorescence validation of individual EGR2 siRNAs identified two functional siRNAs targeting EGR2, providing evidence that EGR2 acts as a potential driver of senescence.

Within this Chapter and Chapter 4, it has been shown that EGR2 siRNA knockdown reverses various phenotypes of senescence, as demonstrated by an increase in cell number (Chapter 4 Figure 4.6, Chapter 5 Figure 5.8), altered nuclear and cellular morphology towards a p16+p21 siRNA knockdown phenotype (Chapter 4 Figure 4.7, Figure 4.10, and Chapter 5 Figure 5.8) and decreased p16 and p21 expression (Chapter 4 Figure 4.14). Further validation of EGR2 as a driver of senescence and exploration of the EGR2-knockdown reversed phenotype is discussed in Chapter 6 Section 6.3.

5.7.1 Investigating the relationship between EGR2, p16, and p21 driving senescence

Multiple studies have identified a role for EGR2 in the up-regulation of p21 expression (Le *et al.*, 2005; Zhu *et al.*, 2008; Pospisil *et al.*, 2011; Srinivasan *et al.*, 2012). Furthermore, ChIP performed in EGR2 overexpressing murine T cells demonstrated that EGR2 directly binds to the p21 promoter (Zhu *et al.*, 2008). In line with this literature, p21 protein levels decreased in DS HMFs following EGR2 knockdown (see Chapter 4 Figure 4.14), and EGR2 binding sites were identified in the p21 promoter (see Section 5.2.1), suggesting that EGR2 directly up-regulates p21 expression in HMF replicative senescence. Interestingly, p16 protein levels were also observed to decrease in DS HMFs following EGR2 knockdown (see Chapter 4 Figure 4.14), and the p16 promoter was identified to contain EGR2 binding sites (see Section 5.6.1), indicating a potential role for EGR2 regulating p16 expression. In support of this, EGR2 was the only siRNA identified to reverse senescence, although modestly, in the HMFs without additional knockdown of p16 or p21, potentially indicating that EGR2 is essential for driving senescence upstream of both the p16/pRB and p53/p21 pathways (see Chapter 4 Figure 4.6, Chapter 5 Figure 5.8, schematic Figure 5.13). To date, there is no evidence linking EGR2 to p16 in the literature. In order to investigate the direct relationship between

EGR2 and p16, ChIP for EGR2 could be used to determine whether EGR2 binds to the p16 promoter, and if this is enriched within the DS HMFs and HMECs. Furthermore, p21, p53, TERT, other hits identified in Chapter 4, including MYL12A, FRAS1, JUP, ACTG1, FN1, and other genes of interest identified in this Chapter, including p15, S100A4, MUM1L1, CST6, FXYD3, PLCG2, ZPLD1, FUT2, SORT1, and FMO4, could be investigated as potential direct EGR2 targets using ChIP analysis. In order to achieve this, a ChIP-grade antibody would need to be developed, as discussed in more detail in Chapter 6 Section 6.3.1.

Fascinatingly, p21 siRNA knockdown in DS HMFs stimulated a decrease in EGR2 protein levels (see Section 5.5), suggesting the presence of a feedback loop to regulate the levels of EGR2 during senescence (Figure 5.13). Previous evidence for EGR2 feedback loops exist in the literature, as NAB2, a protein known to bind to EGR2 and inhibit its transcriptional activity, has also been identified as a direct EGR2 transcriptional target which is activated following EGR2 binding to the promoter, thus forming a feedback loop to regulate EGR2 levels (Kumbrink, Gerlinger and Johnson, 2005; Srinivasan *et al.*, 2007). As p21 primarily regulates gene transcription in senescence via pRB-mediated inhibition of E2F-regulated genes, it would be interesting to determine whether p21 regulates EGR2 protein levels indirectly through the E2F family (see schematic Figure 5.13). In order to further explore this relationship, the EGR2 locus could be investigated for the presence of inhibitory E2F family member binding sites. Subsequently, ChIP could be performed using an antibody raised against the inhibitory E2F family member identified to possess a binding site within the EGR2 promoter to determine whether E2F binding to the EGR2 promoter is enriched in DS HMFs. Furthermore a plasmid overexpressing the inhibitory E2F family member could be transduced into DS HMFs and a luciferase assay used to determine whether EGR2 promoter activation is inhibited.

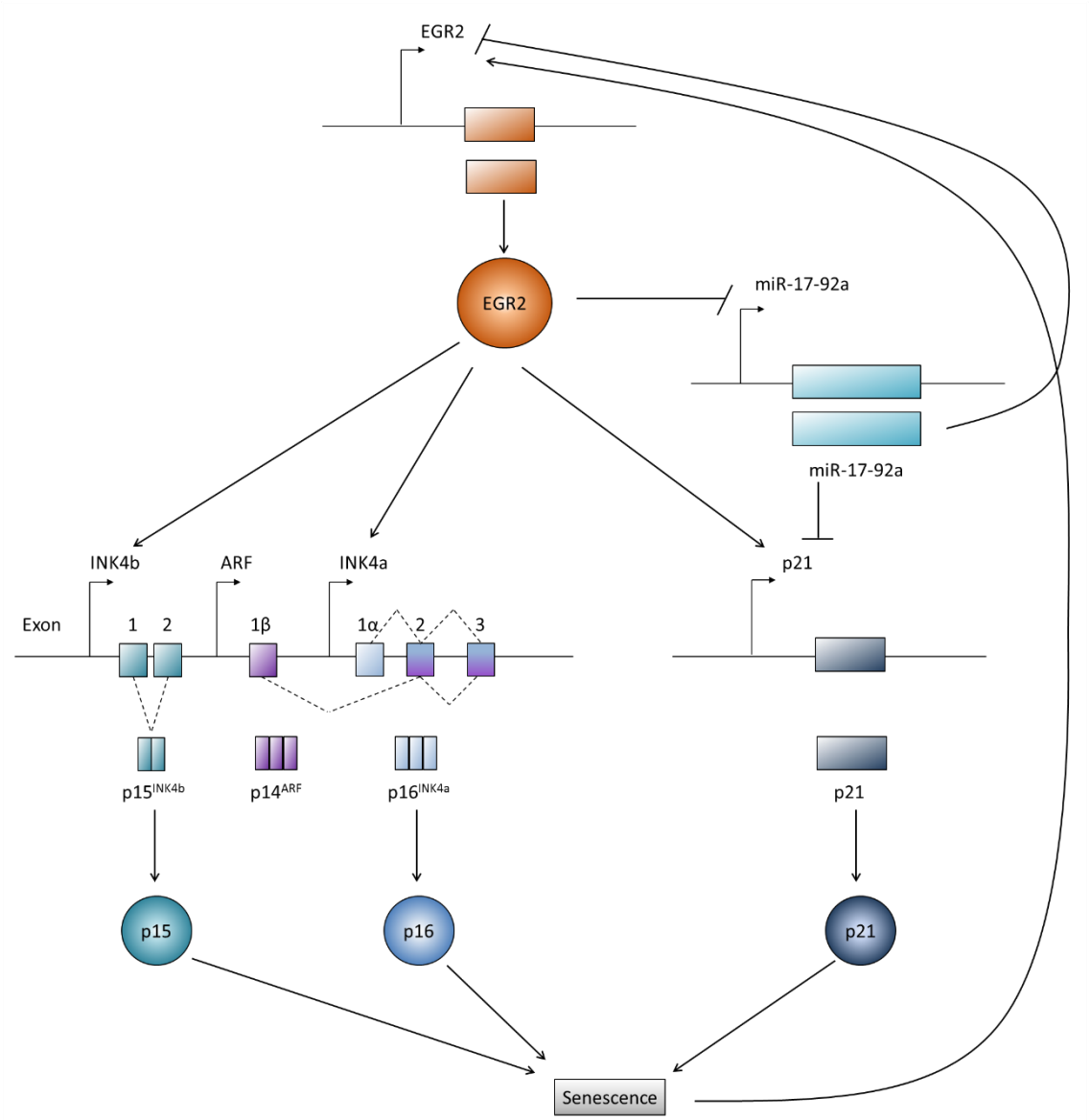

Figure 5.13 Schematic summarising the proposed relationship between EGR2, p16, p21, p15, and the miR-17-92a cluster in senescence. Theoretical relationship between EGR2 (orange), and the senescence effectors: p16 (light blue); p15 (green); p21 (blue), and the miR-17-92a cluster (light green): EGR2 directly up-regulates p15, p16, and p21 expression, and inhibits transcription of the miR-17-92a. In a theoretical feedback loop, p21 inhibition of E2F transcription factor in senescence prevents binding of inhibitory E2F family members to EGR2 and subsequent transcriptional inhibition. Furthermore, in another theoretical feedback mechanism, the miR-17-92a cluster could function to inhibit EGR2 transcription.

Additionally, EGR2 has been found to directly repress the miR-17-92 cluster which encodes seven related microRNAs known to play important roles in cell proliferation by down-regulating expression of p21 amongst other mechanisms (Pospisil *et al.*, 2011). Crucially, large-scale microarray analysis has demonstrated that the miR-17-92 cluster is down-regulated during replicative senescence in multiple cell types *in vitro*, including adult human dermal fibroblasts (Hackl *et al.*, 2010), as well as in organismal ageing represented by three different *ex vivo* tissue types, including T cells isolated from the peripheral blood of healthy individuals (Hackl *et al.*, 2010). These findings are confirmed by a study looking at foetal lung IMR-90 fibroblast replicative senescence (Dhahbi *et al.*, 2011). Furthermore, previous work in the lab. has shown that miR-106a, and -18a from the miR-17-92 cluster are down-regulated in senescent HMECs (Overhoff *et al.*, 2014). Given this, future work could investigate whether the miR-17-92 cluster is down-regulated in DS compared to EP HMFs using qRTPCR. In addition, expression of the miR-17-92 cluster could be investigated following EGR2 siRNA knockdown in DS HMFs using qRTPCR. Furthermore, EGR2 has been identified as a target gene of miR-106b, part of the miR-17-92 cluster, with significant EGR2 up-regulation observed following transfection with a miR-106b inhibitor (Tang *et al.*, 2015), indicating the presence of an auto-regulatory feedback loop with the miRNA cluster (Figure 5.13). As the miR-17-92 cluster is known to be oncogenic and up-regulated in cancer (reviewed in Fuziwara & Kimura 2015), over-expression of these miRNAs in DS HMFs could induce senescence bypass not reversal, however given that EGR2 has been identified as a target gene of the miR-17-92 cluster, it would be interesting to investigate levels of EGR2, p16, and p21 using immunofluorescence following miRNA overexpression in DS HMFs. The data generated here would inform the role of the miR-17-92 cluster in EGR2-driven HMF senescence and determine the relationship between EGR2, p16, p21, and the miR-17-92 cluster (Figure 5.13).

Fascinatingly, p15 was also identified as a putative EGR2 transcriptional target in the previous analysis (see Section 5.2.1). In the SASP pathway, TGF-β up-regulates p16, p21, and p15 through the SMAD complex (see Section 1.1.3). Similarly, EGR2 is a known target of TGF-β through the canonical SMAD pathway in foreskin fibroblasts (Fang *et al.*, 2011). Importantly, SMAD3 was identified as a reversal hit in combination with p21 siRNA in the DS HMF siRNA screen (see Section 4.3.1). To explore this further and

determine whether EGR2-driven senescence occurs downstream of the canonical SMAD/TGF-β pathway, a small-scale siRNA screen targeting the TGF-β pathway could be performed in the adult DS HMFs with immunofluorescence staining for DAPI, EGR2, and Cell Mask to investigate the effect on cell number, morphology, and EGR2 protein levels.

To understand further the downstream pathways and mechanisms through which EGR2 may drive senescence, future work could explore the panel of genes up-regulated in HMEC senescence which contain an EGR2 binding site identified in Section 5.2.1, as well as the genes identified in Section 5.2.2 to also be directly regulated by EGR2 in other cellular contexts. To identify genes with increased expression during HMF senescence which have decreased expression following EGR2 siRNA knockdown, a microarray or qRTPCR array could be performed comparing EP HMFs, DS HMFs, and EGR2 siRNA transfected DS HMFs. Following validation, the genes identified here could represent novel EGR2 targets and drivers of senescence and provide mechanistic insight into the route of EGR2-driven senescence. Further elucidation of the mechanism through which EGR2 drives senescence will be discussed in Chapter 6 Section 6.3.2.

Chapter 6 Discussion

6.1 Senescence reversal in HMFs

As outlined in Section 1.7, this project explores the reversal of DS HMFs to a state similar to that of proliferating cells. As discussed in Section 1.7, previous work exploring mTOR inhibition in 'near-senescent' human neonatal fibroblasts has shown that senescence onset is delayed (Walters *et al*., 2016) and permanent loss of proliferative potential is prevented in human and rodent cell lines induced to senesce via exogenous p16 or p21 expression (Demidenko *et al*., 2009). However, senescent cells were not stimulated to proliferate. As discussed in Section 1.7 and Section 3.4.2, the most recent work investigating p16/pRB and p53/p21 pathway knockdown as a route for senescence reversal concluded that high levels of p16 expression provide a barrier to senescence reversal in human fibroblasts (Beausejour *et al*., 2003). As such, the data presented in this project has demonstrated for the first time that deep senescence can be effectively reversed in normal adult HMFs with high levels of both p16 and p21 expression using siRNA transfection targeting p16 and p21, as characterised by the loss of a number of classic senescence markers, including cell cycle arrest, senescence-associated nuclear and cellular morphology, oxidative damage, and expression of CDKIs, p16 and p21, as demonstrated in Chapter 3.

6.1.1 Future work to further profile the DS and reversed phenotype

Replicative senescence is induced in response to a DDR triggered by critically short telomeres (see Section 1.2). In order to further validate DS HMFs and explore the reversed HMF phenotype, additional senescence markers could be explored in EP, DS, and p16+p21 siRNA transfected DS HMFs. For example, it would be interesting to investigate telomere length using qRTPCR, the presence of TAF using confocal microscopy (Hewitt *et al.*, 2012), and telomerase activity using the TRAP assay. Previous examination of 8-oxoG levels revealed that p16+p21 siRNA transfected DS HMFs have decreased cellular oxidative damage compared to DS HMFs (see Section 3.3.2). Given that senescence induction is triggered by a DDR in response to DNA damage, further investigation of 53BP1, a well-known DDR factor, and γ-H2AX, a histone marker present at double-strand DNA breaks, (see Section 1.2) could be performed using immunofluorescence. Together, these data could be used to assess whether p16+p21 siRNA transfected DS HMFs reverse telomere shortening, DNA damage, and DDR activation, thus dampening senescence triggers and potentially delaying senescence re-

induction. Interestingly, conditioned medium experiments demonstrated that DS HMFs are able to induce paracrine senescence in EP HMFs (see Section 3.2.4), thus demonstrating the presence of the SASP. Given this, SASP components, including IL-6, IL-8, or chemokine CXCL-2, could be further explored using immunofluorescence, ELISA, or Luminex-based assays. Previous studies of senescence reversal have demonstrated that treatments which induce senescent fibroblasts to alter their cellular morphology without stimulating proliferation have decreased SA-β-Gal activity (Gire and Wynford-Thomas, 1998; Dirac and Bernards, 2003; Correia-Melo *et al.*, 2016; Walters, Deneka-Hannemann and Cox, 2016), suggesting that SA-β-Gal may not be a useful marker for senescence reversal. However, Lowe *et al*. (2015) showed that a substantial fraction of reversed DS HMECs stained negative for SA-β-Gal activity. Given this, it would be interesting to explore SA-β-Gal activity in non-proliferating p16 siRNA transfected DS HMFs; compared to proliferating p21, and p16+p21 siRNA transfected DS HMFs, as well as EP and DS fibroblasts. Together, these studies will further characterise the reversed phenotype following p16+p21 siRNA knockdown in DS HMFs and provide insight into the mechanism of this reversal.

Interestingly, reversal of fibroblast replicative senescence has previously only been achievable in the absence of high levels of p16 expression (see Section 1.7). By contrast, the data presented in this thesis has demonstrated that p16+p21 siRNA knockdown reverses a DS HMF population which expresses both p16 and p21 (see Section 3.3.2). Given this, it would be interesting to perform p16+p21 siRNA knockdown in cell types previously investigated for senescence reversal in the literature (for example, WI38 and BJ fibroblasts), as well as HMFs induced to senesce via other mechanisms including OIS (see Section 1.3.2). This is explored in more detail in Chapter 3 Discussion Section 3.4.2. These studies will determine whether p16+p21 siRNA knockdown reverses senescence in fibroblasts with differing p16 and p21 levels, thus determining whether p16+p21 siRNA knockdown is a universal tool for senescence reversal in fibroblasts and enabling further elucidation of the roles of p16/pRB and p53/p21 pathways in different cellular contexts. Furthermore, understanding the cellular and molecular signatures of OIS-induced senescent fibroblasts could have important implications for therapies which aim to reverse or delay onset of senescence *in vivo*, as explored in further detail in Section 6.4.1. Previous work has shown that senescence is reversible in another cell type

from breast tissue, namely DS HMECs, using p16 siRNA knockdown (Lowe *et al.*, 2015). In order to determine whether reversal is achievable in cells from other tissue types, further experiments could explore whether p16 siRNA or p16+p21 siRNA knockdown induces reversal in cells isolated from different tissues including dermal fibroblasts and keratinocytes.

6.1.2 Characterisation of senescence reversal versus bypass

Senescence is known to be prevalent in the pre-malignant stages of tumourigenesis but absent in malignant tumours. It has therefore been hypothesised that progression to malignancy requires bypass of senescence (reviewed in Collado and Serrano, 2010). This process is characterised by mutations or epigenetic alterations which lead to inactivation of the p16/pRB and p53/p21 pathways, telomerase activation, and subsequent infinite cell proliferation (reviewed in Shay and Wright, 2005). Given that cancer cells may have arisen via bypass of senescence, they may retain phenotypic characteristics shared with senescent cells that are distinct from normal proliferating cells, which can potentially be used as markers of senescence bypass. For example, cells which have bypassed senescence should exhibit infinite proliferation. Importantly, data presented in Chapter 4 Section 4.4.1 showed that p16+p21 siRNA knockdown DS HMFs began reverting to a senescent morphology at seven days post-transfection, suggesting that p16+p21 siRNA knockdown induces transient reversal, not bypass, of senescence. Similar observations were made following senescence reversal in DS HMECs (Lowe *et al.*, 2015). In order to confirm that knockdown induces reversal not bypass, long-term inducible p16+p21 short hairpin RNA (shRNA) knockdown could be performed in DS HMFs and subsequently turned off, thus enabling investigation of the kinetics of senescence re-entry using the senescence markers examined in this thesis and outlined in Section 6.1.1. Furthermore, the duration of inducible p16+p21 shRNA knockdown in DS HMFs could be explored to determine whether prolonged shRNA knockdown induces further loss of senescence markers, subsequently delaying re-entry into senescence.

Of relevance, it is well-established that altered DNA methylation is a hallmark of cancer (reviewed in Sproul & Meehan 2013). Recent work has demonstrated the presence of a senescence-associated methylome within fibroblasts and HMECs which resembles the methylation landscape in cancer (Cruickshanks *et al.*, 2013; Lowe *et al.*, 2015). Furthermore, this altered methylation landscape is retained in cells which bypass

senescence (Cruickshanks *et al.*, 2013). Previous work in our lab. has defined senDMPs in DS HMECs relative to EP cells using an Illumina 450K array, and demonstrated that senescence reversal in DS HMECs following p16 siRNA knockdown effectively reversed the senDMP signature (Lowe *et al.*, 2015). Profiling of methylation dynamics in EP, DS, and p16+p21 siRNA knockdown DS HMFs using an Illumina EPIC array for >900,000 cytosine residues would enable identification of senDMPs in HMFs, and determine whether p16+p21 siRNA knockdown in DS HMFs enables reversal of the senDMP signature. In addition, the senDMPs identified in p16+p21 siRNA knockdown DS HMFs could be cross-compared with the DMRs identified in senescent IMR-90 fibroblasts and SV40 T-antigen expressing IMR-90 cells which bypassed senescence (Cruickshanks *et al*. 2013), to determine whether there is significant overlap between the methylation profile in p16+p21 siRNA knockdown HMFs and IMR-90 fibroblasts which have bypassed senescence. Cruickshanks *et al*. (2013) also compared senescence-associated DMRs and senescence bypass-associated DMRs with cancer-associated DMRs reported previously for colon and breast cancer and found highly significant overlap. Given this, p16+p21 siRNA knockdown DS HMFs senDMP signature should be compared with the cancer-associated Illumina 450K methylation profiles available, including colon and breast cancer, within The Cancer Genome Atlas (TCGA) database. Together, these studies will establish if the methylome of DS HMFs resembles cancer methylomes and determine whether p16+p21 knockdown induces reversal or bypass of senescence.

6.1.3 Membrane stiffness may act as a novel marker of replicative senescence in HMFs

As human skin undergoes the ageing process, it is evident that there are significant changes in its mechanical properties (Daly and Odland, 1979). However, the relationship between ageing and the mechanical properties of cells and the cellular microenvironment remains poorly understood. Data presented in Chapter 3 Section 3.3.3 demonstrated that DS HMFs exhibited significantly stiffer membranes than EP fibroblasts, which significantly softened following p16+p21 siRNA knockdown, suggesting that this may be a novel senescence marker *in vitro*. In line with these findings, Kim *et al*. (2015) found that late-passage dermal foreskin fibroblasts showed an increased stiffness approximately three times greater than early-passage cells. In addition, Berdyyeva, Woodworth and Sokolov, 2005 found that epithelial cells exhibit

increased stiffness *in vitro* at later passages due to increased F-actin density in the cytoskeleton. Interestingly, cytochalasin B, a chemical that inhibits polymerisation of F-actin, reduced late-passage epithelial cell membrane stiffness to levels observed in cultures of early-passage cells (Sokolov, Iyer and Woodworth, 2006). In order to determine whether membrane stiffening is a universal feature of senescence, future work could investigate membrane stiffness in senescent epithelial cells as well as HMFs induced to senesce via other triggers. Given that both fibroblast and epithelial cells have been identified to exhibit increased stiffness at later passages nearing senescence (Berdyyeva, Woodworth and Sokolov, 2005; Kim *et al.*, 2015), it is hypothesised that HMF membrane stiffening occurs prior to senescence induction, potentially acting as a driver of senescence. In order to explore the kinetics of stiffening, membrane stiffness could be measured at multiple intervals between EP and DS HMFs. To explore whether membrane stiffening is a potential driver of senescence, future work could investigate whether treatment of DS HMFs with cytochalasin B reduces senescence-associated membrane stiffness and the senescence markers examined in this thesis and outlined in Section 6.1.1 could also be assessed to determine whether senescence reversal is induced following membrane softening. Conversely, further experiments could be performed using jasplakinolide, a drug which polymerises and stabilises actin filaments (Bubb *et al.*, 1994), to investigate whether increased actin polymerisation in EP HMFs induces senescence, as assessed by the senescence markers examined in this thesis. Interestingly, a study by Schulze *et al*. 2012 showed that dermal fibroblasts isolated from older healthy female donors (>60 years old) were stiffer than those isolated from younger donors (<42 years old), suggesting that dermal fibroblasts exhibit a significant increase in stiffness during ageing *in vivo.* To explore this further, future work could investigate membrane stiffness alongside senescence markers, such as p16 and p21 expression, in fibroblasts isolated from donors of differing ages. Together, these studies may identify membrane stiffness as a novel, universal senescence marker *in vitro* and *in vivo* as well as a potential driver of senescence.

The biomechanical properties of the cellular microenvironment are known to regulate fundamental cell processes, such as proliferation, via ECM-cell and cell-cell interactions (reviewed in Provenzano and Keely, 2011). To explore the effect of external mechanical forces on senescence markers, proliferating HMFs were seeded onto substrates of

varying stiffnesses coated with collagen in collaboration with Ana Laly, a PhD student in Dr Connelly's group. The preliminary data generated from these experiments indicated that culture of HMFs on a softer substrate increased proliferation as well as decreased p21 levels in comparison with HMFs seeded onto collagen-treated plastic (data not shown). The data suggests that the stiffness of the extracellular microenvironment may play a role in senescence induction. Interestingly, it has been shown that fibroblasts can adjust their membrane stiffness to match substrate stiffness (Solon *et al.*, 2007), indicating the presence of a signalling pathway between sensing the stiffness of the microenvironment and regulation of internal cellular stiffness. In order to assess whether a relationship exists between substrate stiffness, membrane stiffness, and senescence induction, the membrane stiffness of near-senescent HMFs seeded on substrates of differing stiffnesses could be investigated alongside the senescence markers outlined in this thesis.

6.2 siRNA screening hits are enriched for cytoskeletal and cell adhesion processes

The successful reversal of deep senescence in adult HMFs using p16 and p21 siRNA subsequently provided the opportunity to screen for novel siRNAs that induced reversal in both DS HMECs and HMFs, using the 28 driver siRNAs identified in a screen of 200 genes in DS HMECs. This strategy revealed 45 siRNAs in DS HMFs which significantly increased cell number in comparison to the control, including 22 driver siRNAs functional within both HMFs and HMECs and 23 interactors identified in the HMFs. It is important to note that an initial genome-wide siRNA screen in DS HMFs may have identified additional hits specific to the fibroblast context. However, further investigation of the top 14 siRNAs identified using this strategy revealed 10 siRNAs which ranked highly as reversal hits in analyses of morphology and p16 and p21 levels. Of these, three encoded genes with disparate functions grouped as 'other'; five encoded genes involved with cytoskeleton and cell adhesion; and two encoded transcription factors, including EGR2, which will be discussed in more detail in Section 6.3 and Section 6.4.

Given the discussion explored in Section 6.1.3, it is noteworthy that the top 10 hits were enriched for genes with cytoskeletal and cell adhesion function. Based on these hits, a

theoretical mechanism by which mechanical force regulates intracellular signalling via the extracellular matrix is proposed in Chapter 4 Section 4.5.2. In summary, external mechanical forces or internal forces generated by NMII and MYL12A via ACTG1 may stretch diffuse FN1 in the ECM into fibrils, thus activating signal propagation to the nucleus potentially via integrins and integrin-like kinases, cadherin signalling and JUP or other transmembrane proteins, such as FRAS1, subsequently altering gene expression and driving senescence induction. In order to explore this theoretical mechanism and potentially identify other drivers of senescence, a siRNA screen for reversal could be performed in DS HMFs which investigates interactors within this network, including NMII (Park *et al.*, 2011), fibronectin-binding partner integrin α5β1 (Huveneers *et al.*, 2008), ILK, an integrin-binding cytoplasmic protein, and other extracellular matrix components such as smooth muscle alpha actin (α-SMA), F-actin or vimentin (Chen *et al.*, 2006). In order to validate these four hits as drivers of senescence, the siRNA pools could be deconvoluted and validated using high content analysis, immunofluorescence, qRTPCR, and western blotting. In addition, membrane stiffness could be investigated as a senescence marker following siRNA knockdown of these hits in DS HMFs. To complement these experiments, inducible overexpression of the hits in EP HMFs could be performed to determine whether premature senescence is induced. Together, these studies may elucidate the mechanism through which mechanical force drives senescence induction.

6.3 EGR2 may represent a novel driver of senescence

6.3.1 Further validation of EGR2 as a driver of senescence

As described in Chapter 4, further investigation of the top 14 siRNAs revealed EGR2 as the top hit for reversal in multiple analyses, including increasing cell proliferation when transfected alone as well reversing senescent cellular and nuclear morphology in a dose-dependent manner. Accordingly, EGR2 was selected for validation and further investigation. As effective knockdown at the protein level must be achieved in order to inhibit gene function, an important post-screening validation step was establishing that EGR2 knockdown was achieved following siRNA transfection, as explored in detail in Chapter 5. To support these endeavours, transcript knockdown following siRNA transfection could be assessed using qRTPCR. Of note, EGR2 possesses multiple

transcript variants which encode two isoforms: A, and the slightly shorter isoform B (see Section1.8.1). Before assessing transcript knockdown, it will be important to examine the relative abundance of isoform expression in EP and DS HMFs and HMECs using isoform specific primers and qRTPCR. As the individual EGR2 siRNAs used in this project knockdown both isoforms (see Section 5.4), the relative isoform abundance could be examined post-EGR2 siRNA knockdown using qRTPCR analysis. Further work could investigate isoform-A-specific EGR2 siRNA knockdown compared to knockdown of both isoforms in order to determine the relative contributions of EGR2 isoforms driving senescence. Identification of the functional EGR2 isoform(s) in senescence will be important for design of further experiments, including monoclonal antibody generation, inducible shRNA or inducible overexpression, as discussed in more detail below.

To extend EGR2 protein knockdown validation, future work could explore the potential EGR2 post translational modifications. Attempts could be made to remove these modifications in order to improve EGR2 band resolution and enable EGR2 protein levels to be investigated using western blotting. As explored in Chapter 5, a potential post-translational modification could be N-terminal O-GlcNAc glycosylation, and this can be removed from proteins using commercially available hexosaminidases (Zachara, Vosseller and Hart, 2011). In order to ensure that deglycosylation has been performed, a positive control should be included, such as ovalbumin which bears terminal GlcNAc residues and migrates several KDa lower on a 10-12% gel following deglycosylation. If deglycosylation does not improve the anti-EGR2 (H220) band resolution, a monoclonal antibody specific for the known functional isoform EGR2 could be developed. Following this, the monoclonal anti-EGR2 antibody would be validated for detection of an appropriate band or bands using western blotting for DS HMFs and HMECs, and subsequently optimised for immunofluorescence staining in DS HMFs and HMECs. Production of a validated monoclonal antibody which probes the known functional EGR2 isoform(s) in DS HMFs and HMECs would enable further EGR2 investigation in EP, DS and reversed HMFs and HMECs at the protein level as well as further validation of EGR2 siRNA protein knockdown using western blotting and further experiments outlined below.

To further validate EGR2 as a driver of senescence, an inducible EGR2-overexpressing plasmid could be transduced into EP HMFs to investigate whether EGR2 overexpression

induces premature senescence using the senescence markers examined in this thesis and outlined in Section 6.1.1. In addition, long-term inducible EGR2 shRNA knockdown in EP HMFs could be performed to determine whether EGR2 knockdown extends replicative lifespan. Further to this, EGR2 knockdown could be turned off prior to senescence in order to investigate whether long-term EGR2 suppression delays entry into senescence. To determine whether EGR2 shRNA knockdown can induce senescence reversal, HMFs transduced with the inducible EGR2 shRNA construct could be passaged to senescence and EGR2 knockdown turned on post-senescence induction. Following this, inducible EGR2 shRNA knockdown could then be turned off, thus enabling investigation of senescence re-entry in reversed DS HMFs.

6.3.2 Exploring the mechanism of EGR2 driving fibroblast replicative senescence

In order to further explore the reversed DS HMF phenotype following EGR2 siRNA knockdown, the senescence markers outlined in Section 6.1.1 and Section 6.1.3 could be investigated and compared to p16+p21 siRNA knockdown DS HMFs, including DNA damage markers, the SASP and membrane stiffness. Together, these studies may identify whether EGR2 regulates particular processes during senescence induction and help to elucidate the mechanism by which EGR2 drives senescence.

As discussed in Section 6.1.2 for p16+p21 siRNA knockdown, characterisation of the methylation profile following EGR2 siRNA knockdown in DS HMFs could be performed using an Illumina EPIC array. The data generated here could be cross-compared with EP and DS methylation profiles to determine whether the EGR2 siRNA knockdown methylation profile resembles either the proliferating methylation profile or the senescence-associated methylation profile present during senescence bypass or indeed, if the DS HMF profile remains unaltered. In addition, the data could be cross-compared with the 'bypass' signature generated by Cruickshanks *et al*. (2013) and cancer-associated methylation profiles present in the TCGA. It would also be interesting to cross-compare the EGR2 siRNA knockdown methylation profile with the p16+p21 siRNA knockdown profile to identify differentially methylated positions that may elucidate commonalities and differences in the senescence induction mechanism.

Using the ChIP-grade antibody which could be generated as part of the future work presented in Section 6.3.1, the presence of EGR2 binding sites in the promoters of the

INK4/ARF locus, p21, p53, TERT and other genes of interest could be investigated in EP versus DS HMFs using ChIP, as outlined in Chapter 5 Discussion. Given the correlation demonstrated between p16, p21 and EGR2 in Chapter 5, it would also be interesting to investigate whether p16 and members of the E2F family bind to the EGR2 promoter in DS HMFs compared to EP HMFs using ChIP. To identify global EGR2 binding targets during senescence, ChIP-Seq could then be performed comparing EGR2 binding sites in EP and DS HMFs. Further, a microarray or targeted qRTPCR experiment for the reversal hits identified to possess EGR2 binding sites (see Section 5.2) could be performed in inducible EGR2-overexpressing HMFs compared to normal DS HMFs to explore the EGR2-regulated transcriptome. Together, these studies will facilitate cross comparison of the EGR2-regulated transcriptome, EGR2 binding sites and EGR2-regulated methylation dynamics during senescence thus elucidating the mechanism by which EGR2 drives senescence.

Furthermore, a number of senescence-associated signalling pathways have been implicated upstream of EGR2 signalling, including PI3K/AKT/mTOR, MEK/ERK, p38, TGF-β, and the miR-17-92 cluster (see Section 1.8 and Section 5.7). In order to explore the pathways upstream of EGR2 driving senescence, a siRNA screen of genes in these pathways could be performed to identify other hits for senescence reversal. As part of this strategy, EGR2 levels could be investigated in this screen using immunofluorescence staining.

6.3.3 Is EGR2 a universal driver of senescence?

Data presented within this thesis indicates that EGR2 plays a role driving both mammary epithelial cellular senescence and fibroblast replicative senescence. In order to further explore EGR2 as a universal senescence driver, analysis of EGR2 siRNA knockdown could be expanded to encompass HMFs which have undergone senescence induced by other triggers and other senescent cell types including dermal fibroblasts, keratinocytes, and T cells. Mazzatti *et al*. (2007) identified an increase in EGR2 expression during T cell senescence, a process defined by the loss of co-stimulatory molecules (see Section 1.3.3). Interestingly, multiple studies have demonstrated that increased EGR2 expression is a master regulator of T cell anergy, a proliferation-arrested state stimulated by TCR activation in the absence of co-stimulatory molecules (see Section 1.8.4) (Harris *et al.*, 2004; Safford *et al.*, 2005; Anderson *et al.*, 2006; Zhu *et al.*, 2008;

Zheng *et al.*, 2012). Given this, it is hypothesised that down-regulation of co-stimulatory molecules in T cells nearing senescence may potentially stimulate increased EGR2 expression which subsequently inhibits proliferation and induces T cell senescence. In order to investigate this, analysis of proliferation using high content microscopy could be performed following EGR2 siRNA knockdown in senescent T cells. However, T cells are notoriously difficult to transfect and there are significant challenges involved with siRNA delivery techniques. Currently, high voltages are required to be applied to T cells in order to induce transient membrane permeabilisation, frequently resulting in loss of cell viability or cell death (reviewed in Freeley and Long, 2013). Furthermore, siRNA gene silencing using this technique is known to be less efficient in non-activated T cells, i.e. senescent T cells. In future, further elucidation of the mechanism by which EGR2 drives senescence may allow identification of a potential druggable target which could be investigated for treatment in T cell senescence. Importantly, immunosenescence during ageing is in part characterised by a loss of T cells due to T cell senescence (see Section 1.5.1), thus these studies may help to expand our understanding of the mechanism of T cell senescence and identify a potential target to treat immunosenescence in the future.

As EGR2 expression has been identified to increase during T cell senescence *in vitro* (Mazzatti *et al.*, 2007) and a recent whole-blood gene expression meta-analysis looking at over 7,000 human samples showed that EGR2 increases with age (Peters *et al.*, 2015), it would be interesting to explore whether EGR2 expression and protein increases in T cells *in vivo* during human ageing. In order to investigate this, T cells isolated from the peripheral blood of healthy older donors and younger donors using flow cytometry could be interrogated for EGR2 expression using qRTPCR and fluorescence-activated cell sorting (FACS). Further sub-fractionation of older and younger T cells into CD28+ proliferating and CD28- senescent T cells using flow cytometry would enable investigation of EGR2 expression and protein in both proliferating and senescent populations with age (reviewed in Koch *et al*. 2008). The data generated here could determine whether EGR2 expression is increased in the CD28- senescent T cell population in comparison to the proliferating T cell sub-fraction in both older and younger donors, potentially confirming a role for EGR2 expression during T cell senescence *in vivo*.

As the data generated in this thesis indicates that EGR2 drives senescence in fibroblasts and epithelial cells, it is hypothesised that EGR2 expression would increase with age in these cell types *in vivo*. To investigate this, fibroblasts and epithelial cells isolated from older healthy donors could be investigated for increased EGR2 expression in comparison to younger donors using qRTPCR. In addition, future work could investigate whether EGR2 expression is increased *in situ* in sun-protected cutaneous tissue obtained from older healthy donors compared to younger donors using immunohistochemical staining and cell-type specific markers. Together, these studies could help determine whether EGR2 is a universal driver of senescence and, potentially, ageing in humans.

6.4 EGR2 may represent a novel therapeutic target for rejuvenation

6.4.1 Can we target senescence for reversal *in vivo*?

Targeted transient reversal of replicatively senescent populations could potentially rejuvenate aged tissues and exert a beneficial effect on healthspan in humans (see Section 1.6). However, senescence reversal therapies face a number of significant challenges *in vivo*. First, siRNA reversal therapy as a delivery mechanism would need to overcome significant technical challenges, including a high siRNA uptake by the kidney, liver and spleen which function to clear siRNAs, as well as the enzymatic siRNA degradation by nucleases in the blood (Whitehead, Langer and Anderson, 2009). Alternatively, future work elucidating the mechanism driving senescence as outlined in Sections 6.3.1, 6.3.2 and 6.3.3 may lead to the identification of a druggable target for senescence reversal which could subsequently enable investigation of a drug reversal therapy.

However, regardless of the therapeutic delivery strategy, it is important to note that senescence is known to occur as a tumour suppressor mechanism *in vivo*. As outlined in Section 6.1.1, future work could investigate whether reversal is achievable in OIS fibroblasts using EGR2 siRNA knockdown. If OIS fibroblasts are found to be reversible in a similar manner to DS fibroblasts, the current lack of methodology to distinguish different senescence types *in vivo* presents a significant challenge to both siRNA and drug-dependent senescence reversal therapeutics. In order to enable specific targeting of non-OIS cells and preclude reversal of senescence in pre-cancerous cells, markers

must be identified to distinguish between replicative senescence and OIS *in vivo*. In order to address this, a potential solution could be the development of a delivery system designed to specifically release cargo in replicatively senescent cells. For example, Agostini *et al*. (2012) have developed silica nanoparticles capped with galacto-oligosaccharides which are hydrolysed by SA-β-Gal to release the cargo following internalisation by senescent cells. Identification of an enzyme overexpressed during replicative senescence but not OIS, cancer, or normal cells could enable development of a nanoparticle cap designed to be digested for release specifically in cells which have undergone replicative senescence. To explore this, the differences in gene expression between replicative senescence and OIS could be interrogated to identify an enzyme overexpressed during replicative senescence but not OIS (Nelson *et al.*, 2014). However, following development of this delivery system, there would need to be extensive validation *in vitro* using numerous OIS cell types in order to ensure target specificity as well as preliminary investigation of target specificity in an experimental human context reflecting *in vivo* conditions, as explored in more detail in the following section.

6.4.2 Future work to explore EGR2 as a novel therapeutic target

At present, senescent cell reversal *in vivo* remains unexplored. As there are numerous senescence triggers, cell-type-dependent senescence mechanisms, and roles of senescence *in vivo* (see Introduction Sections 1.3 and 1.5, respectively), further understanding of the mechanisms driving senescence is required in order to evaluate the potential consequences of reversal therapeutics *in vivo*. The data which could be generated in the future work outlined in Section 6.3 may help elucidate these mechanisms. Further, as explored in Section 6.4.1, delivery systems capable of targeting specific senescence types *in vivo* will potentially need to be developed in order to prevent 'off-target' reversal and unintended consequences.

A second promising therapeutic strategy involves deceleration of senescence *in vivo*. Recent studies have demonstrated that delayed senescent cell accumulation *in vivo* exerts a beneficial effect on murine healthspan (see Introduction Section 1.6) (Wang *et al.*, 2010; Schafer *et al.*, 2016). Thus, it would be interesting to ask whether suppression of EGR2, or a target potentially identified within the mechanism of EGR2-driven senescence in Section 6.3, could act as a means of restraining senescence, ageing mechanisms, and potentially extending healthspan. As outlined in Section 6.3.1,

investigation of long-term inducible EGR2 shRNA knockdown in proliferating HMFs could determine whether EGR2 suppression extends replicative lifespan *in vitro*. Furthermore, as outlined in the future work discussed in Section 6.3.3, investigation of EGR2 siRNA knockdown in senescent dermal fibroblasts and keratinocytes could identify EGR2 as a universal driver of senescence. Following this, long-term inducible EGR2 shRNA knockdown in proliferating dermal fibroblasts and keratinocytes could be performed to investigate whether replicative lifespan is extended in multiple cell types.

As the mechanism of human senescence is known to be distinct from murine cell senescence (see Section 1.7), it is important to explore the implications of *in vivo* anti-senescence strategies in a human context. The living skin equivalent (LSE), a three-dimensional organotypic model comprised of dermal fibroblasts and stratified epidermal keratinocytes, has been widely used to study many aspects of cutaneous biology (reviewed in Mertsching *et al*. 2008). Thus, development of an LSE comprised of near-senescent or DS dermal fibroblasts and keratinocytes which re-capitulates the characteristics of skin ageing *in vivo* would enable investigation of anti-senescence therapeutic strategies for senescence suppression or reversal. For example, loss of senescence markers and skin ageing characteristics could be explored following p16+p21 or EGR2 siRNA knockdown treatment in a DS LSE model to determine whether siRNA reversal can be achieved in an *in vivo* context and whether reversal has an effect on skin ageing phenotypes. In addition, investigation of senescence markers and skin ageing features in a near-senescent LSE model could be compared with an LSE comprised of identical passage dermal fibroblasts and keratinocytes which have undergone long-term inducible EGR2 shRNA knockdown to determine whether EGR2 suppression has an effect on skin ageing phenotypes. Furthermore, development of an LSE comprised of both OIS and DS dermal fibroblasts and keratinocytes could enable investigation of the target specificity of the delivery system described in Section 6.4.1 in an experimental setting reflecting *in vivo* aged skin. Together, these studies will help to further our understanding of the mechanisms driving senescence and ageing, as well as explore whether EGR2 can be used as a novel therapeutic target in humans *in vivo* for reversal or suppression of senescence in order to potentially exert a beneficial effect on healthspan.

References

Acosta, J. C., Banito, A., Wuestefeld, T., Georgilis, A., Janich, P., Morton, J. P., Athineos, D., Kang, T.-W., Lasitschka, F., Andrulis, M., Pascual, G., Morris, K. J., Khan, S., Jin, H., Dharmalingam, G., Snijders, A. P., Carroll, T., Capper, D., Pritchard, C., Inman, G. J., Longerich, T., Sansom, O. J., Benitah, S. A., Zender, L. and Gil, J. (2013) 'A complex secretory program orchestrated by the inflammasome controls paracrine senescence.', *Nature Cell Biology*. Nature Publishing Group, 15(8), pp. 978–90. doi: 10.1038/ncb2784.

Acosta, J. C., O'Loghlen, A., Banito, A., Guijarro, M. V., Augert, A., Raguz, S., Fumagalli, M., Da Costa, M., Brown, C., Popov, N., Takatsu, Y., Melamed, J., d'Adda di Fagagna, F., Bernard, D., Hernando, E. and Gil, J. (2008) 'Chemokine Signaling via the CXCR2 Receptor Reinforces Senescence', *Cell*, 133(6), pp. 1006–1018. doi: 10.1016/j.cell.2008.03.038.

Agostini, A., Mondragõn, L., Bernardos, A., Martínez-Máñez, R., Dolores Marcos, M., Sancenõn, F., Soto, J., Costero, A., Manguan-García, C., Perona, R., Moreno-Torres, M., Aparicio-Sanchis, R. and Murguía, J. R. (2012) 'Targeted cargo delivery in senescent cells using capped mesoporous silica nanoparticles', *Angewandte Chemie - International Edition*, 51(42), pp. 10556–10560. doi: 10.1002/anie.201204663.

Alcorta, D. A., Xiong, Y., Phelps, D., Hannon, G., Beach, D. and Barrett, J. C. (1996) 'Involvement of the cyclin-dependent kinase inhibitor p16 (INK4a) in replicative senescence of normal human fibroblasts.', *Proceedings of the National Academy of Sciences of the United States of America*, 93(24), pp. 13742–7. doi: 10.1073/pnas.93.24.13742.

Alimbetov, D., Davis, T., Brook, A. J. C., Cox, L. S., Faragher, R. G. A., Nurgozhin, T. and Zhumadilov, Z. (2016) 'Suppression of the senescence-associated secretory phenotype (SASP) in human fibroblasts using small molecule inhibitors of p38 MAP kinase and MK2', *Biogerontology*. Springer Netherlands, 17(2), pp. 305–315. doi: 10.1007/s10522-015-9610-z.

Anderson, P. O., Manzo, B. A., Sundstedt, A., Minaee, S., Symonds, A., Khalid, S., Rodriguez-Cabezas, M. E., Nicolson, K., Li, S., Wraith, D. C. and Wang, P. (2006) 'Persistent antigenic stimulation alters the transcription program in T cells, resulting in

antigen-specific tolerance', *European Journal of Immunology*, 36(6), pp. 1374–1385. doi: 10.1002/eji.200635883.

Asghar, U., Witkiewicz, A. K., Turner, N. C. and Knudsen, E. S. (2015) 'The history and future of targeting cyclin-dependent kinases in cancer therapy', *Nature Reviews Drug Discovery*, 14(2), pp. 130–146. doi: 10.1038/nrd4504.The.

Astle, M. V, Hannan, K. M., Ng, P. Y., Lee, R. S., George, a J., Hsu, a K., Haupt, Y., Hannan, R. D. and Pearson, R. B. (2012) 'AKT induces senescence in human cells via mTORC1 and p53 in the absence of DNA damage: implications for targeting mTOR during malignancy', *Oncogene*, 31(15), pp. 1949–1962. doi: 10.1038/onc.2011.394.

Atanasoski, S., Boller, D., De Ventura, L., Koegel, H., Boentert, M., Young, P., Werner, S. and Suter, U. (2006) 'Cell cycle inhibitors p21 and p16 are required for the regulation of Schwann cell proliferation', *Glia*, 53(2), pp. 147–157. doi: 10.1002/glia.20263.

Baker, D. J., Childs, B. G., Durik, M., Wijers, M. E., Sieben, C. J., Zhong, J., Saltness, R. A., Jeganathan, K. B., Casaclang Verzosa, G., Pezeshki, A., Khazaie, K., Miller, J. D. and Van Deursen, J. M. (2016) 'Naturally occurring p16 Ink4a -positive cells shorten healthy lifespan', *Nature*. Nature Publishing Group, 530(7589), pp. 1–5. doi: 10.1038/nature16932.

Baker, D. J. and Sedivy, J. M. (2013) 'Probing the depths of cellular senescence', *Journal of Cell Biology*, 202(1), pp. 11–13. doi: 10.1083/jcb.201305155.

Baker, D. J., Wijshake, T., Tchkonia, T., LeBrasseur, N. K., Childs, B. G., van de Sluis, B., Kirkland, J. L. and van Deursen, J. M. (2011) 'Clearance of p16Ink4a-positive senescent cells delays ageing-associated disorders.', *Nature*. Nature Publishing Group, 479(7372), pp. 232–6. doi: 10.1038/nature10600.

Banito, A., Rashid, S. T., Acosta, J. C., Li, S., Pereira, C. F., Geti, I., Pinho, S., Silva, J. C., Azuara, V., Walsh, M., Vallier, L. and Gil, J. (2009) 'Senescence impairs successful reprogramming to pluripotent stem cells', *Genes & Development*, 23(18), pp. 2134–2139. doi: 10.1101/gad.1811609.

Baranwal, S., Naydenov, N. G., Harris, G., Dugina, V., Morgan, K. G., Chaponnier, C. and Ivanov, A. I. (2012) 'Nonredundant roles of cytoplasmic β- and γ-actin isoforms in

regulation of epithelial apical junctions.', *Molecular Biology of the Cell*, 23(18), pp. 3542–53. doi: 10.1091/mbc.E12-02-0162.

Beauséjour, C. M., Krtolica, A., Galimi, F., Narita, M., Lowe, S. W., Yaswen, P. and Campisi, J. (2003) 'Reversal of human cellular senescence: Roles of the p53 and p16 pathways', *EMBO Journal*, 22(16), pp. 4212–4222. doi: 10.1093/emboj/cdg417.

Beckmann, A. M. and Wilce, P. A. (1997) 'Egr transcription factors in the nervous system', *Neurochemistry International*, 31(4), pp. 477–510. doi: 10.1016/S0197-0186(97)00001-6.

Belancio, V. P., Blask, D. E., Deininger, P., Hill, S. M. and Michal Jazwinski, S. (2014) 'The aging clock and circadian control of metabolism and genome stability', *Frontiers in Genetics*, 5(DEC), pp. 1–7. doi: 10.3389/fgene.2014.00455.

Belancio, V. P., Roy-Engel, A. M., Pochampally, R. R. and Deininger, P. (2010) 'Somatic expression of LINE-1 elements in human tissues', *Nucleic Acids Research*, 38(12), pp. 3909–3922. doi: 10.1093/nar/gkq132.

Berdyyeva, T. K., Woodworth, C. D. and Sokolov, I. (2005) 'Human epithelial cells increase their rigidity with ageing in vitro: direct measurements.', *Physics in Medicine and Biology*, 50(1), pp. 81–92. doi: 10.1088/0031-9155/50/1/007.

Bhaumik, D., Scott, G. K., Schokrpur, S., Patil, C. K., Orjalo, A. V., Rodier, F., Lithgow, G. J. and Campisi, J. (2009) 'MicroRNAs miR-146a/b negatively modulate the senescence-associated inflammatory mediators IL-6 and IL-8.', *Aging*, 1(4), pp. 402–411. doi: 10.1016/j.virol.2011.01.029.The.

Bishop, C. L., Bergin, A. M. H., Fessart, D., Borgdorff, V., Hatzimasoura, E., Garbe, J. C., Stampfer, M. R., Koh, J. and Beach, D. H. (2010) 'Primary cilium-dependent and -independent hedgehog signaling inhibits p16INK4A', *Molecular Cell*. Elsevier Inc., 40(4), pp. 533–547. doi: 10.1016/j.molcel.2010.10.027.

Bodnar, A. G., Ouellette, M., Frolkis, M., Holt, S. E., Chiu, C. P., Morin, G. B., Harley, C. B., Shay, J. W., Lichtsteiner, S. and Wright, W. E. (1998) 'Extension of life-span by introduction of telomerase into normal human cells.', *Science*, 279(5349), pp. 349–52. doi: 10.1126/science.279.5349.349.

Bond, J. A., Blaydes, J. P., Rowson, J., Haughton, M. F., Smith, J. R., Wynford-Thomas, D. and Wyllie, F. S. (1995) 'Mutant p53 Rescues Human Diploid Cells from Senescence without Inhibiting the Induction of SDI1/WAF', *Cancer Research*, 55(11), pp. 2404–2409.

Borgdorff, V., Lleonart, M. E., Bishop, C. L., Fessart, D., Bergin, A. H., Overhoff, M. G. and Beach, D. H. (2010) 'Multiple microRNAs rescue from Ras-induced senescence by inhibiting p21(Waf1/Cip1)', *Oncogene*. Nature Publishing Group, 29(15), pp. 2262–2271. doi: 10.1038/onc.2009.497.

Bork, S., Pfister, S., Witt, H., Horn, P., Korn, B., Ho, A. D. and Wagner, W. (2010) 'DNA methylation pattern changes upon long-term culture and aging of human mesenchymal stromal cells', *Aging Cell*, 9(1), pp. 54–63. doi: 10.1111/j.1474-9726.2009.00535.x.

Boutros, M. and Ahringer, J. (2008) 'The art and design of genetic screens: RNA interference.', *Nature Reviews Genetics*, 9(7), pp. 554–66. doi: 10.1038/nrg2364.

Bracken, A. P., Kleine-Kohlbrecher, D., Dietrich, N., Pasini, D., Gargiulo, G., Beekman, C., Theilgaard-Mönch, K., Minucci, S., Porse, B. T., Marine, J. C., Hansen, K. H. and Helin, K. (2007) 'The Polycomb group proteins bind throughout the INK4A-ARF locus and are disassociated in senescent cells', *Genes & Development*, 21(5), pp. 525–530. doi: 10.1101/gad.415507.

Brenner, A. J., Stampfer, M. R. and Aldaz, C. M. (1998) 'Increased p16 expression with first senescence arrest in human mammary epithelial cells and extended growth capacity with p16 inactivation.', *Oncogene*, 17(2), pp. 199–205. doi: 10.1038/sj.onc.1201919.

Bruggeman, S. W. M., Valk-lingbeek, M. E., Stoop, P. P. M. Van Der, Jacobs, J. J. L., Kieboom, K., Tanger, E., Hulsman, D., Leung, C., Arsenijevic, Y., Marino, S. and Lohuizen, M. Van (2011) 'Differentially Affect Cell Proliferation and Neural Stem Cell Self-Renewal in', *Genes & Development*, pp. 1438–1443. doi: 10.1101/gad.1299305.1438.

Brzezińska, A., Magalska, A. and Sikora, E. (2003) 'Proliferation of CD8+ in culture of

human T cells derived from peripheral blood of adult donors and cord blood of newborns', *Mechanisms of Ageing and Development*, 124(4), pp. 379–387. doi: 10.1016/S0047-6374(03)00012-5.

Bubb, M. R., Senderowicz, A. M. J., Sausville, E. A., Duncan, K. L. K. and Korn, E. D. (1994) 'Jasplakinolide, a cytotoxic natural product, induces actin polymerization and competitively inhibits the binding of phalloidin to F-actin', *Journal of Biological Chemistry*, 269(21), pp. 14869–14871. doi: VL - 269.

Buttitta, L. A. and Edgar, B. A. (2007) 'Mechanisms controlling cell cycle exit upon terminal differentiation', *Current Opinion in Cell Biology*, 19(6), pp. 697–704. doi: 10.1016/j.ceb.2007.10.004.

Cao, K., Graziotto, J. J., Blair, C. D., Mazzulli, J. R., Erdos, M. R., Krainc, D. and Collins, F. S. (2011) 'Rapamycin reverses cellular phenotypes and enhances mutant protein clearance in Hutchinson-Gilford progeria syndrome cells.', *Science translational medicine*, 3(89), p. 89ra58. doi: 10.1126/scitranslmed.3002346.

De Cecco, M., Criscione, S. W., Peckham, E. J., Hillenmeyer, S., Hamm, E. A., Manivannan, J., Peterson, A. L., Kreiling, J. A., Neretti, N. and Sedivy, J. M. (2013) 'Genomes of replicatively senescent cells undergo global epigenetic changes leading to gene silencing and activation of transposable elements', *Aging Cell*, 12(2), pp. 247–256. doi: 10.1111/acel.12047.

Chang, J., Wang, Y., Shao, L., Laberge, R.-M., Demaria, M., Campisi, J., Janakiraman, K., Sharpless, N. E., Ding, S., Feng, W., Luo, Y., Wang, X., Aykin-Burns, N., Krager, K., Ponnappan, U., Hauer-Jensen, M., Meng, A. and Zhou, D. (2015) 'Clearance of senescent cells by ABT263 rejuvenates aged hematopoietic stem cells in mice', *Nature Medicine*. Nature Publishing Group, 22(1), pp. 1–9. doi: 10.1038/nm.4010.

Chang, J., Wang, Y., Shao, L., Laberge, R. M., Demaria, M., Campisi, J., Janakiraman, K., Sharpless, N. E., Ding, S., Feng, W., Luo, Y., Wang, X., Aykin-Burns, N., Krager, K., Ponnappan, U., Hauer-Jensen, M., Meng, A. and Zhou, D. (2016) 'Clearance of senescent cells by ABT263 rejuvenates aged hematopoietic stem cells in mice', *Nature Medicine*. Nature Publishing Group, 22(1), pp. 78–83. doi: 10.1038/nm.4010.

Chen, Q., Fischer, A., Reagan, J. D., Yan, L. J. and Ames, B. N. (1995) 'Oxidative DNA damage and senescence of human diploid fibroblast cells.', *Proceedings of the National Academy of Sciences of the United States of America*, 92(10), pp. 4337–41. doi: 10.1073/pnas.92.10.4337.

Chen, W., Kang, J., Xia, J., Li, Y., Yang, B., Chen, B., Sun, W., Song, X., Xiang, W., Wang, X., Wang, F., Wan, Y. and Bi, Z. (2008) 'p53-related apoptosis resistance and tumor suppression activity in UVB-induced premature senescent human skin fibroblasts', *International Journal of Molecular Medicine*, 21(5), pp. 645–653. doi: 10.3892/ijmm.21.5.645.

Chen, X., Li, Z., Feng, Z., Wang, J., Ouyang, C., Liu, W., Fu, B., Cai, G., Wu, C., Wei, R., Wu, D. and Hong, Q. (2006) 'Integrin-linked kinase induces both senescence-associated alterations and extracellular fibronectin assembly in aging cardiac fibroblasts.', *The journals of gerontology: Biological Scienece*, 61A(12), pp. 1232–1245. doi: 61/12/1232 [pii].

Chen, Y. J., Dominguez-Brauer, C., Wang, Z., Asara, J. M., Costa, R. H., Tyner, A. L., Lau, L. F. and Raychaudhuri, P. (2009) 'A conserved phosphorylation site within the forkhead domain of FoxM1B is required for its activation by cyclin-CDK1', *Journal of Biological Chemistry*, 284(44), pp. 30695–30707. doi: 10.1074/jbc.M109.007997.

Chen, Z., Trotman, L. C., Shaffer, D., Lin, H.-K., Dotan, Z. A., Niki, M., Koutcher, J. A., Scher, H. I., Ludwig, T., Gerald, W., Cordon-Cardo, C. and Pandolfi, P. P. (2005) 'Crucial role of p53-dependent cellular senescence in suppression of Pten-deficient tumorigenesis', *Nature*, 436(7051), pp. 725–730. doi: 10.3892/ijo.

Chen, Z., Yue, S. X., Zhou, G., Greenfield, E. M. and Murakami, S. (2015) 'ERK1 and ERK2 regulate chondrocyte terminal differentiation during endochondral bone formation', *Journal of Bone and Mineral Research*, 30(5), pp. 765–774. doi: 10.1002/jbmr.2409.

Childs, B. G., Baker, D. J., Kirkland, J. L., Campisi, J. and van Deursen, J. M. (2014) 'Senescence and apoptosis: dueling or complementary cell fates?', *EMBO Reports*, 15(11), pp. 1139–53. doi: 10.15252/embr.201439245.

Childs, B. G., Baker, D. J., Wijshake, T., Conover, C. A., Campisi, J. and Van Deursen, J.

M. (2016) ‘Senescent intimal foam cells are deleterious at all stages of atherosclerosis’, *Science*, 354(6311), pp. 472–477. doi: 10.1126/science.aaf6659.Senescent.

Chinta, S. J., Lieu, C. A., Demaria, M., Laberge, R. M., Campisi, J. and Andersen, J. K. (2013) ‘Environmental stress, ageing and glial cell senescence: A novel mechanistic link to parkinson’s disease?’, *Journal of Internal Medicine*, 273(5), pp. 429–436. doi: 10.1111/joim.12029.

Choi, H. R., Cho, K. A., Kang, H. T., Lee, J. Bin, Kaeberlein, M., Suh, Y., Chung, I. K. and Park, S. C. (2011) ‘Restoration of senescent human diploid fibroblasts by modulation of the extracellular matrix’, *Aging Cell*, (10), pp. 148–157. doi: 10.1111/j.1474-9726.2010.00654.x.

Chou, J. P. and Effros, R. B. (2013) ‘T cell replicative senescence in human aging.’, *Current pharmaceutical design*, 19(9), pp. 1680–98. doi: 10.2174/1381612811319090016.

Clarke, R. W., Novak, P., Zhukov, A., Tyler, E. J., Cano-Jaimez, M., Drews, A., Richards, O., Volynski, K., Bishop, C. and Klenerman, D. (2016) ‘Low Stress Ion Conductance Microscopy of Sub-Cellular Stiffness’, *Soft Matter*. Royal Society of Chemistry, 12, pp. 7953–7958. doi: 10.1039/C6SM01106C.

Cliby, W. A., Roberts, C. J., Cimprich, K. A., Stringer, C. M., Lamb, J. R., Schreiber, S. L. and Friend, S. H. (1998) ‘Overexpression of a kinase-inactive ATR protein causes sensitivity to DNA-damaging agents and defects in cell cycle checkpoints’, *The EMBO Journal*, 17(1), pp. 159–169.

Collado, M. and Serrano, M. (2010) ‘Senescence in tumours: evidence from mice and humans’, *Nature Reviews Cancer*. Nature Publishing Group, 10(1), pp. 51–57. doi: 10.1038/nrc2772.

Coppé, J.-P., Desprez, P.-Y., Krtolica, A. and Campisi, J. (2010) ‘The senescence-associated secretory phenotype: the dark side of tumor suppression.’, *Annual Review of Pathology*, 5, pp. 99–118. doi: 10.1146/annurev-pathol-121808-102144.

Coppé, J.-P., Patil, C. K., Rodier, F., Sun, Y., Muñoz, D. P., Goldstein, J., Nelson, P. S., Desprez, P.-Y. and Campisi, J. (2008) ‘Senescence-associated secretory phenotypes

reveal cell-nonautonomous functions of oncogenic RAS and the p53 tumor suppressor.', *PLoS Biology*, 6(12), pp. 2853–68. doi: 10.1371/journal.pbio.0060301.

Coqueret, O. and Gascan, H. (2000) 'Functional interaction of STAT3 transcription factor with the cell cycle inhibitor p21(WAF1/CIP1/SDI1)', *Journal of Biological Chemistry*, 275(25), pp. 18794–18800. doi: 10.1074/jbc.M001601200.

Correia-Melo, C., Marques, F. D., Anderson, R., Hewitt, G., Hewitt, R., Cole, J., Carroll, B. M., Miwa, S., Birch, J., Merz, A., Rushton, M. D., Charles, M., Jurk, D., Tait, S. W., Czapiewski, R., Greaves, L., Nelson, G., Bohlooly-Y, M., Rodriguez-Cuenca, S., Vidal-Puig, A., Mann, D., Saretzki, G., Quarato, G., Green, D. R., Adams, P. D., von Zglinicki, T., Korolchuk, V. I. and Passos, J. F. (2016) 'Mitochondria are required for pro-ageing features of the senescent phenotype', *The EMBO Journal*, 35(7), pp. 724–742. doi: 10.15252/embj.201592862.

Cruickshanks, H. A., McBryan, T., Nelson, D. M., Vanderkraats, N. D., Shah, P. P., van Tuyn, J., Singh Rai, T., Brock, C., Donahue, G., Dunican, D. S., Drotar, M. E., Meehan, R. R., Edwards, J. R., Berger, S. L. and Adams, P. D. (2013) 'Senescent cells harbour features of the cancer epigenome.', *Nature Cell Biology*. Nature Publishing Group, 15(12), pp. 1495–506. doi: 10.1038/ncb2879.

Dabrowska, M. and Skoneczny, M. (2011) 'Functional gene expression profile underlying methotrexate-induced senescence in human colon cancer cells', *Tumour Biol.*, 32, pp. 965–976. doi: 10.1007/s13277-011-0198-x.

Daly, C. H. and Odland, G. F. (1979) 'Age-related changes in the mechanical properties of human skin.', *The Journal of Investigative Dermatology*. Elsevier Masson SAS, 73(1), pp. 84–87. doi: 10.1111/1523-1747.ep12532770.

Damalas, A., Kahan, S., Shtutman, M., Ben-Ze'ev, A. and Oren, M. (2001) 'Deregulated beta-catenin induces a p53-and ARF-dependent growth arrest and cooperates with Ras in transformation', *EMBO Journal*, 20(17), p. 4912–22. doi: 10.1093/emboj/20.17.4912.

Das, A., Chendil, D., Dey, S., Mohiuddin, M., Mohiuddin, M., Milbrandt, J., Rangnekar, V. M. and Ahmed, M. M. (2001) 'Ionizing Radiation Down-regulates p53 Protein in Primary Egr-1 -/- Mouse Embryonic Fibroblast Cells Causing Enhanced Resistance to

Apoptosis', *Journal of Biological Chemistry*, 276(5), pp. 3279–3286. doi: 10.1074/jbc.M008454200.

Davalos, A. R., Kawahara, M., Malhotra, G. K., Schaum, N., Huang, J., Ved, U., Beausejour, C. M., Coppe, J. P., Rodoer, F. and Campisi, J. (2013) 'p53-dependent release of Alarmin HMGB1 is a central mediator of senescent phenotypes', *Journal of Cell Biology*, 201(4), pp. 613–629. doi: 10.1083/jcb.201206006.

Decker, L. (2006) 'Peripheral Myelin Maintenance Is a Dynamic Process Requiring Constant Krox20 Expression', *Journal of Neuroscience*, 26(38), pp. 9771–9779. doi: 10.1523/JNEUROSCI.0716-06.2006.

Delavaine, L. and La Thangue, N. B. (1999) 'Control of E2F activity by p21Waf1/Cip1.', *Oncogene*, 18(39), pp. 5381–5392. doi: 10.1038/sj.onc.1202923.

Demaria, M., Ohtani, N., Youssef, S. A., Rodier, F., Toussaint, W., Mitchell, J. R., Laberge, R. M., Vijg, J., VanSteeg, H., Dollé, M. E. T., Hoeijmakers, J. H. J., deBruin, A., Hara, E. and Campisi, J. (2014) 'An essential role for senescent cells in optimal wound healing through secretion of PDGF-AA', *Developmental Cell*, 31(6), pp. 722–733. doi: 10.1016/j.devcel.2014.11.012.

Demidenko, Z. N., Zubova, S. G., Bukreeva, E. I., Pospelov, V. A., Pospelova, T. V. and Blagosklonny, M. V. (2009) 'Rapamycin decelerates cellular senescence', *Cell Cycle*, 8(12), pp. 1888–1895. doi: 10.4161/cc.8.12.8606.

Deng, Q., Liao, R., Wu, B. L. and Sun, P. (2004) 'High Intensity ras Signaling Induces Premature Senescence by Activating p38 Pathway in Primary Human Fibroblasts', *Journal of Biological Chemistry*, 279(2), pp. 1050–1059. doi: 10.1074/jbc.M308644200.

van Deursen, J. M. (2014) 'The role of senescent cells in ageing.', *Nature*. Nature Publishing Group, 509(7501), pp. 439–46. doi: 10.1038/nature13193.

Dhahbi, J. M., Atamna, H., Boffelli, D., Magis, W., Spindler, S. R. and Martin, D. I. K. (2011) 'Deep sequencing reveals novel microRNAs and regulation of microRNA expression during cell senescence', *PLoS ONE*, 6(5). doi: 10.1371/journal.pone.0020509.

Dimri, G. P., Itahana, K., Acosta, M. and Campisi, J. (2000) 'Regulation of a Senescence

Checkpoint Response by the E2F1 Transcription Factor and p14 ARF Tumor Suppressor', *Molecular and Cellular Biology*, 20(1), pp. 273–285.

Dimri, G. P., Lee, X., Basile, G., Acosta, M., Scott, G., Roskelley, C., Medrano, E. E., Linskens, M., Rubelj, I. and Pereira-Smith, O. (1995) 'A biomarker that identifies senescent human cells in culture and in aging skin in vivo.', *Proceedings of the National Academy of Sciences of the United States of America*, 92(20), pp. 9363–7. doi: DOI 10.1073/pnas.92.20.9363.

Dirac, A. M. G. and Bernards, R. (2003) 'Reversal of senescence in mouse fibroblasts through lentiviral suppression of p53', *Journal of Biological Chemistry*, 278(14), pp. 11731–11734. doi: 10.1074/jbc.C300023200.

Doncel-Perez, E., Mateos-Hernandez, L., Pareja, E., Garcia-Forcada, A., Villar, M., Tobes, R., Romero Ganuza, F., Vila del Sol, V., Ramos, R., Fernandez de Mera, I. G. and de la Fuente, J. (2015) 'Expression of Early Growth Response Gene-2 and Regulated Cytokines Correlates with Recovery from Guillain-Barre Syndrome', *The Journal of Immunology*, 196(11), pp. 1102–1107. doi: 10.4049/jimmunol.1502100.

Dumaz, N., Milne, D. M., Jardine, L. J. and Meek, D. W. (2001) 'Critical roles for the serine 20, but not the serine 15, phosphorylation site and for the polyproline domain in regulating p53 turnover', *Biochemical Journal*, 359, pp. 459–464.

Durinck, S., Spellman, P. T., Birney, E. and Huber, W. (2009) 'Mapping Identifiers for the Integration of Genomic Datasets with the R/Bioconductor package biomaRt', *Nature Protocols*, 4(8), pp. 1184–1191. doi: 10.1016/j.pestbp.2011.02.012.Investigations.

Dyson, N. (1998) 'The regulation of E2F by pRB-family proteins', *Genes & Development*, 12(617), pp. 2245–2262. doi: 10.1101/gad.12.15.2245.

Echeverri, C. J., Beachy, P. A., Baum, B., Boutros, M., Buchholz, F., Chanda, S. K., Downward, J., Ellenberg, J., Fraser, A. G., Hacohen, N., Hahn, W. C., Jackson, A. L., Kiger, A., Linsley, P. S., Lum, L., Ma, Y., Mathey-Prevot, B., Root, D. E., Sabatini, D. M., Taipale, J., Perrimon, N. and Bernards, R. (2006) 'Minimizing the risk of reporting false positives in large-scale RNAi screens', *Nature Methods*, 3(10), pp. 777–779. doi:

10.1038/nmeth1006-777.

Erusalimsky, J. D. (2009) 'Vascular endothelial senescence: from mechanisms to pathophysiology.', *Journal of Applied Physiology*, 106(1), pp. 326–32. doi: 10.1152/japplphysiol.91353.2008.

di Fagagna, F. d'Adda, Reaper, P. M., Clay-Farrace, L., Fiegler, H., Carr, P., von Zglinicki, T., Saretzki, G., Carter, N. P. and Jackson, S. P. (2003) 'A DNA damage checkpoint response in telomere-initiated senescence', *Nature*, 426(6963), pp. 194–198. doi: 10.1038/nature02118.

Fagnoni, F. F., Vescovini, R., Mazzola, M., Bologna, G., Nigro, E., Lavagetto, G., Franceschi, C., Passeri, M. and Sansoni, P. (1996) 'Expansion of cytotoxic CD8+ CD28- T cells in healthy ageing people, including centenarians.', *Immunology*, 88(4), pp. 501–507.

Falschlehner, C., Steinbrink, S., Erdmann, G. and Boutros, M. (2010) 'High-throughput RNAi screening to dissect cellular pathways: A how-to guide', *Biotechnology Journal*, 5(4), pp. 368–376. doi: 10.1002/biot.200900277.

Falvella, F. S., Colombo, F., Spinola, M., Campiglio, M., Pastorino, U. and Dragani, T. a (2008) 'BHLHB3: a candidate tumor suppressor in lung cancer.', *Oncogene*, 27, pp. 3761–3764. doi: 10.1038/sj.onc.1211038.

Fang, F., Ooka, K., Bhattachyya, S., Wei, J., Wu, M., Du, P., Lin, S., Del Galdo, F., Feghali-Bostwick, C. A. and Varga, J. (2011) 'The early growth response gene Egr2 (alias Krox20) is a novel transcriptional target of transforming growth factor-β that is up-regulated in systemic sclerosis and mediates profibrotic responses', *American Journal of Pathology*, 178(5), pp. 2077–2090. doi: 10.1016/j.ajpath.2011.01.035.

Ferbeyre, G., De Stanchina, E., Querido, E., Baptiste, N., Prives, C. and Lowe, S. W. (2000) 'PML is induced by oncogenic ras and promotes premature senescence', *Genes & Development*, 14(16), pp. 2015–2027. doi: 10.1101/gad.14.16.2015.

Fire, A., Xu, S., Montgomery, M. K., Kostas, S. A., Driver, S. E. and Mello, C. C. (1998) 'Potent and specific genetic interference by double-stranded RNA in Caenorhabditis elegans', *Nature*, 391(6669), pp. 806–811. doi: 10.1038/35888.

Flachsbart, F., Franke, A., Kleindorp, R., Caliebe, A., Blanché, H., Schreiber, S. and Nebel, A. (2010) 'Mutation Research / Fundamental and Molecular Mechanisms of Mutagenesis Investigation of genetic susceptibility factors for human longevity – A targeted nonsynonymous SNP study', *Mutation Research - Fundamental and Molecular Mechanisms of Mutagenesis*. Elsevier B.V., 694(1–2), pp. 13–19. doi: 10.1016/j.mrfmmm.2010.08.006.

Freeley, M. and Long, A. (2013) 'Advances in siRNA delivery to T-cells: potential clinical applications for inflammatory disease, cancer and infection', *Biochem. J*, 455, pp. 133–147. doi: 10.1042/BJ20130950.

Freund, A., Laberge, R.-M., Demaria, M. and Campisi, J. (2012) 'Lamin B1 loss is a senescence-associated biomarker.', *Molecular Biology of the Cell*, 23(11), pp. 2066–75. doi: 10.1091/mbc.E11-10-0884.

Freund, A., Orjalo, A. V, Desprez, P.-Y. and Campisi, J. (2010) 'Inflammatory Networks during Cellular Senescence: Causes and Consequences', *Trends in Molecular Medicine*, 16(5), pp. 238–246. doi: 10.1016/j.pestbp.2011.02.012.Investigations.

Freund, A., Patil, C. K. and Campisi, J. (2011) 'p38MAPK is a novel DNA damage response-independent regulator of the senescence-associated secretory phenotype', *The EMBO Journal*. Nature Publishing Group, 30(8), pp. 1536–1548. doi: 10.1038/emboj.2011.69.

Fuziwara, C. S. and Kimura, E. T. (2015) 'Insights into Regulation of the miR-17-92 Cluster of miRNAs in Cancer.', *Frontiers in Medicine*, 2(September), p. 64. doi: 10.3389/fmed.2015.00064.

Gabet, Y., Baniwal, S. K., Leclerc, N., Shi, Y., Kohn-Gabet, A. E., Cogan, J., Dixon, A., Bachar, M., Guo, L., Turman, J. E. and Frenkel, B. (2010) 'Krox20/EGR2 deficiency accelerates cell growth and differentiation in the monocytic lineage and decreases bone mass', *Blood*, 116(19), pp. 3964–3971. doi: 10.1182/blood-2010-01-263830.

Garbe, J. C., Bhattacharya, S., Merchant, B., Bassett, E., Swisshelm, K., Feiler, H. S., Wyrobek, A. J. and Stampfer, M. R. (2009) 'Molecular distinctions between stasis and telomere attrition senescence barriers shown by long-term culture of normal human

mammary epithelial cells', *Cancer Research*, 69(19), pp. 7557–7568. doi: 10.1158/0008-5472.CAN-09-0270.

Gargaun, E., Seferian, A. M., Cardas, R., Le Moing, A.-G., Delanoe, C., Nectoux, J., Nelson, I., Bonne, G., Bihoreau, M.-T., Deleuze, J.-F., Boland, A., Masson, C., Servais, L. and Gidaro, T. (2016) 'EGR2 mutation enhances phenotype spectrum of Dejerine–Sottas syndrome', *Journal of Neurology*, 263(7), pp. 1456–1458. doi: 10.1007/s00415-016-8153-9.

Garinis, G. a, van der Horst, G. T. J., Vijg, J. and Hoeijmakers, J. H. J. (2008) 'DNA damage and ageing: new-age ideas for an age-old problem.', *Nature Cell Biology*, 10(11), pp. 1241–1247. doi: 10.1038/ncb1108-1241.

Geng, Y. Q., Guan, J. T., Xu, X. H. and Fu, Y. C. (2010) 'Senescence-associated beta-galactosidase activity expression in aging hippocampal neurons', *Biochemical and Biophysical Research Communications*. Elsevier Inc., 396(4), pp. 866–869. doi: 10.1016/j.bbrc.2010.05.011.

Gil, J., Bernard, D., Martínez, D. and Beach, D. (2004) 'Polycomb CBX7 has a unifying role in cellular lifespan.', *Nature Cell Biology*, 6(1), pp. 67–72. doi: 10.1038/ncb1077.

Gil, J. and Peters, G. (2006) 'Regulation of the INK4b-ARF-INK4a tumour suppressor locus: all for one or one for all.', *Nature Reviews Molecular Cell Biology*, 7(9), pp. 667–77. doi: 10.1038/nrm1987.

Gillian, A. L. and Svaren, J. (2004) 'The Ddx20/DP103 Dead Box Protein Represses Transcriptional Activation by Egr2/Krox-20', *Journal of Biological Chemistry*, 279(10), pp. 9056–9063. doi: 10.1074/jbc.M309308200.

Gire, V. and Wynford-Thomas, D. (1998) 'Reinitiation of DNA synthesis and cell division in senescent human fibroblasts by microinjection of anti-p53 antibodies.', *Molecular and Cellular Biology*, 18(3), pp. 1611–21.

Gomez-Sanchez, J. A., Gomis-Coloma, C., Morenilla-Palao, C., Peiro, G., Serra, E., Serrano, M. and Cabedo, H. (2013) 'Epigenetic induction of the Ink4a/Arf locus prevents Schwann cell overproliferation during nerve regeneration and after tumorigenic challenge', *Brain*, 136(7), pp. 2262–2278. doi: 10.1093/brain/awt130.

Goronzy, J. J. and Weyand, C. M. (2013) 'Understanding immunosenescence to improve responses to vaccines', *Nature Immunology*, 14(5), pp. 428–436. doi: 10.1038/ni.2588.

Grassmann, F., Friedrich, U., Fauser, S., Schick, T., Milenkovic, A., Schulz, H. L., von Strachwitz, C. N., Bettecken, T., Lichtner, P., Meitinger, T., Arend, N., Wolf, A., Haritoglou, C., Rudolph, G., Chakravarthy, U., Silvestri, G., McKay, G. J., Freitag-Wolf, S., Krawczak, M., Smith, R. T., Merriam, J. C., Merriam, J. E., Allikmets, R., Heid, I. M. and Weber, B. H. F. (2015) 'A Candidate Gene Association Study Identifies DAPL1 as a Female-Specific Susceptibility Locus for Age-Related Macular Degeneration (AMD)', *Neuromolecular Medicine*. Springer US, 17, pp. 111–120. doi: 10.1007/s12017-015-8342-1.

Grunewald, T. G., Bernard, V., Gilardi-Hebenstreit, P., Raynal, V., Surdez, D., Aynaud, M.-M., Mirabeau, O., Cidre-Aranaz, F., Tirode, F., Zaidi, S., Perot, G. euml lle, Jonker, A. H., Lucchesi, C., Le Deley, M.-C. eacute cile, Oberlin, O., Rard, P. M.-B. eacute, Ron, A. eacute lie S. V. eacute, Reynaud, S., Lapouble, E., Boeva, V., Frio, T. R., Alonso, J., Bhatia, S., Pierron, G. euml lle, Cancel-Tassin, G., Cussenot, O., Cox, D. G., Morton, L. M., Machiela, M. J., Chanock, S. J., Charnay, P. and Delattre, O. (2015) 'Chimeric EWSR1-FLI1 regulates the Ewing sarcoma susceptibility gene EGR2 via a GGAA microsatellite', *Nature Genetics*, 47(9), pp. 1–9. doi: 10.1038/ng.3363.

Hackl, M., Brunner, S., Fortschegger, K., Schreiner, C., Micutkova, L., Mück, C., Laschober, G. T., Lepperdinger, G., Sampson, N., Berger, P., Herndler-Brandstetter, D., Wieser, M., Kühnel, H., Strasser, A., Rinnerthaler, M., Breitenbach, M., Mildner, M., Eckhart, L., Tschachler, E., Trost, A., Bauer, J. W., Papak, C., Trajanoski, Z., Scheideler, M., Grillari-Voglauer, R., Grubeck-Loebenstein, B., Jansen-Dürr, P. and Grillari, J. (2010) 'miR-17, miR-19b, miR-20a, and miR-106a are down-regulated in human aging', *Aging Cell*, 9(2), pp. 291–296. doi: 10.1111/j.1474-9726.2010.00549.x.

Hänzelmann, S., Beier, F., Gusmao, E. G., Koch, C. M., Hummel, S., Charapitsa, I., Joussen, S., Benes, V., Brümmendorf, T. H., Reid, G., Costa, I. G. and Wagner, W. (2015) 'Replicative senescence is associated with nuclear reorganization and with DNA methylation at specific transcription factor binding sites', *Clinical Epigenetics*, 7(1), p. 19. doi: 10.1186/s13148-015-0057-5.

Hara, E., Smith, R., Parry, D., Tahara, H., Stone, S. and Peters, G. (1996) 'Regulation of p16CDKN2 expression and its implications for cell immortalization and senescence.', *Molecular and Cellular Biology*, 16(3), pp. 859–67. doi: 10.1128/MCB.16.3.859.

Harris, J. E., Bishop, K. D., Phillips, N. E., Mordes, J. P., Greiner, D. L., Rossini, A. a and Czech, M. P. (2004) 'Early growth response gene-2, a zinc-finger transcription factor, is required for full induction of clonal anergy in CD4+ T cells.', *Journal of Immunology*, 173(12), pp. 7331–7338. doi: 10.4049/jimmunol.173.12.7331.

Hayflick, L. and Moorhead, P. S. (1961) 'The serial cultivation of human diploid cell strains.', *Journal of Chemical Information and Modeling*, 53(9), pp. 1689–1699. doi: 10.1017/CBO9781107415324.004.

Herdegen, T., Kiessling, M., Bele, S., Bravo, R., Zimmermann, M. and Gass, P. (1993) 'The KROX-20 transcription factor in the rat central and peripheral nervous systems: novel expression pattern of an immediate early gene-encoded protein', *Neuroscience*, 57(1), pp. 41–52. doi: 10.1016/0306-4522(93)90110-2.

Herranz, N., Gallage, S., Mellone, M., Wuestefeld, T., Klotz, S., Hanley, C. J., Raguz, S., Acosta, J. C., Innes, A. J., Banito, A., Georgilis, A., Montoya, A., Wolter, K., Dharmalingam, G., Faull, P., Carroll, T., Martínez-Barbera, J. P., Cutillas, P., Reisinger, F., Heikenwalder, M., Miller, R. A., Withers, D., Zender, L., Thomas, G. J. and Gil, J. (2015) 'mTOR regulates MAPKAPK2 translation to control the senescence-associated secretory phenotype.', *Nature Cell Biology*, 17(9), pp. 1205–17. doi: 10.1038/ncb3225.

Hewitt, G., Jurk, D., Marques, F. D. M., Correia-Melo, C., Hardy, T., Gackowska, A., Anderson, R., Taschuk, M., Mann, J. and Passos, J. F. (2012) 'Telomeres are favoured targets of a persistent DNA damage response in ageing and stress-induced senescence.', *Nature Communications*, 3, p. 708. doi: 10.1038/ncomms1708.

Hoare, M., Ito, Y., Kang, T.-W., Weekes, M. P., Matheson, N. J., Patten, D. A., Shetty, S., Parry, A. J., Menon, S., Salama, R., Antrobus, R., Tomimatsu, K., Howat, W., Lehner, P. J., Zender, L. and Narita, M. (2016) 'NOTCH1 mediates a switch between two distinct secretomes during senescence', *Nature Cell Biology*, 18(9), pp. 979–992. doi: 10.1038/ncb3397.

Holst, C. R., Nuovo, G. J., Esteller, M., Chew, K., Baylin, S. B., Herman, J. G. and Tlsty, T. D. (2003) 'Methylation of p16 INK4a Promoters Occurs in Vivo in Histologically Normal Human Mammary Epithelia Methylation of p16 INK4a Promoters Occurs in Vivo in Histologically Normal Human', *Cancer*, pp. 1596–1601.

Hossain, S., de la Cruz-Morcillo, M. A., Sanchez-Prieto, R. and Almazan, G. (2012) 'Mitogen-activated protein kinase p38 regulates krox-20 to direct schwann cell differentiation and peripheral myelination', *Glia*, 60(7), pp. 1130–1144. doi: 10.1002/glia.22340.

Huschtscha, L. I., Noble, J. R., Neumann, A. a, Moy, E. L., Barry, P., Melki, J. R., Clark, S. J. and Reddel, R. R. (1998) 'Advances in Brief Loss of pl6INK4 Expression by Methylation Is Associated with Lifespan Extension of Human Mammary Epithelial Cells1', *Cancer Research*, 58, pp. 3508–3512.

Huveneers, S., Truong, H., Fässler, R., Sonnenberg, A. and Danen, E. H. J. (2008) 'Binding of soluble fibronectin to integrin alpha5 beta1 - link to focal adhesion redistribution and contractile shape.', *Journal of cell science*, 121(Pt 15), pp. 2452–2462. doi: 10.1242/jcs.033001.

Iannello, A., Thompson, T. W., Ardolino, M., Lowe, S. W. and Raulet, D. H. (2013) 'p53-dependent chemokine production by senescent tumor cells supports NKG2D-dependent tumor elimination by natural killer cells.', *The Journal of experimental medicine*, 210(10), pp. 2057–69. doi: 10.1084/jem.20130783.

Jackson, D. A., Hassan, A. B., Errington, R. J. and Cook, P. R. (1993) 'Visualization of focal sites of transcription within human nuclei.', *The EMBO journal*, 12(3), pp. 1059–65.

Jacobs, J. J., Kieboom, K., Marino, S., DePinho, R. a and van Lohuizen, M. (1999) 'The oncogene and Polycomb-group gene bmi-1 regulates cell proliferation and senescence through the ink4a locus.', *Nature*, 397(6715), pp. 164–168. doi: 10.1038/16476.

Jacobs, J. J. L. and De Lange, T. (2004) 'Significant Role for p16INK4a in p53-Independent Telomere-Directed Senescence', *Current Biology*, 14, pp. 2302–2308. doi: 10.1016/j.

Janzen, V., Forkert, R., Fleming, H. E., Saito, Y., Waring, M. T., Dombkowski, D. M., Cheng, T., DePinho, R. A., Sharpless, N. E. and Scadden, D. T. (2006) 'Stem-cell ageing modified by the cyclin-dependent kinase inhibitor p16INK4a', *Nature*, 443(7110), pp. 421–426. doi: nature05159 [pii] 10.1038/nature05159.

Jeck, W. R., Siebold, A. P. and Sharpless, N. E. (2012) 'Review: A Meta-Analysis of GWAS Studies and Age-Associated Diseases', *Aging Cell*, 11(5), pp. 727–731. doi: 10.1016/j.pestbp.2011.02.012.Investigations.

Jolma, A., Yan, J., Whitington, T., Toivonen, J., Nitta, K. R., Rastas, P., Morgunova, E., Enge, M., Taipale, M., Wei, G., Palin, K., Vaquerizas, J. M., Vincentelli, R., Luscombe, N. M., Hughes, T. R., Lemaire, P., Ukkonen, E., Kivioja, T. and Taipale, J. (2013) 'DNA-binding specificities of human transcription factors', *Cell*. Elsevier Inc., 152(1–2), pp. 327–339. doi: 10.1016/j.cell.2012.12.009.

Jun, J.-I. and Lau, L. F. (2010) 'The matricellular protein CCN1 induces fibroblast senescence and restricts fibrosis in cutaneous wound healing.', *Nature Cell Biology*, 12(7), pp. 676–85. doi: 10.1038/ncb2070.

Jun, J.-I. and Lau, L. F. (2016) 'CCN2 induces cellular senescence in fibroblasts', *Journal of Cell Communication and Signaling*. Journal of Cell Communication and Signaling. doi: 10.1007/s12079-016-0359-1.

Jurk, D., Wang, C., Miwa, S., Maddick, M., Korolchuk, V., Tsolou, A., Gonos, E. S., Thrasivoulou, C., Jill Saffrey, M., Cameron, K. and von Zglinicki, T. (2012) 'Postmitotic neurons develop a p21-dependent senescence-like phenotype driven by a DNA damage response', *Aging Cell*, 11(6), pp. 996–1004. doi: 10.1111/j.1474-9726.2012.00870.x.

Kang, C., Xu, Q., Martin, T. D., Li, M. Z., Demaria, M., Aron, L., Lu, T., Yankner, B. A., Campisi, J. and Elledge, S. J. (2015) 'The DNA damage response induces inflammation and senescence by inhibiting autophagy of GATA4.', *Science*, 349(6255), p. aaa5612. doi: 10.1126/science.aaa5612.

Kang, T.-W., Yevsa, T., Woller, N., Hoenicke, L., Wuestefeld, T., Dauch, D., Hohmeyer, A., Gereke, M., Rudalska, R., Potapova, A., Iken, M., Vucur, M., Weiss, S.,

Heikenwalder, M., Khan, S., Gil, J., Bruder, D., Manns, M., Schirmacher, P., Tacke, F., Ott, M., Luedde, T., Longerich, T., Kubicka, S. and Zender, L. (2011) 'Senescence surveillance of pre-malignant hepatocytes limits liver cancer development', *Nature*. Nature Publishing Group, 479(7374), pp. 547–551. doi: 10.1038/nature10599.

Kato, J., Matsushime, H., Hiebert, S. W., Ewen, M. E. and Sherr, C. J. (1993) 'Direct binding of cyclin D to the retinoblastoma gene product (pRb) and pRb phosphorylation by the cyclin D-dependent kinase CDK4', *Genes & Development*, 7(3), pp. 331–342. doi: 10.1101/gad.7.3.331.

Khidekel, N., Ficarro, S. B., Clark, P. M., Bryan, M. C., Swaney, D. L., Rexach, J. E., Sun, Y. E., Coon, J. J., Peters, E. C. and Hsieh-Wilson, L. C. (2007) 'Probing the dynamics of O-GlcNAc glycosylation in the brain using quantitative proteomics', *Nature Chem Biol*, 3(6), pp. 339–348. doi: nchembio881 [pii]\r10.1038/nchembio881.

Kim, K. S., Park, H. K., Lee, J. W., Kim, Y. Il and Shin, M. K. (2015) 'Investigate correlation between mechanical property and aging biomarker in passaged human dermal fibroblasts', *Microscopy Research and Technique*, 78(4), pp. 277–282. doi: 10.1002/jemt.22472.

Kim, Y., Byun, H., Jee, B. A., Seo, Y., Kim, Y., Park, M. H., Chung, H., Woo, H. G. and Yoon, G. (2013) 'Implications of time-series gene expression profiles of replicative senescence', *Aging Cell*, 12, pp. 622–634. doi: 10.1111/acel.12087.

Kitaura, H., Shinshi, M., Uchikoshi, Y., Ono, T., Tsurimoto, T., Yoshikawa, H., Iguchi-ariga, S. M. M. and Ariga, H. (2000) 'Reciprocal Regulation via Protein-Protein Interaction between c-Myc and p21 cip1 / waf1 / sdi1 in DNA Replication and Transcription', *Journal of Biological Chemistry*, 275(14), pp. 10477–10483. doi: 10.1074/jbc.275.14.10477.

Klenerman, D., Shevchuk, A., Novak, P., Korchev, Y. E. and Davis, S. J. (2013) 'Imaging the cell surface and its organization down to the level of single molecules', *Philos Trans R Soc Lond B Biol Sci*, 368(1611), p. 20120027. doi: 10.1098/rstb.2012.0027.

Koch, S., Larbi, A., Derhovanessian, E., Ozcelik, D., Naumova, E. and Pawelec, G. (2008) 'Multiparameter flow cytometric analysis of CD4 and CD8 T cell subsets in young and

old people.', *Immunity & Ageing*, 5, p. 6. doi: 10.1186/1742-4933-5-6.

Koetz, K., Bryl, E., Spickschen, K., O'Fallon, W. M., Goronzy, J. J. and Weyand, C. M. (2000) 'T cell homeostasis in patients with rheumatoid arthritis', *Proceedings of the National Academy of Sciences of the United States of America*, 97(16), pp. 9203–9208. doi: 10.1073/pnas.97.16.9203.

Komori, H., Enomoto, M., Nakamura, M., Iwanaga, R. and Ohtani, K. (2005) 'Distinct E2F-mediated transcriptional program regulates p14ARF gene expression.', *The EMBO journal*, 24(21), pp. 3724–36. doi: 10.1038/sj.emboj.7600836.

Kosar, M., Bartkova, J., Hubackova, S., Hodny, Z., Lukas, J. and Bartek, J. (2011) 'Senescence-associated heterochromatin foci are dispensable for cellular senescence, occur in a cell type- And insult-dependent manner, and follow expression of p16ink4a', *Cell Cycle*, 10(3), pp. 457–468. doi: 10.4161/cc.10.3.14707.

Kowalska, E., Ripperger, J. a, Hoegger, D. C., Bruegger, P., Buch, T., Birchler, T., Mueller, A., Albrecht, U., Contaldo, C. and Brown, S. a (2013) 'NONO couples the circadian clock to the cell cycle.', *Proceedings of the National Academy of Sciences of the United States of America*, 110(5), pp. 1592–9. doi: 10.1073/pnas.1213317110.

Krishnamurthy, J., Ramsey, M. R., Ligon, K. L., Torrice, C., Koh, A., Bonner-Weir, S. and Sharpless, N. E. (2006) 'p16INK4a induces an age-dependent decline in islet regenerative potential', *Nature*, 443(7110), pp. 453–457. doi: nature05092 [pii] 10.1038/nature05092.

Krishnamurthy, J., Torrice, C., Ramsey, M. R., Kovalev, G. I., Al-regaiey, K., Su, L. and Sharpless, N. E. (2004) 'Ink4a/Arf expression is a biomarker of aging', *Journal of Clinical Investigation*, 114(9), pp. 1299–1307. doi: 10.1172/JCI200422475.The.

Krizhanovsky, V., Yon, M., Dickins, R. A., Hearn, S., Simon, J., Miething, C., Yee, H., Zender, L. and Lowe, S. W. (2008) 'Senescence of Activated Stellate Cells Limits Liver Fibrosis', *Cell*, 134(4), pp. 657–667. doi: 10.1016/j.cell.2008.06.049.

Krones-Herzig, A., Adamson, E. and Mercola, D. (2003) 'Early growth response 1 protein, an upstream gatekeeper of the p53 tumor suppressor, controls replicative senescence.', *Proceedings of the National Academy of Sciences of the United States of*

America, 100(6), pp. 3233–3238. doi: 10.1073/pnas.2628034100.

Krtolica, A., Parrinello, S., Lockett, S., Desprez, P. Y. and Campisi, J. (2001) 'Senescent fibroblasts promote epithelial cell growth and tumorigenesis: a link between cancer and aging.', *Proceedings of the National Academy of Sciences of the United States of America*, 98(21), pp. 12072–7. doi: 10.1073/pnas.211053698.

Krude, T., Jackman, M., Pines, J. and Laskey, R. A. (1997) 'Cyclin/Cdk-Dependent Initiation of DNA Replication in a Human Cell-Free System', *Cell*. Cell Press, 88(1), pp. 109–119. doi: 10.1016/S0092-8674(00)81863-2.

Kuilman, T., Michaloglou, C., Mooi, W. J. and Peeper, D. S. (2010) 'The essence of senescence', *Genes & Development*, 24(22), pp. 2463–2479. doi: 10.1101/gad.1971610.

Kumazaki, T. (1992) 'Cellular Aging and Expression of Fibronectin', *HIJM*, 41(4), pp. 101–104.

Kumazaki, T., Kobayashi, M. and Mitsui, Y. (1993) 'Enhanced expression of fibronectin during in vivo cellular aging of human vascular endothelial cells and skin fibroblasts'. Experimental Cell Research, pp. 396–402.

Kumbrink, J., Gerlinger, M. and Johnson, J. P. (2005) 'Egr-1 induces the expression of its corepressor Nab2 by activation of the Nab2 promoter thereby establishing a negative feedback loop', *Journal of Biological Chemistry*, 280(52), pp. 42785–42793. doi: 10.1074/jbc.M511079200.

Labaer, J., Garrett, M. D., Stevenson, L. F., Slingerland, J. M., Sandhu, C., Chou, H. S., Fattaey, A. and Harlow, E. (1997) 'New functional activities for the p21 family of CDK inhibitors', *Genes & Development*, 11(7), pp. 847–862. doi: 10.1101/gad.11.7.847.

Labalette, C., Bouchoucha, Y. X., Wassef, M. A., Gongal, P. A., Le Men, J., Becker, T., Gilardi-Hebenstreit, P. and Charnay, P. (2011) 'Hindbrain patterning requires fine-tuning of early krox20 transcription by Sprouty 4.', *Development*, 138(2), pp. 317–26. doi: 10.1242/dev.057299.

Laberge, R.-M., Sun, Y., Orjalo, A. V, Patil, C. K., Freund, A., Zhou, L., Curran, S. C., Davalos, A. R., Wilson-edell, K. A., Liu, S., Limbad, C., Demaria, M., Li, P., Hubbard, G.

B., Ikeno, Y., Javors, M., Desprez, P.-Y., Benz, C. C., Kapahi, P., Nelson, P. S. and Campisi, J. (2015) 'MTOR regulates the pro-tumorigenic senescence-associated secretory phenotype by promoting IL1A translation.', *Nature Cell Biology*, 17(8), pp. 1049–61. doi: 10.1038/ncb3195.

Ladha, M. H., Lee, K. Y., Upton, T. M., Reed, M. F. and Ewen, M. E. (1998) 'Regulation of exit from quiescence by p27 and cyclin D1-CDK4.', *Molecular and Cellular Biology*, 18(11), pp. 6605–15.

Lanna, A., Henson, S. M., Escors, D. and Akbar, A. N. (2015) 'AMPK-TAB1 activated p38 drives human T cell senescence', *Nature Immunology*, 15(10), pp. 965–972. doi: 10.1038/ni.2981.AMPK-TAB1.

Laurenti, E., Frelin, C., Xie, S., Ferrari, R., Dunant, C. F., Zandi, S., Neumann, A., Plumb, I., Doulatov, S., Chen, J., April, C., Fan, J. B., Iscove, N. and Dick, J. E. (2015) 'CDK6 levels regulate quiescence exit in human hematopoietic stem cells', *Cell Stem Cell*. The Authors, 16(3), pp. 302–313. doi: 10.1016/j.stem.2015.01.017.

Lauritsen, J.-P. H., Kurella, S., Lee, S.-Y., Lefebvre, J. M., Rhodes, M., Alberola-Ila, J. and Wiest, D. L. (2008) 'Egr2 is required for Bcl-2 induction during positive selection.', *Journal of Immunology*, 181(11), pp. 7778–7785. doi: 181/11/7778 [pii].

Lavin, M. F. and Shiloh, Y. (1997) 'THE GENETIC DEFECT IN ATAXIA-TELANGIECTASIA', *Annual Review of Immunology*, (1), pp. 177–202.

Le, N., Nagarajan, R., Wang, J. Y. T., Araki, T., Schmidt, R. E. and Milbrandt, J. (2005) 'Analysis of congenital hypomyelinating Egr2Lo/Lo nerves identifies Sox2 as an inhibitor of Schwann cell differentiation and myelination.', *Proceedings of the National Academy of Sciences of the United States of America*, 102(Track II), pp. 2596–2601. doi: 10.1073/pnas.0407836102.

LeBlanc, S. E., Jang, S. W., Ward, R. M., Wrabetz, L. and Svaren, J. (2006) 'Direct regulation of myelin protein zero expression by the Egr2 transactivator', *Journal of Biological Chemistry*, 281(9), pp. 5453–5460. doi: 10.1074/jbc.M512159200.

Lee, B. Y., Han, J. A., Im, J. S., Morrone, A., Johung, K., Goodwin, E. C., Kleijer, W. J., DiMaio, D. and Hwang, E. S. (2006) 'Senescence-associated β-galactosidase is

lysosomal β-galactosidase', *Aging Cell*, 5(2), pp. 187–195. doi: 10.1111/j.1474-9726.2006.00199.x.

Lee, S. L., Sadovsky, Y., Swirnoff, a H., Polish, J. a, Goda, P., Gavrilina, G. and Milbrandt, J. (1996) 'Luteinizing hormone deficiency and female infertility in mice lacking the transcription factor NGFI-A (Egr-1).', *Science*, 273(5279), pp. 1219–1221. doi: 10.1126/science.273.5279.1219.

Levi, G., Topilko, P., Schneider-Maunoury, S., Lasagna, M., Mantero, S., Cancedda, R. and Charnay, P. (1996) 'Defective bone formation in Krox-20 mutant mice.', *Development*, 122(1), pp. 113–20.

Lewis, D. E., Merched-Sauvage, M., Goronzy, J. J., Weyand, C. M. and Vallejo, A. N. (2004) 'Tumor necrosis factor-α and CD80 modulate CD28 expression through a similar mechanism of T-cell receptor-independent inhibition of transcription', *Journal of Biological Chemistry*, 279(28), pp. 29130–29138. doi: 10.1074/jbc.M402194200.

Li, S., Symonds, A. L. J., Zhu, B., Liu, M., Raymond, M. V., Miao, T. and Wang, P. (2011) 'Early growth response gene-2 (egr-2) regulates the development of b and t cells', *PLoS ONE*, 6(4), pp. 1–9. doi: 10.1371/journal.pone.0018498.

Li, X., Zhang, Z., Yu, M., Li, L., Du, G., Xiao, W. and Yang, H. (2013) 'Involvement of miR-20a in promoting gastric cancer progression by targeting early growth response 2 (EGR2).', *International Journal of Molecular Sciences*, 14(8), pp. 16226–16239. doi: 10.3390/ijms140816226.

Li, Y., Song, X., Ma, Y., Liu, J., Yang, D. and Yan, B. (2004) 'DNA binding, but not interaction with Bmal1, is responsible for DEC1-mediated transcription regulation of the circadian gene mPer1.', *The Biochemical journal*, 382, pp. 895–904. doi: 10.1042/BJ20040592.

Lim, S. and Kaldis, P. (2013) 'Cdks, cyclins and CKIs: roles beyond cell cycle regulation.', *Development*, 140(15), pp. 3079–93. doi: 10.1242/dev.091744.

Lin, A. W., Barradas, M., Stone, J. C., Van Aelst, L., Serrano, M. and Lowe, S. W. (1998) 'Premature senescence involving p53 and p16 is activated in response to constitutive MEK/MAPK mitogenic signaling', *Genes & Development*, 12(19), pp. 3008–3019. doi:

10.1101/gad.12.19.3008.

Liu, D. and Hornsby, P. J. (2007) 'Senescent human fibroblasts increase the early growth of xenograft tumors via matrix metalloproteinase secretion', *Cancer Research*, 67(7), pp. 3117–3126. doi: 10.1158/0008-5472.CAN-06-3452.

Liu, Q., Guntuku, S., Cui, X., Matsuoka, S., Cortez, D., Tamai, K., Luo, G., Carattini-rivera, S., Demayo, F., Bradley, A., Donehower, L. A. and Elledge, S. J. (2000) 'Chk1 is an essential kinase that is regulated by Atr and required for the G 2 / M DNA damage checkpoint', *Genes & Development*, 6(Genes & Development), pp. 1448–1459.

Liu, X., Shi, H., Liu, B., Li, J., Liu, Y. and Yu, B. (2015) 'MIR-330-3p controls cell proliferation by targeting early growth response 2 in non-small-cell lung cancer', *Acta Biochimica et Biophysica Sinica*, 47(6), pp. 431–440. doi: 10.1093/abbs/gmv032.

Liu, Y., Sanoff, H. K., Cho, H., Burd, C. E., Torrice, C., Ibrahim, G., Thomas, N. E. and Sharpless, N. E. (2009) 'Expression of p16INK4a in peripheral blood T-cells is a biomarker of human aging', *Aging Cell*, 8(4), pp. 439–448. doi: 10.1111/j.1474-9726.2009.00489.x.Expression.

Lowe, D., Horvath, S. and Raj, K. (2016) 'Epigenetic clock analyses of cellular senescence and ageing', *Oncotarget*, 7(8), pp. 8524–8531.

Lowe, R., Overhoff, M. G., Ramagopalan, S. V, Garbe, J. C., Koh, J., Stampfer, M. R., Beach, D. H., Rakyan, V. K. and Bishop, C. L. (2015) 'The senescent methylome and its relationship with cancer, ageing and germline genetic variation in humans.', *Genome Biology*. Genome Biology, 16, p. 194. doi: 10.1186/s13059-015-0748-4.

Luciano, R. L. and Wilson, A. C. (2003) 'HCF-1 Functions as a Coactivator for the Zinc Finger Protein Krox20', *Journal of Biological Chemistry*, 278(51), pp. 51116–51124. doi: 10.1074/jbc.M303470200.

Lujambio, A., Akkari, L., Simon, J., Grace, D., Tschaharganeh, D. F., Bolden, J. E., Zhao, Z., Thapar, V., Joyce, J. A., Krizhanovsky, V. and Lowe, S. W. (2013) 'Non-cell-autonomous tumor suppression by p53', *Cell*. Elsevier Inc., 153(2), pp. 449–460. doi: 10.1016/j.cell.2013.03.020.

Luo, Y., Hurwitz, J. and Massagué, J. (1995) 'Cell-cycle inhibition by independent CDK

and PCNA binding domains in p21Cip1.', *Nature*, pp. 159–161. doi: 10.1038/375159a0.

Marais, A., Ji, Z., Child, E. S., Krause, E., Mann, D. J. and Sharrocks, A. D. (2010) 'Cell cycle-dependent regulation of the forkhead transcription factor FOXK2 by CDK·cyclin complexes', *Journal of Biological Chemistry*, 285(46), pp. 35728–35739. doi: 10.1074/jbc.M110.154005.

Martin, N., Beach, D. and Gil, J. (2014) 'Ageing as developmental decay: Insights from p16INK4a', *Trends in Molecular Medicine*, 20(12), pp. 667–674. doi: 10.1016/j.molmed.2014.09.008.

Mathelier, A., Fornes, O., Arenillas, D. J., Chen, C. Y., Denay, G., Lee, J., Shi, W., Shyr, C., Tan, G., Worsley-Hunt, R., Zhang, A. W., Parcy, F., Lenhard, B., Sandelin, A. and Wasserman, W. W. (2016) 'JASPAR 2016: A major expansion and update of the open-access database of transcription factor binding profiles', *Nucleic Acids Research*, 44(D1), pp. D110–D115. doi: 10.1093/nar/gkv1176.

Matheny, C., Day, M. L. and Milbrandt, J. (1994) 'The nuclear localization signal of NGFI-A is located within the zinc finger DNA binding domain.', *The Journal of biological chemistry*, 269(11), pp. 8176–81.

Matsuoka, S., Huang, M. and Elledge, S. J. (1998) 'Linkage of ATM to Cell Cycle Regulation by the Chk2 Protein Kinase', *Science*, 282, pp. 1893–1896. doi: 10.1126/science.282.5395.1893.

Matsushime, H., Quelle, D. E., Shurtleff, S. a, Shibuya, M., Sherr, C. J. and Kato, J. Y. (1994) 'D-type cyclin-dependent kinase activity in mammalian cells.', *Molecular and Cellular Biology*, 14(3), pp. 2066–76. doi: 10.1128/MCB.14.3.2066.Updated.

Matthews, C., Gorenne, I., Scott, S., Figg, N., Kirkpatrick, P., Ritchie, A., Goddard, M. and Bennett, M. (2006) 'Vascular smooth muscle cells undergo telomere-based senescence in human atherosclerosis: Effects of telomerase and oxidative stress', *Circulation Research*, 99(2), pp. 156–164. doi: 10.1161/01.RES.0000233315.38086.bc.

Matys, V., Kel-Margoulis, O. V., Fricke, E., Liebich, I., Land, S., Barre-Dirrie, A., Reuter, I., Chekmenev, D., Krull, M., Hornischer, K., Voss, N., Stegmaier, P., Lewicki-Potapov, B., Saxel, H., Kel, A. E. and Wingender, E. (2006) 'TRANSFAC(R) and its module

TRANSCompel(R): transcriptional gene regulation in eukaryotes', *Nucleic Acids Research*, 34(suppl_1), pp. D108-110. doi: 10.1093/nar/gkj143.

Mazzatti, D. J., White, A., Forsey, R. J., Powell, J. R. and Pawelec, G. (2007) 'Gene expression changes in long-term culture of T-cell clones: Genomic effects of chronic antigenic stress in aging and immunosenescence', *Aging Cell*, 6(2), pp. 155–163. doi: 10.1111/j.1474-9726.2007.00269.x.

Mehta, I. S., Figgitt, M., Clements, C. S., Kill, I. R. and Bridger, J. M. (2007) 'Alterations to nuclear architecture and genome behavior in senescent cells', *Annals of the New York Academy of Sciences*, 1100, pp. 250–263. doi: 10.1196/annals.1395.027.

Mertsching, H., Weimer, M., Kersen, S. and Brunner, H. (2008) 'Human skin equivalent as an alternative to animal testing.', *GMS Krankenhaushygiene interdisziplinär*, 3(1), p. Doc11.

Miah, M. A., Byeon, S. E., Ahmed, M. S., Yoon, C. H., Ha, S. J. and Bae, Y. S. (2013) 'Egr2 induced during DC development acts as an intrinsic negative regulator of DC immunogenicity', *European Journal of Immunology*, 43(9), pp. 2484–2496. doi: 10.1002/eji.201243046.

Miao, T., Raymond, M., Bhullar, P., Ghaffari, E., Symonds, A. L. J., Meier, U. C., Giovannoni, G., Li, S. and Wang, P. (2013) 'Early growth response gene-2 controls IL-17 expression and Th17 differentiation by negatively regulating Batf.', *Journal of Immunology*, 190(1), pp. 58–65. doi: 10.4049/jimmunol.1200868.

Michaloglou, C., Vredeveld, L. C. W., Soengas, M. S., Denoyelle, C., Kuilman, T., van der Horst, C. M. a M., Majoor, D. M., Shay, J. W., Mooi, W. J. and Peeper, D. S. (2005) 'BRAFE600-associated senescence-like cell cycle arrest of human naevi.', *Nature*, 436(August), pp. 720–724. doi: 10.1038/nature03890.

Mikešová, E., Hühne, K., Rautenstrauss, B., Mazanec, R., Baránková, L., Vyhnálek, M., Horáček, O. and Seeman, P. (2005) 'Novel EGR2 mutation R359Q is associated with CMT type 1 and progressive scoliosis', *Neuromuscular Disorders*, 15(11), pp. 764–767. doi: 10.1016/j.nmd.2005.08.001.

Moiseeva, O., Bourdeau, V., Roux, A., Deschênes-Simard, X. and Ferbeyre, G. (2009)

'Mitochondrial dysfunction contributes to oncogene-induced senescence.', *Molecular and Cellular Biology*, 29(16), pp. 4495–507. doi: 10.1128/MCB.01868-08.

Molofsky, A. V, Slutsky, S. G., Joseph, N. M., He, S., Pardal, R., Krishnamurthy, J., Sharpless, N. E. and Morrison, S. J. (2006) 'Increasing p16INK4a expression decreases forebrain progenitors and neurogenesis during ageing', *Nature*, 443(7110), pp. 448–452. doi: nature05091 [pii] 10.1038/nature05091.

Muñoz-Espín, D., Cañamero, M., Maraver, A., Gómez-López, G., Contreras, J., Murillo-Cuesta, S., Rodríguez-Baeza, A., Varela-Nieto, I., Ruberte, J., Collado, M. and Serrano, M. (2013) 'Programmed cell senescence during mammalian embryonic development.', *Cell*, 155(5), pp. 1104–18. doi: 10.1016/j.cell.2013.10.019.

Muñoz-Espín, D. and Serrano, M. (2014) 'Cellular senescence: From physiology to pathology', *Nature Reviews Molecular Cell Biology*. Nature Publishing Group, 15(7), pp. 482–496. doi: 10.1038/nrm3823.

Munro, J., Barr, N. I., Ireland, H., Morrison, V. and Parkinson, E. K. (2004) 'Histone deacetylase inhibitors induce a senescence-like state in human cells by a p16-dependent mechanism that is independent of a mitotic clock', *Experimental Cell Research*, 295(2), pp. 525–538. doi: 10.1016/j.yexcr.2004.01.017.

Myouzen, K., Kochi, Y., Shimane, K., Fujio, K., Okamura, T., Okada, Y., Suzuki, A., Atsumi, T., Ito, S., Takada, K., Mimori, A., Ikegawa, S., Yamada, R., Nakamura, Y. and Yamamoto, K. (2010) 'Regulatory polymorphisms in EGR2 are associated with susceptibility to systemic lupus erythematosus', *Human Molecular Genetics*, 19(11), pp. 2313–2320. doi: 10.1093/hmg/ddq092.

Nacher, V., Carretero, A., Navarro, M., Armengol, C., Llombart, C., Rodríguez, A., Herrero-Fresneda, I., Ayuso, E. and Ruberte, J. (2006) 'The quail mesonephros: A new model for renal senescence?', *Journal of Vascular Research*, 43(6), pp. 581–586. doi: 10.1159/000096076.

Nafez, S., Oikawa, K., Odero, G. L., Sproule, M., Ge, N., Schapansky, J., Abrenica, B., Hatherell, A., Cadonic, C., Zhang, S., Song, X., Kauppinen, T., Glazner, G. W., Grilli, M., Czubryt, M. P., Eisenstat, D. D. and Albensi, B. C. (2015) 'Early growth response 2 (Egr-

2) expression is triggered by NF-KB activation', *Molecular and Cellular Neuroscience*. Elsevier Inc., 64, pp. 95–103. doi: 10.1016/j.mcn.2014.12.008.

Nagarajan, R., Svaren, J., Le, N., Araki, T., Watson, M. and Milbrandt, J. (2001) 'EGR2 mutations in inherited neuropathies dominant-negatively inhibit myelin gene expression', *Neuron*, 30(2), pp. 355–368. doi: 10.1016/S0896-6273(01)00282-3.

Nakajima, T., Schulte, S., Warrington, K. J., Kopecky, S. L., Frye, R. L., Goronzy, J. J. and Weyand, C. M. (2002) 'T-Cell–Mediated Lysis of Endothelial Cells in Acute Coronary Syndromes Takako', *Gene Expression*, 105(5), pp. 570–575.

Narita, M., Nũnez, S., Heard, E., Narita, M., Lin, A. W., Hearn, S. A., Spector, D. L., Hannon, G. J. and Lowe, S. W. (2003) 'Rb-mediated heterochromatin formation and silencing of E2F target genes during cellular senescence', *Cell*, 113(6), pp. 703–716. doi: 10.1016/S0092-8674(03)00401-X.

Naylor, R., Baker, D. and van Deursen, J. (2013) 'Senescent Cells: A Novel Therapeutic Target for Aging and Age-Related Diseases', *Clinical Pharmacology & Therapeutics*, 93(1), pp. 105–116. doi: 10.1038/clpt.2012.193.Senescent.

Naylor, R. M., Baker, D. J. and van Deursen, J. M. (2012) 'Senescent Cells: A Novel Therapeutic Target for Aging and Age-Related Diseases', *Clinical Pharmacology & Therapeutics*, 93(1), pp. 105–116. doi: 10.1038/clpt.2012.193.

Nelson, D. M., McBryan, T., Jeyapalan, J. C., Sedivy, J. M. and Adams, P. D. (2014) 'A comparison of oncogene-induced senescence and replicative senescence: implications for tumor suppression and aging', *Age*, 36(3), p. 9637. doi: 10.1007/s11357-014-9637-0.

Nelson, G., Wordsworth, J., Wang, C., Jurk, D., Lawless, C., Martin-Ruiz, C. and von Zglinicki, T. (2012) 'A senescent cell bystander effect: Senescence-induced senescence', *Aging Cell*, 11(2), pp. 345–349. doi: 10.1111/j.1474-9726.2012.00795.x.

O'Leary, N. A., Wright, M. W., Brister, J. R., Ciufo, S., Haddad, D., McVeigh, R., Rajput, B., Robbertse, B., Smith-White, B., Ako-Adjei, D., Astashyn, A., Badretdin, A., Bao, Y., Blinkova, O., Brover, V., Chetvernin, V., Choi, J., Cox, E., Ermolaeva, O., Farrell, C. M., Goldfarb, T., Gupta, T., Haft, D., Hatcher, E., Hlavina, W., Joardar, V. S., Kodali, V. K., Li,

W., Maglott, D., Masterson, P., McGarvey, K. M., Murphy, M. R., O'Neill, K., Pujar, S., Rangwala, S. H., Rausch, D., Riddick, L. D., Schoch, C., Shkeda, A., Storz, S. S., Sun, H., Thibaud-Nissen, F., Tolstoy, I., Tully, R. E., Vatsan, A. R., Wallin, C., Webb, D., Wu, W., Landrum, M. J., Kimchi, A., Tatusova, T., DiCuccio, M., Kitts, P., Murphy, T. D. and Pruitt, K. D. (2016) 'Reference sequence (RefSeq) database at NCBI: Current status, taxonomic expansion, and functional annotation', *Nucleic Acids Research*, 44(D1), pp. D733–D745. doi: 10.1093/nar/gkv1189.

Ohtani, N., Zebedee, Z., Huot, T. J., Stinson, J. a, Sugimoto, M., Ohashi, Y., Sharrocks, a D., Peters, G. and Hara, E. (2001) 'Opposing effects of Ets and Id proteins on p16INK4a expression during cellular senescence.', *Nature*, 409(6823), pp. 1067–1070. doi: 10.1038/35059131.

Okamura, T., Fujio, K., Shibuya, M., Sumitomo, S., Shoda, H., Sakaguchi, S. and Yamamoto, K. (2009) 'CD4+CD25-LAG3+ regulatory T cells controlled by the transcription factor Egr-2.', *Proceedings of the National Academy of Sciences of the United States of America*, 106(33), pp. 13974–9. doi: 10.1073/pnas.0906872106.

Ono, K., Tanaka, T., Tsunoda, T., Kitahara, O., Kihara, C., Okamoto, A., Ochiai, K., Takagi, T. and Nakamura, Y. (2000) 'Identification by cDNA microarray of genes involved in ovarian carcinogenesis', *Cancer Research*, 60(18), pp. 5007–5011.

Orjalo, A. V, Bhaumik, D., Gengler, B. K., Scott, G. K. and Campisi, J. (2009) 'Cell surface-bound IL-1alpha is an upstream regulator of the senescence-associated IL-6/IL-8 cytokine network.', *Proceedings of the National Academy of Sciences of the United States of America*, 106(40), pp. 17031–6. doi: 10.1073/pnas.0905299106.

Overhoff, M. G., Garbe, J. C., Koh, J., Stampfer, M. R., Beach, D. H. and Bishop, C. L. (2014) 'Cellular senescence mediated by p16INK4A-coupled miRNA pathways', *Nucleic Acids Research*, 42(3), pp. 1606–1618. doi: 10.1093/nar/gkt1096.

Pagès, H., Aboyoun, P., Gentleman, R. and Debroy, S. (2016) 'String objects representing biological sequences, and matching algorithms', *R package version 2.42.1*.

Panossian, L., Fenik, P., Zhu, Y., Zhan, G., McBurney, M. W. and Veasey, S. (2011) 'SIRT1 regulation of wakefulness and senescence-like phenotype in wake neurons.', *The*

Journal of neuroscience : the official journal of the Society for Neuroscience, 31(11), pp. 4025–4036. doi: 10.1523/JNEUROSCI.5166-10.2011.

Parish, S. T., Wu, J. E. and Effros, R. B. (2010) 'Sustained CD28 expression delays multiple features of replicative senescence in human CD8 T lymphocytes', *Journal of Clinical Immunology*, 30(6), pp. 798–805. doi: 10.1007/s10875-010-9449-7.

Park, I., Han, C., Jin, S., Lee, B., Choi, H., Kwon, J. T., Kim, D., Kim, J., Lifirsu, E., Park, W. J., Park, Z. Y., Kim, D. H. and Cho, C. (2011) 'Myosin regulatory light chains are required to maintain the stability of myosin II and cellular integrity.', *The Biochemical journal*, 434, pp. 171–180. doi: 10.1042/BJ20101473.

Parkinson, D. B., Bhaskaran, A., Droggiti, A., Dickinson, S., D'Antonio, M., Mirsky, R. and Jessen, K. R. (2004) 'Krox-20 inhibits Jun-NH2-terminal kinase/c-Jun to control Schwann cell proliferation and death', *Journal of Cell Biology*, 164(3), pp. 385–394. doi: 10.1083/jcb.200307132.

Parrinello, S., Coppe, J.-P., Krtolica, A. and Campisi, J. (2005) 'Stromal-epithelial interactions in aging and cancer: senescent fibroblasts alter epithelial cell differentiation.', *Journal of cell science*, 118(Pt 3), pp. 485–96. doi: 10.1242/jcs.01635.

Passegué, E. and Wagner, E. F. (2000) 'JunB suppresses cell proliferation by transcriptional activation of p16(INK4a) expression.', *The EMBO journal*, 19(12), pp. 2969–79. doi: 10.1093/emboj/19.12.2969.

Passos, J. F., Nelson, G., Wang, C., Richter, T., Simillion, C., Proctor, C. J., Miwa, S., Olijslagers, S., Hallinan, J., Wipat, A., Saretzki, G., Rudolph, K. L., Kirkwood, T. B. L. and von Zglinicki, T. (2010) 'Feedback between p21 and reactive oxygen production is necessary for cell senescence.', *Molecular Systems Biology*, 6(347), p. 347. doi: 10.1038/msb.2010.5.

Pat-Horenczyk, R. and Brom, D. (2007) 'The multiple faces of post-traumatic growth', *Applied Psychology*, 56(3), pp. 379–385. doi: 10.1111/j.1464-0597.2007.00297.x.

Perez-Roger, I., Kim, S. H., Griffiths, B., Sewing, A. and Land, H. (1999) 'Cyclins D1 and D2 mediate Myc-induced proliferation via sequestration of p27(Kip1) and p21(Cip1)', *EMBO Journal*, 18(19), pp. 5310–5320. doi: 10.1093/emboj/18.19.5310.

Peters, J. M. (2006) 'The anaphase promoting complex/cyclosome: a machine designed to destroy', *Nature Reviews Molecular Cell Biology*, 7(9), pp. 644–656. doi: 10.1038/nrm1988.

Peters, M. J., Joehanes, R., Pilling, L. C., Schurmann, C., Conneely, K. N., Powell, J., Reinmaa, E., Sutphin, G. L., Zhernakova, A., Schramm, K., Wilson, Y. A., Kobes, S., Tukiainen, T., NABEC/UKBEC Consortium, Ramos, Y. F., Göring, H. H. H., Fornage, M., Liu, Y., Gharib, S. A., Stranger, B. E., De Jager, P. L., Aviv, A., Levy, D., Murabito, J. M., Munson, P. J., Huan, T., Hofman, A., Uitterlinden, A. G., Rivadeneira, F., van Rooij, J., Stolk, L., Broer, L., Verbiest, M. M. P. J., Jhamai, M., Arp, P., Metspalu, A., Tserel, L., Milani, L., Samani, N. J., Peterson, P., Kasela, S., Codd, V., Peters, A., Ward-Caviness, C. K., Herder, C., Waldenberger, M., Roden, M., Singmann, P., Zeilinger, S., Illig, T., Homuth, G., Grabe, H.-J., Völzke, H., Steil, L., Kocher, T., Murray, A., Melzer, D., Yaghootkar, H., Bandinelli, S., Moses, E. K., Kent, J. W., Curran, J. E., Johnson, M. P., Williams-Blangero, S., Westra, H.-J., McRae, A. F., Smith, J. A., Kardia, S. L. R., Hovatta, I., Perola, M., Ripatti, S., Salomaa, V., Henders, A. K., Martin, N. G., Smith, A. K., Mehta, D., Binder, E. B., Nylocks, K. M., Kennedy, E. M., Klengel, T., Ding, J., Suchy-Dicey, A. M., Enquobahrie, D. A., Brody, J., Rotter, J. I., Chen, Y.-D. I., Houwing-Duistermaat, J., Kloppenburg, M., Slagboom, P. E., Helmer, Q., den Hollander, W., Bean, S., Raj, T., Bakhshi, N., Wang, Q. P., Oyston, L. J., Psaty, B. M., Tracy, R. P., Montgomery, G. W., Turner, S. T., Blangero, J., Meulenbelt, I., Ressler, K. J., Yang, J., Franke, L., Kettunen, J., Visscher, P. M., Neely, G. G., Korstanje, R., Hanson, R. L., Prokisch, H., Ferrucci, L., Esko, T., Teumer, A., van Meurs, J. B. J. and Johnson, A. D. (2015) 'The transcriptional landscape of age in human peripheral blood.', *Nature Communications*, 6, p. 8570. doi: 10.1038/ncomms9570.

Pietschmann, P., Grisar, J., Thien, R., Willheim, M., Kerschan-Schindl, K., Preisinger, E. and Peterlik, M. (2001) 'Immune phenotype and intracellular cytokine production of peripheral blood mononuclear cells from postmenopausal patients with osteoporotic fractures', *Experimental Gerontology*, 36(10), pp. 1749–1759. doi: 10.1016/S0531-5565(01)00125-5.

Poirier, R., Cheval, H., Mailhes, C., Garel, S., Charnay, P., Davis, S. and Laroche, S. (2008) 'Distinct functions of egr gene family members in cognitive processes.',

Frontiers in Neuroscience, 2(1), pp. 47–55. doi: 10.3389/neuro.01.002.2008.

Pospisil, V., Vargova, K., Kokavec, J., Rybarova, J., Savvulidi, F., Jonasova, A., Necas, E., Zavadil, J., Laslo, P. and Stopka, T. (2011) 'Epigenetic silencing of the oncogenic miR-17-92 cluster during PU.1-directed macrophage differentiation', *The EMBO Journal*. Nature Publishing Group, 30(21), pp. 4450–4464. doi: 10.1038/emboj.2011.317.

Postel-Vinay, S., Véron, A. S., Tirode, F., Pierron, G., Reynaud, S., Kovar, H., Oberlin, O., Lapouble, E., Ballet, S., Lucchesi, C., Kontny, U., González-Neira, A., Picci, P., Alonso, J., Patino-Garcia, A., de Paillerets, B. B., Laud, K., Dina, C., Froguel, P., Clavel-Chapelon, F., Doz, F., Michon, J., Chanock, S. J., Thomas, G., Cox, D. G. and Delattre, O. (2012) 'Common variants near TARDBP and EGR2 are associated with susceptibility to Ewing sarcoma.', *Nature Genetics*. Nature Publishing Group, 44(3), pp. 323–327. doi: 10.1038/ng.1085.

Provenzano, P. P. and Keely, P. J. (2011) 'Mechanical signaling through the cytoskeleton regulates cell proliferation by coordinated focal adhesion and Rho GTPase signaling.', *Journal of cell science*, 124(Pt 8), pp. 1195–1205. doi: 10.1242/jcs.067009.

Ramirez, R. D., Morales, C. P., Herbert, B. S., Rohde, J. M., Passons, C., Shay, J. W. and Wright, W. E. (2001) 'Putative telomere-independent mechanisms of replicative aging reflect inadequate growth conditions', *Genes & Development*, 15(4), pp. 398–403. doi: 10.1101/gad.859201.

Rioux, J. D., Xavier, R. J., Taylor, K. D., Silverberg, M. S., Goyette, P., Huett, A., Green, T., Kuballa, P., Barmada, M. M., Datta, L. W., Shugart, Y. Y., Griffiths, A. M., Targan, S. R., Ippoliti, A. F., Bernard, E.-J., Mei, L., Nicolae, D. L., Regueiro, M., Schumm, L. P., Steinhart, A. H., Rotter, J. I., Duerr, R. H., Cho, J. H., Daly, M. J. and Brant, S. R. (2007) 'Genome-wide association study identifies new susceptibility loci for Crohn disease and implicates autophagy in disease pathogenesis.', *Nature Genetics*, 39(5), pp. 596–604. doi: 10.1038/ng2032.

Rodgers, J. T., King, K. Y., Brett, J. O., Cromie, M. J., Charville, G. W., Maguire, K. K., Brunson, C., Mastey, N., Liu, L., Tsai, C.-R., Goodell, M. a and Rando, T. a (2014) 'mTORC1 controls the adaptive transition of quiescent stem cells from G0 to G(Alert).', *Nature*. Nature Publishing Group, 509(7505), pp. 393–6. doi: 10.1038/nature13255.

Rodier, F. and Campisi, J. (2011) 'Four faces of cellular senescence', *Journal of Cell Biology*, 192(4), pp. 547–556. doi: 10.1083/jcb.201009094.

Rodier, F., Coppé, J.-P., Patil, C. K., Hoeijmakers, W. A. M., Muñoz, D. P., Raza, S. R., Freund, A., Campeau, E., Davalos, A. R. and Campisi, J. (2009) 'Persistent DNA damage signaling triggers senescence- associated inflammatory cytokine secretion', *Nature Cell Biology*, 11(8), pp. 973–979. doi: 10.1038/ncb1909.Persistent.

Romagosa, C., Simonetti, S., López-Vicente, L., Mazo, a, Lleonart, M. E., Castellvi, J. and Ramon y Cajal, S. (2011) 'p16(Ink4a) overexpression in cancer: a tumor suppressor gene associated with senescence and high-grade tumors.', *Oncogene*, 30(18), pp. 2087–2097. doi: 10.1038/onc.2010.614.

Romanov, S. R., Kozakiewicz, B. K., Holst, C. R., Stampfer, M. R., Haupt, L. M. and Tlsty, T. D. (2001) 'Normal human mammary epithelial cells spontaneously escape senescence and acquire genomic changes.', *Nature*, 409(6820), pp. 633–637. doi: 10.1038/35054579.

Roos, C. M., Zhang, B., Palmer, A. K., Ogrodnik, M. B., Pirtskhalava, T., Thalji, N. M., Hagler, M., Jurk, D., Smith, L. A., Casaclang-Verzosa, G., Zhu, Y., Schafer, M. J., Tchkonia, T., Kirkland, J. L. and Miller, J. D. (2016) 'Chronic senolytic treatment alleviates established vasomotor dysfunction in aged or atherosclerotic mice', *Aging Cell*, (February), pp. 973–977. doi: 10.1111/acel.12458.

Russo, M. W., Sevetson, B. R. and Milbrandt, J. (1995) 'Identification of NAB1, a repressor of NGFI-A- and Krox20-mediated transcription.', *Proceedings of the National Academy of Sciences of the United States of America*, 92(15), pp. 6873–7. doi: 10.1073/pnas.92.15.6873.

Sadasivam, S. and DeCaprio, J. A. (2013) 'The DREAM complex: Master coordinator of cell cycle dependent gene expression', *Nature Reviews Cancer*, 13(8), pp. 585–595. doi: 10.1038/nrc3556.The.

Safford, M., Collins, S., Lutz, M. A., Allen, A., Huang, C. T., Kowalski, J., Blackford, A., Horton, M. R., Drake, C., Schwartz, R. H. and Powell, J. D. (2005) 'Egr-2 and Egr-3 are negative regulators of T cell activation', *Nature Immunology*, 6(5), pp. 472–480. doi:

10.1038/ni1193.

Šafka Brožková, D., Nevšímalová, S., Mazanec, R., Rautenstrauss, B. and Seeman, P. (2012) 'Charcot-Marie-Tooth neuropathy due to a novel EGR2 gene mutation with mild phenotype - Usefulness of human mapping chip linkage analysis in a Czech family', *Neuromuscular Disorders*, 22(8), pp. 742–746. doi: 10.1016/j.nmd.2012.04.002.

Sage, J., Miller, A. L., Perez-Mancera, P. A., Wysocki, J. M. and Tyler, J. (2003) 'Acute mutation of retinoblastoma gene function is sufficient for cell cycle re-entry', *Nature*, 424(6945), pp. 223–228. doi: 10.1038/nature01745.1.

Sagiv, A., Burton, D. G. A., Moshayev, Z., Vadai, E., Wensveen, F., Ben-Dor, S., Golani, O., Polic, B. and Krizhanovsky, V. (2016) 'NKG2D ligands mediate immunosurveillance of senescent cells', *Aging*, 8(2), pp. 328–344. doi: 10.18632/aging.100897.

Salotti, J., Sakchaisri, K., Tourtellotte, W. G. and Johnson, P. F. (2015) 'An Arf-Egr-C/EBPβ Pathway Linked to Ras-Induced Senescence and Cancer', *Molecular and Cellular Biology*, 35(5), pp. 866–83. doi: 10.1128/MCB.01489-14.

Samuels-Lev, Y., Connor, D. J. O., Bergamaschi, D., Trigiante, G., Hsieh, J., Zhong, S., Campargue, I., Naumovski, L., Crook, T. and Lu, X. (2001) 'ASPP Proteins Specifically Stimulate the Apoptotic Function of p53', *Molecular Cell*, 8, pp. 781–794.

Sandu, C., Liu, T., Malan, A., Challet, E., Pévet, P. and Felder-Schmittbuhl, M.-P. (2015) 'Circadian clocks in rat skin and dermal fibroblasts: differential effects of aging, temperature and melatonin', *Cellular and Molecular Life Sciences*. doi: 10.1007/s00018-014-1809-7.

Schafer, M. J., White, T. A., Evans, G., Tonne, J. M., Verzosa, G. C., Stout, M. B., Mazula, D. L., Palmer, A. K., Baker, D. J., Jensen, M. D., Torbenson, M. S., Miller, J. D., Ikeda, Y., Tchkonia, T., Van Deursen, J. M., Kirkland, J. L. and LeBrasseur, N. K. (2016) 'Exercise prevents diet-induced cellular senescence in adipose tissue', *Diabetes*, 65(6), pp. 1606–1615. doi: 10.2337/db15-0291.

Schneider-Maunoury, S., Topilko, P., Seitanidou, T., Levi, G., Cohen-Tannoudji, M., Pournin, S., Babinet, C. and Charnay, P. (1993) 'Disruption of Krox-20 results in alteration of rhombomeres 3 and 5 in the developing hindbrain', *Cell*, 75(6), pp. 1199–

1214. doi: 10.1016/0092-8674(93)90329-O.

Schulze, C., Wetzel, F., Kueper, T., Malsen, A., Muhr, G., Jaspers, S., Blatt, T., Wittern, K. P., Wenck, H. and Käs, J. A. (2012) 'Stiffening of human skin fibroblasts with age', *Clinics in Plastic Surgery*, 39(1), pp. 9–20. doi: 10.1016/j.cps.2011.09.008.

Schwartz, R. H. (2003) 'T Cell Anergy', *Annual Review of Immunology*, 21, pp. 305–334. doi: 10.1146/annurev.neuro.26.041002.131058.

Sedivy, J. M., Banumathy, G. and Adams, P. D. (2008) 'Aging by epigenetics-A consequence of chromatin damage?', *Experimental Cell Research*, 314(9), pp. 1909–1917. doi: 10.1016/j.yexcr.2008.02.023.

Seluanov, A., Gorbunova, V., Falcovitz, A., Milyavsky, M., Zurer, I., Shohat, G., Sigal, A., Goldfinger, N. and Rotter, V. (2001) 'Change of the Death Pathway in Senescent Human Fibroblasts in Response to DNA Damage Is Caused by an Inability To Change of the Death Pathway in Senescent Human Fibroblasts in Response to DNA Damage Is Caused by an Inability To Stabilize p53', *Molecular and Cellular Biology*, 21(5), pp. 1552–1564. doi: 10.1128/MCB.21.5.1552.

Serrano, M., Lin, A. W., McCurrach, M. E., Beach, D. and Lowe, S. W. (1997) 'Oncogenic ras provokes premature cell senescence associated with accumulation of p53 and p16(INK4a)', *Cell*, 88(5), pp. 593–602. doi: 10.1016/S0092-8674(00)81902-9.

Shah, P. P., Donahue, G., Otte, G. L., Capell, B. C., Nelson, D. M., Cao, K., Aggarwala, V., Cruickshanks, H. A., Rai, T. S., McBryan, T., Gregory, B. D., Adams, P. D. and Berger, S. L. (2013) 'Lamin B1 depletion in senescent cells triggers large-scale changes in gene expression and the chromatin landscape', *Genes & Development*, 27(16), pp. 1787–1799. doi: 10.1101/gad.223834.113.

Sham, M. H., Vesque, C., Nonchev, S., Marshall, H., Whiting, J., Wilkinson, D., Chamay, P., Krumlauf, R., Ridgeway, T. and Hill, M. (1993) 'The Zinc Finger Gene Krox20 Regulates HoxB2 (Hox2.8) during Hindbrain Segmentation', *Cell*, 72, pp. 183–196.

Sharpless, N. E. and Sherr, C. J. (2015) 'Forging a signature of in vivo senescence', *Nature Reviews Cancer*. Nature Publishing Group, 15(7), pp. 397–408. doi: 10.1038/nrc3960.

Shay, J. W. and Wright, W. E. (2005) 'Senescence and immortalization: Role of telomeres and telomerase', *Carcinogenesis*, 26(5), pp. 867–874. doi: 10.1093/carcin/bgh296.

Sherr, C. J. and Roberts, J. M. (1999) 'CDK inhibitors: positive and negative regulators of G1-phase progression.', *Genes & Development*, 13(12), pp. 1501–1512. doi: 10.1101/gad.13.12.1501.

Short, K., Wiradjaja, F. and Smyth, I. (2007) 'Let's stick together: the role of the Fras1 and Frem proteins in epidermal adhesion.', *Life*, 59(7), pp. 427–435. doi: 10.1080/15216540701510581.

Shtutman, M., Zhurinsky, J., Oren, M., Levina, E. and Ben-Ze'ev, A. (2002) 'PML is a target gene of beta-catenin and plakoglobin, and coactivates beta-catenin-mediated transcription.', *Cancer research*, 62(25), pp. 5947–5954.

Sikora, E. (2013) 'Rejuvenation of senescent cells-The road to postponing human aging and age-related disease?', *Experimental Gerontology*. Elsevier Inc., 48(7), pp. 661–666. doi: 10.1016/j.exger.2012.09.008.

Sikora, E., Arendt, T., Bennett, M. and Narita, M. (2011) 'Impact of cellular senescence signature on ageing research', *Ageing Research Reviews*. Elsevier B.V., 10(1), pp. 146–152. doi: 10.1016/j.arr.2010.10.002.

Sokolov, I., Iyer, S. and Woodworth, C. D. (2006) 'Recovery of elasticity of aged human epithelial cells in vitro', *Nanomedicine: Nanotechnology, Biology, and Medicine*, 2(1), pp. 31–36. doi: 10.1016/j.nano.2005.12.002.

Solon, J., Levental, I., Sengupta, K., Georges, P. C. and Janmey, P. A. (2007) 'Fibroblast adaptation and stiffness matching to soft elastic substrates', *Biophysical Journal*, 93(12), pp. 4453–4461. doi: 10.1529/biophysj.106.101386.

Spaulding, C., Guo, W. and Effros, R. B. (1999) 'Resistance to apoptosis in human CD8+ T cells that reach replicative senescence after multiple rounds of antigen-specific proliferation', *Experimental Gerontology*, 34(5), pp. 633–644. doi: 10.1016/S0531-5565(99)00033-9.

Sproul, D. and Meehan, R. R. (2013) 'Genomic insights into cancer-associated aberrant

CpG island hypermethylation', *Briefings in Functional Genomics*, 12(3), pp. 174–190. doi: 10.1093/bfgp/els063.

Srinivasan, R., Jang, S.-W., Ward, R. M., Sachdev, S., Ezashi, T. and Svaren, J. (2007) 'Differential regulation of NAB corepressor genes in Schwann cells.', *BMC molecular biology*, 8, p. 117. doi: 10.1186/1471-2199-8-117.

Srinivasan, R., Sun, G., Keles, S., Jones, E. A., Jang, S. W., Krueger, C., Moran, J. J. and Svaren, J. (2012) 'Genome-wide analysis of EGR2/SOX10 binding in myelinating peripheral nerve', *Nucleic Acids Research*, 40(14), pp. 6449–6460. doi: 10.1093/nar/gks313.

Stampfer, M. R., Bartholomewt, J. C., Smith, H. S. and Bartley, J. C. (1981) 'Metabolism of benzo[a]pyrene by human mammary epithelial cells: toxicity and DNA adduct formation.', *Proceedings of the National Academy of Sciences of the United States of America*, 78(10), pp. 6251–6255.

Stein, G. H., Drullinger, L. F., Soulard, A. and Dulic, V. (1999) 'Differential Roles for Cyclin-Dependent Kinase Inhibitors p21 and p16 in the Mechanisms of Senescence and Differentiation in Human Fibroblasts Differential Roles for Cyclin-Dependent Kinase Inhibitors p21 and p16 in the Mechanisms of Senescence and Differ', *Molecular and Cellular Biology*, 19(3), pp. 2109–2117.

Storer, M., Mas, A., Robert-Moreno, A., Pecoraro, M., Ortells, M. C., Di Giacomo, V., Yosef, R., Pilpel, N., Krizhanovsky, V., Sharpe, J. and Keyes, W. M. (2013) 'Senescence is a developmental mechanism that contributes to embryonic growth and patterning', *Cell*. Elsevier Inc., 155(5), pp. 1119–1130. doi: 10.1016/j.cell.2013.10.041.

Strappazzon, F., Torch, S., Chatellard-Causse, C., Petiot, A., Thibert, C., Blot, B., Verna, J. M. and Sadoul, R. (2010) 'Alix is involved in caspase 9 activation during calcium-induced apoptosis', *Biochemical and Biophysical Research Communications*. Elsevier Inc., 397(1), pp. 64–69. doi: 10.1016/j.bbrc.2010.05.062.

Sun, L., Ryan, D. G., Zhou, M., Sun, T.-T. and Lavker, R. M. (2006) 'EEDA: a protein associated with an early stage of stratified epithelial differentiation.', *Journal of cellular physiology*, 206(1), pp. 103–11. doi: 10.1002/jcp.20433.

Sun, P., Yoshizuka, N., New, L., Moser, B. A., Li, Y., Liao, R., Xie, C., Chen, J., Deng, Q., Yamout, M., Dong, M. Q., Frangou, C. G., Yates, J. R., Wright, P. E. and Han, J. (2007) 'PRAK Is Essential for ras-Induced Senescence and Tumor Suppression', *Cell*, 128(2), pp. 295–308. doi: 10.1016/j.cell.2006.11.050.

Sun, S., Sun, L., Zhou, X., Wu, C., Wang, R., Lin, S. H. and Kuang, J. (2016) 'Phosphorylation-Dependent Activation of the ESCRT Function of ALIX in Cytokinetic Abscission and Retroviral Budding', *Developmental Cell*. Elsevier Inc., 36(3), pp. 331–343. doi: 10.1016/j.devcel.2016.01.001.

Svaren, J., Sevetson, B. R., Apel, E. D., Zimonjic, D. B., Popescu, N. C. and Milbrandt, J. (1996) 'NAB2, a corepressor of NGFI-A (Egr-1) and Krox20, is induced by proliferative and differentiative stimuli.', *Molecular and Cellular Biology*, 16(7), pp. 3545–53.

Swanson, E. C., Manning, B., Zhang, H. and Lawrence, J. B. (2013) 'Higher-order unfolding of satellite heterochromatin is a consistent and early event in cell senescence', *Journal of Cell Biology*, 203(6), pp. 929–942. doi: 10.1083/jcb.201306073.

Swiatek, P. J. and Gridley, T. (1993) 'Perinatal lethality and defects in hindbrain development in mice homozygous for a targeted mutation of the zinc finger gene Krox20', *Genes & Development*, 7(11), pp. 2071–2084. doi: 10.1101/gad.7.11.2071.

Takahashi, A., Ohtani, N., Yamakoshi, K., Iida, S., Tahara, H., Nakayama, K., Nakayama, K. I., Ide, T., Saya, H. and Hara, E. (2006) 'Mitogenic signalling and the p16INK4a-Rb pathway cooperate to enforce irreversible cellular senescence.', *Nature Cell Biology*, 8(11), pp. 1291–1297. doi: 10.1038/ncb1491.

Tang, H., Jiang, H., Zheng, J., Li, J., Wei, Y., Xu, G. and Li, H. (2015) 'International Immunopharmacology MicroRNA-106b regulates pro-allergic properties of dendritic cells and Th2 polarisation by targeting early growth response-2 in vitro', *International Immunopharmacology*. Elsevier B.V., 28(2), pp. 866–874. doi: 10.1016/j.intimp.2015.03.043.

Tchkonia, T., Morbeck, D. E., Von Zglinicki, T., Van Deursen, J., Lustgarten, J., Scrable, H., Khosla, S., Jensen, M. D. and Kirkland, J. L. (2010) 'Fat tissue, aging, and cellular senescence', *Aging Cell*, 9(5), pp. 667–684. doi: 10.1111/j.1474-9726.2010.00608.x.

Tchkonia, T., Zhu, Y., Deursen, J. Van, Campisi, J. and Kirkland, J. L. (2013) 'Cellular senescence and the senescent secretory phenotype: therapeutic opportunities', *The Journal of Clinical Investigation*, 123(3), pp. 966–972. doi: 10.1172/JCI64098.966.

The Wellcome Trust Case Control Consortium (2007) 'Genome-wide association study of 14,000 cases of seven common diseases and 3,000 shared controls.', *Nature*, 447(7145), pp. 661–78. doi: 10.1038/nature05911.

Todorović, V., Desai, B. V, Patterson, M. J. S., Amargo, E. V, Dubash, A. D., Yin, T., Jones, J. C. R. and Green, K. J. (2010) 'Plakoglobin regulates cell motility through Rho- and fibronectin-dependent Src signaling', *Journal of cell science*, 123(Pt 20), pp. 3576–3586. doi: 10.1242/jcs.070391.

Topilko, P., Schneider-Maunoury, S., Levi, G., Baron-Van Evercooren, a, Chennoufi, a B., Seitanidou, T., Babinet, C. and Charnay, P. (1994) 'Krox-20 controls myelination in the peripheral nervous system.', *Nature*, pp. 796–799. doi: 10.1038/371796a0.

Turenne, G. a, Paul, P., Laflair, L. and Price, B. D. (2001) 'Activation of p53 transcriptional activity requires ATM's kinase domain and multiple N-terminal serine residues of p53.', *Oncogene*, 20(37), pp. 5100–5110. doi: 10.1038/sj.onc.1204665.

Unoki, M. and Nakamura, Y. (2001) 'Growth-suppressive effects of BPOZ and EGR2, two genes involved in the PTEN signaling pathway.', *Oncogene*, 20(33), pp. 4457–65. doi: 10.1038/sj.onc.1204608.

Unoki, M. and Nakamura, Y. (2003) 'Methylation at CpG islands in intron 1 of EGR2 confers enhancer-like activity', *FEBS Letters*, 554(1–2), pp. 67–72. doi: 10.1016/S0014-5793(03)01092-5.

Vernier, M., Bourdeau, V., Gaumont-Leclerc, M. F., Moiseeva, O., Bégin, V., Saad, F., Mes-Masson, A. M. and Ferbeyre, G. (2011) 'Regulation of E2Fs and senescence by PML nuclear bodies', *Genes & Development*, 25(1), pp. 41–50. doi: 10.1101/gad.1975111.

Vicente-Manzanares, M., Ma, X., Adelstein, R. S. and Horwitz, A. R. (2009) 'Non-muscle myosin II takes centre stage in cell adhesion and migration', *Nature Reviews Molecular Cell Biology*, 10(11), pp. 778–790. doi: 10.1038/nrm2786.Non-muscle.

Walters, H. E., Deneka-Hannemann, S. and Cox, L. S. (2016) 'Reversal of phenotypes of cellular senescence by pan-mTOR inhibition', *Aging*, 8(2), pp. 231–244. doi: 10.18632/aging.100872.

Wang, C., Maddick, M., Miwa, S., Jurk, D., Czapiewski, R., Saretzki, G., Langie, S. A. S., Godschalk, R. W. L., Cameron, K. and von Zglinicki, T. (2010) 'Adult-onset, short-term dietary restriction reduces cell senescence in mice', *Aging*, 2(9), pp. 555–566. doi: 100196 [pii].

Wang, E. (1995) 'Senescent Human Fibroblasts Resist Programmed Cell Death, and Failure to Suppress bell Is Involved', *Cancer Research*, 55(11), pp. 2284–2292.

Warbrick, E., Lanet, D. P., Glover, D. M. and Coxt, L. S. (1995) 'A small peptide inhibitor of DNA replication defines the site of interaction between the cyclin-dependent kinase inhibitor p21WAF1 and proliferating cell nuclear antigen', *Current Biology*, 5(3), pp. 275–282.

Warner, L. E., Mancias, P., Butler, I. J., McDonald, C. M., Keppen, L., Koob, K. G. and Lupski, J. R. (1998) 'Mutations in the early growth response 2 (EGR2) gene are associated with hereditary myelinopathies', *Nature Genetics*, 18(4), pp. 382–384. doi: 10.1038/ng0498-382 [doi].

Wassermann, S., Scheel, S. K., Hiendlmeyer, E., Palmqvist, R., Horst, D., Hlubek, F., Haynl, A., Kriegl, L., Reu, S., Merkel, S., Brabletz, T., Kirchner, T. and Jung, A. (2009) 'p16INK4a Is a β-Catenin Target Gene and Indicates Low Survival in Human Colorectal Tumors', *Gastroenterology*. AGA Institute American Gastroenterological Association, 136(1), p. 196–205.e2. doi: 10.1053/j.gastro.2008.09.019.

Webley, K., Bond, J. A., Jones, C. J., Blaydes, J. P., Craig, A., Hupp, T. and Wynford-Thomas, D. (2000) 'Posttranslational modifications of p53 in replicative senescence overlapping but distinct from those induced by DNA damage.', *Molecular and Cellular Biology*, 20(8), pp. 2803–8. doi: 10.1128/MCB.20.8.2803-2808.2000.

Weitzman, J. B., Fiette, L., Matsuo, K. and Yaniv, M. (2000) 'JunD protects cells from p53-dependent senescence and apoptosis.', *Molecular Cell*, 6(5), pp. 1109–1119. doi: 10.1016/S1097-2765(00)00109-X.

Whitehead, K. a, Langer, R. and Anderson, D. G. (2009) 'Knocking down barriers: advances in siRNA delivery.', *Nature Reviews Drug discovery*, 8(2), pp. 129–38. doi: 10.1038/nrd2742.

Wiley, C. D., Velarde, M. C., Lecot, P., Liu, S., Sarnoski, E. A., Freund, A., Shirakawa, K., Lim, H. W., Davis, S. S., Ramanathan, A., Gerencser, A. A., Verdin, E. and Campisi, J. (2016) 'Mitochondrial dysfunction induces senescence with a distinct secretory phenotype', *Cell Metabolism*. Elsevier, 23(2), pp. 303–314. doi: 10.1016/j.cmet.2015.11.011.

Williams, G. (1957) 'Pleiotropy, natural selection, and the evolution of senescence', *Evolution*, 11(4), pp. 398–411.

Wu, L. M. N., Wang, J., Conidi, A., Zhao, C., Wang, H., Ford, Z., Zhang, L., Zweier, C., Ayee, B. G., Maurel, P., Zwijsen, A., Chan, J. R., Jankowski, M. P., Huylebroeck, D. and Lu, Q. R. (2016) 'Zeb2 recruits HDAC-NuRD to inhibit Notch and controls Schwann cell differentiation and remyelination.', *Nature Neuroscience*, 19(8), pp. 1060–72. doi: 10.1038/nn.4322.

Wu, Q., Jin, H., Yang, Z., Luo, G., Lu, Y., Li, K., Ren, G., Su, T., Pan, Y., Feng, B., Xue, Z., Wang, X. and Fan, D. (2010) 'MiR-150 promotes gastric cancer proliferation by negatively regulating the pro-apoptotic gene EGR2', *Biochemical and Biophysical Research Communications*. Elsevier Inc., 392(3), pp. 340–345. doi: 10.1016/j.bbrc.2009.12.182.

Xue, W., Zender, L., Miething, C., Dickins, R. A., Hernando, E., Krizhanovsky, V., Cordon-Cardo, C. and Lowe, S. W. (2007) 'Senescence and tumour clearance is triggered by p53 restoration in murine liver carcinomas.', *Nature*, 445(7128), pp. 656–60. doi: 10.1038/nature05529.

Yager, E. J., Ahmed, M., Lanzer, K., Randall, T. D., Woodland, D. L. and Blackman, M. A. (2008) 'Age-associated decline in T cell repertoire diversity leads to holes in the repertoire and impaired immunity to influenza virus', *The Journal of experimental medicine*, 205(3), pp. 711–723. doi: 10.1084/jem.20071140.

Yokota, I., Sasaki, Y., Kashima, L., Idogawa, M. and Tokino, T. (2010) 'Identification and

characterization of early growth response 2, a zinc-finger transcription factor, as a p53-regulated proapoptotic gene', *International Journal of Oncology*, 37, pp. 1407–1416. doi: 10.3892/ijo.

Yosef, R., Pilpel, N., Tokarsky-Amiel, R., Biran, A., Ovadya, Y., Cohen, S., Vadai, E., Dassa, L., Shahar, E., Condiotti, R., Ben-Porath, I. and Krizhanovsky, V. (2016) 'Directed elimination of senescent cells by inhibition of BCL-W and BCL-XL.', *Nature Communications*. Nature Publishing Group, 7, p. 11190. doi: 10.1038/ncomms11190.

Yun, M. H., Davaapil, H. and Brockes, J. P. (2015) 'Recurrent turnover of senescent cells during regeneration of a complex structure.', *eLife*, 4(May), p. e05505. doi: 10.7554/eLife.05505.

Zachara, N. E., Vosseller, K. and Hart, G. W. (2011) 'Detection and analysis of proteins modified by O-Linked N-Acetylglucosamine', *Current Protocols in Protein Science*. doi: 10.1002/0471140864.ps1208s66.

Zhang, M., Wang, Y., Wang, J. S., Liu, J., Liu, M. M. and Yang, H. B. (2015) 'The Roles of Egr-2 in Autoimmune Diseases', *Inflammation*, 38(3), pp. 972–977. doi: 10.1007/s10753-014-0059-z.

Zhang, Y., Xiong, Y. and Yarbrough, W. G. (1998) 'ARF promotes MDM2 degradation and stabilizes p53: ARF-INK4a locus deletion impairs both the Rb and p53 tumor suppression pathways', *Cell*, 92(6), pp. 725–734. doi: 10.1016/S0092-8674(00)81401-4.

Zheng, Y., Zha, Y., Driessens, G., Locke, F. and Gajewski, T. F. (2012) 'Transcriptional regulator early growth response gene 2 (Egr2) is required for T cell anergy in vitro and in vivo.', *The Journal of experimental medicine*, 209(12), pp. 2157–63. doi: 10.1084/jem.20120342.

Zheng, Y., Zha, Y., Spaapen, R. M., Mathew, R., Barr, K., Bendelac, A. and Gajewski, T. F. (2013) 'Egr2-dependent gene expression profiling and ChIP-Seq reveal novel biologic targets in T cell anergy', *Molecular Immunology*. Elsevier Ltd, 55(3–4), pp. 283–291. doi: 10.1016/j.molimm.2013.03.006.

Zhu, B., Symonds, A. L. J., Martin, J. E., Kioussis, D., Wraith, D. C., Li, S. and Wang, P. (2008) 'Early growth response gene 2 (Egr-2) controls the self-tolerance of T cells and

prevents the development of lupuslike autoimmune disease.', *The Journal of experimental medicine*, 205(10), pp. 2295–307. doi: 10.1084/jem.20080187.

Zhu, J., Woods, D., Mcmahon, M. and Bishop, J. M. (1998) 'Senescence of human fibroblasts induced by oncogenic Raf Senescence of human fibroblasts induced by oncogenic Raf', *Genes & Development*, pp. 2997–3007. doi: 10.1101/gad.12.19.2997.

Zhu, Y., Tchkonia, T., Fuhrmann-Stroissnigg, H., Dai, H. M., Ling, Y. Y., Stout, M. B., Pirtskhalava, T., Giorgadze, N., Johnson, K. O., Giles, C. B., Wren, J. D., Niedernhofer, L. J., Robbins, P. D. and Kirkland, J. L. (2016) 'Identification of a novel senolytic agent, navitoclax, targeting the Bcl-2 family of anti-apoptotic factors', *Aging Cell*, 15(3), pp. 428–435. doi: 10.1111/acel.12445.

Zhu, Y., Tchkonia, T., Pirtskhalava, T., Gower, A. C., Ding, H., Giorgadze, N., Palmer, A. K., Ikeno, Y., Hubbard, G. B., Lenburg, M., O'Hara, S. P., Larusso, N. F., Miller, J. D., Roos, C. M., Verzosa, G. C., Lebrasseur, N. K., Wren, J. D., Farr, J. N., Khosla, S., Stout, M. B., Mcgowan, S. J., Fuhrmann-Stroissnigg, H., Gurkar, A. U., Zhao, J., Colangelo, D., Dorronsoro, A., Ling, Y. Y., Barghouthy, A. S., Navarro, D. C., Sano, T., Robbins, P. D., Niedernhofer, L. J. and Kirkland, J. L. (2015) 'The Achilles' heel of senescent cells: From transcriptome to senolytic drugs', *Aging Cell*, (March), pp. 644–658. doi: 10.1111/acel.12344.

Zhuo, W., Ge, W., Meng, G., Jia, S., Zhou, X. and Liu, J. (2015) 'MicroRNA-20a promotes the proliferation and cell cycle of human osteosarcoma cells by suppressing early growth response 2 expression', *Molecular Medicine Reports*, 12(4), pp. 4989–4994. doi: 10.3892/mmr.2015.4098.

Zorick, T. S., Syroid, D. E., Arroyo, E., Scherer, S. S. and Lemke, G. (1996) 'The transcription factors SCIP and Krox-20 mark distinct stages and cell fates in Schwann cell differentiation.', *Molecular and Cellular Neuroscience*, 8(2–3), pp. 129–145. doi: 10.1006/mcne.1996.0052.

Zuehlke, A. D., Beebe, K., Neckers, L. and Prince, T. (2015) 'Regulation and function of the human HSP90AA1 gene', *Gene*. Elsevier B.V., 570(1), pp. 8–16. doi: 10.1016/j.gene.2015.06.018.

Appendix

Senescence marker	Description	References
Arrested proliferation	• Stable G1 cell cycle arrest characterised by reduced BrdU incorporation.	Reviewed in (Sikora *et al.*, 2011)
Altered nuclear and cellular morphology	• Enlarged, flattened cellular morphology. • Enlarged, irregular nuclear morphology. • Down-regulated lamin B1 expression.	Reviewed in (Sikora *et al.*, 2011) (Freund *et al*. 2012)
Expression of tumour suppressor genes	• Increased expression of p15, p16, ARF, p53, and/or p21.	(Alcorta *et al.*, 1996; Gil and Peters, 2006)
DNA damage response	• Telomere dysfunction. • DNA damage foci characterised by γ-H2AX and 53BP1. • Increased oxidative DNA damage foci characterised by 8-oxoG.	(Bodnar *et al.*, 1998) (di Fagagna *et al.*, 2003) (Chen *et al.*, 1995)
Epigenetic alterations	• Genomic DNA hypomethylation. • Hypermethylation at specific sites composes a senescence-associated methylation signature. • SAHF (not universal), characterised by HP1.	(Bork *et al.*, 2010; Cruickshanks *et al.*, 2013; Hänzelmann *et al.*, 2015; Lowe *et al.*, 2015) (Narita *et al.*, 2003; Kosar *et al.*, 2011)
Increased lysosomal activity	• Increased SA-β-Gal activity.	(Dimri *et al.*, 1995)
Senescence-associated secretory phenotype	• Increased secretion of cocktail of factors including inflammatory cytokines (IL-6, IL-8), MMPs, and TGF-β, inducing local inflammation and paracrine senescence.	(Freund *et al.*, 2010; Acosta *et al.*, 2013)

Table A.1 Table summarising commonly used markers of senescence.

Measure	EP	DS	DS + siGLO	DS + p16 siRNA	DS + p21 siRNA	DS + p16+p21 siRNA
Cell number (cells/well)	2,739 ± 189	1,182 ± 156	1,017 ± 106	1,042 ± 150	1,476 ± 238	1,657 ± 214
Nuclear area (μm^2)	215 ± 5	280 ± 5	281 ± 9	273 ± 10	203 ± 8	187 ± 9
Nuclear elongation (AU)	1.37 ± 0.01	1.42 ± 0.03	1.42 ± 0.03	1.42 ± 0.03	1.36 ± 0.04	1.35 ± 0.03
Nuclear roundness (AU)	0.94 ± 0.003	0.91 ± 0.009	0.90 ± 0.01	0.90 ± 0.01	0.92 ± 0.01	0.92 ± 0.007
Cell area (μm^2)	2,110 ± 280	5,832 ± 424	6,341 ± 800	5,668 ± 792	3,407 ± 661	2,908 ± 676
Cell elongation (AU)	1.82 ± 0.003	1.77 ± 0.013	1.80 ± 0.03	1.85 ± 0.07	1.98 ± 0.09	2.02 ± 0.13
BrdU positive nuclei	15% ± 1%	0% ± 0%	1% ± 1%	4% ± 2%	17% ± 6%	32% ± 10%
8-oxoG positive cells	16% ± 4%	71% ± 3%	89% ± 1%	84% ± 2%	62% ± 7%	55% ± 10%
p16+p21+ nuclei	5% ± 1%	62% ± 18%	64% ± 9%	35% ± 12%	23% ± 2%	30% ± 1%
p16+p21- nuclei	6% ± 1%	11% ± 8%	2% ± 1%	2% ± 1%	57% ± 6%	42% ± 2%
p16-p21+ nuclei	37% ± 8%	23% ± 4%	31% ± 10%	59% ± 14%	4% ± 2%	6% ± 0%
p16-p21- nuclei	53% ± 9%	5% ± 6%	3% ± 0%	4% ± 2%	16% ± 2%	22% ± 0%

Table A.2 Table summarising measures analysed for EP, DS, and siRNA transfected DS HMFs.

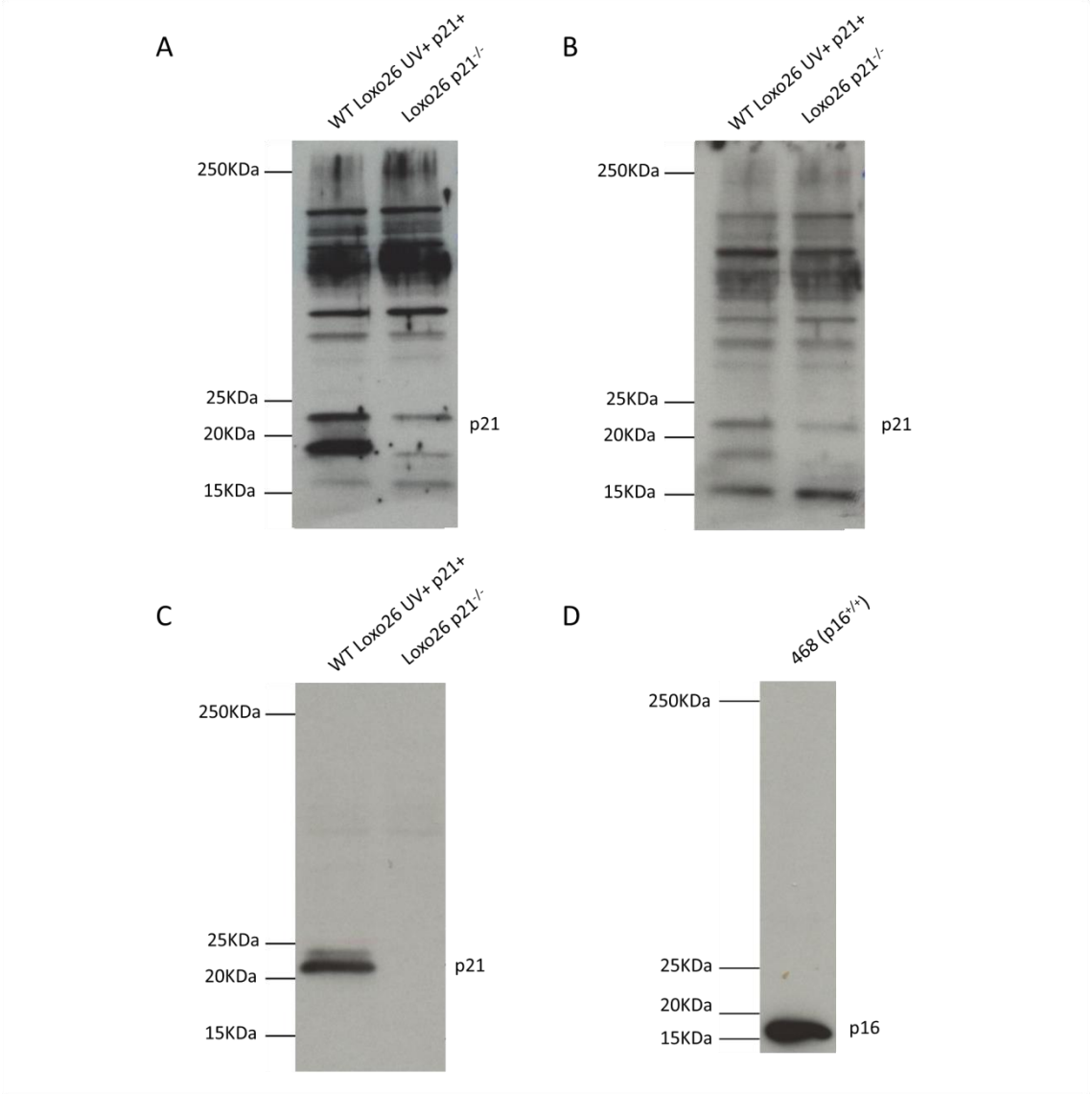

Figure A.1 Uncropped western blots of p21 and p16 in WT Loxo26 UV+ p21+, Loxo26 p21$^{-/-}$, and MDA-MB-468 cells loaded by total protein concentration. Cell lysates were probed for **(A)** rabbit anti-p21 (ab7960), **(B)** rabbit anti-p21 (C-19 sc397), and **(C)** rabbit anti-p21 (12D1) according to Section 2.4. **(D)**. MDA-MB-468 p16-positive cells were probed for mouse anti-p16 (JC8) according to Section 2.4. Antibody dilutions and conditions may be found in Section 2.4.3.

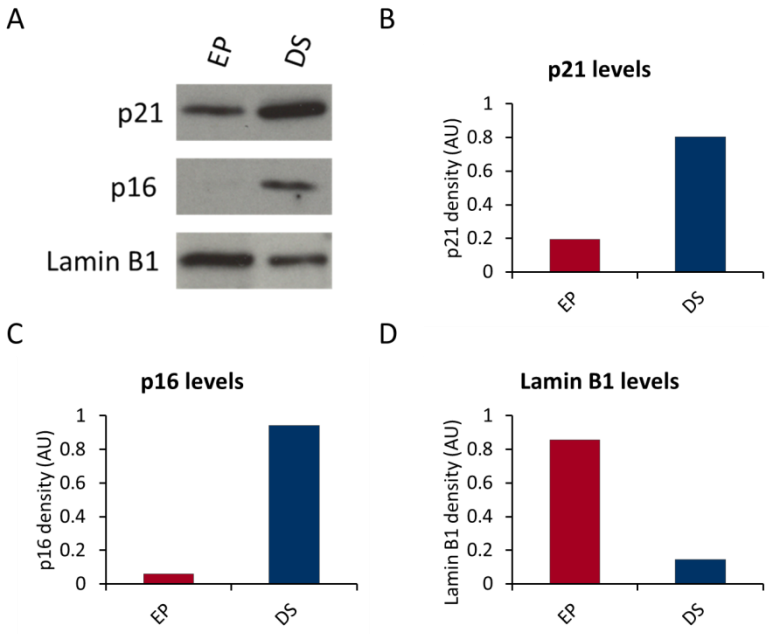

Figure A.2 Western blot analysis of p21, p16 and lamin B1 levels in EP and DS HMFs loaded by cell number. (A) Western blot depicting p21, p16, and lamin B1 levels in EP and DS HMFs. Lysates were probed for rabbit anti-p21 (12D1), mouse anti-p16 (JC8), and the rabbit anti-lamin B1 antibody according to Section 2.4. Antibody dilutions and conditions may be found in Section 2.4.3. **(B)** Densitometry analysis of p21 levels in EP and DS HMFs. **(C)** Densitometry analysis of p16 levels in EP and DS HMFs. **(D)** Densitometry analysis of lamin B1 levels. Analysis was performed using ImageJ software according to Section 2.4.4. Bars denote density levels of one experiment.

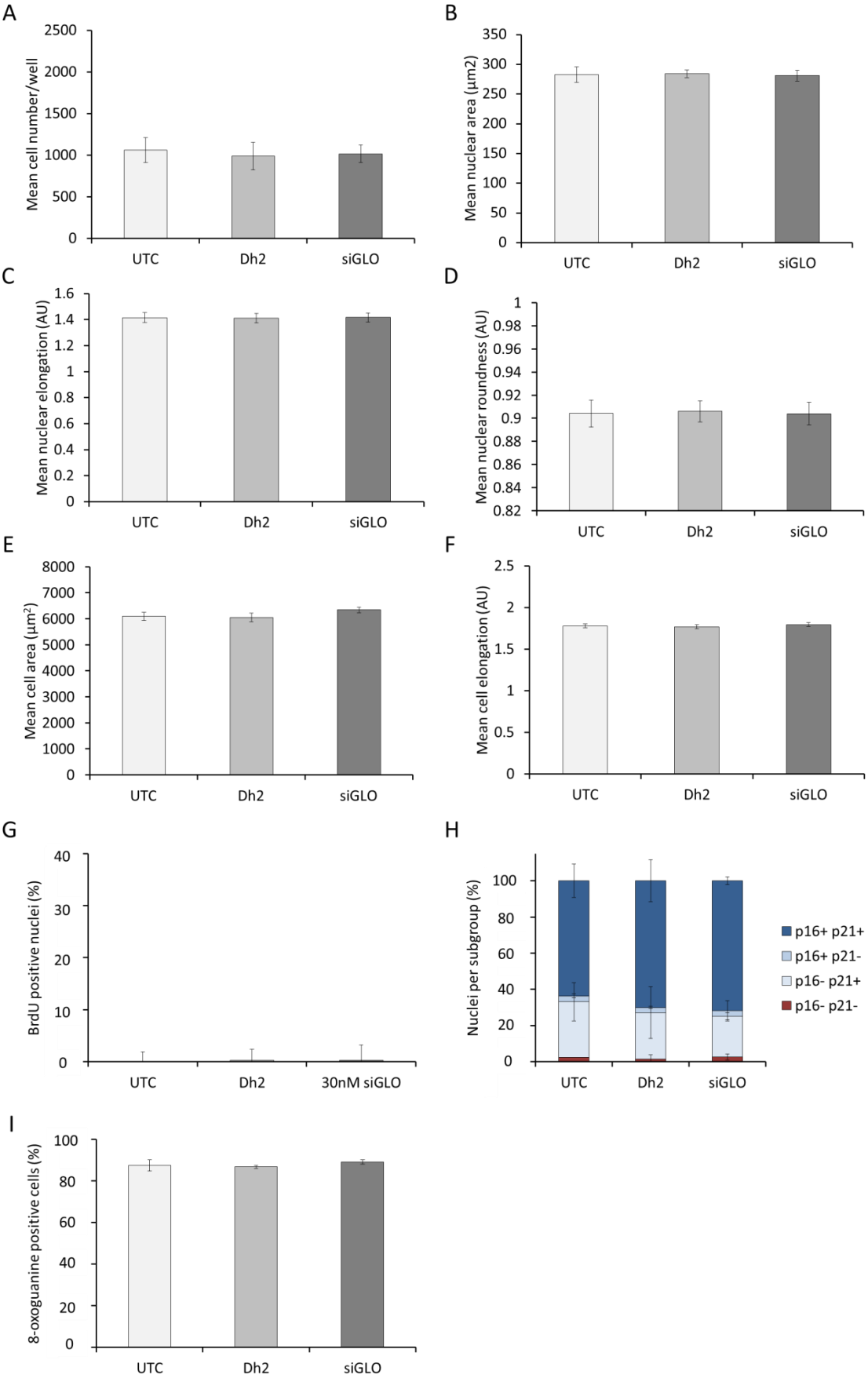
A
Mean cell number/well
2500
2000
1500
1000
500
0
UTC
Dh2
siGLO
B
Mean nuclear area (µm2)
350
300
250
200
150
100
50
0
UTC
Dh2
siGLO
C
Mean nuclear elongation (AU)
1.6
1.4
1.2
1
0.8
0.6
0.4
0.2
0
UTC
Dh2
siGLO
D
Mean nuclear roundness (AU)
1
0.98
0.96
0.94
0.92
0.9
0.88
0.86
0.84
0.82
UTC
Dh2
siGLO
E
Mean cell area (µm²)
8000
7000
6000
5000
4000
3000
2000
1000
0
UTC
Dh2
siGLO
F
Mean cell elongation (AU)
2.5
2
1.5
1
0.5
0
UTC
Dh2
siGLO
G
BrdU positive nuclei (%)
40
30
20
10
0
UTC
Dh2
30nM siGLO
H
Nuclei per subgroup (%)
100
80
60
40
20
0
UTC
Dh2
siGLO
p16+ p21+
p16+ p21-
p16- p21+
p16- p21-
I
8-oxoguanine positive cells (%)
100
80
60
40
20
0
UTC
Dh2
siGLO

Figure A.3 Analysis of untransfected, Dh2 only, and siGLO transfected controls. DS cells were seeded at 15,000 cells/cm^2 in 384-well plate format and were either untransfected (UTC) or forward transfected with either Dh2 alone, or with 30 nM siGLO. Cells were then fixed, stained with DAPI, mouse anti-BrdU Alexa Fluor 488, or mouse anti-p16 (JC8) and rabbit anti-p21 (12D1), or mouse anti-8-oxoG, and donkey anti-mouse Alexa Fluor 488 and goat anti-rabbit Alexa Fluor 546, and Cell Mask. Nuclear and cellular morphologies, BrdU nuclear intensity, p16 and p21 nuclear intensities, and 8-oxoG cellular density was quantitated according to Section 2.7 and Section 2.8. Using the secondary only control, a nuclear intensity threshold was established to define BrdU positive or negative nuclei. Nuclear intensity thresholds were established for p16 and p21 to define positive or negative nuclei. Nuclei were classified into four subgroups: p16 and p21 positive (p16+ p21+); p16 positive and p21 negative (p16+ p21-); p16 negative and p21 positive (p16- p21+); and p16 and p21 negative (p16- p21-). A cellular density threshold was established to define 8-oxoG positive or negative cells. **(A)** Mean cell number/well. **(B)** Mean nuclear area (µm^2). **(C)** Mean nuclear elongation (µm^2). **(D)** Mean nuclear roundness (AU). **(E)** Mean cell area (µm^2). **(F)** Mean cell elongation (AU). N=4. Error bars=SD of four independent experiments, each performed with three replicates. **(G)** Bars denote mean percentage of BrdU positive nuclei. N=1. Error bars=SD of a single experiment containing three replicates. **(H)** Bars denote mean percentage of nuclei per subgroup. N=2. Error bars=SD of two independent experiments, each performed with three replicates. **(I)** Bars denote mean percentage of 8-oxoG positive nuclei. N=2. Error bars=SD of two independent experiments, each performed with three replicates.

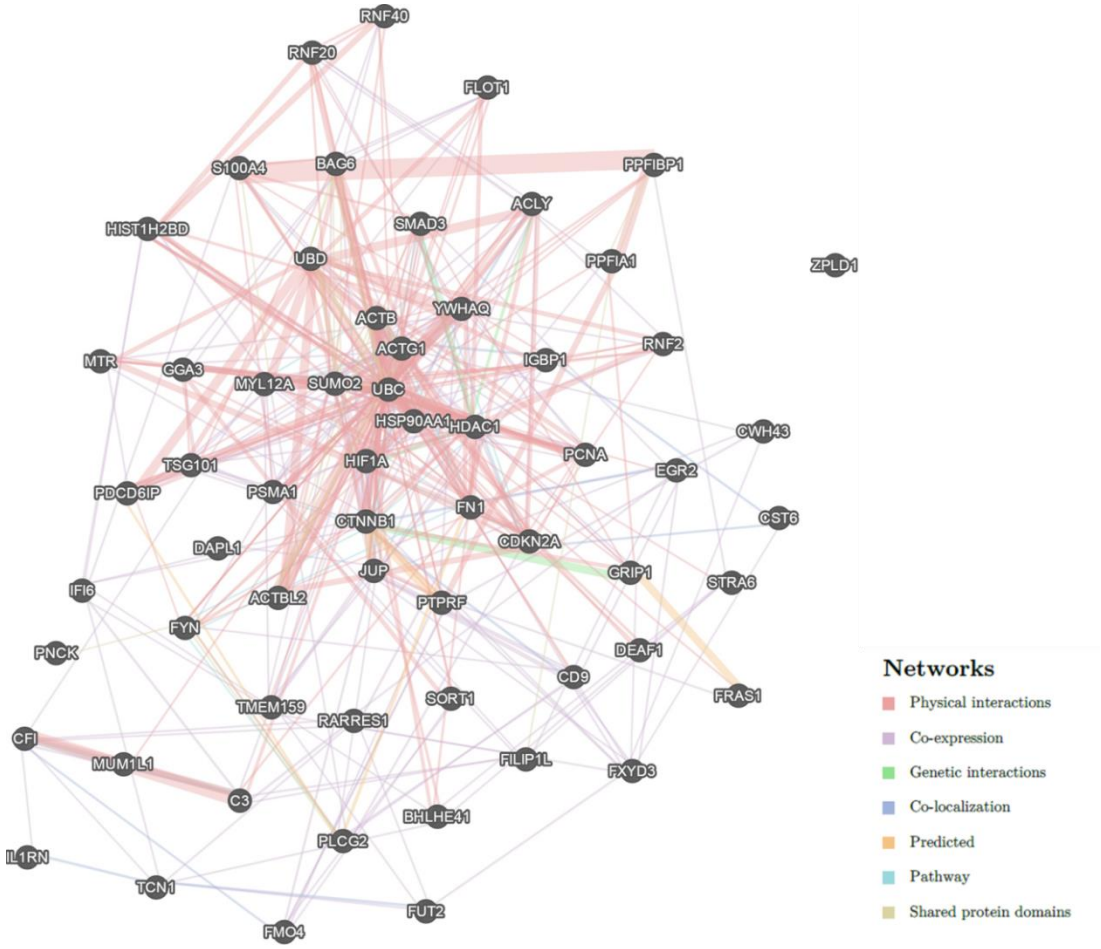

Figure A.4 GeneMANIA interaction network of drivers and interactors. 28 potential drivers of senescence were identified in the previous DS HMEC screen. Using the BioGRID bioinformatics database, 33 interactors were identified which physically interacted with at least two other drivers. To further explore the relationships between drivers and interactors, GeneMANIA was used to generate an interaction network using data from a variety of sources, including physical interactions (red), co-expression (purple), genetic interactions (green), co-localisation (dark blue), predicted interactions (orange), pathways (light blue), and shared protein domains (light green).

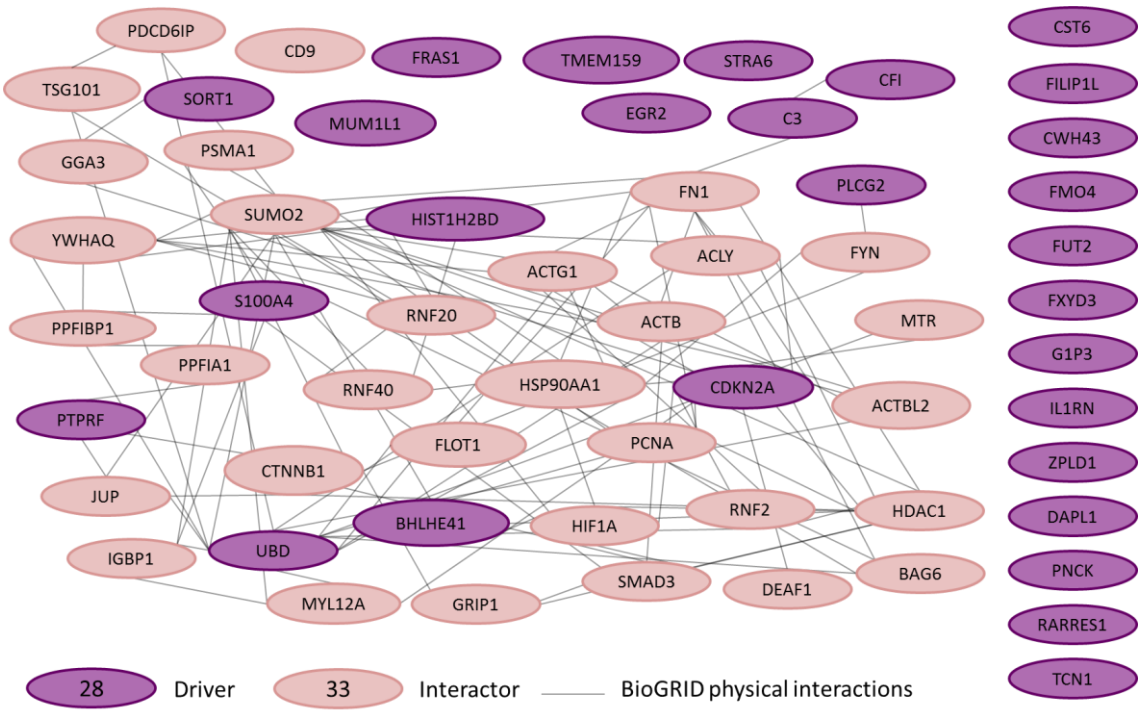

Figure A.5 BioGRID interaction network of drivers and interactors, not including UBC. 28 potential drivers of senescence were identified in the previous DS HMEC screen. Using the BioGRID bioinformatics database, 33 interactors were identified which physically interacted with at least two other drivers. In order to ensure that the previous interactors were not falsely identified, UBC was removed and the protein interaction network re-generated.

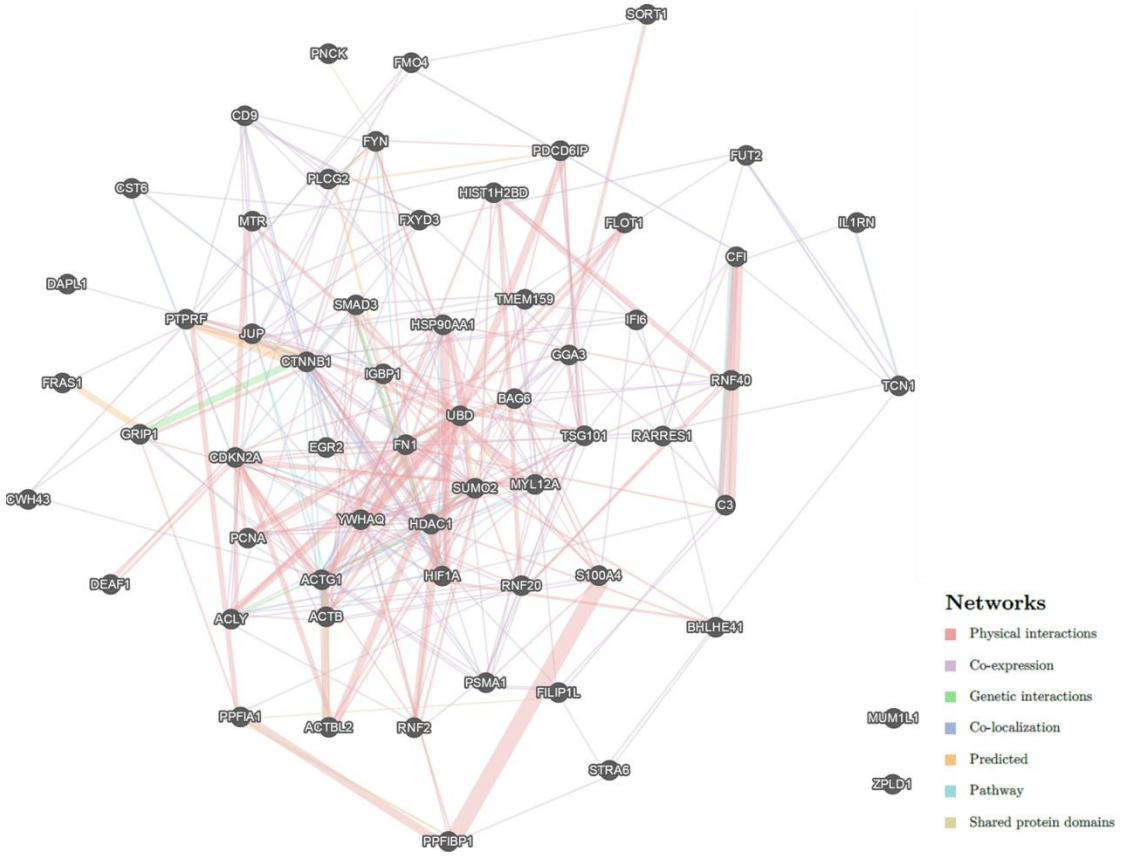

Figure A.6 GeneMANIA interaction network of drivers and interactors, not including UBC. 28 potential drivers of senescence were identified in the previous DS HMEC screen. Using the BioGRID bioinformatics database, 33 interactors were identified which physically interacted with at least two other drivers. In order to ensure that the previous interactors were not falsely identified, UBC was removed and the protein interaction network re-generated using GeneMANIA.

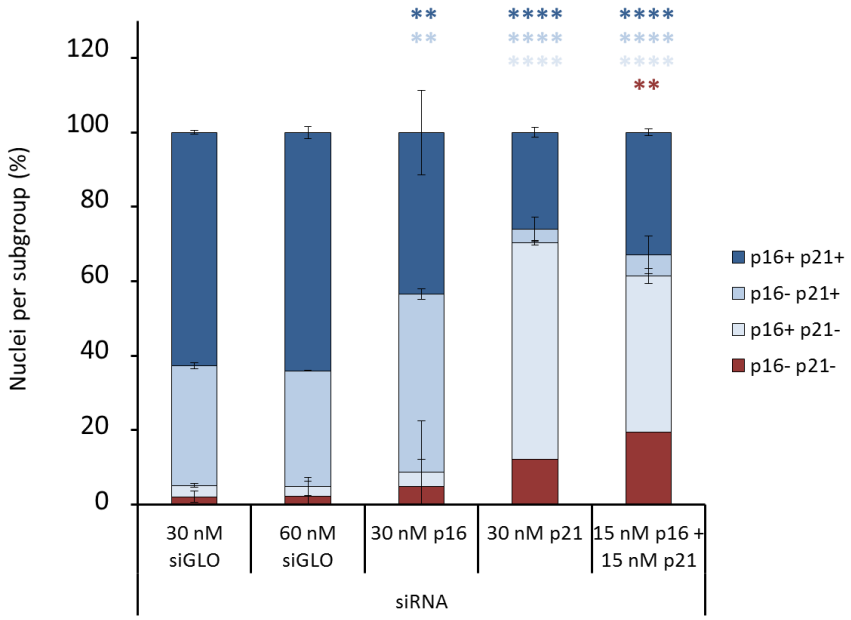

Figure A.7 Comparison of control siRNAs according to p16 and p21 double negative subgroup frequency at day five. Two independent siRNA screens, each in triplicate, were performed for the five day time point in DS HMFs according to Section 2.6.2. Cells were then fixed and stained with DAPI, mouse anti-p16 (JC8), rabbit anti-p21 (12D1), donkey anti-mouse Alexa Fluor 488, and goat anti-rabbit Alexa Fluor 546. Cells were imaged and intensities were quantitated according to Section 2.7 and 2.8. Nuclear intensity thresholds were established for p16 and p21 to define positive or negative nuclei. Nuclei were classified into four subgroups: p16 and p21 positive (p16+ p21+); p16 negative and p21 positive (p16- p21+); p16 positive and p21 negative (p16+ p21-); and p16 and p21 negative (p16- p21-). Bars denote nuclei per subgroup. Two-way ANOVA and Dunnett's test ** $p<0.01$, **** $p<0.0001$ relative to the 30 nM siGLO control. N=2 throughout. Error bars=SD of two independent experiments, each performed with three replicates. Bars denote the 30 nM siGLO control, 60 nM siGLO control, 30 nM p16 siRNA control, 30 nM p21 siRNA control, 15 nM p16 + 15 nM p21 (p16+p21) siRNA.

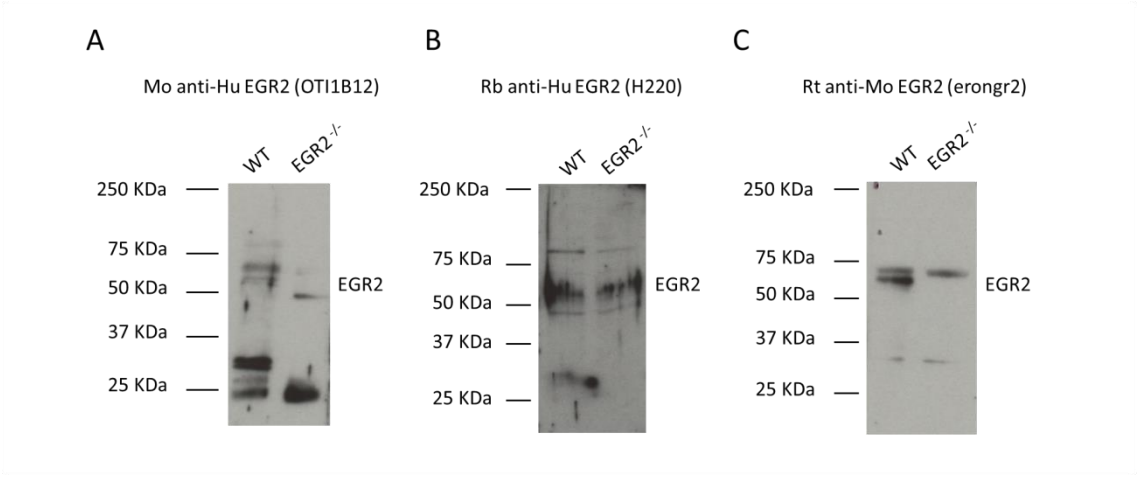

Figure A.8 Uncropped western blots of EGR2 antibodies in wild-type (WT) and Egr-2 knockout mouse lysates loaded by total protein concentration. Lysates of $CD4^+$ T cells isolated from WT and Egr-2 conditional knockout ($EGR2^{-/-}$) mice kindly donated by Prof. Ping Wang and Dr Tizong Miao were probed for **(A)** mouse anti-human EGR2 (OTI1B12) antibody, **(B)** rabbit anti-human EGR2 (H220) antibody, **(C)** rat anti-mouse EGR2 (erongr2) antibody, according to Section 2.4. Antibody dilutions and conditions may be found in Section 2.4.3.

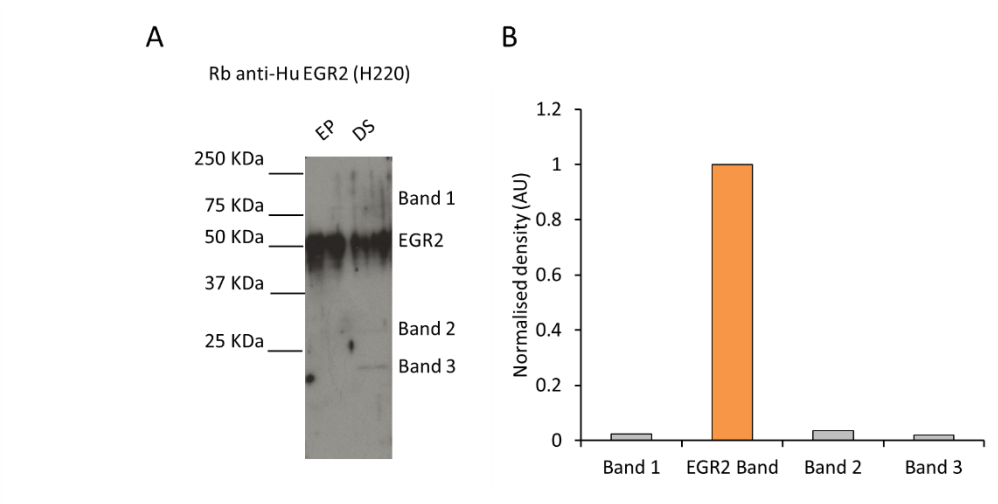

Appendix Figure A.9 Uncropped western blot of rabbit anti-human EGR2 (H220) antibody in EP and DS HMF lysates loaded by cell number. (A) Representative western blot of EP and DS HMFs cell lysates probed for rabbit anti-human EGR2 (H220). **(B)** Densitometry analysis of bands in rabbit anti-human EGR2 (H220) stained siGLO transfected DS HMFs. Analysis was performed using ImageJ software. Bars denote density levels normalised to the EGR2 band. Lysates were probed according to Section 2.4. Antibody dilutions and conditions may be found in Section 2.4.3.

Antibody	Protocol	Condition tried
Rb anti-Hu EGR2 (H220)	Lysate collection	Included phosphatase inhibitors
	Lysate fractionation	Probing nuclear extract
	Laemmli sample buffer	10% β-mercaptoethanol concentration
		4% SDS concentration
	Primary block	.05% PBST versus .1% PBST
		5% milk versus 5% BSA versus no block
Rt anti-Mo EGR2 (erongr2)	Primary concentration	Range between 1:1,000 - 1:100
	Primary incubation	Range between 72 hours – 16 hours
	Secondary concentration	1:10,000 versus 1:5,000

Appendix Table A.3 Optimisation of conditions for anti-EGR2 antibodies using western blotting. The gold standard EGR2 antibody in the literature, rabbit anti-human EGR2 (PRB-236P), was discontinued in October 2015 due to batch variability. Consequently, a number of EGR2 antibodies were tested and optimised in order to identify a suitable EGR2 antibody.

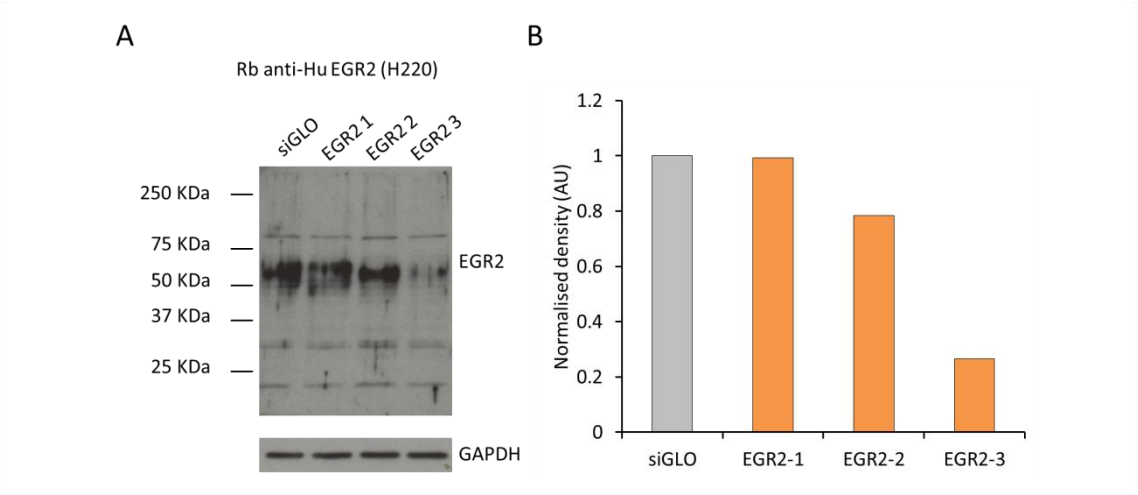

Appendix Figure A.10 Uncropped western blot of rabbit anti-human EGR2 (H220) antibody in DS HMFs transfected with individual EGR2 siRNAs loaded with total protein concentration. **(A)** Representative western blot of DS HMFs transfected with 30 nM siGLO (siGLO), or 30 nM individual EGR2 siRNA (EGR2-1, EGR2-2, EGR2-3) cell lysates were probed for rabbit anti-human EGR2 (H220). **(B)** Densitometry analysis of EGR2 bands in rabbit anti-human EGR2 (H220) probed siGLO transfected DS HMFs. Analysis was performed using ImageJ software. Bars denote density levels normalised to the EGR2 band in siGLO control. Lysates were probed according to Section 2.4. Antibody dilutions and conditions may be found in Section 2.4.3.